Origin of the heaviest elements: The rapid neutron-capture process

John J. Cowan[*]

HLD Department of Physics and Astronomy, University of Oklahoma, 440 West Brooks Street, Norman, Oklahoma 73019, USA

Christopher Sneden[†]

Department of Astronomy, University of Texas, 2515 Speedway, Austin, Texas 78712-1205, USA

James E. Lawler[‡]

Physics Department, University of Wisconsin–Madison, 1150 University Avenue, Madison, Wisconsin 53706-1390, USA

Ani Aprahamian[§] and Michael Wiescher[¶]

Department of Physics and Joint Institute for Nuclear Astrophysics, University of Notre Dame, 225 Nieuwland Science Hall, Notre Dame, Indiana 46556, USA

Karlheinz Langanke[**]

GSI Helmholtzzentrum für Schwerionenforschung, Planckstraße 1, 64291 Darmstadt, Germany and Institut für Kernphysik (Theoriezentrum), Fachbereich Physik, Technische Universität Darmstadt, Schlossgartenstraße 2, 64298 Darmstadt, Germany

Gabriel Martínez-Pinedo[††]

GSI Helmholtzzentrum für Schwerionenforschung, Planckstraße 1, 64291 Darmstadt, Germany; Institut für Kernphysik (Theoriezentrum), Fachbereich Physik, Technische Universität Darmstadt, Schlossgartenstraße 2, 64298 Darmstadt, Germany; and Helmholtz Forschungsakademie Hessen für FAIR, GSI Helmholtzzentrum für Schwerionenforschung, Planckstraße 1, 64291 Darmstadt, Germany

Friedrich-Karl Thielemann[‡‡]

Department of Physics, University of Basel, Klingelbergstrasse 82, 4056 Basel, Switzerland and GSI Helmholtzzentrum für Schwerionenforschung, Planckstraße 1, 64291 Darmstadt, Germany

(published 1 February 2021)

The production of about half of the heavy elements found in nature is assigned to a specific astrophysical nucleosynthesis process: the rapid neutron-capture process (*r* process). Although this idea was postulated more than six decades ago, the full understanding faces two types of uncertainties or open questions: (a) The nucleosynthesis path in the nuclear chart runs close to the neutron-drip line, where presently only limited experimental information is available, and one has to rely strongly on theoretical predictions for nuclear properties. (b) While for many years the occurrence of the *r* process has been associated with supernovae, where the innermost ejecta close to the central neutron star were supposed to be neutron rich, more recent studies have cast substantial doubts on this environment.

[*]jjcowan1@ou.edu
[†]chris@astro.as.utexas.edu
[‡]jelawler@wisc.edu
[§]aapraham@nd.edu
[¶]Michael.C.Wiescher.1@nd.edu
[**]k.langanke@gsi.de
[††]g.martinez@gsi.de
[‡‡]f-k.thielemann@unibas.ch

Possibly only a weak *r* process, with no or negligible production of the third *r*-process peak, can be accounted for, while much more neutron-rich conditions, including an *r*-process path with fission cycling, are likely responsible for the majority of the heavy *r*-process elements. Such conditions could result during the ejection of initially highly neutron-rich matter, as found in neutron stars, or during the fast ejection of matter that has previously experienced strong electron captures at high densities. Possible scenarios are the mergers of neutron stars, neutron-star–black hole mergers, but also include rare classes of supernovae as well as hypernovae or collapsars with polar jet ejecta, and possibly also accretion disk outflows related to the collapse of fast rotating massive stars. The composition of the ejecta from each event determines the temporal evolution of the *r*-process abundances during the "chemical" evolution of the Galaxy. Stellar *r*-process abundance observations have provided insight into and constraints on the frequency of and conditions in the responsible stellar production sites. One of them, neutron-star mergers, was just identified thanks to the observation of the *r*-process kilonova electromagnetic transient following the gravitational wave event GW170817. These observations, which are becoming increasingly precise due to improved experimental atomic data and high-resolution observations, have been particularly important in defining the heavy element abundance patterns of the old halo stars, and thus in determining the extent and nature of the earliest nucleosynthesis in the Galaxy. Combining new results and important breakthroughs in the related nuclear, atomic, and astronomical fields of science, this review attempts to answer the question "How were the elements from iron to uranium made?"

DOI: 10.1103/RevModPhys.93.015002

CONTENTS

I. INTRODUCTION AND HISTORICAL REVIEWS

At present we know of 118 elements from charge number $Z = 1$ (H) to $Z = 118$ (Og). Eighty of them have at least one stable isotope (up to $Z = 82$, Pb) with $Z = 43$ (Tc) and $Z = 61$ (Pm) being unstable. Another 11 elements up to $Z = 94$ (Pu) (with the exception of $Z = 93$, Np) are naturally occurring on Earth with sufficiently long half-lives, while the remaining ones with short half-lives have existed only

temporarily either in the laboratory or in explosive astrophysical environments. The question of how this took place in the Universe is a long-standing one. Presently we know that of the natural elements and isotopes only ^{1,2}H, ^{3,4}He, and ^{7}Li originated in the big bang, with problems remaining in understanding the abundance of ^{7}Li (Cyburt *et al.*, 2016; Pitrou *et al.*, 2018). All other elements were synthesized in stars, the first ones forming a few hundred million years after the big bang. The majority of stars, which have long evolutionary phases, are powered by fusion reactions. Major concepts for stellar burning were laid out in the 1950s (Burbidge *et al.*, 1957; Cameron, 1957), including the then called x process, which today is understood via spallation of nuclei by cosmic rays (Prantzos, 2012). During their evolution and in explosive end phases, massive stars can synthesize elements from C through Ti, the iron-peak elements (e.g., $21 \leq Z \leq 30$ from Sc to Zn) and beyond [as outlined over many years; see Howard *et al.* (1972), Woosley and Heger (2007), Wanajo *et al.* (2018), and Curtis *et al.* (2019)]. The major result is that the production of heavier nuclei up to Pb, Bi, and the actinides requires free neutrons, as charged-particle reactions in stellar evolution and explosions lead typically to full chemical or quasiequilibria that favor the abundance of nuclei with the highest nuclear binding energies, occurring in the Fe peak (Hix *et al.*, 2007).

An extremely small number of these heavy isotopes can be produced as a result of charged-particle and photon-induced reactions in explosive nucleosynthesis, the so-called proton-rich p process [see Arnould and Goriely (2003), Nishimura *et al.* (2018), and Travaglio *et al.* (2018), and references therein], and possibly a further contribution resulting from interactions with neutrinos in such environments, including the ν process (Woosley *et al.*, 1990; Heger *et al.*, 2005; Suzuki and Kajino, 2013; Sieverding *et al.*, 2019) and νp process (Fröhlich, Martínez-Pinedo *et al.*, 2006; Pruet *et al.*, 2006; Wanajo, 2006).

The two main processes involving the capture of free neutrons are the slow (s) process and the rapid (r) process (due to low or high densities of neutrons available and the resulting reaction timescales of neutron captures). In the s process, taking place during stellar evolution and passing through nuclei near stability, there is sufficient time for beta decay between two neutron captures. The process timescale ranges from hundreds to thousands of years. For many of these nuclei experimental data are available (Käppeler *et al.*, 2011; Karakas and Lattanzio, 2014; Reifarth, Lederer, and Käppeler, 2014). To allow for the production of the heaviest nuclei over a timescale of seconds, the r process operates far from stability, which requires high neutron densities. This involves highly unstable nuclei, for which little experimental data are currently available. In addition, the quest for the stellar origin of the required conditions involved a large number of speculations for many decades (Cowan, Thielemann, and Truran, 1991; Arnould, Goriely, and Takahashi, 2007). There are also observational indications of intermediate neutron-capture processes between the s process and the r process, e.g., the i process (Cowan and Rose, 1977), possibly occurring in super–asymptotic giant branch stars (Jones, Ritter *et al.*, 2016). Figure 1 gives an overview of the major

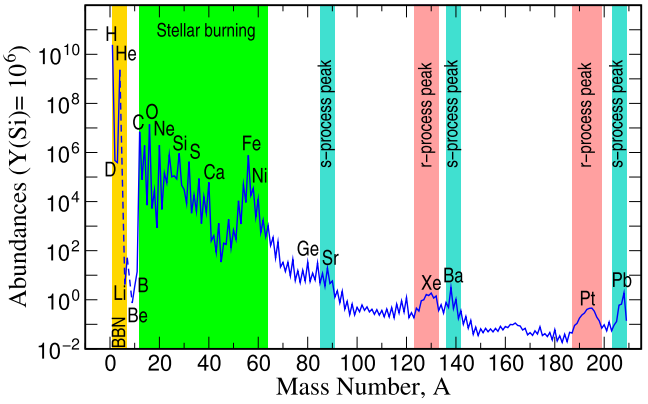

FIG. 1. Abundances Y_i of elements and their isotopes in the Solar System as a function of mass number $A_i = Z_i + N_i$. $A_i Y_i$ is equal to the mass fraction of isotope i, and the sum of mass fractions amounts to 1, $\sum_i A_i Y_i = 1$. A scaling, leading for historical reasons to an abundance of 10^6 for the element Si is utilized. Element ratios are obtained from solar spectra, the isotopic ratios from primitive meteorites and terrestrial values (Asplund *et al.*, 2009; Lodders, Palme, and Gail, 2009). These values represent a snapshot in time of the abundances within the gas that formed the Solar System.

contributions to the Solar System abundances. It includes the big bang (light elements H, He, and Li and their isotopes ^{1,2}H, ^{3,4}He, and ^{7}Li, given in yellow) plus stellar sources contributing via winds and explosions to the interstellar medium until the formation of the Solar System. These stellar burning abundances result from charged-particle reactions up to the Fe group in stellar evolution and explosions (green in Fig. 1) and neutron-capture processes. The latter are a superposition of understood slow neutron captures (s process) in helium burning of stars (with abundance maxima at closed neutron shells for stable nuclei, turquoise in Fig. 1), and a rapid neutron-capture process (r process, pink in Fig. 1), leading to abundance maxima shifted to lighter nuclei in comparison to the s process. We note that the contributions of the i, p, ν, and νp processes are minor and thus are not readily apparent in the figure. The focus of this review is on the r process and an understanding of how the corresponding isotopes were synthesized in nature.

Over the years there have been a number of comprehensive reviews on this topic [for a selected list see Hillebrandt (1978), Cowan, Thielemann, and Truran (1991), Arnould, Goriely, and Takahashi (2007), Qian and Wasserburg (2007), Sneden, Cowan, and Gallino (2008), Thielemann *et al.* (2011), Thielemann, Eichler, Panov, Pignatrari, and Wehmeyer (2017), Thielemann, Eichler, Panov, and Wehmeyer (2017), and references therein], as well as recent parallel efforts (Horowitz *et al.*, 2019; Kajino *et al.*, 2019). To get clues on the r-process origin, a wide range of subtopics need to be addressed: (1) nuclear physics input to understand the nucleosynthesis path far from stability, (2) nucleosynthesis modeling to find out conditions for neutron densities and temperatures that can reproduce the r-process abundances found in nature, (3) determining whether proposed astrophysical sites can match such conditions, (4) observations of stellar abundances throughout galactic history to find out

which of these sites can contribute during which period of galactic evolution, (5) to do so with good precision a detailed study of the atomic physics is required for identifying the strengths of absorption lines needed to determine abundances, and (6) detections of long-lived radioactive species that can hint toward understanding the frequencies of *r*-process events in the Galaxy. Thus, a number of connected fields, including atomic physics, nuclear physics, stellar spectroscopy, stellar explosion modeling, and galactic chemical evolution are involved in attempting to answer the long-standing problem "How were the elements from iron to uranium made?," one of the *Eleven Science Questions for the New Century* addressed by the National Academy of Sciences in 2003 (National Research Council, 2003). Detailed discussions are given in later sections; here we list a number of considered scenarios.

While there have been many parametric studies in the early days, assuming a set of neutron densities and temperatures (Seeger, Fowler, and Clayton, 1965; Kodama and Takahashi, 1975; Kratz *et al.*, 1986, 1988; 1993; Freiburghaus *et al.*, 1999; Pfeiffer *et al.*, 2001), the long-standing question is, where an *r* process with neutron densities of 10^{26} cm^{-3} and higher, producing highly unstable neutron-rich isotopes of all heavy elements and permitting a fast buildup of the heaviest elements up to the actinides, can take place.

As discussed later with respect to observations, there are indications that a "weak" and a "strong" *r* process occur in nature, and the strong component is probably the dominant one, accounting essentially for Solar System *r*-process abundances. But some old stars, although displaying abundances of *r*-process elements, including Eu, show a strongly declining trend toward heavy elements, and it is not clear whether the third *r*-process peak with $A = 195$ or even the actinides are present. In our review we focus mostly on the strong *r* process but discuss observations and possible sites of the weak *r* process as well. There have been many suggestions relating the site of the strong *r* process to the following:

(1) The innermost ejecta of regular core-collapse supernovae (core-collapse SNe or CCSNe) (Schramm, 1973; Sato, 1974; Hillebrandt, Takahashi, and Kodama, 1976; Hillebrandt, 1978; Takahashi, Witti, and Janka, 1994; Witti, Janka, and Takahashi, 1994; Woosley *et al.*, 1994; Qian and Woosley, 1996; Hoffman, Woosley, and Qian, 1997; Terasawa *et al.*, 2001; Thompson, Burrows, and Meyer, 2001; Wanajo *et al.*, 2001; Qian and Wasserburg, 2007; Farouqi *et al.*, 2010; Roberts, Woosley, and Hoffman, 2010; Martínez-Pinedo *et al.*, 2012; Roberts, Reddy, and Shen, 2012; Arcones and Thielemann, 2013; Mirizzi, 2015). However, despite all remaining uncertainties in the explosion mechanism, recent conclusions are that at most a weak *r* process can occur under these conditions (Wanajo, Janka, and Müller, 2011; Martínez-Pinedo *et al.*, 2012; Roberts, Reddy, and Shen, 2012; Curtis *et al.*, 2019), because weak interactions with electron neutrinos and antineutrinos from the newly formed hot protoneutron star either will make initially neutron-rich matter less neutron rich or even proton rich or, in the case of slightly neutron-rich matter, sufficiently high entropies will not be attained. Another option for a weak *r* process exists in so-called quark deconfinement supernovae, where after the collapse of a massive star, leading to a protoneutron star, a quark-hadron phase transition sets in that causes the subsequent supernova explosion (Fischer *et al.*, 2018; Fischer, Wu *et al.*, 2020).

(2) Outer layers of supernova explosions, e.g., the helium layer where neutrons are created by (α, n) reactions, have also been suggested (Truran, Cowan, and Cameron, 1978; Thielemann, Arnould, and Hillebrandt, 1979, Cowan, Cameron, and Truran, 1980, 1983, 1985; Hillebrandt *et al.*, 1981; Klapdor *et al.*, 1981; Cameron, Cowan, and Truran, 1983; Thielemann, Metzinger, and Klapdor, 1983), and later the collapsing ONeMg core of massive stars was also suggested (Wheeler, Cowan, and Hillebrandt, 1998). The emergence of realistic preexplosion stellar models made this site less likely. Further options include (for low abundances of heavy elements in the early Galaxy) sufficient amounts of neutrons in the He shell, provided via neutrino interactions (Epstein, Colgate, and Haxton, 1988; Nadyozhin and Panov, 2007). But this scenario, with low neutron number densities, would not be able to produce the solar *r*-process pattern with its correct peak locations (Banerjee, Haxton, and Qian, 2011; Qian, 2014; Banerjee *et al.*, 2016).

(3) Special classes of core-collapse events of massive stars with fast rotation and high magnetic fields. They can lead either to highly magnetized neutron stars (magnetars) and neutron-rich jet ejecta [magnetohydrodynamical (MHD) jet supernovae] along the polar axis (Symbalisty, Schramm, and Wilson, 1985; Cameron, 2003; Nishimura *et al.*, 2006, 2017; Winteler *et al.*, 2012; Mösta *et al.*, 2014, 2015, 2018; Nishimura, Takiwaki, and Thielemann, 2015; Halevi and Mösta, 2018; Obergaulinger, Just, and Aloy, 2018) or to black holes (BHs), polar jets, and black hole accretion disk outflows (hypernovae and collapsars). The latter have been attributed to neutron-rich jet ejecta (Fujimoto, Nishimura, and Hashimoto, 2008; Ono *et al.*, 2012) and/or the creation of *r*-process elements in black hole accretion disks (Pruet, Woosley, and Hoffman, 2003; Pruet, Thompson, and Hoffman, 2004; Siegel, Barnes, and Metzger, 2019). The first type of events showed quite some promise for producing *r*-process ejecta, but the necessity that high precollapse magnetic fields exist puts constraints on this scenario. The second option (collapsars) stands for a high-angular-momentum subset of rotating stars that form black holes in combination with long-duration gamma-ray bursts (GRBs). A variant of this based on the spiraling in of a neutron star (NS) via merger with a giant in a binary system (leading eventually to accretion, black hole formation, and a black hole accretion disk) was suggested by Grichener and Soker (2019).

(4) Ejecta from binary NS (or BH-NS) mergers were studied for many years before the first detection of such an event (Lattimer and Schramm, 1974; Symbalisty and Schramm, 1982; Eichler *et al.*, 1989, 2015; Freiburghaus, Rosswog, and Thielemann, 1999; Rosswog *et al.*, 2000; Goriely, Bauswein, and Janka, 2011;

Rosswog *et al.*, 2014; Wanajo *et al.*, 2014; Goriely *et al.*, 2015; Just *et al.*, 2015; Mendoza-Temis *et al.*, 2015; Ramirez-Ruiz *et al.*, 2015; Shibagaki *et al.*, 2016; Wu *et al.*, 2016; Lippuner *et al.*, 2017; Thielemann, Eichler, Panov, and Wehmeyer, 2017). After the gravitational wave detection GW170817 of a neutron-star merger with a combined total mass of about 2.74 $M_\odot$ (Abbott *et al.*, 2017b, 2019), accompanied by a kilonova observation supporting the production of heavy elements [see Metzger (2017b), Tanaka *et al.* (2017), and Villar *et al.* (2017)], this type of event has attracted special attention; see the reviews by Rosswog *et al.* (2018), Horowitz *et al.* (2019), and Shibata and Hotokezaka (2019), and references therein. More recent gravitational wave observations point to further neutron-star mergers (e.g., GW190425, with a combined total mass of ~3.4 $M_\odot$) (B. P. Abbott *et al.*, 2020), or even neutron-star–black hole mergers, e.g., GW190426 and GW190814, with a combined total mass in excess of 7 and 25 $M_\odot$ (Lattimer, 2019; R. Abbott *et al.*, 2020a; R. Abbott *et al.*, 2020b). The three last mentioned events had no observed electromagnetic counterpart, due to either nonexistence or nondetection, with the latter related to a large distance and/or missing precise directions (Ackley *et al.*, 2020; Barbieri *et al.*, 2020; Foley *et al.*, 2020; Kyutoku *et al.*, 2020). Whether the smaller 2.6 $M_\odot$ binary member in GW190814 is actually a massive neutron star or an extremely small black hole is still under debate (Godzieba, Radice, and Bernuzzi, 2020).

Most of the previously mentioned astrophysical sites involve ejection of material from high densities and a neutron star or black hole produced during core collapse or a compact binary merger. Hence the high density equation of state that ultimately determines the transition from a neutron star to a black hole plays an important role in the modeling of these objects. We do not discuss this topic further here but refer the interested reader to reviews on the nuclear equation of state (Lattimer, 2012; Hebeler *et al.*, 2015; Özel and Freire, 2016; Oertel *et al.*, 2017; Bauswein and Stergioulas, 2019; Tews, Margueron, and Reddy, 2019).

Before we discuss the *r*-process astrophysical sources in detail, a lot of groundwork has to be laid out. Section II provides an overview of observations (including the atomic physics for their correct interpretation), while Sec. VII discusses the physics relevant for the description of *r*-process electromagnetic transients, Sec. III addresses the basic working of an *r* process and which conditions are needed for its successful operation, Secs. IV and V discuss the impact played by nuclear physics (with experimental and theoretical investigations), and Sec. VI passes through the astrophysical sites that can fulfill the required conditions. Section VIII combines these astrophysical sites and shows how their role in galactic evolution connects with Sec. II. Finally in the summary (Sec. IX), after having presented all possible connections, we discuss the remaining issues and open questions, i.e., whether a single *r*-process site has been identified by now or whether we still might need several sources to explain observations throughout galactic evolution.

II. OBSERVATIONS

A. Stellar abundances of neutron-capture elements in metal-poor stars

Stellar abundance observations over decades have provided fresh evidence about the nature and extent of heavy element nucleosynthesis. In the case of the *s* process there is direct observational evidence of *in situ* stellar nucleosynthesis with the observation of the radioactive element Tc, first discovered by Merrill (1952). Additional stellar abundance studies have strongly linked this type of nucleosynthesis to evolved He shell-burning asymptotic giant branch stars (Busso, Gallino, and Wasserburg, 1999; Käppeler *et al.*, 2011; Karakas and Lattanzio, 2014). There is no similar example for the *r* process, related to nucleosynthesis during stellar evolution, as it requires extensive neutron fluxes obtainable only in explosive events. Some elements are formed exclusively or almost so only in the *r* process, such as Eu, Os, Ir, Pt, Th, and U. Their presence in old galactic very metal-poor (VMP) halo stars is a clear indication that this process occurred in violent astrophysical sites early in the history of the Galaxy; see Sneden, Cowan, and Gallino (2008) and Thielemann, Eichler, Panov, and Wehmeyer (2017), and references therein.

Identification of *r*-process-rich stars began with the discovery of overabundances of neutron-capture elements in the field red giant HD 115444 (Griffin *et al.*, 1982). This was followed by the identification of an *r*-process pattern in the well-known bright giant HD 122563, even though its overall neutron-capture element level is depressed relative to Fe (Sneden and Parthasarathy, 1983; Honda *et al.*, 2006). An initial abundance survey in metal-poor (MP) stars (Gilroy *et al.*, 1988) considered 20 red giants, finding a common and easily spotted pattern of increasing overabundances from Ba ($Z = 56$) to Eu ($Z = 63$) among the rare-earth elements. With better echelle spectrographic data came discoveries of many more *r*-process-rich stars, leading Beers and Christlieb (2005) to subclassify them as "*r* I" with $0.3 \leq [\mathrm{Eu/Fe}] \leq +1.0$ and $[\mathrm{Ba/Eu}] < 0$, and as "*r* II" with $[\mathrm{Eu/Fe}] > +1.0$ and $[\mathrm{Ba/Eu}] < 0$.

The most detailed deconvolution of abundances into nucleosynthetic contributions exists for the Solar System, as we have accurate abundances down to the isotopic level as a result of meteoritic and solar atmospheric measurements (Cameron, 1959; Asplund *et al.*, 2009; Lodders, Palme, and Gail, 2009); see Fig. 1. Identifying the *r*-process contributions to the Solar System neutron-capture abundances is usually accomplished by first determining the *s*-process fractions (Arlandini *et al.*, 1999; Käppeler, 1999; Burris *et al.*, 2000; Käppeler *et al.*, 2011). The remaining (residual) amount of the total elemental abundance is assumed to be the solar *r*-process contribution; see Figs. 1 and 2. Aside from the so-called *p* process (Arnould and Goriely, 2003; Rauscher *et al.*, 2013; Nishimura *et al.*, 2018), which accounts for the minor heavy element isotopes on the proton-rich side of the valley of instability, as well as the ν process (Woosley *et al.*, 1990) and the νp process (Fröhlich, Martínez-Pinedo *et al.*, 2006), only the *s* and *r* processes are needed to explain nearly all of the solar heavy element abundances.

Early observations of CS 22892-052 (Sneden *et al.*, 1994, 2003) and later CS 31082-001 [see Hill *et al.* (2002), Siqueira

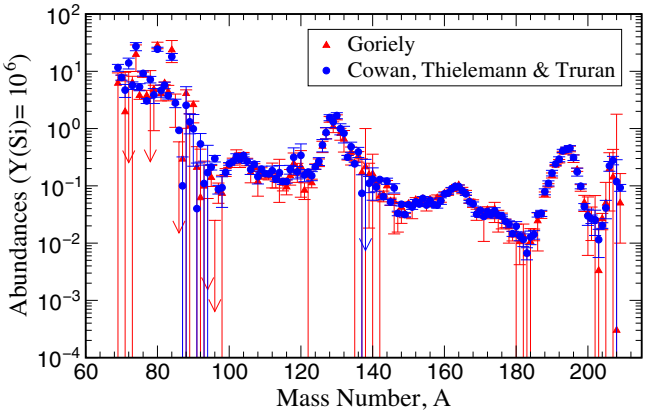

FIG. 2. Solar *r*-process abundances as determined by Cowan, Thielemann, and Truran (1991) and Goriely (1999). The largest uncertainties are clearly visible for $A \lesssim 100$ (weak *s*-process region) and around lead.

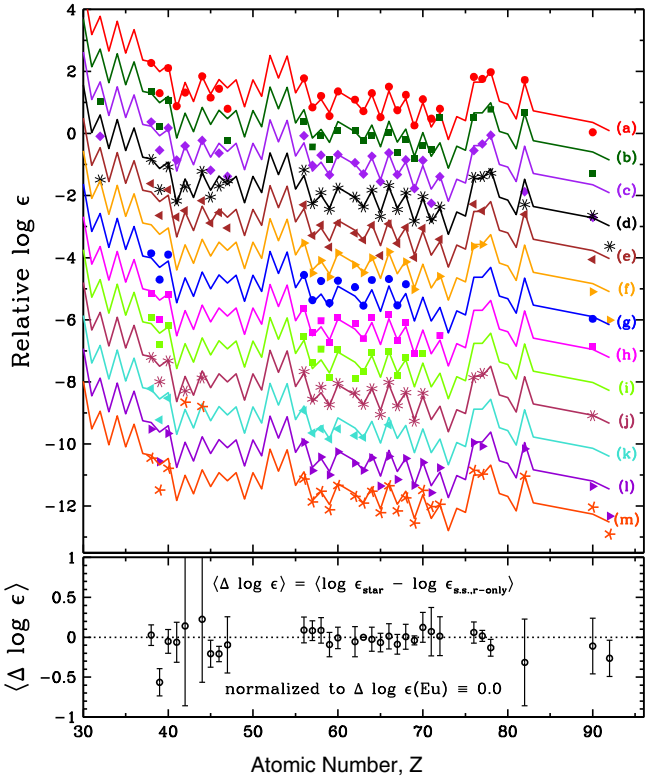

FIG. 3. Top panel: neutron-capture abundances in 13 *r*-II stars (points) and the scaled Solar System *r*-process-only abundances of Siqueira *et al.* (2013), adapted mostly from Simmerer *et al.* (2004). The stellar and Solar System distributions were normalized to agree for the element Eu ($Z = 63$), and vertical shifts were then applied in each case for plotting clarity. The stellar abundance sets are (a) CS 22892-052 (Sneden and Cowan, 2003), (b) HD 115444 (Westin *et al.*, 2000), (c) BD + 17 3248 (Cowan *et al.*, 2002), (d) CS 31082-001 (Siqueira *et al.*, 2013), (e) HD 221170 (Ivans *et al.*, 2006), (f) HD 1523 + 0157 (Frebel *et al.*, 2007), (g) CS 29491-069 (Hayek *et al.*, 2009), (h) HD 1219-0312 (Hayek *et al.*, 2009), (i) CS 22953-003 (François *et al.*, 2007), (j) HD 2252-4225 (Mashonkina, Christlieb, and Eriksson, 2014), (k) LAMOST J110901.22 + 075441.8 (Li *et al.*, 2015), (l) RAVE J203843.2-002333 (Placco *et al.*, 2017), and (m) 2MASS J09544277 + 5246414 (Holmbeck *et al.*, 2018). Bottom panel: mean abundance differences for the 13 stars with respect to the Solar System *r*-process values.

[Eu/Ba] $> +0.3$) can be seen even in MP stars with bulk deficiencies in neutron-capture elements. In Fig. 4 we show differences in abundances between stellar observations and those of the Solar System attributed only to the *r* process. Figure 4 is similar in structure to those followed by Honda *et al.* (2007) and Roederer, Cowan *et al.* (2010). As defined in the figure, if $\Delta \log \epsilon = 0$, then the stellar neutron-capture abundance set is identical to the Solar System *r*-process-only distribution. This is the case for elements in the atomic number range $Z = 57$–78 such as

[Eu/Ba] $> +0.3$) can be seen even in MP stars with bulk deficiencies in neutron-capture elements. In Fig. 4 we show differences in abundances between stellar observations and those of the Solar System attributed only to the *r* process. Figure 4 is similar in structure to those followed by Honda *et al.* (2007) and Roederer, Cowan *et al.* (2010). As defined in the figure, if $\Delta \log \epsilon = 0$, then the stellar neutron-capture abundance set is identical to the Solar System *r*-process-only distribution. This is the case for elements in the atomic number range $Z = 57$–78 such as

et al. (2013), and references therein], indicated a "purely" or "complete" Solar System *r*-process abundance pattern; see Fig. 3. The total abundances of these mostly rare-earth elements in the stars were smaller than in the Sun but with the same relative proportions, i.e., scaled. This indicated that these stars, which likely formed early in the history of the Galaxy, had already experienced pollution from a robust *r* process.

However, the growing literature on abundance analyses of VMP stars has added to our knowledge of the average *r*-process pattern and has served to highlight departures from that pattern. Additions to the observational results since the review by Sneden, Cowan, and Gallino (2008) include Roederer, Sneden *et al.* (2010), Roederer, Schatz *et al.* (2014), Li *et al.* (2015), Roederer *et al.* (2016), Aoki *et al.* (2017), Roederer (2017), Yong *et al.* (2017), Hansen *et al.* (2018), Roederer, Hattori, and Valluri (2018), Sakari *et al.* (2018), and Ezzeddine *et al.* (2020). Additional observations from Travaglio *et al.* (2004), Cowan *et al.* (2005), Hansen and Primas (2011), Hansen *et al.* (2012), Aoki *et al.* (2013), Ural *et al.* (2015), and Wu *et al.* (2016) showed that there is a complex relationship between light and heavy neutron-capture elements. In particular it has been found in some stars that there is significant observed star-to-star abundance scatter of lighter neutron-capture elements ($Z \leq 50$), the opposite of heavier ones ($Z \geq 56$), as shown in Fig. 3. For heavy neutron-capture elements, particularly among the well-studied rare-earth elements, an *r*-process origin does not always mean perfect agreement with the solar *r*-process pattern. So-called truncated (or incomplete or limited) *r*-process stars have been identified with sharp abundance falloffs toward the heavy end of the rare-earth elements (Honda *et al.*, 2006, 2007; Roederer, Cowan *et al.*, 2010; Boyd *et al.*, 2012). These observed abundance patterns can be described as having a range of *r*-process "completeness," with some stars showing only partial agreement. The differences in these abundance patterns have led to a flurry of stellar models and calculations to identify a site or sites for the *r* process, and to determine why stars show differences in these heavy element patterns. In addition to the suggested operation of a weak *r* process, two further processes have gained currency: the so-called lighter element primary process (LEPP) of still unknown origin (Travaglio *et al.*, 2004), and the *i* process; see Cowan and Rose (1977), as well as Denissenkov *et al.* (2017) and references therein. While the LEPP and the *i* process may explain certain individual stellar abundances, their contributions to the total Solar System (s.s.) abundances appear to be small.

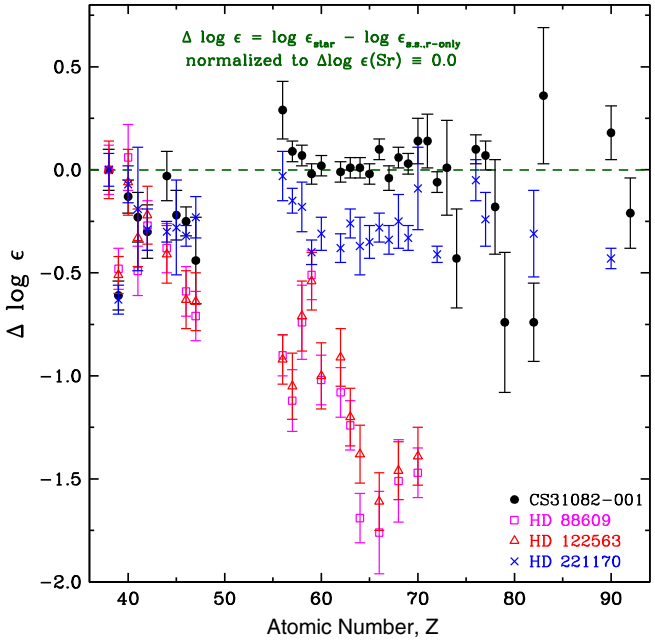

FIG. 4. Differences between stellar and *r*-process-only Solar System (s.s.) abundances for four VMP stars with *r*-process abundance mixes, modeled after Fig. 5 given by Honda *et al.* (2007) and Fig. 11 given by Roederer, Sneden *et al.* (2010). The "s.s., *r*-only" abundances are those given by Siqueira *et al.* (2013), mostly from Simmerer *et al.* (2004). The stellar abundance sets are CS31082-001 (Siqueira *et al.*, 2013), HD 88609 (Honda *et al.*, 2007), HD 122563 (Honda *et al.*, 2006), and HD 221170 (Ivans *et al.*, 2006).

La–Pt in CS31082-001 (Siqueira *et al.*, 2013). All extremely *r*-process-rich stars (classified as "*r* II": [Eu/Fe] $> +1$) have similar abundance runs in the heavy neutron-capture elements, as previously discussed. However, many MP stars with a clear dominance of the *r* process, as defined by [Eu/Ba] $> +0.3$, have abrupt dropoffs in abundance through the rare-earth domain. The most dramatic examples are the truncated *r*-process stars shown in Fig. 4: HD 122563 (Honda *et al.*, 2006) and HD 88609 (Honda *et al.*, 2007). Intermediate cases are abundant, as shown by Roederer, Sneden *et al.* (2010).

To understand the types and nature of the nucleosynthesis, and to identify the stellar sites and the identities of the first stars in our Galaxy, demands highly precise stellar abundance observations. Those require both high-resolution spectrographic measurements and accurate atomic data. Thus, the discovery of MP stars renewed efforts to improve atomic data for many heavy (beyond the Fe-group) neutron-capture elements (Sneden *et al.*, 2009), as discussed in Sec. II.B.

B. Atomic data for the analysis of neutron-capture elements in metal-poor stars

Despite the need for improved transition probabilities, the identification of lines from neutron-capture elements in stellar spectra has been possible for most elements using readily available laboratory data from about the middle of the 20th century. Wavelengths of spectral lines of such elements were measured during the first half of the 20th century using large grating spectrographs such as 10 m Rowland circle instruments. These early wavelength measurements often achieved 1 part per million (ppm) accuracy and were compiled in the well-known atomic energy level series by Moore (1971) and for the rare-earth elements by Martin, Zalubas, and Hagan (1978). The latter included more data from Fourier transform spectrometers (FTSs) and thus achieved $\simeq$0.01 ppm or 10 ppb accuracy in many cases. All of these spectroscopic data are now available online.[1] Although modern optical frequency comb lasers could add many additional digits to energy levels, this technology has not yet been widely applied because of the difficulty in simultaneously using it on large numbers of spectral lines.

The situation with respect to transition probabilities changed with the development of tunable dye lasers originally by Sorokin and Lankard (1966) in the United States and Schäfer, Schmidt, and Volze (1966) in Germany. Although it took some time to thoroughly control dye laser performance, many research groups had organic dye lasers with broad tunability, narrow bandwidths (comparable to or less than Doppler widths), short (few nanosecond) pulse durations, and repetition rates in the tens of hertz. Nonlinear techniques, using crystals and/or gas cells, are needed to access IR and UV wavelengths, and those were also becoming increasingly available. The remaining challenge is to make free atoms and ions of various elements in the periodic table in an optically thin sample with a low collision rate. There are several methods, including sputtering metal cathodes, in a low pressure gas cell (Hannaford and Lowe, 1981), laser-driven plasma sources (Svanberg *et al.*, 1994), and the hollow cathode atom–ion-beam source (Duquette, Salih, and Lawler, 1981; Salih and Lawler, 1983). The broadly tunable organic dye lasers, in combination with a technique to make low pressure samples of metal atoms and ions, opened the possibility of using time-resolved laser-induced-fluorescence (TRLIF) to measure accurate and precise (about a few percent) radiative lifetimes of upper levels on interest in atoms and ions. These lifetimes provide an accurate and precise total decay rate for transition probabilities from the selected upper level.

Emission branching fractions (BFs) in rich spectra still represented a challenge. The same visible and UV capable FTS instruments (Brault, 1976), used to improve energy levels, became the "workhorse" of efforts on BFs in complex spectra. Reference Ar I and II lines became internal standards for many laboratory spectra from hollow cathode lamps recorded using FTS instruments; see Whaling, Carle, and Pitt (1993) and references therein. The advantages of interferometric instruments such as the 1 m FTS of the National Solar Observatory on Kitt Peak, Arizona, were critical for BF measurements in complex spectra. This instrument has a large etendue common to all interferometric spectrometers, wave number accuracy to 1 part in 10^8, a limit of resolution as small as 0.01 cm^{-1}, broad spectral coverage from the UV to the IR, and the capability of recording a million point spectrum in minutes (Brault, 1976). Hollow cathode lamps that yield emission spectra for neutral and singly ionized atoms are available for essentially the entire periodic table.

[1]See http://physics.nist.gov/asd.

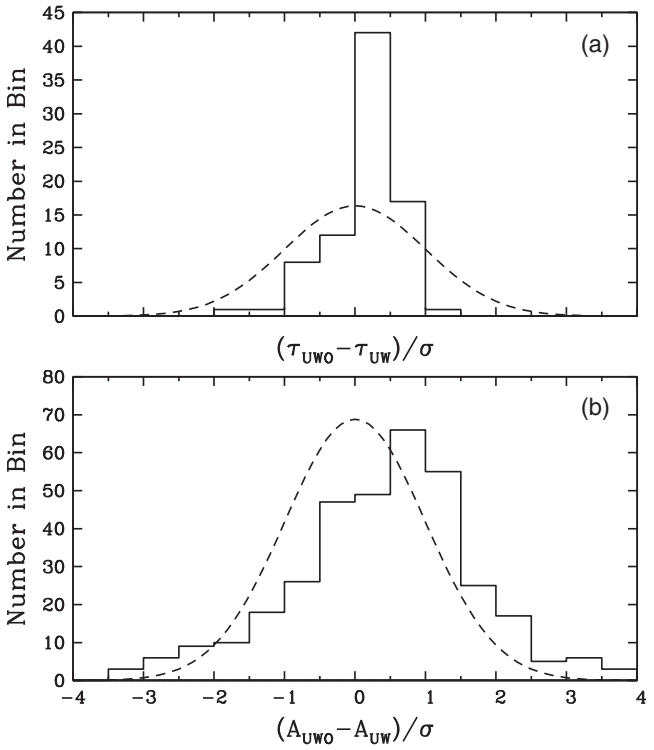

FIG. 5. Comparisons of laboratory data on Sm II from University of Western Ontario (UWO) and University of Wisconsin (UW) groups. (a) Histogram of differences in lifetimes (τ divided by their uncertainties added in quadrature), along with a dashed line representing a 1 standard deviation Gaussian. (b) Similar histogram and Gaussian representation for transition probabilities (A values). Adapted from Lawler *et al.*, 2008.

Interest in rare-earth elements is a natural part of the study of neutron-capture elements in MP stars. Atoms and ions with open f shells have many transitions in the optical spectrum; see Sec. VII for their relevance in kilonova light curves. Rare-earth elements have important applications in general lighting and in optoelectronics because of their rich visible spectra. Rare-earth elements in MP stars are convenient for spectroscopic studies in the optical region accessible to ground-based telescopes. Europium is a nearly pure r-process element and lanthanum is a nearly pure s-process element in Solar System material. Although none of the r-process peaks are in the rare-earth row, the accessibility from the ground is a major advantage for rare-earth elements.

Rare-earth elements tend to be singly ionized in the photospheres of F, G, and K stars of interest for many elemental abundance studies. The spectrum of singly ionized samarium (Sm II) has received special attention (Lawler *et al.*, 2006; Rehse *et al.*, 2006). Lawler *et al.* (2008) completed comparisons from the two sets of measurements. Figure 5 shows a histogram of lifetime measurement differences between the two studies with a 1 standard deviation Gaussian superposed, as well as a similar histogram comparison for Einstein A coefficients that include BFs. These histograms indicate that radiative lifetime uncertainties are overly conservative and that BF uncertainties are satisfactory but perhaps slightly too optimistic in at least one of the two sets of measurements.

Uncertainties in radiative lifetimes from TRLIF experiments have proven to be easier to minimize than uncertainties in emission BFs. Various techniques can conveniently be used to check for optical depth (vary the atom–ion-beam intensity), to check for collisional effects (throttle a vacuum pump), and to eliminate errors from Zeeman quantum beats (zero the magnetic field in the experimental region for short lifetimes and introduce a high, 30 G, magnetic field for long lifetimes). Benchmark lifetimes in simple spectra such as He I, Be I, Be II, and Mg II, which are well known from accurate theory, can be periodically remeasured as an end-to-end test of the TRLIF experiment (Den Hartog, Wickliffe, and Lawler, 2002). There are multiple challenges in BF measurements. It is essential to have a reliable relative radiometric calibration and a source that is optically thin for strong lines of interest. One must resolve lines of interest from nearby blending partners and line identifications must be correct. The last two constraints are most easily achieved using FTS instruments due to their exceptional resolving power and absolute wave number accuracy and precision. Weak lines from an upper level of interest are most vulnerable to blending, poor signal-to-noise ratios, and other problems. Uncertainty migrates to weak lines because BFs from an upper level of interest sum to unity by definition.

Elements with wide hyperfine structure and/or a wide range of isotopes require some additional effort, but in most cases the needed hyperfine splitting (hfs) data can be extracted from FTS spectra. The existence of even a few pieces of hfs data from single frequency laser measurements is helpful since such data can serve to constrain nonlinear least square fitting of partially resolved hfs patterns in FTS data. Laboratory transition probability measurements on rare-earth ions were summarized during a study of Ce II by Lawler *et al.* (2009) and were applied to five r-process-rich VMP stars in a companion paper by Sneden *et al.* (2009). The most striking conclusion from the decade-long rare-earth study is that the relative r-process abundance pattern is stable over time and space. Third r-process peak elements, including Os, Ir, and Pt, were observed in MP stars by Cowan *et al.* (2005). Some useful lines of Os I and Ir I are accessible to ground-based studies. Lines suitable for abundance studies of many lighter neutron-capture elements are not accessible via ground-based observation. Elements near the first r-process peak such as As and Se have their valence electrons in nearly closed p shells. The large gap between the ground and first resonance levels exists in both the neutral and ion energy level structure, although the neutral atom population is dominant in most stars of interest for both of these elements. A similar problem arises for Te at the second r-process peak with only deep UV lines. Hubble Space Telescope (HST) time was allocated for a study of Te I lines in multiple MP stars (Roederer *et al.*, 2012). The success of the Te study inspired a careful search through the HST archives for one or more stars with sufficiently deep UV spectral coverage for observations on all three r-process peaks (Roederer and Lawler, 2012). The star HD 160617 is likely the only such star with sufficiently deep UV spectral coverage. Laboratory datasets for many of the lighter r-process elements are included. Laboratory datasets for many of the lighter r-process elements could be improved, but a successor telescope to HST with a high-resolution spectrograph and UV capability will be needed to exploit improvements in the laboratory data.

The discovery of a single line of U II in a MP star (complicated by being located on the shoulders of a much

stronger Fe I line) by Cayrel *et al.* (2001) was a milestone in stellar spectroscopy. Despite this complication, there is some confidence in its identification. Thorium is also an element of choice for stellar chronometry (Sneden *et al.*, 2003).

C. Abundance trends in galactic and extragalactic stars

As discussed in Sec. II.A, the galactic MP stars show indications of neutron-capture abundances; in fact, it appears as if all such stars (to an observational limit) exhibit some level of neutron-capture abundances. In addition, observations have indicated the presence of elements such as Ba in nearby dwarf spheroidal galaxies (Shetrone, Bolte, and Stetson, 1998; Shetrone *et al.*, 2003; Venn *et al.*, 2003; Skúladóttir *et al.*, 2019). Recently there has been evidence of these elements in ultrafaint dwarf (UFD) galaxies, structures of only about 10^4 $M_\odot$ and possibly also that they may be the building blocks and substructures of the early Galaxy (Brauer *et al.*, 2019). To date more than ten UFDs have been discovered around our Galaxy, metal poor with metallicities of [Fe/H] ≈ -3 (Kirby *et al.*, 2013; Frebel and Norris, 2015; Ji *et al.*, 2019; Simon, 2019), and most of them show low *r*-process enhancements. However, one of them (Reticulum II) shows highly *r*-process-enhanced stars that are comparable to galactic *r*-process-rich stars such as CS 22892-052 (Roederer, 2013, 2017; Ji *et al.*, 2016; Ji and Frebel, 2018), which seems to trace back to one early *r*-process event. In addition to Reticulum II, a further dwarf galaxy Tucana III was recently observed and also shows *r*-process features (Hansen *et al.*, 2017; Marshall *et al.*, 2019).

We show in Fig. 6 [see Roederer (2013) and references therein] a compilation of abundances in both galactic and extragalactic stars. In these observations the Sr abundance acts as a surrogate for the overall metallicity of these stars and Ba indicates the enrichment of neutron-capture elements. The figure illustrates that stars down to the lowest metallicities contain Sr and/or Ba. In a solar mix these are predominantly *s*-process elements; i.e., their *s*-process isotopes dominate in present solar abundances. If massive stars with fast rotation rates had already contributed some *s*-process in early galactic evolution (Frischknecht *et al.*, 2016), this could be due to such *s*-process sources. However, global trends in which observed elemental or isotopic ratios can be deconvolved into *s*- and *r*-process contributions show an *s*-process appearance only in later periods of galactic evolution. Thus, this compilation strongly suggests that all of these stars have been enriched in *r*-process material, which also has implications for early nucleosynthesis in galaxies.

Clues about early galactic nucleosynthesis are also found through a comparison of elements with different nucleosynthesic origins. We show one such comparison in Fig. 7, observed in halo stars, i.e., containing elements synthesized prior to the formation of these stars. It is evident that alpha elements such as Mg appear early in galactic evolution at low metallicities, originating from fast evolving massive stars and core-collapse supernovae as their final end points. Such events occur with a high frequency during galactic evolution and show little scatter. Common *r*-process elements like Eu, however, display an extensive scatter. These observations, combined with those from ultrafaint dwarf galaxies, indicate that the heavy *r*-process elements are made in rare events that contribute significant amounts of material, when they occur; see Fig. 7. Such abundance comparisons can be used to put constraints on the site or sites for the *r* process in terms of (a) ejecta composition, (b) amount of *r*-process ejecta, and

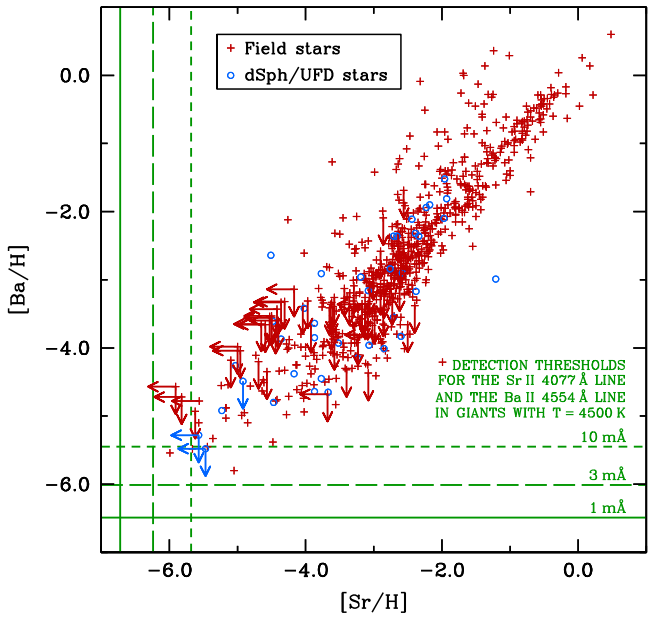

FIG. 6. Abundances of [Sr/Fe] vs [Ba/Fe] in a large number of galactic and extragalactic stars. From Roederer, 2013.

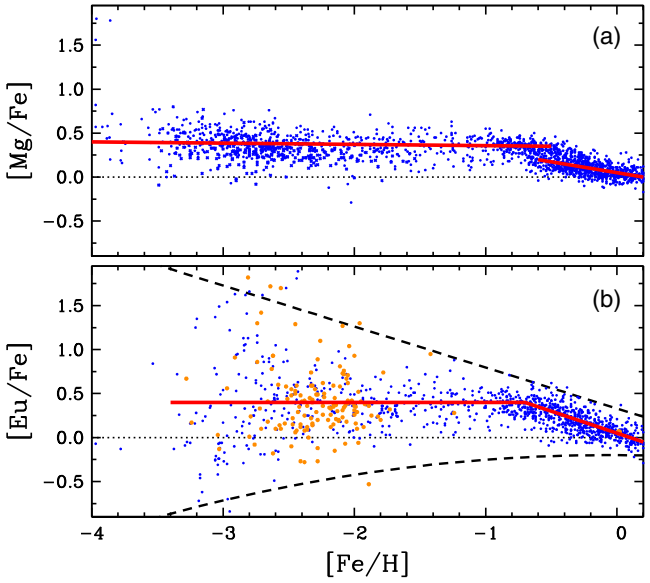

FIG. 7. Abundances as a function of metallicity for (a) [Mg/Fe]and (b) [Eu/Fe]. Red solid lines are approximate fits to the averages of halo, thick disk, and thin disk stars. Black dashed lines in (b) highlight the growing star-to-star scatter in [Eu/Fe] with decreasing metallicity. Individual data points were taken from Fulbright (2000), Hill *et al.* (2002), Reddy *et al.* (2003), Cayrel *et al.* (2004), Cohen *et al.* (2004), Simmerer *et al.* (2004), Barklem *et al.* (2005), Reddy, Lambert, and Allende Prieto (2006), François *et al.* (2007), Bensby, Feltzing, and Oey (2014), Roederer, Schatz *et al.* (2014), and Battistini and Bensby (2016). Adapted from Sneden, Cowan, and Gallino, 2008.

(c) their mixing with the extended interstellar medium in order to understand the history of element formation in the Galaxy (i.e., galactic chemical evolution). With respect to (a) Ji, Drout, and Hansen (2019) analyzed extended sets of low-metallicity observations with $[Fe/H] < -2.5$ (attempting to select stars being polluted only by single events) and $[Eu/Ba] > 0.4$ (to ensure a pure *r*-process origin avoiding *s*-process contributions) with the aim of finding the typical lanthanide plus actinide fraction X_{La} among the global *r*-process element distribution. This permits one, on the one hand, to look for variations among old stars, indicating apparently a different result for the bulk of low-metallicity stars with $\log X_{La} \approx -1.8$, while the most *r*-process enriched stars with $[Eu/Fe] > 0.7$ have $\log X_{La} > -1.5$. This measure will also permit comparisons to future kilonova events if observations allow one to determine this quantity; see Sec. VII. With respect to (b) and (c) of the previous list we return to galactic evolution issues in Sec. VIII after having presented the nucleosynthesis yields of different astrophysical sites.

The eventual demise of the Hubble Space Telescope, which is able to obtain high-quality UV observations, will hamper future progress in the observation of heavy elements in low-metallicity stars. The James Webb Space Telescope, the scientific "successor" of HST, will have no UV capability but an IR capability. Identification of neutron-capture element lines in the IR region could provide new avenues for understanding the operation and nature of the *r* process; see Sec. II.B.

D. The role of long-lived radioactive species

Identification and detailed spectroscopic analysis of a handful of *r*-II stars, including CS 22892-052 (Sneden *et al.*, 1994, 2003), CS 31082-001 [see Hill *et al.* (2002), Siqueira *et al.* (2013), and references therein], and HE 1523-0901 (Frebel *et al.*, 2007), brought forth detections of the long-lived heavy neutron-capture radioactive elements Th ($t_{1/2} = 13.0$ Gyr) and U ($t_{1/2} = 4.6$ Gyr), which can be made only in the *r* process, and in addition neutron-capture element abundances ranging from $Z \approx 30$ to 92, indicating also an *r*-process pattern. This makes detailed comparisons possible between observations and *r*-process theory. More Th detections have been made since then, and more recently U has also been detected in some halo stars. Because of its shorter half-life, its abundance is inherently smaller and detections are difficult. Shown in Fig. 8 is a uranium detection in 2MASS J09544277 + 5246414, the most actinide-enhanced *r*-II star known.

These Th and U discoveries led to cosmochronology estimates, independent of a cosmological model, based solely on decay half-lives of involved isotopes. This method requires, however, Th/U ratios from theoretical *r*-process predictions (geared to fit a solar *r*-process pattern) plus the observed abundance ratios. It has enabled estimates on the decay time since the birth of a star (when the addition of new material from nucleosynthesis sites stopped) and promising results have been obtained (Cowan, Thielemann, and Truran, 1991; Cowan *et al.*, 1999; Kratz, Möller *et al.*, 2000; Schatz *et al.*, 2002; Hill *et al.*, 2017). The same can in principle also

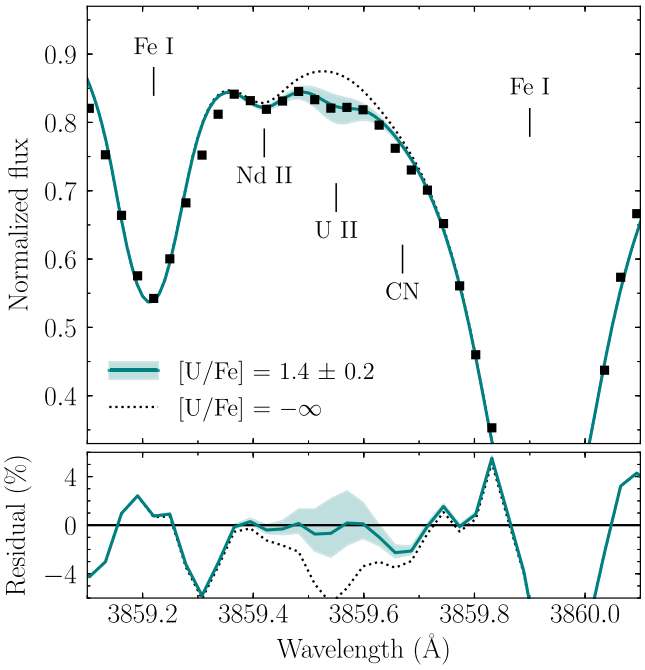

FIG. 8. Synthesis and derived abundance for U in the star 2MASS J09544277 + 5246414. From Holmbeck *et al.*, 2018.

be done by utilizing the Th/Eu ratio for some stars, yielding values in concordance with cosmological age estimates (as previously mentioned). The fact that some stars seem to have experienced an "actinide boost," i.e., an enhanced amount of Th and U relative to lighter *r*-process elements, could point to a nonuniversal *r*-process production pattern and possibly varying *r*-process compositions from different productions sites. This made the [Th/Eu]chronology uncertain or non-reliable for such stars (Cayrel *et al.*, 2001; Honda *et al.*, 2004), as they had experienced a nonsolar *r*-process contribution, while [U/Th]did not show these anomalies (Mashonkina, Christlieb, and Eriksson, 2014). Such an actinide boost is found mostly in stars with metallicities $[Fe/H] \approx -3$. This indicates that (a) an *r* process was already contributing to early galactic evolution, but also (b) with possibly varying conditions for producing the heaviest elements, which are dependent on the *r*-process site. It has proved difficult to obtain U detections in many stars and it remains to be seen how such actinide boosts are distributed as a function of metallicity; see Fig. 9.

In addition to observations of long-lived radioactive species seen via the spectra of stars throughout galactic evolution, there have also been detections in deep-sea sediment, indicating more recent additions of these elements to Earth. While the discussion in Sec. II.C points to rare strong *r*-process events in the early Galaxy, the latter detections suggest the same in recent history. Long-lived radioactive species can act as a witness of recent additions to the Solar System that are dependent on their half-lives. Davis and McKeegan (2014) gave a review on the signature of radioactive isotopes alive in the early Solar System. Two specific isotopes have been utilized in recent years to measure such activities in deep-sea sediment. One of them (^{60}Fe) has a half-life of 2.6×10^6 yr and can indicate recent additions from events occurring up to

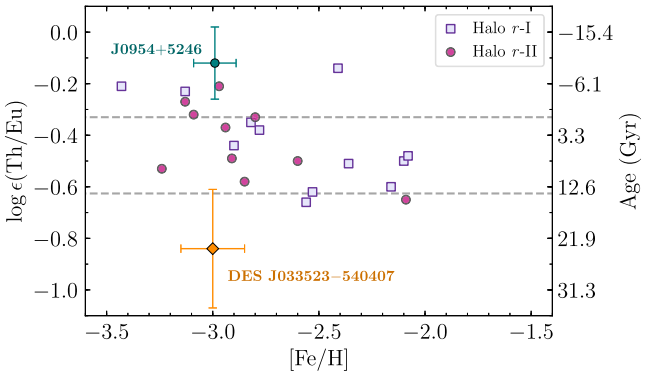

FIG. 9. Th/Eu ratios for stars with detected thorium abundances. One can see that at low metallicities around $[Fe/H] \approx -3$ a number of so-called actinide-boost stars can be found. If utilizing initial *r*-process production ratios that fit solar *r* abundances (Schatz *et al.*, 2002), unreasonable, and even negative, ages of these stars are obtained, which is not at all consistent with their metallicity, which points to the formation of these stars in the early Galaxy. From Holmbeck *et al.*, 2018.

several million years ago. ^{60}Fe is produced during the evolution and explosion of massive stars, leading to supernovae (Thielemann, Hirschi *et al.*, 2011; Wanajo, Janka, and Müller, 2013; Limongi and Chieffi, 2018; Thielemann *et al.*, 2018). It is found in deep-sea sediment that incorporated stellar debris from a nearby explosion about 2×10^6 yr ago (Knie *et al.*, 2004; Ludwig *et al.*, 2016; Wallner *et al.*, 2016; Sørensen, Svensmark, and Gråe Jørgensen, 2017). Such a contribution is consistent with a supernova origin and related occurrence frequencies from witnessing the last nearby event. Another isotope utilized ^{244}Pu has a half-life of 8.1×10^7 yr and would contain a collection from quite a number of contributing events. If the strong *r*-process would take place in every core-collapse supernova from massive stars, about 10^{-4}–10^{-5} $M_\odot$ of *r*-process matter would need to be ejected per event to explain the present day solar abundances (see Fig. 39). The recent ^{244}Pu detection (Wallner *et al.*, 2015) is lower than expected from such predictions by 2 orders of magnitude, suggesting that considerable actinide nucleosynthesis is rare (permitting substantial decay since the last nearby event). This indicates that regular core-collapse supernovae did not contribute significantly to the strong *r* process in the solar neighborhood for the past few hundred million years, but it does not exclude a weak *r*-process contribution with minor Eu production (Fields *et al.*, 2019; Wallner *et al.*, 2019). Thus, in addition to the inherent problems of regular core-collapse supernova models (discussed in later sections) to provide conditions required for a strong *r* process (also producing the actinides in solar *r*-process proportions), these observational constraints from nearby events also challenge them as the source of main *r*-process contributions. A recent study of the origin of the strong *r* process with continuous accretion of interstellar dust grains into the inner Solar System (Hotokezaka, Piran, and Paul, 2015) concluded that the experimental findings (Wallner *et al.*, 2015) are in agreement with an *r*-process origin from a rare event. This can explain the ^{244}Pu existing initially in the early Solar System as well as the low level of more recent additions witnessed in deep-sea sediment over the past few hundred million years.

E. Kilonova observations

For many years a connection between observations of short-duration gamma-ray bursts (sGRBs), supernovalike electromagnetic transients (macronovae to kilonovae), and compact binary mergers has been postulated (Piran, 2005). The first observational evidence of an excess of near-infrared emission over the standard GRB afterglow came in 2013 with the observation of GRB 130603B by Tanvir *et al.* (2013)[2] and suggested a thermal component consistent with kilonova emissions. Further, evidence has been obtained from a reanalysis of the GRB 060614 (Yang *et al.*, 2015), GRB 050709 (Jin *et al.*, 2016), and GRB 070809 (Jin *et al.*, 2020) afterglow data, including a first estimate of the kilonova emission temperature (Jin *et al.*, 2015); see Gompertz *et al.* (2018) for a review of kilonova candidates associated with short GRB observations.

Following Li and Paczyński (1998), the first predictions of light curves powered by radioactive decay were done by Metzger, Martínez-Pinedo *et al.* (2010), Goriely, Bauswein, and Janka (2011), and Roberts *et al.* (2011). These initial studies used gray opacities appropriate to the Fe-rich ejecta in type Ia supernovae (SNe Ia) and predicted peak luminosities at timescales of a day in the blue. However, the opacity of heavy *r*-process elements is substantially higher due to the high density of line transitions associated with the complex atomic structure of lanthanides and actinides. This led to a light curve peak at timescales of a week in the red or near infrared (Barnes and Kasen, 2013; Kasen, Badnell, and Barnes, 2013; Tanaka and Hotokezaka, 2013). Metzger *et al.* (2015) speculated about the possibility that in fast expanding ejecta unburned neutrons are left and led via their decay to a ultraviolet or blue precursor event. Early blue emission has also been suggested to originate from the hot cocoon that surrounds the GRB jet as it crosses the ejecta (Gottlieb, Nakar, and Piran, 2018).

On August 17, 2017, the gravitational wave event GW170817 was observed (Abbott *et al.*, 2017b) and identified as a merger of two neutron stars. With the combination of gravitational wave signals and electromagnetic observations, its location was identified (Abbott *et al.*, 2017a), a weak sGRB detected (Abbott *et al.*, 2017e) (weak probably due to an off-axis observation) (Mooley *et al.*, 2018; Wu and MacFadyen, 2018), accompanied by secondary x-ray and radio signals.

Within 11 h of the merger the electromagnetic transient, named AT 2017gfo, was observed in the ultraviolet, optical, and near-infrared wavelength bands in the galaxy NGC 4993 (Arcavi *et al.*, 2017; Chornock *et al.*, 2017; Coulter *et al.*, 2017; Cowperthwaite *et al.*, 2017; Drout *et al.*, 2017; Evans *et al.*, 2017; Kasliwal *et al.*, 2017; Nicholl *et al.*, 2017; Pian *et al.*, 2017; Smartt *et al.*, 2017; Soares-Santos *et al.*, 2017; Tanvir *et al.*, 2017). The left panel of Fig. 10 shows the bolometric light curve for the two-week-long epoch of detailed observations. The figure also includes late-time

[2]See https://kilonova.space for an up-to-date catalog of kilonova observations.

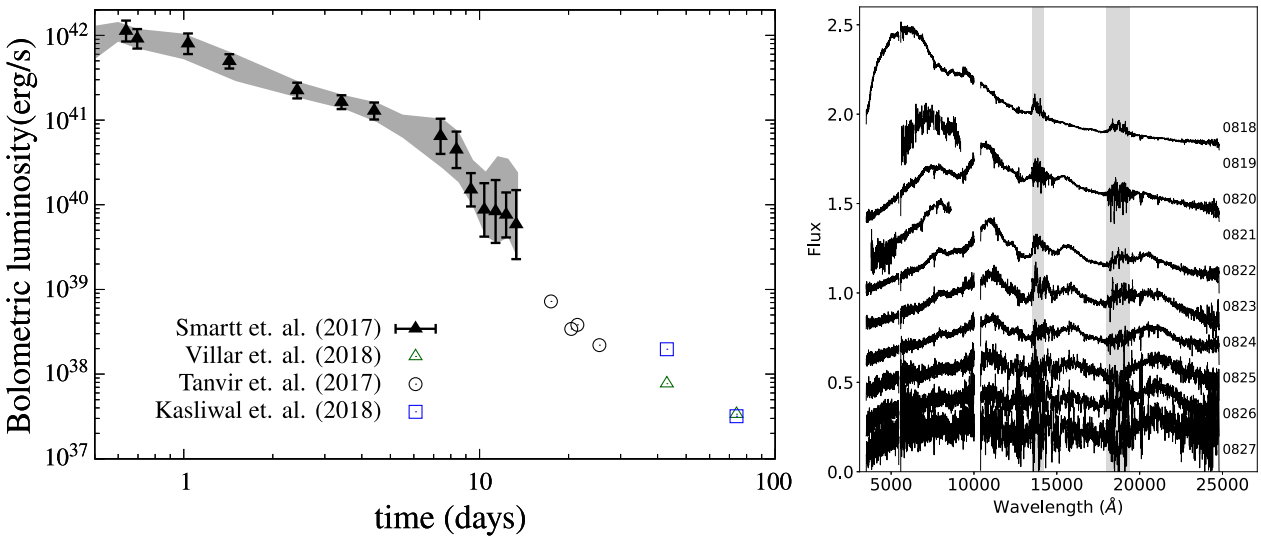

FIG. 10. Left panel: bolometric light curve of AT 2017gfo, the kilonova associated with GW170817. The filled black triangles are from Smartt *et al.* (2017). Uncertainties derived from the range of values given in the literature (Cowperthwaite *et al.*, 2017; Smartt *et al.*, 2017; Waxman *et al.*, 2018) are shown as a gray band. Also shown are lower limits on the late-time luminosity as inferred from the Ks band with VLT/HAWK-I (Tanvir *et al.*, 2017) (empty circles) and the 4.5 μm detections by the Spitzer Space Telescope from Villar *et al.* (2018) (empty triangles) and Kasliwal *et al.* (2019) (empty squares). Adapted from Wu, Barnes *et al.*, 2019. Right panel: evolution of the kilonova flux spectrum during the first 10 d. Each spectrum is labeled by the observation epoch. The shaded areas mark the wavelength ranges with low atmospheric transmission. From Pian *et al.*, 2017.

observations from the Ks band with the VLT/HAWK-I (Tanvir *et al.*, 2017) and 4.5 μm detections by the Spitzer Space Telescope (Villar *et al.*, 2018; Kasliwal *et al.*, 2019). The right panel of Fig. 10 shows the evolution of the kilonova flux spectra from the X-shooter Very Large Telescope (VLT) spectrograph during the first 10 d from Pian *et al.* (2017). Further analysis of these spectra even led to the first identification of an element, Sr (Watson *et al.*, 2019).

The luminosity and its evolution agreed with predictions for the light powered by the radioactive decay of heavy nuclei synthesized via the *r* process in the neutron-rich merger ejecta (Li and Paczyński, 1998; Metzger, Martínez-Pinedo *et al.*, 2010; Roberts *et al.*, 2011; Barnes and Kasen, 2013; Rosswog *et al.*, 2018); see Sec. VII. Additional evidence is provided by the spectral or color evolution, which requires models with at least two components. Simulations suggest that at least three components are necessary to account for the ejecta of neutron-star mergers: dynamic, winds, and secular outflows from the disk (Perego, Radice, and Bernuzzi, 2017). Combining all observations Villar *et al.* (2017) found a best-fit kilonova model consisting of three components: a "blue" lanthanide-poor component (opacity $\kappa = 0.5$ cm^2 g^{-1}) with $M_{\rm ej} \approx 0.020$ M$_\odot$, moving with a velocity of approximately $0.27c$, an intermediate opacity "purple" component ($\kappa = 3$ cm^2 g^{-1}) with $M_{\rm ej} \approx 0.047$ M$_\odot$ at $0.15c$, and a "red" lanthanide-rich component ($\kappa = 10$ cm^2 g^{-1}) with $M_{\rm ej} \approx 0.011$ M$_\odot$ at $0.14c$. The three-component model is compatible with a two-component model containing only blue and red components. The blue component is expected to contain light *r*-process elements with a negligible mass fraction of lanthanides to actinides $X_{\rm lan} \lesssim 10^{-4}$ (Kasen *et al.*, 2017). The mass fraction of lanthanides to actinides necessary to account for the reddening of the spectra has been inferred to be $X_{\rm lan} \sim 10^{-3}$–10^{-2} (Kasen *et al.*, 2017; Tanaka *et al.*, 2017; Waxman *et al.*, 2018) and hence contains both light and heavy *r*-process material assuming solar proportions. The purple component corresponds to ejecta with a small but non-negligible lanthanide fraction. The early blue emission has been interpreted to originate from the fastest outer layers of the ejecta originating from material ejected in the polar direction and containing exclusively light *r*-process nuclei (Metzger and Fernández, 2014; Drout *et al.*, 2017; Nicholl *et al.*, 2017); see Kawaguchi, Shibata, and Tanaka (2018) and Waxman *et al.* (2018) for alternative explanations. The later transition of the emission colors to the near infrared suggest ejecta containing heavy *r*-process elements originating from the postmerger accretion disk ejecta given their smaller velocities and larger masses (Kasen *et al.*, 2017; Perego, Radice, and Bernuzzi, 2017; Siegel and Metzger, 2017, 2018; Fernández *et al.*, 2019; Siegel, 2019); see Sec. VI.B. The total amount of ejecta has been estimated at $M_{\rm ej} \approx 0.03$–0.08 M$_\odot$ (Cowperthwaite *et al.*, 2017; Kasen *et al.*, 2017; Kasliwal *et al.*, 2017; Perego, Radice, and Bernuzzi, 2017; Villar *et al.*, 2017; Kawaguchi, Shibata, and Tanaka, 2018; Waxman *et al.*, 2018). However, those estimates are based on spherically symmetric models, while more realistic geometries may lead to different predictions (Kawaguchi, Shibata, and Tanaka, 2020; Korobkin *et al.*, 2020b). This observation provided the first direct indication that *r*-process elements are produced in neutron-star mergers including estimates of the amount of ejecta, composition, and morphology. Additional information about kilonova modeling and the connection of these observations with models of compact binary mergers is given in Sec. VII.

III. BASIC WORKING OF THE *r* PROCESS AND NECESSARY ENVIRONMENT CONDITIONS

A. Modeling composition changes in astrophysical plasmas

Before discussing the working of the *r* process in detail, we give an introduction to the methods, including how the buildup of elements in astrophysical plasmas can be described and determined. The mechanism to model composition changes is based on nuclear reactions, occurring in environments with a given temperature and density. Integrating the product of the reaction cross section $\sigma(E)$ times the relative velocity $v(E)$ over the energy distribution of reacting partners at a given T, abbreviated as $\langle\sigma v\rangle(T)$, determines the probability of reactions happening. For most conditions in stellar evolution and explosions a Maxwell-Boltzmann distribution is attained (Clayton, 1968; Rolfs and Rodney, 1988; Iliadis, 2007; Lippuner and Roberts, 2017). Nuclear decays can be expressed via the decay constant λ, related to the half-life of a nucleus $t_{1/2}$ via $\lambda = \ln 2/t_{1/2}$. Interactions with photons (photodisintegrations) are described by the integration of the relevant cross section over the energies of the photon Planck distribution for the local temperature. This results in an effective temperature-dependent "decay constant" $\lambda(T)$. Reactions with electrons (electron captures on nuclei) (Fuller, Fowler, and Newman, 1980; Langanke and Martínez-Pinedo, 2001, 2003; Juodagalvis *et al.*, 2010) or neutrinos (Langanke and Kolbe, 2001, 2002; Kolbe *et al.*, 2003) can be treated in a similar way, also resulting in effective decay constants λ, which can depend on temperature T and density ρ (determining for electrons whether degenerate or nondegenerate Fermi distributions are in place). The λ's for neutrinos require their energy distributions (Tamborra *et al.*, 2012) from detailed radiation transport, not necessarily reflecting the local conditions (Liebendörfer *et al.*, 2005; Liebendörfer, Whitehouse, and Fischer, 2009; Janka, 2017b; Richers *et al.*, 2017; Burrows *et al.*, 2018; Pan *et al.*, 2019).

All these reactions contribute to changes of the abundances Y_i, related to number densities $n_i = \rho Y_i/m_u$ and mass fractions of the corresponding nuclei via $X_i = A_i Y_i$, where A_i is the mass number of nucleus i, $\sum_i X_i = 1$, ρ denotes the density of the medium, and m_u is the atomic mass unit. The reaction network equations for the time derivatives of the abundances Y_i include three types of terms (Hix and Thielemann, 1999)

$$\frac{dY_i}{dt} = \sum_j P^i_j \lambda_j Y_j + \sum_{j,k} P^i_{j,k} \frac{\rho}{m_u} \langle j,k\rangle Y_j Y_k + \sum_{j,k,l} P^i_{j,k,l} \frac{\rho^2}{m_u^2} \langle j,k,l\rangle Y_j Y_k Y_l, \quad (1)$$

summing over all reaction partners related to the different summation indices. The P's include an integer (positive or negative) factor N^i (appearing with one, two, or three lower indices for one-body, two-body, or three-body reactions), describing whether (and how often) nucleus i is created or destroyed in this reaction. Additional correction factors $1/m!$ are applied for two-body and three-body reactions in case two or even three identical partners are involved. This leads to $P^i_j = N^i_j$, $P^i_{j,k} = N^i_{j,k}/m(j,k)!$, or $P^i_{j,k,l} = N^i_{j,k,l}/m(j,k,l)!$. $m(i,j)$ is equal to 1 for $i \neq j$ and it is equal to 2 for $i = j$, $m(i,j,k)$ can have the values 1 (for nonidentical reaction partners), 2 for two identical partners, and 3 for three identical partners. Thus, this additional correction factor is 1 for nonidentical reaction partners, $1/2 = 1/2!$ for two identical partners or even $1/6 = 1/3!$ for three identical partners. The λ's stand for decay rates (including decays, photodisintegrations, electron captures, and neutrino-induced reactions), $\langle j,k\rangle$ for $\langle\sigma v\rangle$ of reactions between nuclei j and k. Although in astrophysical environments true three-body reactions are negligible, a sequence of two two-body reactions (with an intermediate extremely short-lived nucleus) is typically written as a three-body reaction term, resulting in the expression $\langle j,k,l\rangle$ (Nomoto, Thielemann, and Miyaji, 1985; Görres, Wiescher, and Thielemann, 1995). The nuclei involved in the first reaction, including the highly unstable intermediate nucleus, are typically in chemical equilibrium (discussed later). A survey of computational methods to solve nuclear networks was given by Hix and Thielemann (1999), Timmes (1999), Hix and Meyer (2006), and Lippuner and Roberts (2017). The solution of the set of differential equations, defined in Eq. (1), provides the changes of individual nuclear abundances for any burning process in astrophysical environments, requiring the inclusion of all possible reactions and the relevant nuclear physics input.[3] In astrophysical applications the composition changes determined by Eq. (1) cause related energy generation that couples to the thermodynamics and hydrodynamics of the event (Mueller, 1986). For large reaction networks that can be computationally rather expensive due to two effects: (a) Nuclear reaction timescales vary by orders of magnitude and the resulting reaction networks represent so-called stiff systems of differential equations that can be solved only with implicit computational methods, requiring large systems of nonlinear equations with several Newton-Raphson iterations. (b) The size of time steps needed to follow nuclear composition changes can be much smaller than those relevant for hydrodynamic changes. For these reasons in most cases the problem is split into hydrodynamics and thermodynamics parts with a limited reaction network, sufficient for the correct energy generation, and postprocessing of the obtained thermodynamic conditions with a detailed nucleosynthesis network; see Curtis *et al.* (2019), Ebinger *et al.* (2019), and references therein.

If matter experiences explosive burning at high temperatures and densities, the reaction rates for fusion reactions and the photodisintegration rates (due to a Planck photon distribution extending to high energies) are large. This will lead to chemical equilibria, i.e., balancing of forward and backward flows in reactions, in particular, also for proton or neutron-capture reactions $p + (Z,A) \rightleftarrows (Z+1, A+1) + \gamma$ and $n + (Z,A) \rightleftarrows (Z, A+1) + \gamma$, corresponding to a relation between the chemical potentials $\mu_p + \mu(Z,A) = \mu(Z+1, A+1)$ and $\mu_n + \mu(Z,A) = \mu(Z, A+1)$ as the chemical potential of photons vanishes. If this is the case not only for a

[3]For data repositories see https://jinaweb.org/reaclib/db, https://nucastro.org/reaclib.html, http://www.kadonis.org, and http://www.astro.ulb.ac.be/pmwiki/Brusslib/HomePage.

particular reaction but also across the entire nuclear chart, the complete reaction sequence is in chemical equilibrium, i.e., $Z\mu_p + N\mu_n = \mu(Z, A)$, which is termed complete chemical or nuclear statistical equilibrium (NSE) (Clayton, 1968; Hix and Thielemann, 1999). For Boltzmann distributions (which apply in general in astrophysical plasmas, with the exception of highly degenerate conditions, where Fermi distributions have to be utilized for the chemical potentials) (Thielemann and Truran, 1986; Bravo and García-Senz, 1999; Yakovlev *et al.*, 2006; Haensel, Potekhin, and Yakovlev, 2007), the abundances of nuclei can be expressed by nuclear properties like the binding energies $B(Z, A)$, the abundances of free neutrons and protons, and environment conditions like temperatures T and densities ρ, leading to the abundance of nucleus i (with Z_i protons and N_i neutrons or $A_i = Z_i + N_i$ nucleons (Clayton, 1968)

$$Y_i = Y_n^{N_i} Y_p^{Z_i} \frac{G_i(T) A_i^{3/2}}{2^{A_i}} \left(\frac{\rho}{m_u}\right)^{A_i - 1} \times \left(\frac{2\pi\hbar^2}{m_u kT}\right)^{3(A_i-1)/2} \exp\left(\frac{B_i}{kT}\right), \quad (2)$$

where B_i is the nuclear binding energy of the nucleus. G_i corresponds to the partition function of nucleus i, as the ground and excited state population is in thermal equilibrium. Reactions moderated by the weak interaction, i.e., β decays, electron captures, and charged-current neutrino interactions, change the overall proton-to-nucleon ratio $Y_e = \sum Z_i Y_i$ and occur on longer timescales than particle captures and photodisintegrations. They are not necessarily in equilibrium and have to be followed explicitly. Thus, as a function of time the NSE abundances depend on density $\rho(t)$, temperature $T(t)$, and proton-to-nucleon ratio $Y_e(t)$, which is determined by weak interactions that act on longer timescales and have not necessarily reached an equilibrium. Mass and charge conservation lead to these two equations that determine the values of Y_n and Y_p:

$$\sum_i A_i Y_i = Y_n + Y_p + \sum_{i,(A_i>1)} (Z_i + N_i) Y_i(\rho, T, Y_n, Y_p) = 1,$$
$$\sum_i Z_i Y_i = Y_p + \sum_{i,(Z_i>1)} Z_i Y_i(\rho, T, Y_n, Y_p) = Y_e. \quad (3)$$

In general, high densities favor heavy nuclei due to the high power of ρ^{A_i-1}, and high temperatures favor light nuclei due to $(kT)^{-3(A_i-1)/2}$ in Eq. (2). In the intermediate regime $\exp(B_i/kT)$ favors tightly bound nuclei, with the highest binding energies in the mass range $A = 50$–60 of the Fe group, but depending on the given Y_e. The width of the composition distribution is determined by the temperature as derived by Clayton (1968).

Under certain conditions, i.e., insufficiently high temperatures when not all reactions are fast enough, especially due to small reaction rates caused by Q values that are too small, i.e., proton or neutron binding energies across magic proton or neutron numbers (closed shells), a full NSE does not emerge and only certain areas of the nuclear chart are in equilibrium, called quasiequilibrium groups (or QSEs). This happens during the early and late phases of explosive burning, before or after conditions for a full NSE have been fulfilled. (In the latter case this is referred to as "freeze-out.") A typical situation is a breakup in three groups, the Fe group above Ca ($N = Z = 20$), the Si group between Ne ($N = Z = 10$) and Ca, the light group from neutrons and protons up to He, and nuclei not in equilibrium from there up to Ne, as discussed by Hix and Thielemann (1999).

A so-called α-rich charged-particle freeze-out is a special case of such QSE conditions, when the buildup of nuclei beyond ^{4}He is hampered by the need of "three-body" reaction sequences, involving highly unstable ^{8}Be (e.g., $\alpha + \alpha + \alpha \rightarrow {}^{12}\mathrm{C} + \gamma$ or $\alpha + \alpha + n \rightleftarrows {}^9\mathrm{Be}$), which are strongly dependent on the density of matter; see Fig. 11. The first part of these reaction sequences involves a chemical equilibrium for $\alpha + \alpha \rightleftarrows {}^8\mathrm{Be}$ that is strongly shifted to the left side of the reaction equation due to the half-life of ^{8}Be ($t_{1/2} = 6.7 \times 10^{-17}$ s). Reasonable amounts of ^{8}Be, which permit the second stage of these reaction sequences via an alpha or neutron capture, can be built up only for high densities. The reaction rates for the combined three-body reactions have a quadratic dependence on density in comparison to a linear density dependence in two-body fusion reactions. Therefore, for low densities the NSE cannot be kept and an overabundance of alpha particles (^{4}He) remains, permitting only a much smaller fraction of heavier elements to be formed than in a NSE (determined by binding energies of nuclei). This α-rich freeze-out leads to two features: (a) the abundance of nuclei heavier than ^{4}He is strongly reduced in comparison to their NSE abundances, and

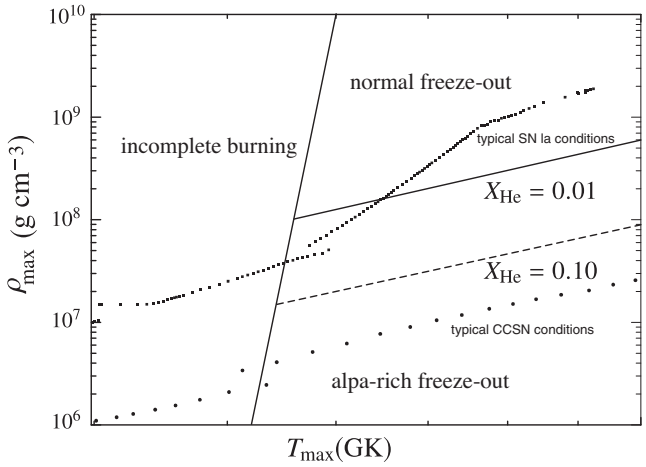

FIG. 11. Plane of maximum temperatures and densities (Woosley, Arnett, and Clayton, 1973), indicating for explosive Si burning the boundaries of conditions after freeze-out of charged-particle reactions with an adiabatic expansion for an electron fraction $Y_e = 0.498$. High densities, permitting three-body reactions to build up C and heavier nuclei, lead to a normal freeze-out NSE composition. For lower densities unburned α particles remain; i.e., the final outcome is a so-called α-rich freeze-out (see the lines of remaining He mass fractions X_{He}). Also displayed are typical conditions experienced in Si-burning mass zones of SNe Ia and CCSNe, determining the nucleosynthesis outcome of such explosions.. Adapted from Thielemann, Nomoto, and Yokoi, 1986, Thielemann, Hashimoto, and Nomoto, 1990, and Thielemann, Nomoto, and Hashimoto, 1996.

(b) the abundance maximum of the fewer heavy nuclei is shifted via final alpha captures to heavier nuclei relative to a NSE. While this maximum would normally be around Fe and Ni (the highest binding energies) with $A = 50$–60, it can be shifted up to A of about 90 for α mass fractions X_{He} after freeze-out in excess of 40%; see Figs. 11 and 17, as well as Hoffman, Woosley, and Qian (1997) and Freiburghaus *et al.* (1999).

Other quasiequilibrium conditions are encountered in proton- or neutron-rich environments. The first case permits proton captures and reverse photodisintegrations, causing QSE clusters along isotonic lines in the nuclear chart, connected via β^+ decays and/or (α, p) reactions on longer timescales (Rembges *et al.*, 1997). For the second case Burbidge *et al.* (1957) [followed up later by Seeger, Fowler, and Clayton (1965)] had already postulated in their 1957 review that isotopic lines in the nuclear chart are in quasiequilibrium for neutron-rich *r*-process conditions (i.e., via neutron captures and their reverse photodisintegrations), connected via β^- decays on longer timescales. The latter are discussed in more detail later with respect to the *r* process. Quasiequilibrium along isotonic and isotopic lines typically acts close to the proton or neutron drip lines, respectively. Thus, small reaction Q values are involved for proton or neutron captures, and only small photon energies for the inverse reactions are needed to establish such an equilibrium. This changes temperature requirements somewhat. A full NSE, close to stability with Q values of the order of 8–10 MeV, is established only for temperatures around 4 to 5 GK (as a rule of thumb temperatures kT need to exceed $Q/30$) (Thielemann *et al.*, 2018). For Q values of the order of 1 to 2 MeV close to the drip lines such equilibria can still be established at temperatures in excess of about 1–1.5 GK.

B. Special features of the *r* process and the role of neutron densities and temperatures

In Sec. III.A we explained how a complete NSE or QSE subgroups could be established. Here we want to discuss the special case of QSE subgroups along isotopic chains before entering a description of the possible sites that permit such quasiequilibria. When charged-particle reactions are frozen, the only connection between isotopic chains is given by weak processes, i.e., β decay, or for large mass number fission and alpha decay (producing lighter nuclei). High neutron densities make the timescales for neutron capture much faster than those for β decay and can produce nuclei with neutron-separation energies $S_n \sim 2$ MeV and less (close to the neutron drip line, where S_n goes down to 0). This is the energy gained (Q value) when capturing a neutron on nucleus $A-1$ or the photon energy required to release a neutron from nucleus A via photodisintegration. For temperatures around 1 GK, (γ, n) photodisintegrations in a thermal plasma can still be active for such small reaction S_n values (as previously discussed). With both reaction directions being faster than astrophysical (and β-decay) timescales a chemical equilibrium between neutron captures and photodisintegrations is attained. This establishes quasiequilibrium clusters along isotopic chains of heavy nuclei. The abundance distribution in each isotopic chain follows the ratio of two neighboring isotopes

$$\frac{Y(Z,A+1)}{Y(Z,A)} = n_n \frac{G(Z,A+1)}{2G(Z,A)} \left[\frac{A+1}{A}\right]^{3/2} \times \left[\frac{2\pi\hbar^2}{m_u kT}\right]^{3/2} \exp\left(\frac{S_n(A+1)}{kT}\right), \quad (4)$$

with partition functions G, the nuclear-mass unit m_u, and the neutron-separation (or neutron binding) energy of nucleus $(Z, A+1)$, $S_n(A+1)$. This relation for a chemical equilibrium of neutron captures and photodisintegrations in an isotopic chain follows from utilizing the appropriate chemical potentials (see Sec. III.A) or equivalently due to the fact that the cross sections for these reactions and their reverses are linked via detailed balance between individual states in the initial and the final nucleus of each capture reaction. The abundance ratios are dependent only on $n_n = \rho Y_n / m_u$, T, and S_n. S_n introduces the dependence on nuclear masses, i.e., a nuclear-mass model for these neutron-rich unstable nuclei. Under the assumption of an $(n,\gamma) \rightleftarrows (\gamma, n)$ equilibrium, no detailed knowledge of neutron-capture cross sections is needed.

Given that $Y(A+1)/Y(A)$ first rises with increasing neutron excess before it decreases farther out [caused by the last two factors in Eq. (4)], this leads to abundance maxima in each isotopic chain that are determined only by the neutron number density n_n and the temperature T. Approximating $Y(Z,A+1)/Y(Z,A) \simeq 1$ at the maximum, as well as $G(Z,A+1) \approx G(Z,A)$, the neutron-separation energy S_n has to be the same for the abundance maxima in all isotopic chains, defining the so-called *r*-process path.

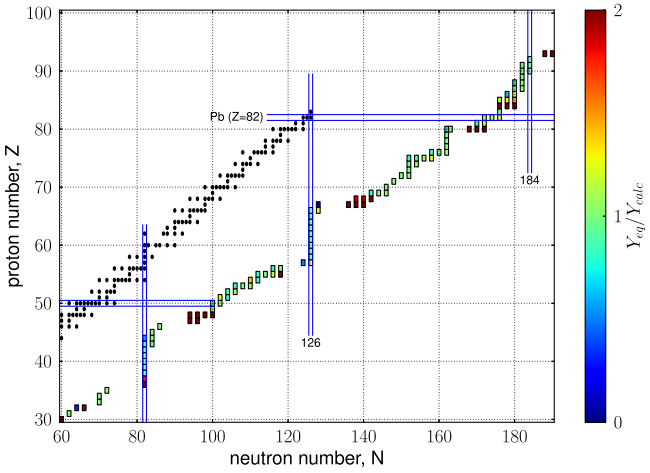

FIG. 12. The figure shows the line of stability (black solid squares), the proton and neutron magic numbers (blue horizontal and vertical lines), and an *r*-process path. The conditions here are taken from a neutron-star merger environment that is further discussed later. The position of the path follows from a chemical equilibrium between neutron captures and photodisintegrations in each isotopic chain [$(n,\gamma) \rightleftarrows (\gamma, n)$ equilibrium]. However, the calculation was performed with a complete nuclear network, containing more than 3000 nuclei. The colors along the path indicate how well the full network calculation follows such an $(n,\gamma) \rightleftarrows (\gamma, n)$ equilibrium. It can be seen that such full calculations agree with this equilibrium approach within a factor of 2 along the *r*-process path, which continues to the heaviest nuclei. From Eichler *et al.*, 2015.

Figure 12 shows such an *r*-process path for $S_n \simeq 2$ MeV, when utilizing masses based on the finite-range droplet model (FRDM) (Möller *et al.*, 1995); for a detailed discussion of nuclear properties far from stability see Secs. IV and V. In environments with sufficiently high neutron densities, the *r* process continues to extremely heavy nuclei and finally encounters the neutron-shell closure $N = 184$, where fission plays a dominant role. Figure 12 also displays the line of stability. As the speed along the *r*-process path is determined by β decays, which are longer closer to stability, abundance maxima will occur at the top end of the kinks in the *r*-process path at neutron-shell closures $N = 50$, 82, 126. After decay to stability at the end of the process, these maxima appear at the corresponding mass numbers *A*. These *A*'s are smaller than those of stable nuclei for the same neutron-shell closures. The latter experience the smallest neutron-capture cross sections and cause the *s*-process maxima.

Figure 13 shows the regions of the nuclear chart where fission dominates and the location of fission fragments for various mass models and fission barriers. Nuclear properties like mass models, fission, and weak interactions are discussed in detail in Secs. IV and V. Early *r*-process calculations always made use of an $(n,\gamma) \rightleftarrows (\gamma,n)$ equilibrium but had to assume neutron densities, temperatures, and a specific duration time (before the final decay to stability, via β-decay and β-delayed neutron emission) (Burbidge *et al.*, 1957; Seeger, Fowler, and Clayton, 1965; Kodama and Takahashi, 1975). It was realized that with such calculations a unique set of conditions could not reproduce solar *r*-process abundances. Within this approach and with increasing knowledge of nuclear properties, Kratz *et al.* (1993) and Pfeiffer *et al.*, 2001 provided a series of parameter studies. An optimal fit for the three *r*-process peaks and the amount of matter in the actinides required a superposition of at least four components.

Dynamical calculations with varying $n_n(t)$ and $T(t)$ and while discarding the $(n,\gamma) \rightleftarrows (\gamma,n)$ equilibrium follow the abundance changes in detail (Blake and Schramm, 1976; Truran, Cowan, and Cameron, 1978; Cowan, Cameron, and Truran, 1980, 1985; Cameron, Cowan, and Truran, 1983). These calculations showed that the *r* process can operate under two different regimes with significantly different nuclear physics demands (Wanajo, 2007; Arcones and Martínez-Pinedo, 2011): a "hot" *r* process in which the temperatures are large enough to reach $(n,\gamma) \rightleftarrows (\gamma,n)$ equilibrium and a "cold" *r* process in which the temperatures are so low that photodissociation reactions are irrelevant (Blake and Schramm, 1976). Notice that the differentiation between hot and cold refers to the temperature conditions during the neutron-capture phase and not during the earlier phase when the seeds are formed; see Sec. III.C. Material could initially be cold and later reheated by nuclear processes, resulting in a hot *r* process or initially hot and during the expansion cool to low temperatures, producing a cold *r* process. In general, astrophysical environments produce a broad range of conditions in which both high and low temperatures are reached, as illustrated in Fig. 14. In some cases the material can reach such low densities that free neutrons remain after the *r* process (brown lines in the figure) with potentially important observational consequences

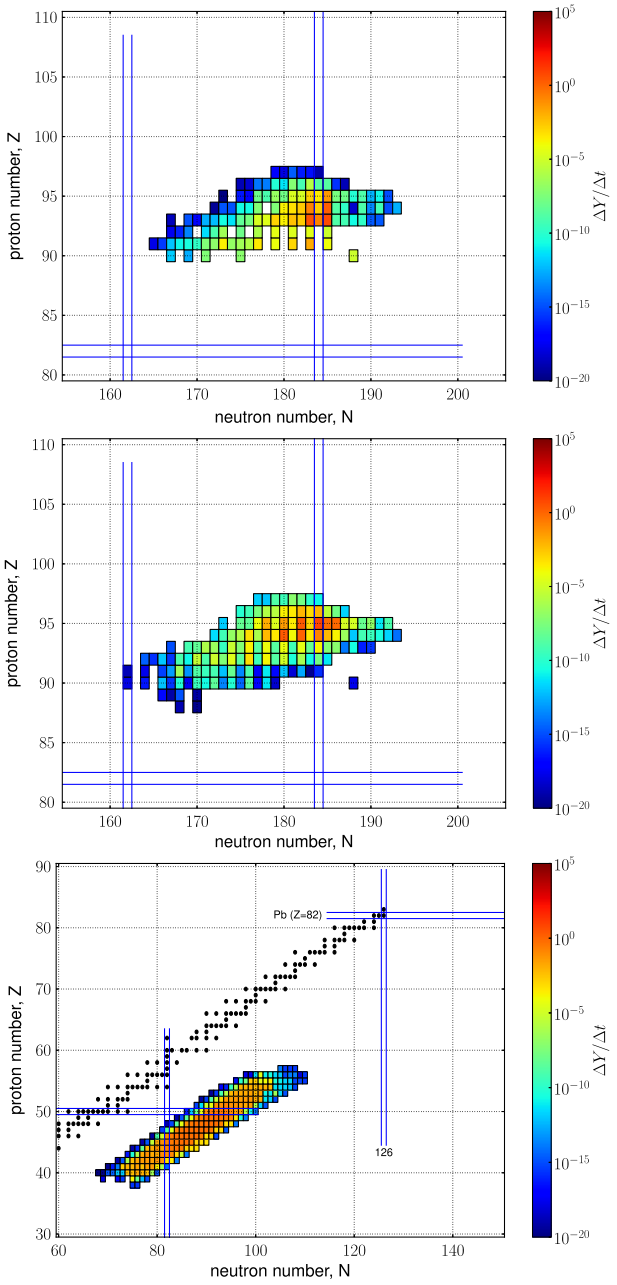

FIG. 13. Color-coded time derivatives of nuclear abundances *Y* during an *r*-process simulation describing the destruction via (top panel) neutron-induced fission and (center panel) β-delayed fission (Panov *et al.*, 2010) and (bottom panel) the production of fission fragments (Kelic, Ricciardi, and Schmidt, 2008). The largest destruction rates occur at or close to the neutron closure $N = 184$ due to the smallest fission barriers encountered at these locations. Fission fragments are produced in a broad distribution, ranging in mass number *A* from 115 to 155. From Eichler *et al.*, 2015.

(Metzger *et al.*, 2015). Figure 14 also shows the nuclear energy generation during the *r* process (lower panel) that is particularly relevant for neutron-rich conditions, as expected in dynamic ejecta from neutron-star mergers (see Sec. VI.B.1) and for simulations of kilonova *r*-process electromagnetic transients (see Sec. VII).

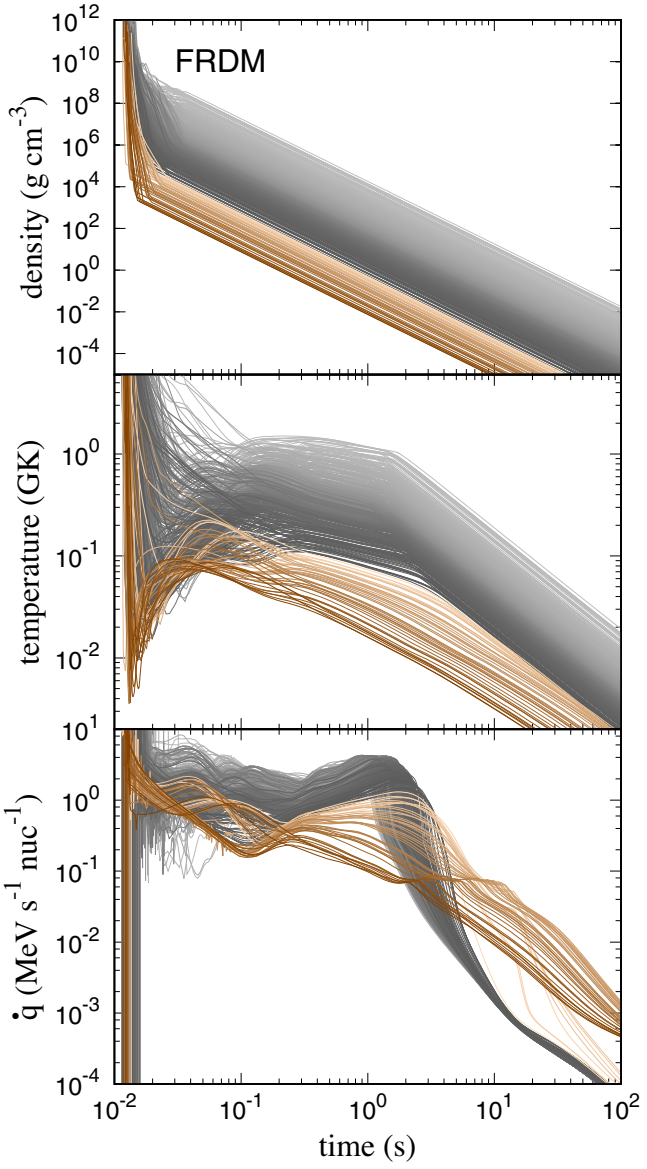

FIG. 14. Evolution of temperature, density, and nuclear energy generation for different trajectories corresponding to material ejected dynamically in neutron-star mergers. Gray (darker) [brown (lighter)] lines correspond to the "slow (fast) ejecta" discussed in Sec. VI.B.1. For both gray and brown lines, light (dark) colors correspond to hotter (colder) conditions. Adapted from Mendoza-Temis *et al.*, 2015.

Following the freeze-out of charged-particle reactions, the *r* process typically consists of two phases: an initial phase dominated by neutron captures and, depending on temperature, photodissociations and a later phase in which neutron captures and β decays operate on similar timescales during the decay to stability in what is typically known as *r*-process freeze-out. The transition between the two phases occurs when the neutron-to-seed ratio (i.e., the ratio of free neutrons to heavy nuclei) reaches values close to 1. This is illustrated in Fig. 15. The upper panel shows the evolution of the abundances of neutrons, alpha particles, and heavy nuclei for a typical trajectory from those shown in Fig. 14. The lower panel shows the effective neutron lifetime τ_n, the average radiative neutron-capture timescale per nucleus $\tau_{(n,\gamma)}$, the average photodissociation timescale per nucleus $\tau_{(\gamma,n)}$, and the average β-decay timescale per nucleus τ_β, defined as the inverse of their average destruction rates per nucleus for the respective processes

$$\frac{1}{\tau_n} = \left|\frac{1}{Y_n}\frac{dY_n}{dt}\right|, \tag{5a}$$

$$\frac{1}{\tau_{(n,\gamma)}} = \frac{\sum_{Z,A} Y(Z,A) n_n \langle \sigma v \rangle_{A,Z}}{\sum_{Z,A} Y(Z,A)}, \tag{5b}$$

$$\frac{1}{\tau_{(\gamma,n)}} = \frac{\sum_{Z,A} Y(Z,A) \lambda_\gamma(Z,A)}{\sum_{Z,A} Y(Z,A)}, \tag{5c}$$

$$\frac{1}{\tau_\beta} = \frac{\sum_{Z,A} Y(Z,A) \lambda_\beta(Z,A)}{\sum_{Z,A} Y(Z,A)}. \tag{5d}$$

Thus, the last three equations provide the neutron-capture rate on an average seed nucleus [averaged over all nuclei with their abundances $Y(Z,A)$], the photodisintegration (γ, n) rate, and the β-decay rate, respectively, which are the inverse of the corresponding average reaction timescales.

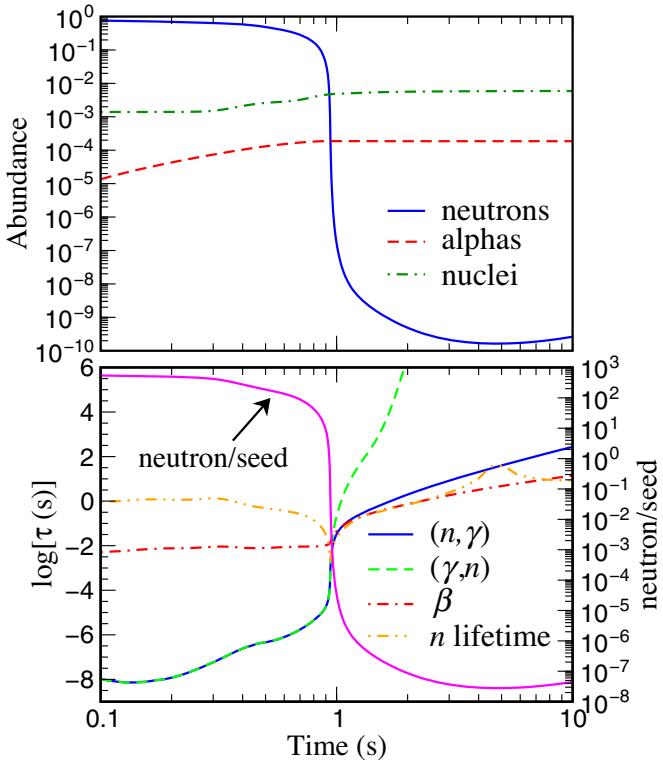

FIG. 15. Upper panel: evolution of the abundances of neutrons, alpha particles, and heavy nuclei during the *r* process. Bottom panel: evolution of the neutron-to-seed ratio and average timescales for neutron captures, photodissociation, and β decays. The absolute value of the neutron lifetime, defined in the text, is also shown. Notice that for $t \lesssim 1$ s neutron-capture and photodissociation timescales coincide.

Figure 15 shows results of calculations with an initial neutron-to-seed nucleus ratio $n_s \sim 600$, allowing for several fission cycles before the end of the r process, i.e., subsequent sequences of fission, leading to lighter fission fragments that can again capture neutrons until heavier nuclei are produced, encountering fission again and the production of fission fragments. The impact of fission cycling, doubling the number of heavy nuclei with each cycle, can be seen in the upper panel of Fig. 15 by the increase in the abundance of heavy nuclei. A similar increase is also seen in the abundances of alpha particles due mainly to the α decay of translead nuclei. At early times (< 1 s) the neutron abundance is large and changes slowly with time. This is a consequence of the almost identical (n,γ) and (γ,n) timescales as the temperatures are large enough to maintain $(n,\gamma) \rightleftarrows (\gamma,n)$ equilibrium. Neglecting the production of neutrons by β decay and fission one finds the following relation for $1/\tau_n$, corresponding to Eq. (5a), which is equal to the difference between average neutron destructions via neutron capture and productions via photodisintegrations per nucleus divided by the neutron-to-seed nucleus ratio n_s:

$$\frac{1}{\tau_n} = \frac{1}{n_s}\left(\frac{1}{\tau_{(n,\gamma)}} - \frac{1}{\tau_{(\gamma,n)}}\right), \tag{6}$$

thereby illustrating the important role played by the neutron-to-seed ratio. Whenever $n_s > 1$, the effective neutron lifetime is large and there is enough time for the r process to pass via successive β decays through many isotopic chains and reach a β-flow equilibrium (Kratz *et al.*, 1993; Freiburghaus *et al.*, 1999). The time derivative $\dot{Y}(Z)$ of the abundance in an entire isotopic chain $Y(Z) = \sum_N Y(Z,N)$, due to β decays, is given by

$$\sum_N \lambda_\beta(Z,N)Y(Z,N) = Y(Z)\sum_N \lambda_\beta(Z,N)\frac{Y(Z,N)}{Y(Z)} = Y(Z)\lambda_\beta^{\mathrm{eff}}(Z) = \mathrm{const}, \tag{7}$$

with $\lambda_\beta^{\mathrm{eff}}(Z)$ the effective decay rate of the entire chain. In a β-flow equilibrium this flux is constant through all affected Z's. As decay rates are related to half-lives via $\lambda = \ln 2/t_{1/2}$, the abundance of a complete isotopic chain is proportional to its effective β-decay half-life $Y(Z) \propto t_{1/2}^{\mathrm{eff}}(Z)$; see Fig. 16.

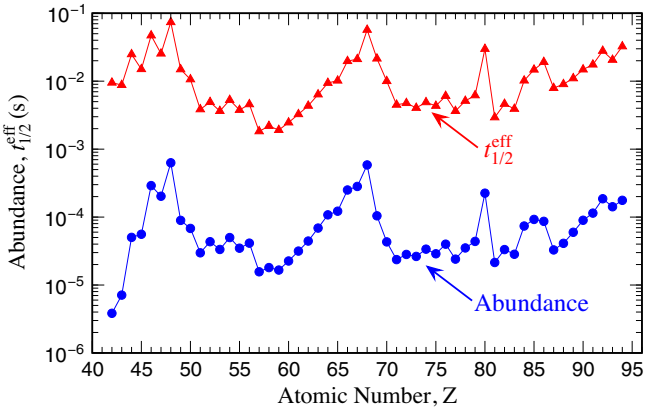

FIG. 16. r-process elemental abundances at freeze-out compared to the effective β-decay half-life of an isotopic chain.

During this early phase, the r-process path is determined mainly by the two-neutron separation energies S_{2n} as only even neutron number nuclei are present due to the pairing effect on binding energies; see Fig. 12. Typically, S_{2n} values decrease smoothly with neutron excess with a sudden decrease at magic neutron numbers. However, for several mass models the S_{2n} are either constant or show a saddle point behavior in regions where there is a transition from deformed to spherical nuclei or vice-versa just before or after magic shell closures. This leads also to saddle points in contour lines of constant S_n in the nuclear chart and translates to the appearance of gaps in the r-process path (see Fig. 12) producing troughs in the abundance distribution (Thielemann *et al.*, 1994; Arcones and Martínez-Pinedo, 2011) before the onset of the freeze-out of neutron captures. These troughs have been extensively discussed in the literature [see Chen *et al.* (1995), Pfeiffer, Kratz, and Thielemann (1997), and references therein] as a signature of quenching of the $N = 82$ shell gap. However, whether the related behavior of neutron separation energies is due to quenching of shell effects far from stability or insufficiency in the challenging treatment of nuclei around the transition from well deformed to spherical is still under debate (Grawe, Langanke, and Martínez-Pinedo, 2007).

Before freeze-out the nuclei with the strongest impact in the r-process dynamics are those with the longest β-decay half-lives. These are the nuclei closest to stability at or just after the magic shell closures. Uncertainties in the nuclear physics properties of those nuclei may have a strong impact on the final abundances. This is particularly the case for nuclei located after the $N = 82$ shell closure. This is confirmed by sensitivity studies (Mumpower *et al.*, 2016) that explore the impact on r-process abundances due to variations of nuclear properties.

Once the r process reaches $n_s \approx 1$, there is an important change in the dynamics. Nuclei start to compete for the few available neutrons and the effective neutron lifetime decreases dramatically; see Eq. (6) and Fig. 15. The effective neutron lifetime increases again once the β-decay timescale becomes shorter than the (n,γ) timescale, resulting in a more gradual decline of n_s at later times. The evolution after $n_s \lesssim 1$ is known as r-process freeze-out. During this phase, the timescales of neutron captures and β decays become similar. It is precisely the competition between neutron captures and β decays (often followed by neutron emission) during the decay to stability that is responsible for smoothing the r-process abundances. Just before the freeze-out the abundances exhibit strong oscillations versus mass number. However, after freeze-out they are rather smooth, in agreement with the Solar System r-process abundances. This is a characteristic feature of the r process when compared to the s process. In the latter case, there is almost never a competition between β decays and neutron captures, and hence the abundances show a strong sensitivity on A.

Any process that produces neutrons during freeze-out can affect the final abundances. This includes β-delayed neutron emission and fission, with the first one dominating for $n_s \lesssim 150$. One should keep in mind that the impact of neutron

production is nonlocal, in the sense that neutrons can be produced in one region of the nuclear chart and captured in another. The freeze-out is responsible of shaping the final abundances. The rare-earth peak is known to be formed during the *r*-process freeze-out. At low n_s, this is due to a competition between neutron captures and β decays (Surman *et al.*, 1997), at high n_s, when fission is important, the fission yields also play an important role (Steinberg and Wilkins, 1978; Panov, Korneev, and Thielemann, 2008; Goriely *et al.*, 2013; Eichler *et al.*, 2015). The freeze-out also has a strong impact on the abundances at the *r*-process peaks at $A \sim 130$ and 195 (Mendoza-Temis *et al.*, 2015). Owing to the large n_s, material accumulates at the $N = 184$ shell closure with $A \sim 280$. During the decay to β stability the material fissions, producing nuclei with $A \lesssim 140$ and neutrons. Depending on the fission rates and yields used it may result in significantly different final abundances (Eichler *et al.*, 2015; Goriely and Martínez-Pinedo, 2015; Giuliani *et al.*, 2020; Vassh *et al.*, 2020). Neutrons emitted by fission have a strong impact on the abundances of the third *r*-process peak. Depending on the masses of nuclei around $N = 130$ (Mendoza-Temis *et al.*, 2015) and the β-decay rates of nuclei with $Z \gtrsim 80$ (Eichler *et al.*, 2015) the peak could be shifted to higher mass numbers relative to Solar System abundances.

After having discussed here the general working of and the nuclear physics input for an *r* process, Sec. III.C discusses how to obtain the required neutron-to-seed ratios. Possible astrophysical sites are discussed in Sec. VI. However, independently the influence of nuclear uncertainties should be analyzed, which we do in Secs. IV and V. They can also affect the validity of suitable astrophysical environments. Recent studies of the impact of mass models, β-decay half-lives, and fission rates and fragment distributions were performed by Arcones and Martínez-Pinedo (2011), Eichler *et al.* (2015), Goriely (2015), Mendoza-Temis *et al.* (2015), Marketin *et al.* (2016), Mumpower *et al.* (2016, 2018), Panov, Lutostansky, and Thielemann (2016), Vassh *et al.* (2019), Giuliani *et al.* (2020), and Vassh *et al.* (2020).

C. How to obtain the required neutron-to-seed ratios

Explosive environments with high temperatures exceeding about 5 GK lead to a NSE consisting of neutrons, protons, and α particles, as discussed in Sec. III.A. Y_e, which affects the NSE composition, is given by the initial abundances and the weak interactions, which determine the overall neutron-to-proton (free and in nuclei) ratio. Essentially all sites of interest for the *r* process, whether starting out with hot conditions or emerging from cold neutron-star material, which heats up during the buildup of heavier nuclei, pass through such a NSE phase. Thus, both cases will lead to similar compositions of light particles and nuclei before the subsequent cooling and expansion of matter, still governed initially by the trend of keeping matter in NSE before the charged-particle freeze-out and the onset of neutron captures in the *r* process.

In hot environments the total entropy is dominated by the black-body photon gas radiation. In such radiation-dominated plasmas the entropy is proportional to T^3/ρ (Hartmann, Woosley, and El Eid, 1985; Woosley and Hoffman, 1992; Meyer, 1993; Witti, Janka, and Takahashi, 1994); i.e., the

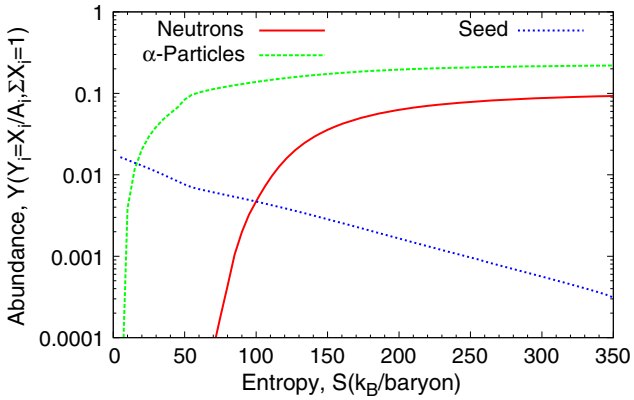

FIG. 17. Abundances of neutrons Y_n, ^{4}He (α particles), Y_α, and so-called seed nuclei $Y_{\rm seed}$ (in the mass range $50 \le A \le 100$), resulting after the charged-particle freeze-out of explosive burning (for $Y_e = 0.45$), as a function of entropy in the explosively expanding plasma. One can realize that the ratio of neutrons to seed nuclei ($n_s = Y_n/Y_{\rm seed}$) increases with entropy. The number of neutrons per seed nucleus determines whether the heaviest elements (actinides) can be produced in a strong *r* process, requiring $A_{\rm seed} + n_s \gtrsim 230$. From Farouqi *et al.*, 2010.

combination of high temperatures and low densities leads to high entropies. Thus, high entropies lead to an α-rich freeze-out (see Fig. 11), and (depending on the entropy) only small amounts of Fe-group and heavier elements are produced, essentially the matter that passed the three-body bottleneck reactions (triple alpha or $\alpha\alpha n$) transforming He to Be and/or C. One can also realize this when examining Fig. 17, obtained from detailed nucleosynthesis calculations, while not assuming any equilibrium conditions. Initially NSE has been obtained. However, depending on the entropy, different types of charged-particle freeze-out occur, paving the way to the subsequent evolution.

The calculation for Fig. 17 starts out with matter in a NSE composition for $Y_e = 0.45$ at $T_0 = 8$ GK and a density ρ_0 corresponding to the given entropy. The expansion from those conditions follows on a so-called free-fall timescale $t_{ff} = [3\pi/(32G\rho_0)]^{1/2}$ (the timescale on which a homogeneous gas cloud of initial density ρ_0 would contract). This timescale is comparable to the expansion caused by an explosion. Figure 17 shows how, with increasing entropies, the alpha mass fraction ($X_\alpha = 4Y_\alpha$) is approaching a constant value and the amount of heavier elements (which would provide the seed nuclei for a later *r* process) is going to zero. This is similar to the big bang, where extremely high entropies permit essentially only the production of elements up to He, and small amounts of Li. In opposition to the big bang, experiencing proton-rich conditions, $Y_e = 0.45$ chosen here is slightly neutron rich, leading at high entropies predominantly to He and free neutrons. The small amount of heavier nuclei after this charged-particle freeze-out (in the mass range of $A = 50$–100), depending on the entropy or α richness of the freeze-out, can then act as seed nuclei for capture of the free neutrons. Once the charged-particle freeze-out has occurred, resulting in a high neutron-to-seed ratio n_s, the actual *r* process (powered by the rapid capture of neutrons) can start, at temperatures below 3 GK. Whether this *r* process

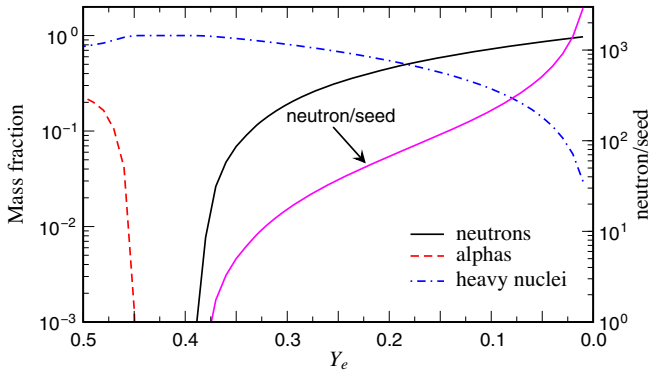

FIG. 18. Evolution of the mass fractions of neutrons, alpha particles, and heavy nuclei vs Y_e (left y-axis scale) and neutron-to-seed ratio (right y-axis scale) at a temperature of 3 GK for an adiabatic expansion with an entropy per nucleon of $s = 20k_B$.

is a hot or cold one, as discussed in Sec. III.B, depends on the resulting neutron densities and temperatures.

For both cases, the neutron-to-seed ratio n_s determines the mass range of nuclei to be produced. Starting with $A =$ 50–100 nuclei, the production of lanthanides requires $n_s \sim 50$, while for actinides an $n_s \sim 150$ is needed.

When considering the result of these investigations, there remain two options for a strong r process in matter that has been heated sufficiently to pass through NSE: (a) for moderately neutron-rich conditions with Y_e not much smaller than 0.5, only extremely high entropies can provide the necessary environment; see Fig. 17 and Freiburghaus *et al.* (1999). (b) For extremely low entropies, when after charged-particle freeze-out only NSE-seed nuclei and free neutrons remain ($Y_n + A_{\rm seed} Y_{\rm seed} = 1$ with $Y_e = Z_{\rm seed} Y_{\rm seed}$) the n_s ratio $Y_n/Y_{\rm seed}$ becomes essentially entropy independent $n_s \approx A_{\rm seed}[Z_{\rm seed}/(A_{\rm seed} Y_e) - 1]$, such that only extremely neutron-rich matter ($Y_e \lesssim 0.15$) can support a strong r process. Figure 18 shows such a case of low entropies per nucleon using $s = 20k_B$, which is typical for matter ejected in neutron-star mergers. It shows several quantities as a function of Y_e. Making a comparison with Fig. 17 at $S = 20$ ($s = 20k_B$) and for $Y = 0.45$ one finds consistent results, i.e., essentially only alpha particles and heavy nuclei (no free neutrons) with typical charges $Z_{\rm seed} \approx 28$ and $A_{\rm seed} \approx 63$. Only for $Y_e \lesssim$ 0.38 do free neutrons start to appear, while lanthanides are produced for $Y_e \lesssim 0.25$; see Lippuner and Roberts (2015) for a systematic study of the astrophysical conditions necessary to produce lanthanides.

IV. EXPERIMENTAL DEVELOPMENTS FOR *r*-PROCESS STUDIES

The r-process path runs through nuclei with extreme neutron excess. Most of these nuclei have yet not been produced in the laboratory and their properties are experimentally unknown. Hence the major nuclear physics input required for r-process simulation must largely be modeled, although recent measurements have led to a significant decrease in uncertainties. Intermediate-mass r-process nuclei could be produced at existing radioactive ion-beam facilities like CERN/Isolde, GSI, and, more recently, RIKEN. Significant advance, however, is expected in the future when key r-process nuclei, including those around the third r-process peak, become accessible at next-generation radioactive ion-beam (RIB) facilities like FAIR and FRIB. This is discussed in more detail in the following sections. Data taken at these facilities will not only directly substitute theory predictions but also serve as stringent and valuable constraints to advanced model predictions for even inaccessible nuclei.

Sections IV and V deal with the nuclear ingredients needed for r-process simulations. At first we discuss the various experimental approaches to produce and study neutron-rich nuclei and summarize the experimental data relevant for r-process nucleosynthesis that have been achieved recently. In Sec. V we present the nuclear models applied to interpret the experimental results and derive the vast nuclear datasets needed for large-scale simulations. We focus on theoretical advances achieved by improved models and experimental constraints and guidance and finally discuss the impact on the improved nuclear data on our understanding of r-process nucleosynthesis.

There has been considerable experimental effort over the last 40 years to explore the nuclear physics of the r process and the structure and properties of r-process nuclei along the projected reaction path, a goal that is nearly equivalent to exploring the evolution of nuclear structure toward the limits of stability. This was one of the strong motivations toward the development of facilities capable of producing radioactive ion beams. The experiments have concentrated on measurement of masses, β decay and β-delayed neutron emission probabilities of neutron-rich nuclei toward and even at the anticipated r-process path. Recently new methods have been developed for the study of neutron-capture reactions on nuclei near or at the r-process path. A multitude of experimental probes have been used to facilitate the production and separation of neutron-rich short-lived nuclei and to measure their specific properties. The traditional tools in the past ranged from extracting fission products from reactors to the use of spontaneous fission sources to the analysis of short-lived reaction products at spallation and fragmentation facilities. The enormous progress in producing neutron-rich isotopes with increasing intensity and resolution was enabled by the simultaneous progress in the development of new experimental techniques and detectors. The traditional approach of tape collection and decay analysis leading to half-life and β–end point determination for single separation products was replaced by large-scale ring experiments for measuring hundreds of masses at once, or complementary to that by sophisticated trapping experiments for determining the masses and decay properties of individual neutron-rich nuclei with unprecedented accuracy. The utilization of these facilities and techniques produced and will produce a wealth of data that will primarily address the needs for knowledge about the properties of neutron-rich nuclei near or at the r-process path; see Fig. 19.

These studies provided important information and input for r-process simulations based on the $(n,\gamma) \rightleftarrows (\gamma,n)$ equilibrium assumptions. Specific challenges remained, such as the (n,γ) nuclear cross section reaction data for simulating the r-process nucleosynthesis after freeze-out. The associated reaction cross

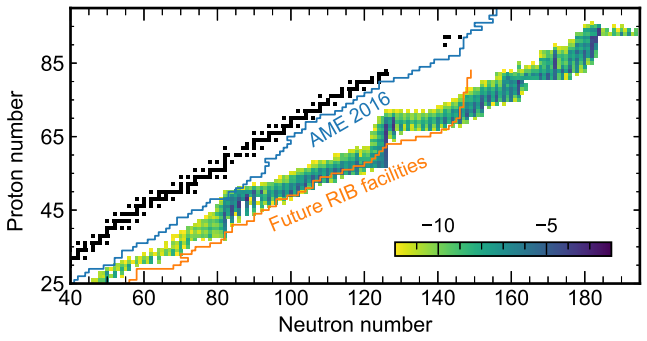

FIG. 19. Nuclear chart with stable nuclei indicated by black squares, the limit of known masses from the 2016 Atomic Mass Evaluation (blue line), the future reach of radioactive ion-beam (RIB) facilities like FRIB or FAIR, and abundance results (color coded) at neutron freeze-out from an *r*-process calculation, utilizing the FRDM masses, combined with Thomas-Fermi fission barriers. Adapted from Giuliani *et al.*, 2020.

sections and reaction rates that are now used in dynamic *r*-process simulations rely entirely on statistical model calculations, utilizing Hauser-Feshbach codes like SMOKER, NON-SMOKER,[4] and TALYS.[5] It is not clear how reliable these predictions for the (n,γ) reaction rates are and how valid they are for reactions on neutron-rich closed-shell nuclei that are characterized by low Q values (neutron binding energies) (Rauscher, Thielemann, and Kratz, 1997). In fact, it is expected that far from stability the direct-capture component dominates, possibly permitting an $(n,\gamma) \rightleftarrows (\gamma,n)$ equilibrium down to low temperatures (Mathews *et al.*, 1983), but how reliable are the predictions for the strength of such direct-capture components (Goriely, 1998; Arnould, Goriely, and Takahashi, 2007)? A direct measurement of neutron-capture reactions on short-lived neutron-rich nuclei is challenging and certainly will not be feasible in the near future. Experimental developments have focused on two approaches that combine theory and experiment to get at the neutron-capture cross sections, the β-Oslo method (Guttormsen, Ramsøy, and Rekstad, 1987; Spyrou *et al.*, 2014, 2017; Tornyi *et al.*, 2014) and surrogate reactions (Escher *et al.*, 2012; Kozub *et al.*, 2012; Manning *et al.*, 2019; Tang *et al.*, 2020), mostly (d,p) to get access to (n,γ) rates. New initiatives have also recently been proposed for direct neutron-capture studies at ring experiments (Reifarth *et al.*, 2017). This proposal is particularly challenging since the idea is to combine, for the first time, a method that couples radioactive beam with radioactive target experiments.

We next discuss in detail the facilities and approaches presently used for the production of neutron-rich nuclei on or near the *r*-process path, along with some of the noteworthy experimental developments in tools and techniques that allow measurements of nuclear masses, β-decay rates, β-delayed neutron emission probabilities, and neutron-capture rates of nuclei required as inputs for reliable simulations of the *r* process.

[4]See https://nucastro.org/reaclib.html.
[5]See http://www.talys.eu/more-about-talys.

A. Production of neutron-rich isotopes

The biggest challenge in experimentally studying isotopes near or at the *r*-process path is the production of these isotopes in sufficient abundances to explore their properties. This is closely correlated with the selectivity of the separators necessary to select the isotopes in question and the sensitivity of the detectors for measuring the respective properties. The overall production of rare isotopes has not significantly improved in recent decades due to the cross section limitations in the production reactions, or the energetics of the facilities to produce beams. However, substantial improvements have been made in the selection process due to innovative techniques in the isotope separation through electromagnetic systems and the increasing utilization of laser-based separation techniques. Enormous progress has also been made on the detection side, and the development of ion trapping techniques has helped overcome many of the statistical limitations in the more traditional measurements of lifetimes, masses, and direct measurements of β-delayed neutron emission probabilities of the extremely neutron-rich nuclei. This section addresses the production of neutron-rich nuclei in reactors, in spontaneous fission sources, in fission products in accelerators, at spallation sources or ISOL facilities, and at fragmentation facilities.

1. Nuclear reactors and fission product sources

One of the traditional methods for the production of neutron-rich nuclei is the extraction and separation of neutron-rich fission products from high flux nuclear reactors. Pioneering work has been done at the TRISTAN separator (McConnell and Talbert, 1975; Talbert *et al.*, 1979) at the Ames Laboratory Research Reactor in Iowa, which was moved in the mid 1970s to the 60 MW High Flux Beam Reactor at Brookhaven National Laboratory (Crease and Seidel, 2000). The fission products were ionized, extracted from a ^{235}U target placed in an ion source located in a beam line close to the reactor core, and separated. A similar separator was installed at the High-Flux Reactor of the Institute Laue Langevin (ILL) in Grenoble, France, where the LOHENGRIN fission fragment separator is used to extract and analyze fission products to study their decay properties (Armbruster *et al.*, 1976). This facility was complemented by the installation of thermoionization separators OSTIS I and II. The OSTIS separator concept (Wünsch, 1978; Münzel *et al.*, 1981) was based on the use of an external neutron guide line bombarding an external ^{235}U source. This approach allowed the measurement of shorter-lived fission products since it reduced the transport times to the ion source. Studies of neutron-rich nuclei were also performed at smaller reactors, even the californium fission source (CARIBU) (Pardo, Savard, and Janssens, 2016) at Argonne National Laboratory, as long as separators were available to select the desired fission product. Measurements of masses, decay half-lives, β-delayed neutron emission probabilities, and γ-ray decay properties were performed with the best techniques available, utilizing moving tape systems. The measurement of neutron-rich isotopes reached close to some of the *r*-process trajectories, in particularly for the alkali isotopes. The measurements on the neutron-rich rubidium isotopes made at that

time (Kratz, 1984) have been rivaled only now, some 30 years later (Lorusso *et al.*, 2015). The main handicaps against reaching the *r*-process path and mapping the neutron-rich nuclei were the fission product distribution and long extraction times for the fission products. All of these measurements had limitations that were overcome with advances and technical developments in detectors, including neutron detection technologies based on ^{6}Li glass, ^{3}He tubes, and ^{3}He spectrometer systems (Kratz *et al.*, 1979; Yeh *et al.*, 1983).

2. Spallation sources and ISOL techniques

The on-line separators for fission products were complemented by ISOLDE (Isotope Separator On-Line DEtector), designed in the mid 1960s for separating spallation products produced by impinging 600 MeV protons from the synchrocyclotron at CERN on a stationary target. The spallation of the heavy target nuclei produced a distribution of target fragments, which were extracted and filtered to separate the desired isotope. The time required for extraction placed a lower limit on the half-life of the isotopes that could be produced by this method. Once extracted, the isotopes were directed to one of several detector stations for measuring the decay properties. The ISOLDE separator was moved in 1990 to the CERN Proton Synchrotron (PS) Booster to increase the yield of the spallation products (Kugler *et al.*, 1992). In a two-step process, the 1 GeV proton beam from the PS Booster, impinging on a Ta or W rod positioned close to the uranium carbide target, produced the fast spallation neutrons to induce fission. This method was essential for suppressing the proton-rich isobaric spallation products that dominated the spallation yield. The new ISOLDE system was one of the most successful sources for neutron-rich isotopes and dominated the production of neutron-rich isotopes for nearly two decades. The implementation of laser ion-source techniques for improving the *Z* selectivity was a significant improvement to studies of neutron-rich nuclei. The laser ionization of the fission products led to a significant reduction in isobar background. This was further improved by using the hyperfine splitting to select or separate specific isomers in neutron-rich isotopes. These gradual improvements of ion-source and separator techniques finally led to the detailed measurement of the *r*-process waiting point nucleus ^{130}Cd, the first milestone in reaching and mapping the *r*-process path (Kratz, Pfeiffer *et al.*, 2000; Dillmann *et al.*, 2003), as well as the recent mass measurements of $^{129-131}$Cd nuclei by Atanasov *et al.* (2015) near the doubly closed magic shell nucleus of ^{132}Sn, a capability that is unmatched to date.

3. Fragmentation sources

Another successful technique for the production of neutron-rich isotopes is the use of fragmentation for the production of neutron-rich, or fusion evaporation for the production of neutron-deficient, isotopes in heavy-ion reactions. The GSI Online Mass Separator was one of the first instruments to utilize fusion evaporation for studying isotopes far from stability using heavy-ion beams from the UNILAC accelerator. The reaction products were stopped in a catcher inside an ion source, from where they were extracted as singly charged atomic or molecular ions and reaccelerated to 60 keV. These beams were implanted, yielding sources for β- or particle-decay spectroscopy (Bruske *et al.*, 1981). This method, however, was more suitable for the study of neutron-deficient isotopes and remained noncompetitive with fission product or spallation based production of neutron-rich isotopes. This instrument was gradually replaced by the projectile fragment separator, known as FRS, to focus on the neutron-rich side of the line of stability (Geissel *et al.*, 1992). Fragmentation was based on smashing a high energy heavy-ion beam on light target material and collecting the fragments through electromagnetic separator systems for subsequent on-line analysis. The great advantage of this technique over the traditional ISOL approach was that even short-lived isotopes could be studied if properly separated. Fragmentation played an increasingly important role for β-decay studies of *r*-process isotopes at the fragment separators at GSI (Kurcewicz *et al.*, 2012), NSCL/MSU in the U.S. (Quinn *et al.*, 2012), and RIKEN in Japan (Lorusso *et al.*, 2015). The measurement of an extremely neutron-rich, doubly closed-shell nucleus ^{78}Ni, at the onset of the *r* process, presented a particularly impressive example on the new relevance of fragment separators for the study of

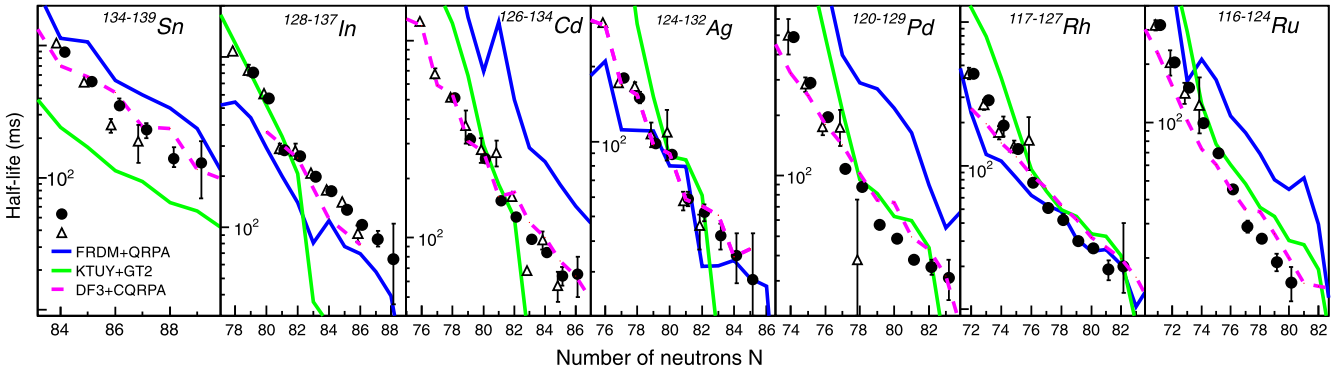

FIG. 20. β-decay half-lives (solid circles) for a number of isotopic chains as a function of neutron number compared to the 2012 NUBASE evaluation (open triangles) (Audi *et al.*, 2012) and the predictions of the models: finite-range droplet model with quasirandom phase approximation (FRDM-QRPA) (dark blue lines) (Möller, Pfeiffer, and Kratz, 2003), gross theory KTUY-GT2 (light green lines) (Tachibana, Yamada, and Yoshida, 1990; Koura *et al.*, 2005), and Fayans density functional with continuum quasirandom phase approximation (DF3-CQRPA) (magenta dashed lines) (Borzov *et al.*, 2008) when available. From Lorusso *et al.*, 2015.

r-process nuclei (Hosmer *et al.*, 2005). The simultaneous measurement of the half-lives of 110 neutron-rich nuclei near the $N = 82$ closed shell at RIKEN (Lorusso *et al.*, 2015) proved to be a substantial step forward for studies of *r*-process nuclei; see Fig. 20. Another example is the systematic study of β-decay half-lives and β-delayed neutron emission processes using the ^{3}He detector array BELEN for 20 heavier isotopes of Au, Hg, Tl, Pb, and Bi in the neutron-rich mass region above the neutron-shell closure $N = 126$ (Caballero-Folch *et al.*, 2016) to probe the feeding pattern of the third *r*-process peak at $A \approx 195$ in astrophysical studies (Caballero *et al.*, 2014; Eichler *et al.*, 2015).

B. Experimental achievements in measuring nuclear properties

In this section, we discuss in more detail the experimental progress in measuring the different nuclear parameters that has been achieved over the four decades of studying nuclei far off the neutron-rich side of stability.

The production of neutron-rich isotopes at ISOL-based systems, both at reactors and at spallation facilities, was limited mainly by the chemistry and extraction time from the ion source. Significant effort went in the development of suitable target materials and ion-source techniques (Ravn, Sundell, and Westgaard, 1975). The choice of isotopes for the study of masses, half-lives, and other decay properties was often dictated by the availability of isotope products rather than physics priorities (Kratz, 2001).

However, over the past decade fragmentation techniques have improved enormously. They allowed the measurement of much shorter-lived neutron-rich radioisotopes, since they were not handicapped by chemical delay processes that were typical for ISOL target systems. With the right target and projectile combination they were able to reach far beyond the range accessible by ISOL facilities. Yet in other cases, such as noble gas and alkali elements, the chemistry conditions are advantageous for ISOL production techniques yielding superior beam intensities. Recent measurements of neutron-rich Rb isotopes (Lorusso *et al.*, 2015) have still been at the limits reached at ISOLDE 20 years earlier (Kratz, 1984; Lhersonneau, Gabelmann *et al.*, 1995; Lhersonneau, Pfeiffer *et al.*, 1995).

Based on the availability of these complementary isotope production modes, in recent decades several new technical developments have led to an enormous improvement in the study of *r*-process masses and decay properties. These have been driven partly by the development of larger high efficiency detection devices, and also by new techniques using storage ring technology to determine masses of multiple isotopes at once, instead of painstakingly extracting and probing one isotope after the other. Other advances have been based on the development of laser traps designed to trap only a few of the selected and collected neutron-rich isotopes and determine their masses and decay characteristics with unprecedented accuracy. The most significant developments are discussed in the following sections.

1. The experimental study of nuclear masses

Mass measurements of selected isotopes near stability have traditionally been performed using mass spectrometers based on magnetic and electric sector fields for separating single isotopes. Modern experimental methods of mass measurement of rare isotopes are generally based on three experimental techniques. Time-of-flight (TOF) mass spectrometry (Meisel and George, 2013) is based on the velocity measurement of short-lived isotopes produced in fragment processes that are analyzed in single-pass spectrometers. The other techniques are frequency-based spectrometry of isotopes in storage rings using Schottky pickup signals of rapidly circulating particles (Litvinov *et al.*, 2004) and Penning traps capable of making measurements with even single trapped particles (Blaum, 2006; Blaum, Dilling, and Nörtershäuser, 2013). The TOF and frequency-based methods are often mentioned as direct mass measurement methods because unknown masses (in fact, mass-to-charge ratios) are directly determined by calibration with well-known masses.

Indirect methods usually rely on the measurement of the energy balance in reaction or decay processes of the isotopes in question. The unknown mass is calculated from known ones in the reaction or decays, plus the determined Q values. This classical approach requires a substantial production of the radioactive isotopes in question to ensure sufficient statistical reliability of the data.

2. Mass measurements in storage rings

Spectrometry of masses at storage rings allows the simultaneous measurements of many nuclei. The ions produced at fragmentation facilities are then stored in storage rings where the relative frequencies of ion revolutions or relative revolution times of the stored ions are related to their relative mass-to-charge ratios and velocities (Yan *et al.*, 2016). To measure the masses of the ions in storage rings, the ions are cooled to minimize the velocity spread. The cooling process requires time, and therefore limits the half-lives that can be measured. This was the principle of the Schottky mass measurement method (Radon *et al.*, 2000; Litvinov *et al.*, 2004). Another approach, named isochronous mass spectrometry (Hausmann *et al.*, 2000, 2001; Sun *et al.*, 2008), removed the limitation on half-lives since it does not depend on cooling. This isochronous mass spectrometry approach resulted in a reduction of the velocity spread by injection of the ions into the isochronous ion optical mode of the ring. That is, the fast and slow ions of the same species are deliberately placed in the longer and shorter orbital paths, respectively, of the ring to yield essentially the same revolution frequency and therefore a reduced velocity spread. Two facilities use these methods for mass measurements at storage rings, the GSI Helmholtz Center in Germany and the Institute of Modern Physics in Lanzhou, China. While these two methods have been used mainly for neutron-deficient nuclei, the masses of $^{129-131}$Cd were recently measured at GSI (Knöbel *et al.*, 2016). There are ongoing plans to implement the same approaches at the Radioactive Isotope Beam Factory in RIKEN and the future FAIR facility at GSI.

3. Mass measurements in traps

Measurements of masses in traps have yielded the most precise and accurate mass measurements to date and present a significant advance over all other methods, including the

storage rings and the traditional β–end point measurements. There are basically two types of traps. Paul traps are based on radio-frequency confinement of ions and Penning traps use electromagnetic fields to trap ions (magnetic fields for radial confinement and electrostatic ones for axial trapping). Coupling of traps to fragmentation or spallation facilities or coupling to spontaneous fissioning sources has significantly extended the reach of high precision and high accuracy measurements, setting new worldwide standards for studies of this fundamental property of the nucleus and its impact on simulations of the *r* process (Blaum, 2006; Blaum, Dilling, and Nörtershäuser, 2013). There are now numerous facilities worldwide, including the Canadian Penning Trap at Argonne National Laboratory; LEBIT at the National Superconducting Cyclotron Laboratory at Michigan State University (MSU) in the United States; TITAN at TRIUMF in Canada; JYFLTRAP in Jyväskylä, Finland; SHIPTRAP at GSI Darmstadt and MAFFTRAP in Munich, Germany; ISOLTRAP at CERN; and RIKEN trap at the SLOWRI facility in Japan. Many of the facilities have implemented or intend to implement multi-reflection time-of-flight spectrograph devices to increase the purity of the ions as well as the range of short-lived exotic nuclei that can be measured. ISOLTRAP at CERN was a pioneer in the field of traps, reaching an uncertainty of a few parts in 10^8 with a resolving power of up to 10^6 with nuclear half-lives of the order of seconds (Eliseev *et al.*, 2013). Exotic neutron-rich nuclei with shorter half-lives required much greater resolving power and led to the introduction of the phase-imaging ion-cyclotron resonance technique (Eliseev *et al.*, 2013). This new technique is based on determining the frequency of the ion by the projection of the ion motion in the trap onto a high-resolution position sensitive microchannel plate detector. The method has been shown to increase the resolving power 40-fold, and at the same time to tremendously increase the speed with which measurements can be made. The higher precision of the measurements has a strong impact on attempts to distinguish sites of the *r* process (Mumpower *et al.*, 2015, 2016; Mumpower, McLaughlin *et al.*, 2017). Recent highlights include precision mass measurement of neutron-rich neodymium and samarium isotopes at the CARIBU facility (Orford *et al.*, 2018), of neutron-rich rare-earth isotopes at JYFLTRAP (Vilen *et al.*, 2018), and neutron-rich gallium isotopes at TITAN (Reiter *et al.*, 2020).

4. Beta-decay studies

Beta-decay measurements are critical for the determination of the half-lives of nuclei along the *r*-process path and for investigating the decay patterns that form the final *r*-process abundance distribution along the line of stability. Beta-decay measurements are typically challenged by the detection efficiency of electrons and neutron-rich ions. This requires not only high production rates at radioactive beam facilities but also sophisticated detector arrangements. New pioneering results for half-lives along the *r*-process path have been measured at RIKEN using stacking of eight silicon double-sided strip detectors such as WAS3ABi (Lorusso *et al.*, 2015; J. Wu *et al.*, 2017) surrounded by an array of 84 high purity germanium (HPGe) detectors of the EURICA array (Söderström *et al.*, 2013). The results are shown in Fig. 20, with a substantially lower experimental uncertainty than previous results, but also indicative of substantial disagreements with the theoretical half-life predictions; see also Sec. V. While silicon has been an excellent choice of detector material, other materials such as Ge with higher Z have recently been commissioned at the NSCL fragmentation facility for use with β-decay experiments. The GeDSSD array shows 50% electron efficiency and greater mechanical stability in allowing the manufacture of thicker detectors (Larson *et al.*, 2013). TRIUMF in Canada has also developed the Scintillating Electron-Positron Tagging Array (SCEPTAR), which comprises 20 thin plastic scintillator beta detectors that surround the implantation point of radioactive ion beams inside a central vacuum chamber surrounded by 16 clover-type, large volume germanium detectors. SCEPTAR has been shown to have an efficiency of ∼80% for electrons emitted from radioactive decays and also provides information on their directions of emission to veto background in the surrounding GRIFFIN HPGe detectors from the bremsstrahlung radiation produced by the stopping of the energetic beta particles. Neutron-rich nuclei are transported to the center of GRIFFIN by a moving tape collector system. The efficiency of this approach has been demonstrated with the measurements of the β-decay half-lives of the ground state and two isomeric states in ^{131}In and the subsequent γ-decay patterns of ^{131}Sn (Dunlop *et al.*, 2019). The sensitivity of this experiment allowed the first detection of γ rays following β-delayed neutron decay for $^{131}\mathrm{In} \rightarrow {}^{130}\mathrm{Sn}$, an important decay branch for many *r*-process nuclei.

5. Beta-delayed neutron emission probability measurements

Beta-delayed neutron emission changes the availability of neutrons and is particularly important since the delayed neutrons can significantly change the abundances of neutron-rich nuclei during freeze-out. While the probabilities of β-delayed neutron emission (P_n) are of great impact for *r*-process simulations, as well as nuclear power reactor designs [for early work see Kratz and Herrmann (1973) and Kratz *et al.* (1982)], the experimental situation is poor since only a few of the P_n values have been measured. Facilities capable of producing neutron-rich nuclei by fragmentation, spallation, or fission sources have invested in a variety of approaches to measure these P_n values.

A number of neutron detection techniques were applied, but multiple counter systems, consisting of a number of ^{3}He counters embedded in a paraffin matrix to thermalize the neutrons for better efficiency, emerged as a standard approach for these kinds of studies. One more recent example was the neutron counter NERO (Pereira *et al.*, 2010), developed at the NSCL/MSU to measure the P_n values of neutron-rich isotopes in the lower mass range that was accessible using fragment production and separation at the A1900 separator. NERO consists of 60 ^{3}He counters embedded in a polyethylene matrix surrounding the collection station to maximize counting efficiency. The efficiency was tested using a ^{252}Cf spontaneous fissioning source and the energy detection range of the detectors was expanded using (α, n) reactions on various target materials. NERO was utilized primarily for the study of medium-mass nuclei in the Co to Cu region (Hosmer

et al., 2010) and in the range of extremely neutron-rich Y, Mo, and Zr isotopes (Pereira *et al.*, 2009), pushing the experiments to nuclei in the $N = 82$ closed neutron-shell region (Montes *et al.*, 2006).

The BELEN detector array is another example of a neutron counter that follows the same concept as NERO. BELEN was conceived as a modular detector that was developed in preparation for experiments at FAIR. Specifically, the DESPEC experiment at FAIR is planned for the measurement of β decays in an array of double-sided silicon detectors called AIDA, in coincidence with the ^{3}He neutron detectors of BELEN, to measure P_n values of exotic nuclei. BELEN-20 consists of two concentric rings of ^{3}He counters (8 and 12 counters, respectively), arranged inside a polyethylene neutron moderator. Early measurements included system testing involving transport of a beam of ions to the center of the neutron detector in front of a Si detector to measure the β decay (Gómez-Hornillos *et al.*, 2011). The most current version of BELEN includes 48 ^{3}He tubes (Calviño *et al.*, 2014; Agramunt *et al.*, 2016) and was recently tested, similarly to BELEN-20, in Jyväskylä, Finland, with fission products produced from the proton-induced fission of thorium. Fission products were swept away by a helium gas jet system into a double Penning trap system that acts as a mass separator, resulting in a relatively pure beam of β-decaying products. The transport system takes on the order of a few hundred milliseconds and imposes a limitation on the lifetimes that can be studied. The BELEN detector is soon to become a part of the largest ever neutron detector of its kind as a part of a 160 ^{3}He counter arrangement being built by the BRIKEN Collaboration for measurements of exotic nuclei at RIKEN. The challenges that remain are the trade-offs between the highest efficiencies and the best energy resolutions for the detection of neutrons. First measurements at the GSI fragment separator focused on the study of nuclei around the $N = 126$ closed shell in the Au to Rn range to determine the half-lives of these isotopes and the P_n values so as to compare them with theoretical model predictions (Caballero-Folch *et al.*, 2016). This work demonstrated that the FRDM coupled with the quasiparticle random phase approximation (QRPA) predictions differ sometimes by up to an order of magnitude from the experimental values. These discrepancies between theoretical predictions and experimental results underline the importance of such studies for exploring the evolution of nuclear structure toward the *r*-process path and beyond.

Recently a new technique was demonstrated in which the challenges of neutron detection were circumvented by measuring the nuclear recoil (Yee *et al.*, 2013), instead of the neutron energy, using traps. The traps can confine a radioactive ion and basically β decay at rest. The emitted radiation emerges with minimal scattering, allowing the measurement of the ion recoil. The β particle is measured in coincidence with the ion, recoiling due to neutron emission, resulting in a time-of-flight spectrum. The proof of principle was demonstrated with a ^{252}Cf fission source, where fission fragments were thermalized in a large volume gas catcher, extracted, bunched, trapped, and mass separated in a Penning trap, then delivered into a β-decay Paul trap. The β particles were detected in a ΔE-E plastic scintillator, while the recoil ions were detected in a microchannel plate detector. The technique allows the measurements of exotic isotopes with half-lives as short as 50 ms while avoiding some of the complications of neutron measurements (Munson *et al.*, 2018; Siegl *et al.*, 2018).

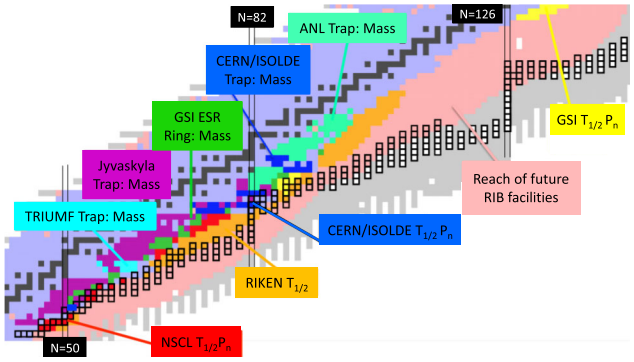

FIG. 21. Summary of recent efforts undertaken at experimental facilities worldwide to attain precise (a) nuclear masses and (b) β-decay properties like half-lives $T_{1/2}$ and delayed neutron probabilities P_n. The individual results at TRIUMF, JYFLTRAP, GSI, CERN, ANL, NSCL, and RIKEN (discussed earlier in this section) are indicated via color coding. Also shown is the region in the nuclear chart in reach of the RIB facilities. Adapted from Horowitz *et al.*, 2019.

Figure 21 provides a summary of the recent experimental efforts and achievements discussed here and in Sec. IV.A.

C. Experiments toward neutron-capture rates

For a long time, the determination of neutron-capture rates on neutron-rich nuclei has been considered of secondary relevance for the simulation of *r*-process nucleosynthesis and scenarios. This is due to the fact that the *r* process is governed by an $(n,\gamma) \rightleftarrows (\gamma,n)$ equilibrium, where the actual reaction rates cancel out as described earlier. However, after freeze-out the equilibrium is no longer maintained and neutron-capture reactions on the neutron-rich reaction products may well shift the abundance distribution toward heavier nuclei. Sensitivity studies with variations of the neutron-capture rates by factors of 10 can result in significant variations in the resulting abundances of the heavy elements (Mumpower *et al.*, 2015). However, the experimental measurements of neutron capture on exotic beams pose significant challenges, in the production of both the exotic nuclei and the neutrons, and in turn in the measurements of the reaction rates.

While the direct measurement of neutron-capture reactions on a stable and even long-lived radioactive isotope for the *s* process has been successful (Guerrero *et al.*, 2017), a similar approach to study neutron capture on short-lived neutron-rich isotopes presents considerable challenges. Most of the *r*-process neutron-capture rates rely on theoretical predictions based on the Hauser-Feshbach statistical model formalism (Rauscher, Thielemann, and Kratz, 1997; Goriely, 1998). To test and verify these predictions a number of indirect methods have been developed in the past decade. These include the so-called Oslo method (Guttormsen, Ramsøy, and Rekstad, 1987) as well as the surrogate reaction technique

(Escher *et al.*, 2012; Kozub *et al.*, 2012; Manning *et al.*, 2019; Tang *et al.*, 2020), while new methods taking a direct experimental approach are being envisioned.

1. Neutron capture on neutron-rich nuclei: β-Oslo method

The Oslo method involves the extraction of level densities and γ-ray strength functions using the measurements of the total deexcitation of a nucleus as a function of energy. The different excitation ranges to be studied are populated by different nuclear reaction modes that can range from light ion transfer reactions to inelastic scattering techniques. This approach requires high intensity beams and the direct measurements of cross sections (Guttormsen, Ramsøy, and Rekstad, 1987) to obtain the level density and strength function data with sufficient statistics for extracting neutron-capture cross sections. A recent adaptation of the Oslo method has been demonstrated in the β-Oslo method, in which the β decay of a neutron-rich nucleus populates the levels at high excitation range and the subsequent γ decay is measured using total absorption spectroscopy (Spyrou *et al.*, 2017). The first version of this approach was developed on the basis of β-decay data obtained at ILL Grenoble and at ISOLDE at CERN (Kratz *et al.*, 1983; Leist *et al.*, 1985). A benchmark test for quantifying the method was the successful comparison between the level density analysis from the study of $^{87}\mathrm{Br}(\beta^{-}n)^{86}\mathrm{Kr}$ through neutron unbound states in $^{87}\mathrm{Kr}$ and the direct $^{86}\mathrm{Kr}(n,\gamma)^{87}\mathrm{Kr}$ resonant neutron-capture data (Raman *et al.*, 1983). An important aspect in this work is the fact that the extracted level density is based on the analysis of the neutron-decay data, selecting configurations prone to neutron capture (and not solely on the γ-decay analysis), which contain all possible excitation modes.

The present β-Oslo method, however, rests mostly on the analysis of γ decay of highly excited states. Neutron unbound states populated by the β decay are less likely to be observed because they primarily decay into the particle rather than the γ channel, as observed in early studies (Raman *et al.*, 1983). Nevertheless, the study of the β-delayed γ decay is a useful tool for determining level densities up to the threshold. The new approach relies on the use of a 4π summing detector device instead of a single Ge detector to analyze the γ-decay pattern. The spectra are then unfolded as a function of excitation energy to determine the nuclear level density and the γ-strength function. The neutron-capture cross section is derived by folding the level density and γ-ray strength function with a nucleon-nucleus optical model potential while adopting statistical assumptions for the neutron transmission channels. The analysis depends critically on a number of assumptions with respect to level density normalization and the optical potential, which possibly introduces systematic uncertainties. However, the largest uncertainty is in the assumption of the density of neutron unbound states above the threshold and the associated neutron strength distribution. This is typically determined from systematics and statistical model simulations. It works well near the stability where the level density above the neutron threshold is high. It becomes more questionable when the method is applied to nuclei at the *r*-process path, where the neutron thresholds and therefore the level density are much lower. A number of measurements have been performed and the extracted results agree well with the predictions of the Hauser-Feshbach simulations (Spyrou *et al.*, 2014), and the uncertainty range in the prediction is claimed to be significantly reduced (Liddick *et al.*, 2016).

The approach suggests a certain redundancy since the experimental data do not consider the neutron strength function above the threshold but instead adopt the one predicted by the same statistical model against which the predicted reaction rates are tested. A study of the systematic uncertainties by Spyrou *et al.* (2017) suggested that the overall uncertainty in the rates obtained by the β-Oslo method is within a factor of ∼3, which is comparable to the uncertainty range of case-optimized Hauser-Feshbach calculations (Beard *et al.*, 2014).

2. Neutron capture by (d,p) surrogate reactions

Single particle transfer reactions such as (d,p) have emerged as a powerful tool for probing the single particle structure of neutron-rich nuclei near the *r*-process path. First (d,p) transfer measurements, using radioactive $^{130,132}\mathrm{Sn}$ beams on CD2 (deuterated polyethylene) targets at the HRIBF of the Oak Ridge National Laboratory, led to a better understanding of the single particle structure of bound states in $^{131,133}\mathrm{Sn}$ (Jones *et al.*, 2010; Kozub *et al.*, 2012). The extracted single particle spectroscopic factors allowed researchers to calculate the direct reaction components for neutron-capture reactions. Higher energy unbound states were not observed. The observation of such states is critical for extracting reliably the single resonant or statistical resonant contributions expected for high level density compound nuclei in (n,γ) reactions. More recently, a similar study was performed at ISOLDE aiming at the determination of the neutron-shell structure below lead and beyond $N=126$ by probing the neutron excitations in $^{207}\mathrm{Hg}$ in the reaction $^{206}\mathrm{Hg}(d,p)^{207}\mathrm{Hg}$ in inverse kinematics (Tang *et al.*, 2020).

The study of the unbound regions of neutron-rich compound nuclei in (n,γ) reactions near the *r*-process path is the primary goal of the surrogate reaction approach, where single particle transfer reactions are utilized to bypass the challenges of measuring neutron-capture cross sections on short-lived nuclei. Neutron-transfer reactions such as (d,p) and $(d,p\gamma)$ are frequently highlighted as surrogates for direct neutron-capture studies (Escher *et al.*, 2012). In surrogate reactions the neutron is carried within a "Trojan" projectile and brought to react with the target. The neutron-capture cross sections on the target nucleus can be extracted by measuring the proton in the final stage (Escher and Dietrich, 2006; Forssén *et al.*, 2007). The first benchmark experiments were performed at the 88-in. cyclotron at Lawrence Berkeley National Laboratory by probing the $^{171,173}\mathrm{Yb}(n,\gamma)$ cross section via the surrogate reaction $^{171,173}\mathrm{Yb}(d,p\gamma)$ using a high intensity deuterium beam (Hatarik *et al.*, 2010). The extracted neutron-capture cross sections agreed within 15% with direct measurements (Wisshak *et al.*, 2000) at energies above 90 keV, while at lower energies considerably larger discrepancies were observed.

In the case of neutron capture on short-lived nuclei, inverse kinematics techniques will be necessary with short-lived radioactive beams interacting with a deuterium target. Neutron-transfer measurement on a radioactive *r*-process nucleus needs large area silicon detector arrays at backward angles in coincidence with an ionization counter at forward angles to detect the beamlike recoils to reduce the beam-induced background. Such a system was developed as the Oak Ridge–Rutgers University Barrel Array (ORRUBA) (Pain *et al.*, 2007). The ORRUBA detector has been used in the center of the Gammasphere Ge array in a combination called Gammasphere Orruba Dual Detectors for $(d, p\gamma)$ studies using stable ^{95}Mo beams (Cizewski *et al.*, 2017), but no conclusive results have been presented. Extracting the neutron-capture cross section out of the surrogate reaction measurements presents its own challenges since it requires proper treatment of nuclear model parameters. Deviations between the results of direct measurements and surrogate reaction studies may reflect insufficient treatment and separation between different reaction mechanisms, such as direct transfer and breakup components (Avrigeanu and Avrigeanu, 2016). While this method is promising, a deeper understanding of the reaction mechanism seems to be necessary (Potel, Nunes, and Thompson, 2015). This was indicated in a recent paper on neutron-capture reactions in neutron-rich Sn nuclei using the surrogate method (Manning *et al.*, 2019). The goal was to determine not the resonant contributions but rather the direct-capture components to low excited states. The spectroscopy method indicated a few single states rather than a broad level distribution. The results deviate from theoretical predictions at a fixed neutron energy of 30 keV, but a broader analysis, including resonances over a wider range of methods, would be necessary for a detailed evaluation.

3. Neutron capture in ring experiments

Recently a new method has been proposed for the direct study of neutron capture on short-lived nuclei, using high intensity radioactive beams in a storage ring on a thermalized neutron target gas produced on line by proton-induced spallation reactions (Reifarth *et al.*, 2017). The cross section of the neutron-capture reactions would be measured in inverse kinematics, detecting the heavy-ion recoils in the ring, using the Schottky method developed at the GSI storage ring facilities (Nolden *et al.*, 2011). This concept is an expansion of earlier work that proposed the use of the high neutron flux in a reactor core as the possible target environment, with the radioactive beam passing through the reactor core in a storage ring (Reifarth and Litvinov, 2014). A number of simulations have demonstrated that both methods seem feasible, albeit technically challenging, since they require the combination of a storage ring facility with either a spallation or fission neutron source. There is a half-life limit that is determined mostly by the production rate at the radioactive ion facility or the beam intensity and the beam losses due to interactions with the rest gas in the ring. Yet such a facility would allow us for the first time to address the challenges of neutron-capture reaction measurements on neutron-rich radioactive isotopes with half-lives less than a minute in the decay products of *r*-process neutron-rich nuclei.

V. NUCLEAR MODELING OF *r*-PROCESS INPUT

A. Nuclear masses

The most basic nuclear property for any *r*-process calculation is the mass of the nuclei involved. It determines the threshold energy for the main reactions during the *r* process: β decay, neutron capture, and photodissociation. Neutron-separation energies S_n are particularly important if the *r* process proceeds in $(n, \gamma) \rightleftarrows (\gamma, n)$ equilibrium, as the reaction path is then fixed at a constant value of S_n for given values of neutron density and temperature of the astrophysical environment. The most commonly used mass tabulations can be grouped into three different approaches: (a) microscopic-macroscopic models like the FRDM approach (Möller *et al.*, 1995, 2015, 2016; Möller, Myers *et al.*, 2012; Möller, Sierk *et al.*, 2012), the extended Thomas-Fermi model with Strutinski integral (ETFSI) approach (Aboussir *et al.*, 1995), the extended Bethe-Weizsäcker formula (Kirson, 2008), and the Weizsäcker-Skyrme mass models (Wang, Liu, and Wu, 2010; Liu *et al.*, 2011); (b) a microscopically inspired parametrization based on the average mean field extracted from the shell model and extended by Coulomb, pairing, and symmetry energies (Duflo and Zuker, 1995); and (c) microscopic models based on the nonrelativistic (Goriely, Chamel, and Pearson, 2016) or relativistic (Sun and Meng, 2008) mean-field models.

All mass models have in common that by fitting a certain set of parameters to known experimental data they are then being used to predict the properties of all nuclei in the nuclear landscape. The models reproduce the experimentally known masses well, with mean deviations between 350 and 600 keV; see Table I. It is quite satisfying to see that when in 2012 a new atomic mass evaluation (AME) (Wang *et al.*, 2012), including 219 new experimental masses, became available, the agreement with data worsened only slightly compared to the comparison with the previous AME. However, when considering only the new experimental masses found in AME-2012, the agreement deteriorates. As the new masses typically involve more exotic nuclei than those found in a previous evaluation, they provide a measure of the capabilities of each model to extrapolate to regions far from stability. This is in general one of the most challenging aspects to address when using a given mass model in *r*-process calculations. Neufcourt

TABLE I. Comparison of the root mean square deviation, in keV, between mass models and experiment. Mass models are FRDM-1992 (Möller *et al.*, 1995), HFB-21 (Goriely, Chamel, and Pearson, 2010), DZ10, DZ31 (Duflo and Zuker, 1995), and WS3 (Liu *et al.*, 2011), and experimental values were taken from 2003 (Audi, Wapstra, and Thibault, 2003) and 2012 evaluations (Wang *et al.*, 2012). The columns labeled "full" consider all masses present in each evaluation, while the column labeled "new" includes masses found in AME-2012 but not those in AME-2003.

Model	AME-2003 (full)	AME-2012 (new)	AME-2012 (full)
FRDM-1992	655	765	666
HFB-21	576	646	584
WS3	336	424	345
DZ10	551	880	588
DZ31	363	665	400

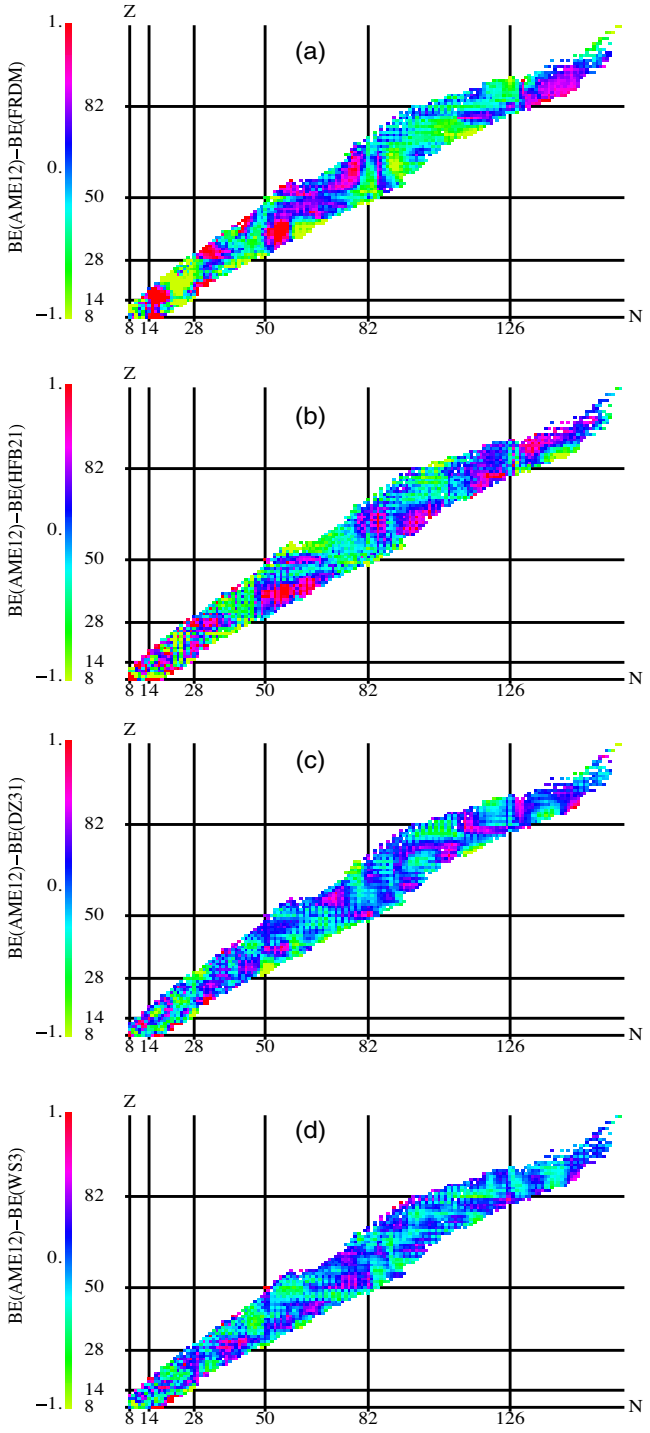

FIG. 22. Differences, in MeV, between experimental energies taken from the 2012 version of the atomic mass evaluation AME12 (Wang *et al.*, 2012) and theoretical binding energies. The following mass models are shown: (a) FRDM-1992 (Möller *et al.*, 1995), (b) HFB-21 (Goriely, Chamel, and Pearson, 2010), (c) DZ31 (Duflo and Zuker, 1995), (d) WS3 (Liu *et al.*, 2011). From Mendoza-Temis, 2014.

et al. (2018) recently applied Bayesian machine-learning techniques to assess the predictive power of global mass models toward more unstable neutron-rich nuclei and provide uncertainty quantification of predictions. Nevertheless, deviations between model and data for neutron-rich nuclei are typically related to bulk properties that may not dramatically affect the abundance predictions, e.g., the symmetry energy whose value is known with an uncertainty of 3.8 MeV to be in the range 29.7–33.5 MeV (Hebeler *et al.*, 2013).

Figure 22 provides a closer comparison between models and data. One notices systematic deviations, such as those for neutron numbers around $N \sim 90$ and 130 just above the neutron-shell closures at $N = 82$ and 126 (Fig. 22). These mass regions are known as "transitional regions" where nuclear shapes change from spherical to deformed configurations, accompanied by a sudden drop in neutron-separation energies. The description of these shape changes is sensitive to correlations that are not fully accounted for in the current mass models. Noticeable differences among the various mass models and the data are also observed in the differences of neutron-separation energies for odd-A and odd-odd nuclei (Arzhanov, 2017), likely pointing to the need for an improved description of neutron-proton correlations. A better description of the transitional region requires beyond-mean-field techniques. The first attempt was presented by Rodríguez, Arzhanov, and Martínez-Pinedo (2015) and based on the generator coordinator method, which considers superpositions of different shapes and restores the breaking of particle number and angular momentum as inherent in the Hartree-Fock-Bogoliubov (HFB) approach. However, first calculations of nuclear masses show only slight effects for nuclei in the $N \sim 90$ range.

Although the differences between the various mass models are rather minute in the transitional regions at $N \sim 90$ and 130, they can have a noticeable impact in r-process simulations. The FRDM (Möller *et al.*, 1995) and version 21 of the Brussels Hartree-Fock-Bogoliubov mass model (HFB21) (Goriely, Chamel, and Pearson, 2010) predict noticeably smaller neutron separation energies than the Duflo-Zuker (Duflo and Zuker, 1995) or the Weizsäcker-Skyrme (WS3) (Wang, Liu, and Wu, 2010; Liu *et al.*, 2011) models in the $N \sim 130$ mass range. As a consequence, for the former two mass tabulations these nuclei act as obstacles in the r-process mass flow and produce a third r-process abundance peak that is narrower in width, overestimated in height, slightly shifted to larger mass numbers, and followed by an abundance trough

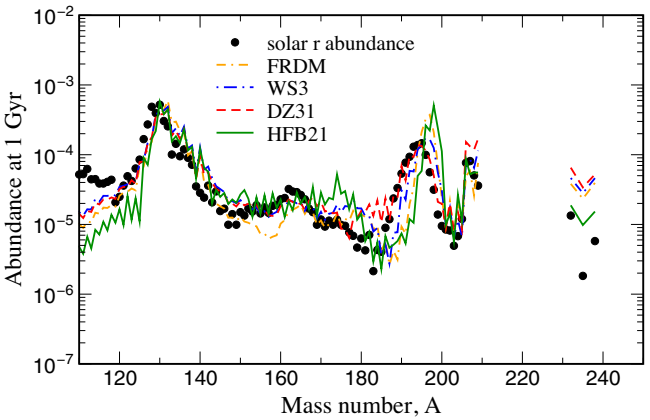

FIG. 23. Final mass-integrated r-process abundances obtained in a neutron-star merger simulation using four different mass models. Adapted from Mendoza-Temis *et al.*, 2015.

just above the peak when compared to simulations using the Duflo-Zuker and WS3 masses and to observational data; see Fig. 23. At $N \sim 90$ the FRDM predicts low neutron separation energies, in contrast to the other mass models (Arcones and Martínez-Pinedo, 2011). As discussed by Mendoza-Temis *et al.* (2015), these low S_n values have consequences for the matter flow between the second and third *r*-process peaks and result in a narrow peak around $A \sim 136$ in the *r*-process abundances at freeze-out, which is, however, washed out at later times due to the continuous production of material in this region by fission. Similar effects were also observed by Martin *et al.* (2016) using masses derived from Skyrme energy density functionals based on different optimization protocols. This allows for systematic studies of uncertainty bands under the same underlying physical model for the description of nuclear masses.

B. Beta-decay half-lives

Nuclear beta decays, which change a neutron into a proton, are responsible for the mass flow to elements with increasingly heavier Z numbers. As the *r* process occurs in a dynamical environment, the time needed for the succession of beta decays to produce thorium and uranium from the seed nuclei available after freeze-out of charged-particle fusion reactions is competing with the dynamical timescale of the explosion, during which matter is transported to larger radii and lower densities. The latter suppresses the neutron number density required for the mass flow to heavier nuclei by neutron captures. Particularly important are beta decays of nuclei with magic neutron numbers N_{mag}, as the matter flow is hindered by the reduced neutron separation energies of the nuclei with $N_{\mathrm{mag}}+1$. Furthermore, because of the extra binding of the magic nuclei, the Q value of their beta decays is relatively reduced, resulting in longer lifetimes.

Calculations of beta decays require two ingredients: the relative energy scale between parent and daughter nuclei (Q value) and the transition strength distribution in the daughter nucleus. We note that the Q values are large for *r*-process nuclei due to the extreme neutron excess. As a consequence uncertainties in this quantity (usually of the order of 0.5–1 MeV) have a mild effect on the half-lives, despite the strong energy dependence of the involved phase space (E^5 for allowed Gamow-Teller transition, and even higher powers for forbidden transitions). However, this strong energy dependence makes the half-life sensitive to the detailed low-lying strength distribution, which is also crucial to determining whether the beta decay is accompanied by the emission of neutrons, i.e., whether the transition proceeds to states in the daughter nucleus above or below the neutron threshold (which is only 2 to 3 MeV in *r*-process nuclei). This so-called β-delayed neutron emission is a source of free neutrons and plays an important role in determining the final *r*-process abundances during the freeze-out of neutron captures (Arcones and Martínez-Pinedo, 2011).

Nucleon-nucleon correlations are responsible for the strong fragmentation of the transition strengths and for its suppression relative to the independent particle model. These correlations are accounted for in the interacting shell model (Caurier *et al.*, 2005), and in fact large-scale shell-model calculations have been proven an appropriate tool to describe nuclear Gamow-Teller distributions (Caurier *et al.*, 1999; Cole *et al.*, 2012) for stellar weak-interaction processes (Langanke and Martínez-Pinedo, 2000, 2003). Shell-model calculations have also proven to be valuable for the calculation of the half-lives of *r*-process key nuclei with magic neutron numbers. For ^{78}Ni the shell model predicted a half-life of 127 ms (Langanke and Martínez-Pinedo, 2003), which was significantly shorter than the value estimated by global models at the time and was subsequently experimentally verified (110 ± 40 ms) (Hosmer *et al.*, 2005). As shown in Fig. 24, the half-lives for the $N = 82$ *r*-process nuclei recently measured at RIKEN (Lorusso *et al.*, 2015) agree well with the earlier shell-model values (Zhi *et al.*, 2013) once the quenching of Gamow-Teller transitions are adjusted to the new ^{130}Cd half-life. The shell-model calculations imply that the half-lives for the $N = 50$ and 82 *r*-process nuclei are dominated by Gamow-Teller transitions and that forbidden strengths contribute only on the few-percent level. This is different for the $N = 126$ *r*-process waiting points. Here two independent large-scale shell-model calculations (Suzuki *et al.*, 2012; Zhi *et al.*, 2013) give evidence that, due to the presence of intruder states with different parity, forbidden transitions contribute significantly and make the half-lives about a factor of 2 shorter than estimated for pure allowed transitions. In turn, the shorter half-lives allow for a faster mass flow through the $N = 126$ waiting points. We note that the relevant forbidden transitions are at low excitation energies, where due to their enhanced phase space energy dependence they can compete with allowed transitions, and hence they have a strong impact on the β-delayed neutron emission probability.

The shell model is the method of choice for β-decay calculations. However, because of the model spaces involved, calculations are possible only for *r*-process nuclei near closed neutron shells. Thus, the global beta-decay rates for *r*-process simulations have to be modeled by less sophisticated many-body models. Traditionally these studies have been performed by calculation of the Gamow-Teller strength distributions within the quasiparticle random phase approximation on the

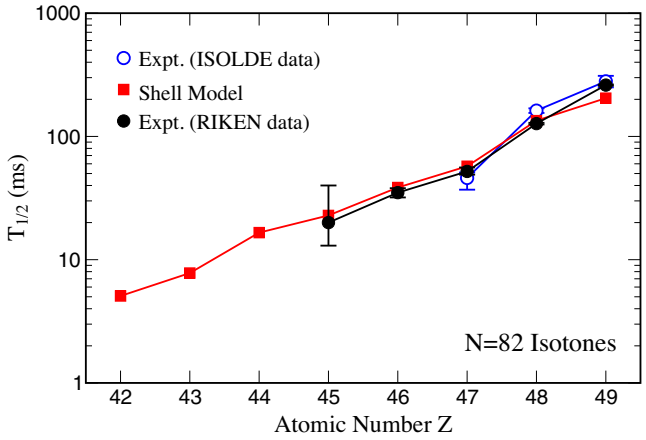

FIG. 24. Comparison of experimental (Pfeiffer *et al.*, 2001; Dillmann *et al.*, 2003; Fogelberg *et al.*, 2004; Lorusso *et al.*, 2015) and shell-model half-lives (Zhi *et al.*, 2013) for $N = 82$ *r*-process nuclei.

basis of the finite-range droplet model (Möller, Nix, and Kratz, 1997) or the ETFSI approach (Borzov and Goriely, 2000). Experimental data for half-lives of *r*-process nuclei around $N = 50$ and 82 (Pfeiffer *et al.*, 2001; Lorusso *et al.*, 2015) showed that these estimates were systematically too long. The FRDM + QRPA model was subsequently extended to include forbidden transitions within the phenomenological "gross theory" (Möller, Pfeiffer, and Kratz, 2003). A promising new road toward globally calculating half-lives for *r*-process nuclei was recently developed by performing QRPA studies on top of the self-consistent Hartree-Fock-Bogoliubov (HFB + QRPA) (Engel *et al.*, 1999) method or density functionals, either nonrelativistic (Borzov, 2003) or relativistic (Marketin, Vretenar, and Ring, 2007). Recent covariant density functional theory ($D3C^* + QRPA$) (Marketin, Huther, and Martínez-Pinedo, 2016), and Skyrme finite-amplitude studies (Mustonen and Engel, 2016; Shafer *et al.*, 2016; Ney, Engel, and Schunck, 2020), which accounted for allowed and forbidden transitions, yielded noticeably shorter half-lives for medium and heavy nuclei than were obtained using the FRDM + QRPA approach.

Shorter half-lives for *r*-process nuclei with $Z > 80$ have a strong impact on the position of the third *r*-process peak (Eichler *et al.*, 2015) and enhance the mass flow through the $N = 126$ waiting points (Mendoza-Temis *et al.*, 2015). The latter implies more material available for fission, thus affecting the abundances of the second *r*-process peak, and the late-time α decays from the decaying *r*-process matter in a neutron-star merger event (Wu, Barnes *et al.*, 2019). Studies of the influence on beta decays on the *r*-process abundances for different astrophysical sites were reported by Mumpower *et al.* (2016), Shafer *et al.* (2016), and Kajino and Mathews (2017).

In principle, the transformation of neutrons into protons can also be achieved by charged-current (ν_e, e^-) reactions. In fact, there have been various suggestions of how neutrino-induced reactions on nuclei might affect *r*-process nucleosynthesis (Haxton *et al.*, 1997; Qian *et al.*, 1997; Meyer, McLaughlin, and Fuller, 1998; Otsuki *et al.*, 2000; Terasawa *et al.*, 2004). All these studies were based on the assumption that the *r*-process operates in the neutrino-driven wind scenario in the presence of strong neutrino fluxes. These assumptions are not supported by modern supernova simulations. In the neutron-star merger scenario neutrino fluxes once the *r* process operates are too low to substantially influence the abundances by charged-current reactions (Roberts *et al.*, 2017). However, the initial proton-to-neutron ratio of the matter ejected in neutron-star mergers and its spatial and time dependence are set by weak reactions on free nucleons; see Sec. VI.

C. Neutron captures

During the *r*-process phase, in which the temperature is large enough ($T \gtrsim 1$ GK), neutron captures and their inverse reactions, photodissociations, are in equilibrium. The rates become relevant once the nucleosynthesis process drops out of this equilibrium. During this period of decreasing temperatures, it is mainly neutron capture that matters.

The neutron-capture and photodissociation rates for *r*-process nuclei (the latter can be derived by detailed balance from the former) are traditionally determined within the statistical model. This assumes a sufficiently high density of states in the daughter nucleus at the relevant capture energies just above the neutron threshold, which is not given for the most neutron-rich nuclei close to the neutron drip line. A systematic estimate about the range of nuclei for which the statistical model is applicable to calculate neutron-capture rates was given by Rauscher, Thielemann, and Kratz (1997). It has been proposed that for the most neutron-rich nuclei the capture rates should be calculated using a direct-capture approach based on a potential (Mathews *et al.*, 1983; Rauscher *et al.*, 1998; Otsuki *et al.*, 2010; Xu and Goriely, 2012; Xu *et al.*, 2014). In such an approach the rate is often determined by a single resonance in the Gamow window (Loens *et al.*, 2012). This makes rate predictions quite uncertain, as nuclear models are not capable of predicting the resonance energies with sufficient accuracy. It has therefore been suggested that the final states should be described by a level density rather than by discrete levels (Goriely, 1997; Ejnisman *et al.*, 1998). Calculations of neutron-capture rates, which include a statistical component and a direct contribution, were reported by Mocelj *et al.* (2007).

The main ingredients of statistical model calculations within the Hauser-Feshbach approach are the nuclear level density, the γ-strength function for the decay of the compound state, and various light-particle potentials. The γ transition can occur with different multipolarities, requiring either different ($E1$) or equal parities ($M1$, $E2$) between the involved states. To also fulfill angular-momentum selection rules requires knowledge of parity- and angular-momentum-dependent level densities.

There has been significant progress in modeling nuclear level densities in recent years. With the shell-model Monte Carlo (SMMC) approach (Johnson *et al.*, 1992; Koonin, Dean, and Langanke, 1997) a tool became available that allows one to determine level densities in unprecedentedly large model spaces. The method to derive level densities within the SMMC was presented by Nakada and Alhassid (1997), Ormand (1997), and Langanke (1998) and then systematically extended to explore the parity dependence (Alhassid, Liu, and Nakada, 1999) and angular-momentum dependence (Alhassid, Liu, and Nakada, 2007). Özen, Alhassid, and Nakada (2015) explored the collective vibrational and rotational enhancement factors, finding that the decay of these enhancement factors is correlated with the pairing and shape phase transitions. The vanishing of pairing and its effect on the level density was studied by Langanke (2006). In the Bethe Fermi gas (BFG) level density formula this vanishing has been described by a temperature-dependent pairing parameter (Grossjean and Feldmeier, 1985; Mustafa *et al.*, 1992; Junghans *et al.*, 1998) for which Langanke (2006) gives a parametrization on the basis of the SMMC calculations. SMMC calculations have been performed for many midmass and heavy nuclei. These include even-even, odd-A, and odd-odd nuclei, allowing one to microscopically test the standard prescription in the BFG level density to describe the systematic differences in these nuclei due to the pairing effect by a pairing shift parameter (Cowan, Thielemann, and Truran, 1991; Rauscher and Thielemann, 2000).

These calculations have initiated and guided attempts to extend a microscopically derived parity dependence into phenomenological level density formulas like the BFG approach. This is achieved by deriving the excitation-energy-dependent parity ratio in the level density using the assumption of Poisson distributed independent quasiparticles combined with occupation numbers obtained from the BCS model, in this way including pairing (Alhassid *et al.*, 2000). Mocelj *et al.* (2007) applied this approach to the large set of *r*-process nuclei (also incorporating a temperature-dependent pairing parameter suggested from SMMC studies), and its effects on astrophysically relevant reaction rates were studied by Loens *et al.* (2008). This improved level density description is part of the statistical model packages NON-SMOKER and SMARAGD developed by Rauscher (Rauscher and Thielemann, 2001; Rauscher, 2011).

A different path to derive parity-dependent and angular-momentum-dependent level densities has been followed by Goriely and co-workers, based on a combinatorial approach within HFB calculations. This approach has also been incorporated into a statistical model package and applied to the calculation of neutron-capture rates for *r*-process nuclei within the Brussels Nuclear Library for Astrophysics Applications (usually called BRUSLIB)[6] (Goriely, Hilaire, and Koning, 2008; Koning, Hilaire, and Goriely, 2008; Hilaire *et al.*, 2010; Goriely, Hilaire, and Girod, 2012).

Traditionally the different γ-strength functions have been described using global parametrizations (Cowan, Thielemann, and Truran, 1991) that were adjusted to photodissociation for $E1$ transitions or electron scattering data for $M1$ transitions (Cowan, Thielemann, and Truran, 1991). Recently $E1$-strength functions that were microscopically calculated for individual nuclei within the framework of the HFB model (Goriely and Khan, 2002; Goriely, Khan, and Samyn, 2004) or based on the relativistic mean-field model (Litvinova *et al.*, 2009) became available. These calculations support the presence of enhanced dipole strength at energies just above the neutron threshold; see also Rauscher (2008). Experimentally such enhanced strength is observed as "pygmy dipole strength" in nuclei with large neutron excess, like those involved in *r*-process nucleosynthesis (Adrich *et al.*, 2005). As shown by Goriely (1998) this enhanced dipole strength can have a significant impact on neutron-capture cross sections.

Dipole γ-strength functions determined from particle-γ coincidence data in neutron pickup and inelastic scattering data for several midmass nuclei exhibit an upbend of the strength toward $E_\gamma = 0$ (Guttormsen *et al.*, 2005; Larsen *et al.*, 2006, 2007). The data also allow for the derivation of the nuclear level density, making a few assumptions (the Oslo method) (Schiller *et al.*, 2000); see Sec. IV.C.1. The impact of this upbend on neutron-capture rates for *r*-process nuclei has been studied (Larsen and Goriely, 2010; Larsen *et al.*, 2015, 2019), and a potential increase of the capture rate by up to 2 orders of magnitude has been calculated. The origin of the low-energy upbend has not yet been completely identified. Coherent adding of magnetic moments of high-j orbitals has been suggested as a possible mechanism for low-energy $M1$ enhancement (Schwengner, Frauendorf, and Larsen, 2013; Brown and Larsen, 2014; Schwengner, Frauendorf, and Brown, 2017), while a low-energy upbend in the $E1$ strength was obtained within finite-temperature relativistic QRPA calculations (Litvinova and Belov, 2013). An upbend in the $M1$-strength function has also been found in large-scale shell-model calculations for selected pf-shell nuclei (Sieja, 2017) and $A \gtrsim 100$ (Sieja, 2018). Goriely *et al.* (2018) performed large-scale calculations of $E1$- and $M1$-strength functions using a combination of shell-model and Gogny-(HFB + QRPA) calculations.

Several general questions regarding basic assumptions made in statistical model evaluations of capture rates have been addressed in large-scale shell-model calculations of the $M1$-strength functions for several midmass nuclei (similar studies for $E1$ transitions are still prohibited by computing limitations, as they require the inclusion of two major shells) (Loens *et al.*, 2012). The results are briefly summarized as follows. (a) The shell-model $M1$-strength functions turned out to give smaller cross sections than the usually adopted parametrizations. (b) The scissors mode, a fundamental orbital $M1$ excitation observed in deformed nuclei at low energies (Bohle *et al.*, 1984), might lead to a noticeable enhancement of the capture rates. (c) The assumption of the Brink hypothesis, i.e., that the strength function is the same for all nuclear states (Brink, 1955, 1957), is valid only to moderate accuracy. (d) The cross section calculated microscopically using a state-by-state approach had the largest contribution from a single state with $M1$ excitations that occur in the Gamow window. Such a nuclear structure effect cannot be caught with any global parametrization. The potential impact of the $M1$ scissors mode on *r*-process neutron-capture cross sections was subsequently revisited by Mumpower, Kawano *et al.* (2017).

The transmission coefficients required in statistical model calculations of astrophysical rates (Cowan, Thielemann, and Truran, 1991; Rauscher and Thielemann, 2000) are calculated on the basis of global optical potentials. For the proton and neutron potentials several rather reliable potentials exist (Jeukenne, Lejeune, and Mahaux, 1977; Bauge, Delaroche, and Girod, 2001; Koning and Delaroche, 2003; Goriely and Delaroche, 2007). The situation is different for the α-optical potential. Although several global potentials exist (McFadden and Satchler, 1966; Demetriou, Grama, and Goriely, 2002, 2003; Kiss *et al.*, 2009; Mohr *et al.*, 2013), none of them are able to consistently describe the existing data at low energies in statistical model approaches. Using ^{64}Zn as an example, Mohr, Gyürky, and Fülöp (2017) explored the sensitivity of the α-induced reaction cross section to the variation of different alpha-optical potential (and other parameters in the statistical model). Attempts have been made to cure the problem. Rauscher (2013) suggested that a consideration of Coulomb excitation leads to better agreement with the data. Demetriou, Grama, and Goriely (2002), Mohr *et al.* (2020), and Szücs *et al.* (2020) showed that a modified imaginary part of the optical potential, particularly at large radii, can improve the reproduction of experimental reaction data at low energies. Based on a large set of α-induced reaction data at

[6]See http://www.astro.ulb.ac.be/bruslib.

sub-Coulomb energies, Avrigeanu, Avrigeanu, and Mănăilescu (2014) and Avrigeanu and Avrigeanu (2015) presented a global α-optical potential for nuclei in the mass range $45 \leq A \leq 209$.

D. Fission

Fission plays an important role in the *r* process, particularly within the NS-NS merger scenario. Fission determines the region of the nuclear chart at which the flow of neutron captures and beta decays stops (Thielemann, Metzinger, and Klapdor, 1983; Petermann *et al.*, 2012; Giuliani, Martínez-Pinedo, and Robledo, 2018; Mumpower *et al.*, 2018; Vassh *et al.*, 2019; Giuliani *et al.*, 2020). In the case of dynamic cold ejecta from mergers, several fission cycles are expected to operate before all neutrons are used (Korobkin *et al.*, 2012; Goriely, 2015; Goriely and Martínez-Pinedo, 2015). It has been suggested that fission is responsible for producing a robust *r*-process pattern (Korobkin *et al.*, 2012; Rosswog *et al.*, 2014; Goriely, 2015) in which the abundances of nuclei with $A \lesssim 140$ are determined during the *r*-process freeze-out from the fission yields of nuclei with $A \lesssim 280$ (Mendoza-Temis *et al.*, 2015).

The description of fission for *r*-process nuclei is challenging, as it sensitively depends on the knowledge of the fission barriers for a broad range of neutron-rich nuclei. In addition, the evolution of the shell structure as function of neutron excess is uncertain. Several competing reaction channels need to be modeled, including neutron capture, neutron-induced fission, beta decay, β-delayed fission, spontaneous fission, alpha decay, and gamma-induced fission. Hence, parallel to the calculation of fission barriers one has to develop models for all the different reaction channels. Several studies have computed barriers for *r*-process nuclei (Howard and Möller, 1980; Myers and Świątecki, 1999; Mamdouh *et al.*, 2001; Goriely *et al.*, 2009; Erler *et al.*, 2012; Möller *et al.*, 2015; Giuliani, Martínez-Pinedo, and Robledo, 2018). It has been shown that the dominating fission channel during *r*-process nucleosynthesis is neutron-induced fission (Panov *et al.*, 2005; Martínez-Pinedo *et al.*, 2007; Petermann *et al.*, 2012). However, the necessary reaction rates have been computed for a limited set of barriers (Thielemann, Cameron, and Cowan, 1989; Panov *et al.*, 2005, 2010; Goriely *et al.*, 2009; Giuliani, Martínez-Pinedo, and Robledo, 2018; Giuliani *et al.*, 2020). This hinders studies of the sensitivity of the *r*-process abundances to the fission barriers. Because of the dominance of neutron-induced fission, the fission barrier itself is the most important quantity for the determination of reliable fission rates, as the fission process occurs at energies just above the fission barrier. In this case, the inertial mass parameter plays a minor role, as tunneling through the barrier has only a negligible contribution. This fact, however, simplifies calculations considerably as the calculation of the inertial mass parameter is rather challenging (Sadhukhan *et al.*, 2013; Giuliani, Robledo, and Rodríguez-Guzmán, 2014; Giuliani, Martínez-Pinedo, and Robledo, 2018).

In addition to the description of the different fission reaction channels, the corresponding fission yields, which depend on the excitation energies of the compound nucleus (Kelic, Ricciardi, and Schmidt, 2008, 2009; Sadhukhan, Nazarewicz, and Schunck, 2016; Schmidt *et al.*, 2016; Zhang, Schuetrumpf, and Nazarewicz, 2016; Schmidt and Jurado, 2018; Schmitt, Schmidt, and Jurado, 2018; Mumpower *et al.*, 2020; Sadhukhan *et al.*, 2020; Vassh *et al.*, 2020), have to be known for *r*-process simulations. As discussed, the fission yields determine the abundance of *r*-process elements in the second *r*-process peak and above and can play an important role for abundance distribution of rare-earth elements (Bengtsson and Howard, 1975; Steinberg and Wilkins, 1978; Panov, Korneev, and Thielemann, 2008; Goriely *et al.*, 2013; Eichler *et al.*, 2015; Vassh *et al.*, 2019).

We emphasize that during the last phase of the *r* process alpha decays compete with fission. This competition determines the final abundances of Pb, U, and Th and of long-lived actinides. Consequently, an improved description of transuranic nuclides is necessary for the determination of the *r*-process abundances produced in neutron-star mergers, with important consequences for the kilonova light curves (Barnes *et al.*, 2016; Hotokezaka *et al.*, 2016; Rosswog *et al.*, 2017; Wanajo, 2018; Zhu *et al.*, 2018; Wu, Barnes *et al.*, 2019).

VI. ASTROPHYSICAL SITES AND THEIR EJECTA COMPOSITION

In Sec. III we discussed conditions that any astrophysical site should attain to produce *r*-process nuclei. They reduce to particular combinations of entropy, expansion timescale, and Y_e in the ejecta. As a minimum requirement the ejecta should be characterized by a high neutron-to-seed nuclei ratio. This is certainly the case for neutron-rich matter, pointing naturally to neutron stars as an important reservoir of neutrons. However, ejecting material from the deep gravitational field of a neutron star requires a cataclysmic event. This could be associated either with the birth of a neutron star in a supernova explosion or with ejecta from a compact binary merger involving a neutron star, leading logically to the most promising sites for a strong *r* process: (i) the innermost ejecta of regular core-collapse supernovae, (ii) a special class of core-collapse supernovae (magnetorotational MHD-jet supernovae or collapsars), with fast rotation and high magnetic fields responsible for their explosion mechanism, which can produce neutron-rich jet ejecta along the poles or from accretion disk outflows, and (iii) ejecta from binary neutron-star mergers or neutron-star black hole systems that are naturally neutron rich and that had already been considered extensively before the observation of GW170817.

A common feature of these scenarios, which is discussed in detail later, is that matter reaches such high temperatures that nuclei are dissociated into free nucleons, and neutrinos become the main cooling mechanism. Those neutrinos and, in particular, electron flavor (anti)neutrinos can interact with the ejecta and reset the composition that is commonly determined by a balance between the following reactions:

$$\nu_e + n \rightleftarrows p + e^-, \tag{8}$$

$$\bar{\nu}_e + p \rightleftarrows n + e^+. \tag{9}$$

In the case of neutrino-driven winds, and potentially also for neutron-star merger ejecta, the material is subject long enough to these processes to reach an equilibrium between neutrino and antineutrino captures (Qian and Woosley, 1996; Thompson, Burrows, and Meyer, 2001; Martínez-Pinedo *et al.*, 2017), resulting in

$$Y_e = Y_{e,\mathrm{eq}} = \left[1 + \frac{L_{\bar{\nu}_e} W_{\bar{\nu}_e}}{L_{\nu_e} W_{\nu_e}} \frac{\varepsilon_{\bar{\nu}_e} - 2\Delta + \Delta^2/\langle E_{\bar{\nu}_e}\rangle}{\varepsilon_{\nu_e} + 2\Delta + \Delta^2/\langle E_{\nu_e}\rangle}\right]^{-1}, \tag{10}$$

with L_{ν_e} and $L_{\bar{\nu}_e}$ the neutrino and antineutrino luminosities, $\varepsilon_\nu = \langle E_\nu^2\rangle/\langle E_\nu\rangle$ the ratio between the second moment of the neutrino spectrum and the average neutrino energy (as is the case for antineutrinos), $\Delta = 1.2933$ MeV the neutron-proton mass difference, and $W_\nu \approx 1 + 1.01\langle E_\nu\rangle/(m_u c^2)$, $W_{\bar{\nu}} \approx 1\text{–}7.22\langle E_{\bar{\nu}}\rangle/(m_u c^2)$ the weak-magnetism correction to the cross sections for neutrino and antineutrino absorption (Horowitz, 2002), with m_u the nucleon mass.

If matter is exposed long enough to neutrinos to reach an equilibrium, these reactions turn matter neutron rich provided that the following condition is fulfilled:

$$\varepsilon_{\bar{\nu}_e} - \varepsilon_{\nu_e} > 4\Delta - \left[\frac{L_{\bar{\nu}_e} W_{\bar{\nu}_e}}{L_{\nu_e} W_{\nu_e}} - 1\right](\varepsilon_{\bar{\nu}_e} - 2\Delta). \tag{11}$$

One should keep in mind an important difference between neutrino emission from protoneutron stars formed in core-collapse supernovae and the emission from a neutron-star merger remnant; see Fig. 25. In the supernova case, we deal with the deleptonization of a hot neutron star, and consequently we expect slightly higher fluxes for ν_e's than for $\bar{\nu}_e$'s. However, owing to the fact that the $\bar{\nu}_e$ spectrum is slightly hotter than the ν_e spectrum, the luminosities of the two flavors are similar. According to Eq. (11) this implies that the average energies between $\bar{\nu}_e$ and ν_e should differ by at least $4\Delta \approx 5.2$ MeV to produce neutron-rich ejecta. Such large differences are not reached in any modern neutrino-wind simulation (Fischer *et al.*, 2010; Hüdepohl *et al.*, 2010; Martínez-Pinedo *et al.*, 2012; Roberts, Reddy, and Shen, 2012; Martínez-Pinedo, Fischer, and Huther, 2014; Mirizzi, Mangano, and Saviano, 2015; Fischer, Guo *et al.*, 2020).

In the case of a neutron-star merger the initial configuration corresponds to a cold neutron-rich neutron star. Because of the merger dynamics the final merger remnant and accretion disk is heated to large temperatures. The large temperatures favor the production of electron-positron pairs and the material tends to protonize toward the new equilibrium Y_e on timescales of hundreds of microseconds as determined by the weak-interaction timescale in matter affected by neutrino interactions (Beloborodov, 2003; Arcones *et al.*, 2010). During this phase the luminosities and average energies of $\bar{\nu}_e$ are much larger than those of ν_e (see the right panels of Fig. 25), reducing the required energy difference of Eq. (11). Hence, even if the impact of neutrino reactions in mergers is expected to be substantial (Perego *et al.*, 2014; Wanajo *et al.*, 2014; Martin *et al.*, 2015, 2018; Sekiguchi *et al.*, 2015, 2016; Foucart *et al.*, 2016) the late ejecta affected by neutrino interactions are still expected to be neutron-rich enough to produce a weak r process, while early dynamic ejecta, emerging from spiral arms after the collision, stay in any case neutron rich and lead to a strong r process.

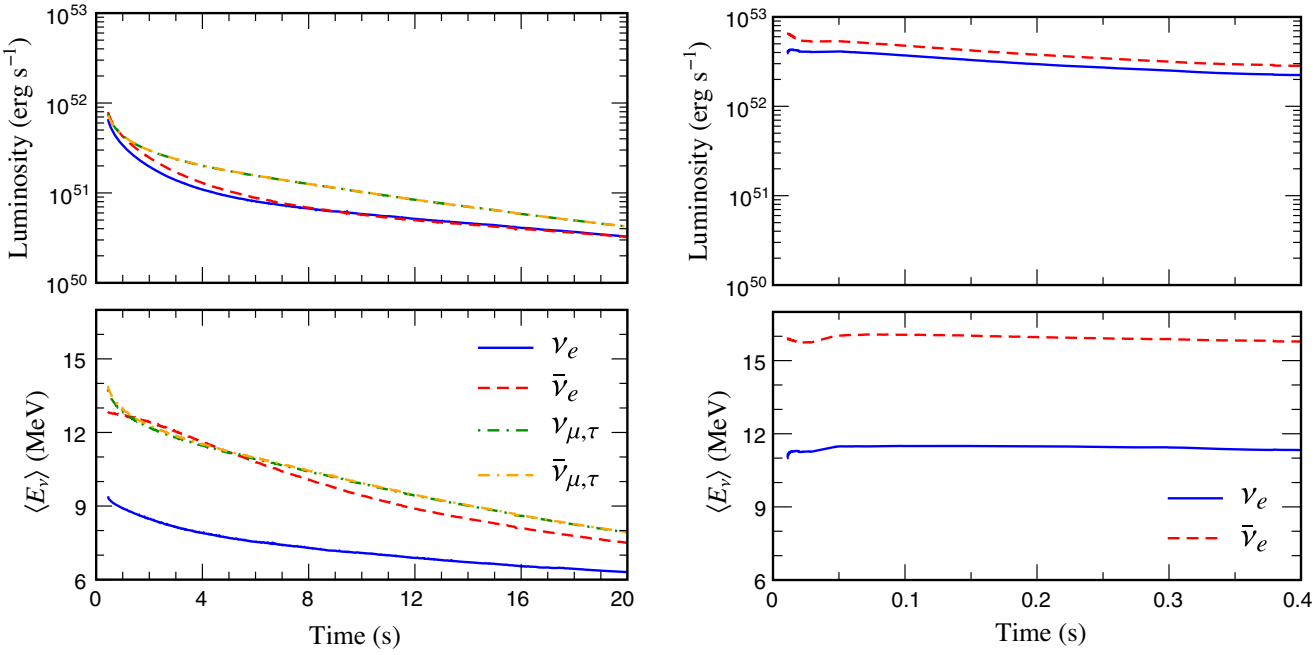

FIG. 25. Left panels: evolution of the luminosities and average energies of neutrinos emitted during the protoneutron star cooling phase following a core-collapse supernova explosion. Adapted from Martínez-Pinedo, Fischer, and Huther, 2014. Right panels: luminosities and average energies of neutrinos emitted after a NS-NS merger that forms a hypermassive neutron star surrounded by an accretion disk. Adapted from Perego, Yasin, and Arcones, 2017.

There is also an important difference between the nucleosynthesis operating in neutrino heated ejecta for supernova and mergers. In the supernova case, due to the high entropies and moderate electron fractions, the material suffers an α-rich freeze-out; see Fig. 17. Under these conditions, if the material is subject to strong neutrino fluxes during the phase of alpha formation, the so-called α effect (Meyer, McLaughlin, and Fuller, 1998) drives the composition to $Y_e \approx 0.5$, hindering the occurrence of an r process. In the case of merger ejecta, due to the more moderate entropies, no alpha formation takes place for $Y_e \lesssim 0.45$ (see Fig. 18), and hence the α effect plays no role.

The previous discussion neglects neutrino flavor transformations and their impact on the Y_e of the ejected material. In the supernova case, the existence of similar spectra for all neutrino flavors hinders the impact of neutrino active-active flavor transformations; see Wu *et al.* (2015). Active-sterile transformations, involving sterile neutrinos on the eV mass scale, as suggested by the reactor (Mention *et al.*, 2011) and gallium (Giunti *et al.*, 2012) anomalies, tend to drive the composition to be more neutron rich (Nunokawa *et al.*, 1997; McLaughlin *et al.*, 1999; Wu *et al.*, 2014; Pllumbi *et al.*, 2015). As discussed, in the case of mergers the $\bar{\nu}_e$ fluxes dominate over those of ν_e. Hence, the neutrino self-interaction potential has a different sign than the neutrino matter potential in the Hamiltonian that describes flavor transformations. This induces conversions via matter-neutrino resonances (Malkus *et al.*, 2012; Foucart *et al.*, 2015; Malkus, McLaughlin, and Surman, 2016; Zhu, Perego, and McLaughlin, 2016; Frensel *et al.*, 2017) and fast pairwise conversions (Wu and Tamborra, 2017; Wu, Tamborra *et al.*, 2017). The existing investigations point to a potential impact on Y_e and thus on the resulting nucleosynthesis.

After this general outline, discussing in detail how weak interactions are setting the stage for the resulting Y_e (and entropy), as they are the dominant criteria for the operation of an r process, we discuss in the following potential environments or sites related to either massive stars or compact objects in binary systems. This leaves out sites of neutron-rich ejecta from core-collapse supernovae (Hillebrandt, 1978), ruled out since the neutrino-powered explosion mechanism has been established (Bethe, 1990), as well as an r process in He layers due to the $^{13}\mathrm{C}(\alpha, n)^{16}\mathrm{O}$ reaction, ruled out since realistic models of massive stars are available (Woosley, Heger, and Weaver, 2002).

A. Possible *r*-process sites related to massive stars

1. Neutrino winds from core-collapse supernovae

Supernovae have been thought to be the origin of the strong r process for many years; see the reviews by Cowan, Thielemann, and Truran (1991), Sumiyoshi *et al.* (2001), and Arnould, Goriely, and Takahashi (2007). While the prompt explosion mechanism has been shown to fail (Bethe, 1990), the development of multidimensional neutrino radiation transport simulations has shown that the neutrino-delayed explosion mechanism remains the most promising scenario to explain the observations; see Kotake *et al.* (2012), Burrows (2013, 2018, 2020), Foglizzo *et al.* (2015), Hix *et al.* (2016), Janka, Melson, and Summa (2016), Müller (2016), Janka (2017a), and Cabezón *et al.* (2018) for reviews. These simulations predict that after the onset of the supernova explosion the hot protoneutron star enters the so-called Kelvin-Helmholtz cooling phase. During this phase, which lasts around 10 s, the protoneutron star deleptonizes, emitting neutrinos of all flavors. Those neutrinos are responsible for producing an outflow of matter known as neutrino-driven wind (Duncan, Shapiro, and Wasserman, 1986) that is expected to operate in each supernova explosion that produces a neutron star. The basic properties of the wind are well understood, based on semianalytical models (Duncan, Shapiro, and Wasserman, 1986; Qian and Woosley, 1996; Hoffman, Woosley, and Qian, 1997; Otsuki *et al.*, 2000; Thompson, Burrows, and Meyer, 2001; Arcones and Thielemann, 2013). These models relate the relevant nucleosynthesis conditions (see Sec. III.C) to fundamental properties including neutrino luminosities, average energy, and mass and radius of the protoneutron star. Early simulations and parametric models (Meyer *et al.*, 1992; Woosley and Hoffman, 1992; Takahashi, Witti, and Janka, 1994; Witti, Janka, and Takahashi, 1994; Woosley *et al.*, 1994; Freiburghaus *et al.*, 1999; Farouqi *et al.*, 2010; Arcones and Martínez-Pinedo, 2011; Kratz, Farouqi, and Möller, 2014) led to impressive results. However, large uncertainties remained, particularly in the determination of entropy and Y_e. Figure 26 shows that the solar r-process abundances can be reproduced, especially when utilizing modern input from nuclear-mass models, but requiring a superposition of entropies of up to $280k_B$ per baryon (and $Y_e < 0.5$).

The development of hydrodynamic simulations (Arcones, Janka, and Scheck, 2007; Arcones and Janka, 2011) showed that such high entropies were out of reach. Nevertheless, they still allowed for the occurrence of a weak r process (Roberts,

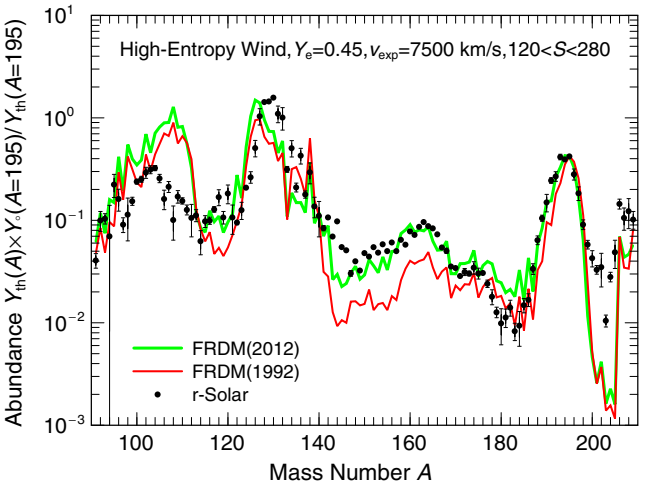

FIG. 26. Results of an r-process calculation assuming an initial $Y_e = 0.45$, adiabatic expansion of matter in a so-called neutrino wind with a given expansion speed v_{exp} of ejected mass shells, and a superposition of entropies S between $120k_B$/baryon and $280k_B$/baryon with equal amounts of matter ejected per entropy interval. Changes due to the utilization of an improved nuclear-mass model are indicated (Möller, Myers *et al.*, 2012; Möller *et al.*, 2016). From Kratz, Farouqi, and Möller, 2014.

Woosley, and Hoffman, 2010; Arcones and Montes, 2011; Akram *et al.*, 2020). Further progress, including the development of neutrino radiation hydrodynamics simulations that follow the entire cooling phase (Fischer *et al.*, 2010; Hüdepohl *et al.*, 2010; Roberts, 2012), improvements in the treatment of neutrino opacities in the decoupling region (Horowitz *et al.*, 2012; Martínez-Pinedo *et al.*, 2012; Roberts, Reddy, and Shen, 2012; Martínez-Pinedo, Fischer, and Huther, 2014; Rrapaj *et al.*, 2015; Bollig *et al.*, 2017; Janka, 2017b; Roberts and Reddy, 2017; Fischer, Guo *et al.*, 2020), and the treatment of convection in the protoneutron star (Roberts *et al.*, 2012; Mirizzi *et al.*, 2016) showed that most or all of the ejecta are proton rich. Under these conditions the nucleosynthesis proceeds via the νp process (Fröhlich, Martínez-Pinedo *et al.*, 2006; Pruet *et al.*, 2006; Wanajo, 2006), producing neutron-deficient isotopes (Fröhlich *et al.*, 2006), including light *p*-process nuclei like ^{92}Mo (Martínez-Pinedo, Fischer, and Huther, 2014; Pllumbi *et al.*, 2015; Eichler *et al.*, 2018; Wanajo *et al.*, 2018).

This result can be understood by considering that in neutrino-driven winds matter is ejected by neutrino energy deposition and is subject to neutrino reactions for a sufficiently long time to permit Y_e to attain the equilibrium value given in Eq. (10). Modern simulations predict similar spectra of ν_e and $\bar{\nu}_e$ leading to proton-rich ejecta; see Fig. 25. These results are robust against the inclusion of neutrino flavor transformations between active flavors (Pllumbi *et al.*, 2015; Wu *et al.*, 2015) but may be affected by the active-sterile flavor transformations (Wu *et al.*, 2014; Pllumbi *et al.*, 2015).

2. Electron-capture supernovae

A way out of the problem in which neutrino irradiation is turning matter proton rich is by considering matter that is ejected promptly with little exposure to neutrinos. This occurs in the so-called electron-capture supernovae in the stellar mass range 8–10 $M_\odot$ (Jones, Hirschi, and Nomoto, 2014), which could lead to a weak *r* process (Kitaura, Janka, and Hillebrandt, 2006; Janka *et al.*, 2008; Wanajo *et al.*, 2009; Wanajo, Janka, and Müller, 2011), possibly producing nuclei up to Eu, but not up to and beyond the third *r*-process peak; for more details see Mirizzi *et al.* (2016). However, there are also strong indications, based on multidimensional hydrodynamic simulations of the oxygen deflagration (Jones, Röpke *et al.*, 2016) and nuclear physics data on the electron-capture rate on ^{20}Ne (Martínez-Pinedo *et al.*, 2014; Kirsebom *et al.*, 2019a, 2019b), that intermediate-mass stars may end their lives as thermonuclear supernovae triggered by electron captures on ^{20}Ne; see Nomoto and Leung (2017a) for a recent review.

3. Neutrino-induced *r* process in the He shell

One of the major requirements for an *r* process to take place is to attain a sufficiently high neutron-to-seed ratio. As already discussed for the high entropy wind, this can also be achieved via a low seed abundance. Banerjee, Haxton, and Qian (2011) and Banerjee *et al.* (2016), following on an idea by Epstein, Colgate, and Haxton (1988), showed that for core-collapse supernovae with metallicities as low as $[\mathrm{Fe/H}] \leq 3$, i.e., those with an extremely low seed abundance, the neutrons released in the He shell by $^4\mathrm{He}(\bar{\nu}_e, e^+n)^3\mathrm{H}$ can be captured to produce nuclei with mass numbers up to $A = 200$ in the stellar mass range of 11–15 $M_\odot$ that are subsequently ejected during the supernova explosion. The caveat of this environment is, that while a sufficiently high neutron-to-seed ratio permits the production of heavy nuclei via neutron captures, the relatively low neutron density n_n leads to an abundance pattern between the *r* process and an *s* process with peaks shifted to higher mass numbers than found for solar *r* abundances. Thus, such a process cannot be an explanation for solar *r*-process abundances and abundance patterns observed in low-metallicity stars.

4. Quark deconfinement supernovae

This scenario considers objects that undergo core collapse and form a central compact protoneutron star, but the neutrino emission from the hot protoneutron star and accreted matter is not sufficient to prevent a further collapse with ongoing mass accretion. The question is whether this second collapse leads directly to black hole formation or can come to a halt (Fischer *et al.*, 2018). A specific equation of state effect was initially introduced by Sagert *et al.* (2009) and Fischer *et al.* (2011), with a quark-hadron phase transition taking place just at the appropriate density and temperature conditions. When adjusting the equation of state properties to presently observed maximum neutron-star masses, Fischer, Wu *et al.* (2020) showed that in such supernovae explosions, expected for a certain stellar mass range, an *r* process can take place in the innermost ejecta. When examining their results, they showed that abundance up to the third *r*-process peak can be obtained; however, the relative abundances beyond the second *r*-process peak are strongly suppressed with respect to solar.

Summarizing the previous discussion, there remains a possibility that core-collapse supernovae can produce *r*-process elements, but they probably do not support a solar-type *r* process up to the third *r*-process peak.

5. Magnetorotational supernovae with jets

Core-collapse with fast rotation and strong magnetic fields is considered to lead to neutron stars with extremely high magnetic fields of the order of 10^{15} G (magnetars) (Duncan and Thompson, 1992; Kramer, 2009; Kaspi and Beloborodov, 2017; Beniamini *et al.*, 2019), connected to a special class of supernovae (Kasen and Bildsten, 2010; Greiner *et al.*, 2015; Nicholl, Guillochon, and Berger, 2017). Such supernovae, induced by strong magnetic fields and/or fast rotation of the stellar core, i.e., MHD SNe, could provide an alternative and robust astronomical source for the *r* process (Symbalisty, Schramm, and Wilson, 1985). Nucleosynthetic studies were carried out by Nishimura *et al.* (2006) based on MHD simulations that exhibited a successful *r* process in jetlike explosions. One important question is whether these earlier results, assuming axis symmetry, also hold in full three-dimensional (3D) simulations, i.e., whether they lead to the ejection of jets along the polar axis. Newtonian 3D MHD simulations with an effective general-relativistic gravitational potential (Marek *et al.*, 2006) and improved treatment of neutrino physics were performed by Winteler *et al.* (2012) for a 15 $M_\odot$ progenitor, utilizing an initial dipole magnetic field of 5×10^{12} G and a ratio of magnetic to gravitational binding

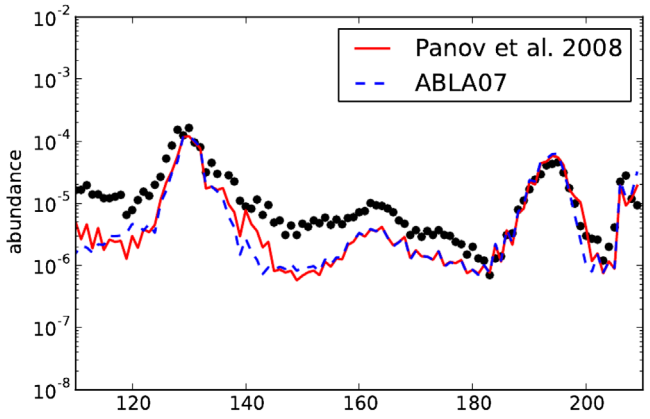

FIG. 27. In a MHD-jet supernova the winding up of magnetic field lines causes the "squeezing out" of polar jets along the rotation axis (Winteler *et al.*, 2012). This environment leads to low entropies, much lower than those discussed in Fig. 17. But in opposition to the Y_e values utilized in Fig. 17, the collapse to high densities resulted in large amounts of electron captures and Y_e values close to 0.1–0.15; see the top of the panel as well as Fig. 18. Such low Y_e's, as under neutron-star merger conditions (where even values as low as 0.03–0.05 can be attained; see Sec. VI.A.6), lead to a strong r process and abundance predictions displayed in the bottom of the panel [shown for the two fission fragment distributions utilized (Kelic, Ricciardi, and Schmidt, 2008; Panov, Korneev, and Thielemann, 2008)]. As Y_e is only moderately low, the effect of late neutron capture by fission neutrons is also moderate, thus avoiding a final shift of the third r-process peak, as indicated in Figs. 32 and 33. From Thielemann, Eichler, Panov, Pignatrari, and Wehmeyer, 2017.

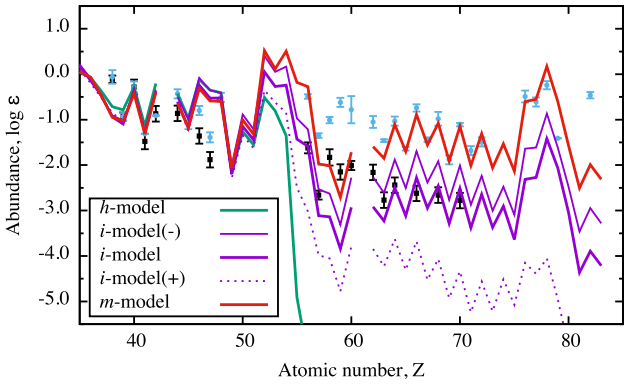

FIG. 28. Abundances from nucleosynthesis calculations with varying ratios of magnetic field strength vs the neutrino heating of regular core-collapse SNe, increasing for the models h, $i-$, i, $i+$, and m. For comparison abundances from MP stars with a weak r process are also shown, i.e., HD122563 (black squares) (Honda *et al.*, 2006), and solar-type r-process observations from CS22892-052 (blue circles) (Sneden *et al.*, 1996). Abundances are normalized for $Z = 40$ of HD122563. Observations of low-metallicity stars with strong r-process contributions vary for abundances below $Z = 50$ (Sneden, Cowan, and Gallino, 2008). From Nishimura *et al.*, 2017.

energy $E_{\rm mag}/W = 2.63 \times 10^{-8}$. These calculations supported and confirmed the ejection of polar jets in three dimensions, attaining magnetic fields of the order of 5×10^{15} G and $E_{\rm mag}/W = 3.02 \times 10^{-4}$ at core bounce, with a successful r process up to and beyond the third r-process peak at $A = 195$; see Fig. 27. Subsequent general-relativistic simulations in 3D MHD (Mösta *et al.*, 2014), involving a 25 $M_\odot$ progenitor with an initial magnetic field of 10^{12} G, led in the early phase to jet formation but experienced afterward a kink instability, deforming the jetlike feature. This probably marks a transition between jetlike explosions and deformed explosions, depending on critical limits in stellar mass, initial rotation, and magnetic fields.

Further high-resolution investigations [resolving the magnetorotational instability (MRI) (Mösta *et al.*, 2015)] have shown that this mechanism can produce magnetar-strength magnetic fields and lead to magnetorotationally powered explosions, even for smaller initial magnetic fields, probably causing the majority of magnetars (Beniamini *et al.*, 2019). However, these are not prompt jetlike explosions on timescales of tens of microseconds, but rather deformed (dual-lobe) explosions on timescales of hundreds of microseconds that experienced the previously mentioned kink instability (Mösta *et al.*, 2018). This underlines the fact that only for high initial magnetic fields can such kink instabilities and long exposures to neutrinos (increasing Y_e) be avoided, ensuring a strong r process. Halevi and Mösta (2018) also analyzed the dependence on the alignment between rotation axis and magnetic fields, where the most aligned cases result in the strongest r process. Recent studies of this phenomenon have been undertaken (Obergaulinger, Just, and Aloy, 2018; Bugli *et al.*, 2020; Obergaulinger and Aloy, 2020; Reichert, Obergaulinger, and Arcones, 2020). The major constraint is the prerequisite of high initial magnetic fields combined with high rotation rates leading to an early (prompt) polar jetlike ejection of neutron-rich matter. In delayed ejections matter experiences interactions with neutrinos, which enhance Y_e and weaken the strength of the r process, as in the supernova neutrino wind (see the previous discussion on that topic).

A number of 2D axisymmetric simulations tested nucleosynthesis features (Nishimura, Takiwaki, and Thielemann, 2015; Shibagaki *et al.*, 2016; Nishimura *et al.*, 2017; Reichert, Obergaulinger, and Arcones, 2020), depending on a variety of conditions in terms of rotation rates, initial magnetic fields, and ratios of neutrino luminosities versus magnetic field strengths. Nishimura *et al.* (2017) performed a series of long-term explosion simulations based on special relativistic MHD (Takiwaki, Kotake, and Sato, 2009; Takiwaki and Kotake, 2011), with outcomes from prompt magnetic jets over delayed magnetic explosions up to dominantly neutrino-powered explosions, determined by the ratio of magnetic field strengths relative to neutrino heating. This also causes a variation of r-process nucleosynthesis results (see Fig. 28), from full-blown strong r-process environments, over a weak r process, not producing nuclei of the third r-process peak, down to no r process at all. Thus, the production for heavy neutron-capture elements varies strongly, with either Fe and Zn dominant as in regular core-collapse SNe or Eu dominant, indicating a strong r process. This is shown in Fig. 29.

The relative fraction that such MHD-jet supernovae contribute to all core-collapse supernovae depends on the distribution of precollapse magnetic field strength and rotation

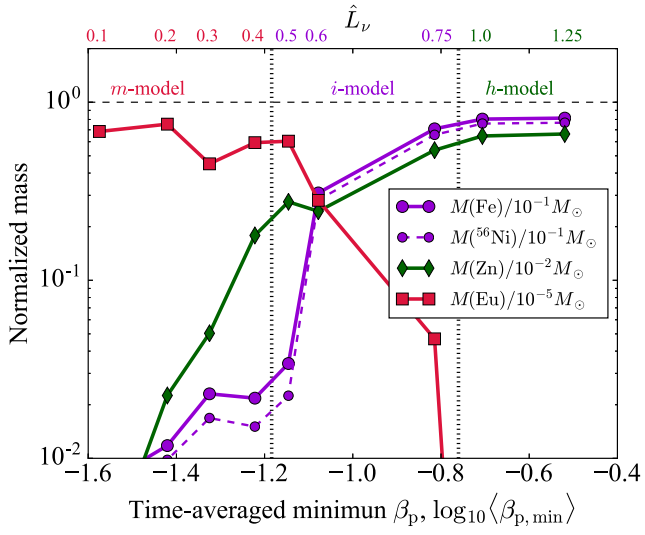

FIG. 29. Nucleosynthesis features of rotating core-collapse SN models (h, $i-$, i, $i+$, m) with varying ratios of neutrino luminosity and magnetic field strengths, as in Fig. 28. Model m represents a strong MHD-jet supernova. One can see the transition from a regular core-collapse SN pattern, dominated by ^{56}Ni, total Fe (after decay), and Zn, to a strong r-process pattern with a high Eu abundance. From Nishimura *et al.*, 2017.

among progenitor stars, which are probably metallicity dependent. Higher metallicities lead to stronger stellar wind loss, accompanied by a loss of angular momentum and thus reducing the fast rotation necessary for this type of SN explosion. These events would eject only small amounts of Fe-group nuclei in case of strong r processing (Nishimura, Takiwaki, and Thielemann, 2015; Nishimura *et al.*, 2017). Figure 29 shows how the Ni/Eu ratio (and similarly the Fe/Eu ratio) varies strongly as a function of neutrino heating versus magnetic field effects. Thus, these types of supernovae alone would be able to provide a large spread in Eu/Fe and might even explain the variations in actinides versus Eu, seen in a number of cases at low metallicities (Wehmeyer, Pignatari, and Thielemann, 2015; Thielemann, Eichler, Panov, Pignatari, and Wehmeyer, 2017). The influence of the explosion mechanism of this type of rare supernovae on their light curves and spectra was discussed by Siegel, Barnes, and Metzger (2019).

6. Collapsars, hypernovae, long-duration gamma-ray bursts

One of the most interesting developments in the study of SNe is the discovery of some highly energetic supernovae [for a review see Nomoto *et al.* (2006)], named hypernovae, whose kinetic energy [in spherically symmetric analysis; see also Piran (2005)] exceeds 10^{52} erg. The most luminous and powerful of these objects, the type Ic supernova (SN Ic) 1998bw (Galama *et al.*, 1998; Patat *et al.*, 1998), was probably linked to the gamma-ray burst GRB 980425, thus establishing for the first time a connection between long-duration gamma-ray bursts (lGRBs) and the well-studied phenomenon of core-collapse SNe. However, SN 1998bw was exceptional, indicating that it synthesized $\sim$0.5 $M_\odot$ of ^{56}Ni with an estimated explosion energy of $E \sim 3 \times 10^{52}$ erg (Iwamoto *et al.*, 1998; Woosley, Eastman, and Schmidt, 1999).

The questions are, where should these events be placed in the stellar mass range and which other features should be related? For nonrotating massive stars only the regular supernova "branch" (with neutron stars as final outcome) can be attained, followed toward increasing stellar mass by a faint or failed supernova branch (leading eventually to black holes, but not to gamma-ray bursts and high ejecta masses). Thus, massive stars, which fail to explode as supernovae via neutrino-powered explosions, will eventually experience the formation of a central BH (Kuroda *et al.*, 2018; Pan *et al.*, 2018). However, rotating BHs and the formation of accretion disks with accretion rates of $\approx 0.1\ M_\odot\ s^{-1}$ can lead, for certain conditions (strong magnetic fields), to lGRBs or hypernovae, also called collapsars. The collapsar model was proposed by Woosley (1993), MacFadyen and Woosley (1999), MacFadyen, Woosley, and Heger (2001), Nagataki *et al.* (2007), Nagataki (2011), and Sekiguchi and Shibata (2011) and includes neutrino heating from the accretion disk and the winding of strong magnetic fields, causing MHD jets (Fujimoto *et al.*, 2006; Ono *et al.*, 2012; McKinney, Tchekhovskoy, and Blandford, 2013; Janiuk, Sukova, and Palit, 2018). Early hydrodynamic simulations (injecting explosion energies artificially) were performed by introducing high explosion energies (up to 10^{52} erg) in either a spherically symmetric way or aspherically to understand jetlike explosions (MacFadyen and Woosley, 1999; Nakamura *et al.*, 2001; Nomoto *et al.*, 2006; Nomoto, Kobayashi, and Tominaga, 2013; Nomoto, 2017).

The basic (consensus) picture has been the following: explosion energies can be found up to 5×10^{52} erg, ^{56}Ni ejecta up to 0.5 $M_\odot$, and relativistic jets responsible for lGRBs exist. There exists uncertainty in predicting Y_e due to weak interactions, and especially neutrino transport. The observational constraint of high ^{56}Ni ejecta argues for a dominant Y_e in matter of the order of 0.5. High explosion energies also lead to high entropies and a strong α-rich freeze-out, including large amounts of ^{45}Sc (which is difficult to produce in other environments), ^{64}Zn (from ^{64}Ge decay), and also other Fe-group elements. Nakamura *et al.* (2001) and Nomoto (2017) concluded that larger abundance ratios for (Zn, Co, V, Ti)/Fe and smaller (Mn, Cr)/Fe ratios are expected than for normal SNe, a feature that seems to be consistent with observations in extremely metal-poor stars.

Self-consistent modeling of the complete event, from collapse, black hole formation, accretion disk modeling, jet ejection, and GRB occurrence is a formidable challenge. Specific investigations, with respect to the role of weak interactions, magnetic fields, and resulting nucleosynthesis in the accretion disk and corresponding outflows, have been undertaken, related either to individual magnetic bubbles (Pruet, Woosley, and Hoffman, 2003; Pruet, Thompson, and Hoffman, 2004) or to the main wind outflows (Beloborodov, 2003; McLaughlin and Surman, 2005; Surman, McLaughlin, and Hix, 2006; Janiuk, 2014, 2017; Siegel and Metzger, 2017; Janiuk and Sapountzis, 2018; Siegel, Barnes, and Metzger, 2019). Beloborodov (2003) found conditions for the minimum accretion rate required,

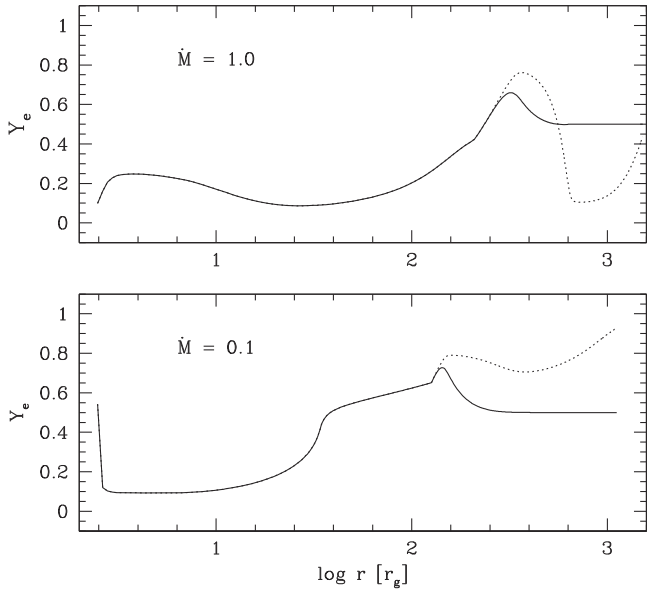

FIG. 30. Radial distribution of Y_e (thick solid line) and proton fraction (dashed line) in a disk, with $\alpha = 0.1$ and $M_{\rm BH} = 3\ {\rm M}_\odot$, for different accretion rates. Y_e indicates neutron-rich conditions deep inside the disk but develops aymptotically to values of 0.5 in the outer layers above $100r_g$ from where the nucleosynthesis outflow will occur. From Janiuk, 2014.

leading to neutron-rich environments with low Y_e's at a given radius

$$\dot{M}_n = 3.821 \times 10^{-3} \left(\frac{r}{3r_g}\right)^{1/2} \left(\frac{\alpha}{0.1}\right) \left(\frac{M_{\rm BH}}{M_\odot}\right)^2 {\rm M}_\odot\,{\rm s}^{-1}. \quad (12)$$

Here $r_g = GM_{\rm BH}/c^2$ is the gravitational radius (half of the Schwarzschild radius), α is the disk viscosity, and $M_{\rm BH}$ is the mass of the central black hole. For typical accretion rates of $0.1\ {\rm M}_\odot\,{\rm s}^{-1}$ this can lead to a low Y_e at small radii in the disk. Larger accretion rates favor smaller Y_e out to larger radii.

Figure 30 shows the Y_e distribution obtained by Janiuk (2014) as a function of the radius. While the central parts of the disk experience a low Y_e, its value reaches $Y_e \approx 0.5$ in the outermost regions and even exceeds 0.5 in the intermediate regions. If the disk outflow occurs from the outer regions, this is consistent with the large ^{56}Ni ejecta observed and found by Pruet, Thompson, and Hoffman (2004), Surman, McLaughlin, and Hix (2006), Janiuk (2014, 2017), and Janiuk and Sapountzis (2018). However, Pruet, Thompson, and Hoffman (2004) also speculated that in the case of strong magnetic fields low Y_e matter can be flung out from more central regions of the disk along magnetic field lines, possibly causing *r*-process production. Additionally, MHD-driven collapsar models, involving black hole accretion disk systems (Nagataki *et al.*, 2007; Fujimoto, Nishimura, and Hashimoto, 2008; Harikae, Takiwaki, and Kotake, 2009), have promoted the argument that the jets produced by the central engine of long-duration gamma-ray bursts can produce heavy *r*-process nuclei (Fujimoto *et al.*, 2007; Fujimoto, Nishimura, and Hashimoto, 2008; Ono *et al.*, 2012; Nakamura *et al.*, 2015). However, we mention here that early studies assumed a simplified treatment of the black hole and the required microphysics. Siegel and Metzger (2017), Janiuk (2019a), and Siegel, Barnes, and Metzger (2019), having performed multi-dimensional MHD simulations for accretion disk outflows, argued that large amounts ($> 0.1\ {\rm M}_\odot$) of *r*-process material can be ejected. If this scenario materializes, it will be sufficient to have about one such event per 1000–10 000 core-collapse supernovae to explain the solar *r*-process abundances.

The open question is whether both large amounts of ^{56}Ni expected for hypernovae and *r*-process ejecta can be produced in the same event. Siegel, Barnes, and Metzger (2019) argued that the ^{56}Ni would have to come from a preceding supernova explosion phase, leaving an intermittent neutron star before further accretion causes black hole formation and a black hole accretion disk. This begs the following questions: (a) At which stellar progenitor masses do we have a transition from the formation of neutron stars to the formation of black holes after collapse? (b) In which transition region do neutron stars initially form, causing a regular supernova explosion, but ongoing accretion leads to a black hole? (c) For which progenitor masses are black holes formed directly during collapse, and how can this be observed? (d) What is the role of rotation and magnetic fields to cause lGRBs, and can we give reliable nucleosynthesis yields for such events? (e) Is there a separation in different types of events, depending on the parameters in (d), leading either to hypernovae and strong ^{56}Ni ejecta or systems with a large outflow of *r*-process elements? (f) Are jets and lGRBs occurring in both types of events?

The scenario suggested by Siegel, Barnes, and Metzger (2019) relates to question (b) and case (c). The main question is whether a strong supernova or hypernova explosion with large Ni production could take place before the accretion disk outflows eject *r*-process material in the same event or *r*-process outflows could occur without causing a hypernova. Further observations will have to constrain such events.

B. Neutron-star and neutron-star–black hole mergers

Neutron stars [for historical references see Landau (1932), Baade and Zwicky (1934), and Hewish and Okoye (1965)], when being part of a compact binary system, lose energy by emission of gravitational waves as predicted by general relativity and are expected to merge (Hulse and Taylor, 1975). Observed systems suggest timescales of $\sim 10^8$ yr for this inspiral (Weisberg and Huang, 2016), but a larger range of timescales is expected, depending on initial separations and excentricities of the orbit. Simultaneously with the discovery of binary pulsars, it was suggested that neutron-star or neutron-star–black hole mergers would eject *r*-process nuclei (Lattimer and Schramm, 1974, 1976; Symbalisty and Schramm, 1982), followed up by a first detailed analysis of possible abundance distributions (Meyer and Schramm, 1988). Later predictions showed that such mergers would be accompanied by neutrino and gamma-ray bursts (Eichler *et al.*, 1989). The first predictions of mass ejection from neutron-star mergers in Newtonian approximation were given by Davies *et al.* (1994), Ruffert, Janka, and Schaefer (1996), and Rosswog *et al.* (1999, 2000). The first detailed nucleosynthesis prediction was provided by Freiburghaus, Rosswog, and Thielemann (1999).

Thereafter, extensive investigations have been undertaken with respect to nucleosynthesis predictions (Panov and Thielemann, 2004; Panov, Korneev, and Thielemann, 2008; Goriely, Bauswein, and Janka, 2011; Korobkin *et al.*, 2012; Bauswein, Goriely, and Janka, 2013; Goriely *et al.*, 2013, 2015; Hotokezaka, Kyutoku, and Shibata, 2013; Panov *et al.*, 2013; Perego *et al.*, 2014; Rosswog *et al.*, 2014; Wanajo *et al.*, 2014; Eichler *et al.*, 2015; Hotokezaka, Piran, and Paul, 2015; Just *et al.*, 2015, 2016; Martin *et al.*, 2015; Mendoza-Temis *et al.*, 2015; Ramirez-Ruiz *et al.*, 2015; Radice *et al.*, 2016; Shibagaki *et al.*, 2016; Wu *et al.*, 2016; Roberts *et al.*, 2017; Martin *et al.*, 2018; Papenfort, Gold, and Rezzolla, 2018; Radice, Perego, Hotokezaka, Fromm *et al.*, 2018; Wojczuk and Janiuk, 2018; Holmbeck, Sprouse *et al.*, 2019). Initial Newtonian approaches (Ruffert and Janka, 2001) have been replaced with conformally flat and fully relativistic treatments (Shibata and Uryū, 2000; Oechslin, Rosswog, and Thielemann, 2002; Oechslin *et al.*, 2004; Shibata and Uryū, 2006; Oechslin, Janka, and Marek, 2007; Shibata and Taniguchi, 2011; Bauswein and Janka, 2012; Bauswein, Goriely, and Janka, 2013; Hotokezaka, Kyutoku, and Shibata, 2013; Wanajo *et al.*, 2014; Sekiguchi *et al.*, 2015, 2016; Radice *et al.*, 2016; Baiotti and Rezzolla, 2017; Bovard *et al.*, 2017; Papenfort, Gold, and Rezzolla, 2018), and further followed by the inclusion of magnetic fields (Price and Rosswog, 2006; Anderson *et al.*, 2008; Liu *et al.*, 2008; Giacomazzo, Rezzolla, and Baiotti, 2009; Obergaulinger, Aloy, and Müller, 2010; Zrake and MacFadyen, 2013; Giacomazzo *et al.*, 2015; Kiuchi *et al.*, 2015) as well as their interplay with neutrinos (Palenzuela *et al.*, 2015; Guilet *et al.*, 2017).

In parallel to NS-NS mergers NS-BH mergers have also been investigated (Rosswog, 2005; Shibata and Uryū, 2006; Chawla *et al.*, 2010; Shibata and Taniguchi, 2011; Korobkin *et al.*, 2012; Wanajo and Janka, 2012; Kyutoku, Ioka, and Shibata, 2013; Foucart *et al.*, 2014; Mennekens and Vanbeveren, 2014; Rosswog *et al.*, 2017; Brege *et al.*, 2018). A common outcome of a NS-NS merger and some NS-BH mergers is the formation of an accretion disk surrounding a central remnant (Ruffert *et al.*, 1997); discussed later.

From the point of view of *r*-process nucleosynthesis, simulations should predict the amount of ejecta, their properties (particularly Y_e), spatial distribution, and temporal evolution. In the following, we discuss the major phases of ejection and the general dependencies on the merging system. The discussion is mostly based on a presentation made by Shibata (2018); see also Shibata and Hotokezaka (2019) and Radice, Bernuzzi, and Perego (2020). Figure 31 summarizes the main ejection channels in compact binary mergers and provides estimates of ejecta mass, Y_e, and velocity. See also Fig. 1 given by Bartos, Brady, and Márka (2013) for estimated behaviors dependent on the mass of the binary components involved.

Because of the emission of gravitational waves, which reduces the eccentricity of the orbit, at times close to coalescence NS-NS systems are expected to have almost circular orbits and spins much smaller than the orbital frequency (Rosswog, 2015). During the coalescence phase matter is ejected dynamically due to angular-momentum conservation on timescales of milliseconds with mildly relativistic speed $v \sim (0.2-0.4)c$ (Rosswog *et al.*, 1999, 2000; Bauswein, Goriely, and Janka, 2013; Hotokezaka, Kiuchi, Kyutoku, Okawa *et al.*, 2013; Palenzuela *et al.*, 2015; Sekiguchi *et al.*, 2015, 2016; Foucart *et al.*, 2016; Radice *et al.*, 2016).

The amount of dynamic ejecta and their properties depend on the compactness of the neutron stars and their mass ratio (Bauswein, Goriely, and Janka, 2013; Hotokezaka, Kiuchi, Kyutoku, Okawa *et al.*, 2013; Radice, Perego, Hotokezaka, Fromm *et al.*, 2018). Two components can be distinguished: cold tidal ejecta in the equatorial plane and shock-heated ejecta originating from the contact interface with a more isotropic distribution. Systems with small mass ratios tend to eject larger amounts of material mainly in the equatorial region, while for similar masses the shock-heated component dominates (Bauswein, Goriely, and Janka, 2013; Hotokezaka, Kiuchi, Kyutoku, Okawa *et al.*, 2013; Palenzuela *et al.*, 2015; Lehner *et al.*, 2016). While the cold tidal ejecta maintain the original low Y_e of the outer regions of the neutron star from which they are ejected, the shock component is heated to high temperatures. This drives electron and positron captures that increase Y_e from a low initial value. As the material moves away, Y_e is further increased by ν_e and $\bar{\nu}_e$ absorption (Wanajo *et al.*, 2014; Goriely *et al.*, 2015; Martin *et al.*, 2015, 2018; Radice *et al.*, 2016; Sekiguchi *et al.*, 2016). The impact of neutrino absorption is sensitive to the evolution of the central remnant (Sekiguchi *et al.*, 2015). The total amount of dynamic ejecta are in the range 10^{-4}–10^{-2} $M_\odot$ (Bauswein, Goriely, and Janka, 2013; Hotokezaka, Kiuchi, Kyutoku, Okawa *et al.*, 2013; Sekiguchi *et al.*, 2015, 2016; Lehner *et al.*, 2016; Radice, Perego, Hotokezaka, Fromm *et al.*, 2018) with an angular mass distribution well approximated by $F(\theta) = \sin^2\theta$ (Perego, Radice, and Bernuzzi, 2017) and a Y_e distribution that can reach $Y_e \sim 0.5$ in the polar region (Shibata *et al.*, 2017; Radice, Perego, Hotokezaka, Fromm *et al.*, 2018; Shibata and Hotokezaka, 2019). Magnetohydrodynamic instabilities, operating during the merger, can produce a third component denoted as "viscous-dynamical" ejecta (Radice, Perego, Hotokezaka, Bernuzzi *et al.*, 2018), with asymptotic velocities extending up to $\sim 0.8c$. The analysis of the tidal deformability from the gravitational wave observations of GW170817 (Abbott *et al.*, 2018; De *et al.*, 2018; Most *et al.*, 2018; Capano *et al.*, 2020), the observation of an electromagnetic transient that disfavors a prompt collapse to a black hole (Bauswein *et al.*, 2017; Margalit and Metzger, 2017, 2019; Shibata *et al.*, 2017; Coughlin *et al.*, 2019), together with nuclear physics constraints (Annala *et al.*, 2018; Fattoyev, Piekarewicz, and Horowitz, 2018; Tews, Margueron, and Reddy, 2018, 2019; Capano *et al.*, 2020) favor moderately compact neutron stars with a radius in the range 8.9–13.2 km. In this case, the major source of ejecta is the contact interface between the neutron stars (Bauswein, Goriely, and Janka, 2013; Sekiguchi *et al.*, 2015; Radice, Perego, Hotokezaka, Fromm *et al.*, 2018). The maximum mass of a neutron star has been constrained to $M_{\max} \lesssim 2.17\ M_\odot$ (Margalit and Metzger, 2017; Shibata *et al.*, 2017; Rezzolla, Most, and Weih, 2018; Ruiz, Shapiro, and Tsokaros, 2018) following the observation of GW170817.

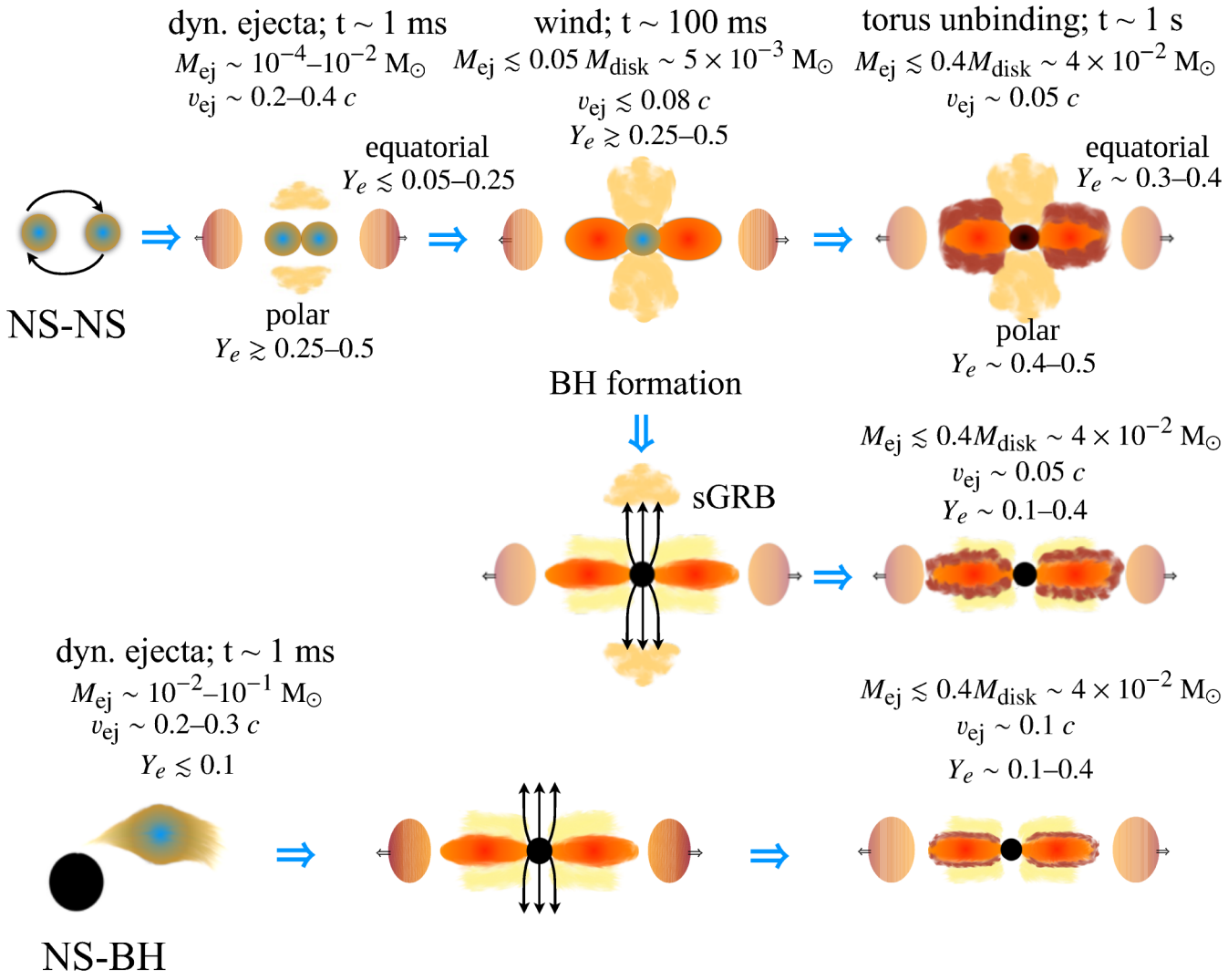

FIG. 31. Ejection channels in compact binary mergers including estimates based on simulations of the ejecta mass, Y_e, and velocity during the different ejection phases. The NS-NS merger system shown in the upper part includes two possible outcomes: a long-lived massive neutron star and a hypermassive neutron star that collapses to a black hole on a timescale shorter than the disk lifetime. The BH-NS merger is shown in the lower part. Adapted from Rosswog *et al.*, 2017.

Recently another NS-NS merger GW190425 with a combined total mass of ~3.4 $M_\odot$ has been observed (B. P. Abbott *et al.*, 2020). The high total mass, together with the absence of an electromagnetic signal, suggests a prompt collapse to a black hole (Foley *et al.*, 2020). In the case of NS-BH systems it is necessary that the NS be tidally disrupted by the BH in order to eject material. Tidal disruption means that the BH tidal force is larger than the self-gravity of the NS. The amount of ejected mass depends on the relative competition between the orbital separation at which tidal disruption occurs and the radius of the innermost stable circular orbit of the BH. The larger this ratio, the larger the amount of ejecta. This requires a large NS radius, a small BH mass or small BH/NS mass ratio, or a high spin for the BH (Kyutoku *et al.*, 2015; Capano *et al.*, 2020). We notice that mass ejection may occur even if the neutron star is disrupted inside the innermost stable circular orbit (Faber *et al.*, 2006). Population synthesis studies favor a BH/NS mass ratio ~7 (Belczynski *et al.*, 2010). This, together with the previously mentioned NS radius constraints, suggests that mass ejection will take place only for a BH with a spin parameter $\chi = cJ/(GM^2) \gtrsim 0.5$ (Foucart, 2012; Foucart *et al.*, 2013, 2014; Kyutoku *et al.*, 2015, 2018; Kawaguchi *et al.*, 2016; Brege *et al.*, 2018). For possible χ values of the recent BH-NS candidate GW190426; see Fig. 4 of Lattimer (2019) and R. Abbott *et al.* (2020b). The tidal dynamic ejecta are much more anisotropic than those of NS-NS mergers. They are mainly concentrated around the orbital plane and often sweep out only half of the plane. The ejected mass can reach ~0.1 $M_\odot$ with asymptotic velocities of $(0.2$–$0.3)c$. The material is extremely neutron rich ($Y_e \lesssim 0.1$) and not affected by neutrino irradiation (Foucart *et al.*, 2014; Kyutoku *et al.*, 2018).

An equally common outcome of compact binary mergers is the production of a rotating torus surrounding the newly formed central object with a typical mass of 0.1 $M_\odot$ (Ruffert *et al.*, 1997; Shibata and Taniguchi, 2006; Radice, Perego, Hotokezaka, Fromm *et al.*, 2018). In the case of BH-NS mergers the central remnant is a BH and we deal with a

neutrino cooled disk that evolves on viscous timescales of seconds. The study of such systems has evolved from the use of α-viscosity prescriptions to parametrize dissipation (Fernández and Metzger, 2013, 2016; Metzger and Fernández, 2014; Fernández *et al.*, 2015; Just *et al.*, 2015, 2016; Wu *et al.*, 2016; Fujibayashi *et al.*, 2018; Wojczuk and Janiuk, 2018) to three-dimensional general-relativistic magnetohydrodynamic simulations (Siegel and Metzger, 2017, 2018; Fernández *et al.*, 2019; Janiuk, 2019b) in which dissipation emerges naturally via the magnetorotational instability. These works find that up to 40% of the disk mass, depending on the BH spin, is unbound in a quasispherical fashion. The electron fraction in the outflow is in the range $Y_e \sim 0.1$–0.4 with velocities $v \approx 0.1c$ (Siegel and Metzger, 2018; Christie *et al.*, 2019; Fernández *et al.*, 2019; Fujibayashi *et al.*, 2020), depending on the efficiency of dissipation in the disk. For the case of NS-NS mergers, the possibilities for the central object are a stable NS, a long-lived massive neutron star [(MNS), i.e., a NS with a mass above the maximum mass for a nonspinning NS and below the one for a uniformly rotating NS], a hypermassive neutron star [(HMNS), i.e., a NS with a mass above the maximum mass for a uniformly rotating NS (Baumgarte, Shapiro, and Shibata, 2000)], or a BH depending primarily on the total mass of the binary M_t (Hotokezaka, Kiuchi, Kyutoku, Muranushi *et al.*, 2013; Shibata, 2018). If M_t exceeds a critical value M_c, the central object produced by the merger collapses promptly to a BH on the dynamical timescale of a few milliseconds (Sekiguchi *et al.*, 2011). On the other hand, if $M_t < M_c$ the resulting HMNS is at least temporarily supported against gravitational collapse by differential rotation and thermal pressure (Hotokezaka, Kiuchi, Kyutoku, Muranushi *et al.*, 2013; Kaplan *et al.*, 2014). The value of M_c depends on the uncertain equation of state (EOS) of nuclear matter, particularly its stiffness, mainly related to the symmetry energy (Baldo and Burgio, 2016; Oertel *et al.*, 2017). The discovery of massive (~ 2 $M_\odot$) neutron stars (Demorest *et al.*, 2010; Antoniadis *et al.*, 2013) places a lower limit of $M_c \gtrsim 2.6$–2.8 $M_\odot$ (Hotokezaka, Kiuchi, Kyutoku, Muranushi *et al.*, 2013). Hydrodynamical simulations of neutron-star mergers for a large sample of temperature-dependent equations of state, show that the ratio between critical mass and the maximum mass of a nonrotating NS are tightly correlated with the compactness of the nonrotating NS (Bauswein, Baumgarte, and Janka, 2013). This allows one to derive semianalytical expressions for the critical mass (Bauswein, Stergioulas, and Janka, 2016; Bauswein and Stergioulas, 2017, 2019) that, combined with the GW170817 constraints on the maximum mass and radius of NS, give $M_c \approx 2.8$ $M_\odot$. It thus appears likely that the canonical $1.35 + 1.35$ $M_\odot$, including GW170817, binary merger goes through a HMNS phase. The duration of this phase depends on angular-momentum transport processes (gravitational wave emission, magnetic fields, etc.) and the EOS as it determines the value of M_c (Shibata, Taniguchi, and Uryū, 2005; Shibata and Taniguchi, 2006; Kiuchi *et al.*, 2009; Hotokezaka *et al.*, 2011; Kastaun, Ciolfi, and Giacomazzo, 2016). For a soft EOS that results in compact initial neutron stars before the merger, the HMNS collapses to a black hole on timescales of several tens of milliseconds, while for a stiff EOS the HMNS is long lived with a lifetime longer than the timescales relevant for matter ejection. The previously mentioned NS radius constraints favor the first case. For the case of prompt collapse to a BH, the BH-torus system evolves similarly to the BH-NS merger case considered earlier. However, systems with large M_t are expected to eject little mass dynamically and produce a low-mass accretion disk. In these cases, the total amount of ejecta, dynamical plus accretion disk, is $\sim 10^{-3}$ $M_\odot$ of neutron-rich material $Y_e \lesssim 0.1$ (Shibata, 2018).

The HMNS torus is characterized by a more important role of neutrino heating that increases the amount of ejecta and raises their Y_e to values that depend on the lifetime of the HMNS remnant (Kaplan *et al.*, 2014; Metzger and Fernández, 2014; Perego *et al.*, 2014; Martin *et al.*, 2015; Lippuner *et al.*, 2017; Fujibayashi *et al.*, 2018). The ejecta consist of two components that are either neutrino driven or viscous driven (also known as secular). The neutrino-driven component is ejected mainly in the polar direction with velocities $v \lesssim 0.08c$ and $Y_e \gtrsim 0.25$ and containing around 5% of the disk mass (Martin *et al.*, 2015; Perego, Radice, and Bernuzzi, 2017). The viscous-driven component occurs mainly in the equatorial direction with a velocity $v \sim 0.05c$ and contains around 40% of the disk mass (Metzger and Fernández, 2014; Lippuner *et al.*, 2017; Fujibayashi *et al.*, 2018). The Y_e distribution depends on the lifetime of the HMNS (Fujibayashi *et al.*, 2018). If the HMNS survives at least for the timescale of neutrino cooling of the disk (~ 10 s), neutrino heating drives Y_e to values above 0.25. If the HMNS collapses to a black hole on a timescale shorter than the disk lifetime, the Y_e distribution is in the range 0.1–0.4, which is similar to the BH-torus case.

Extensive literature relates these events to sGRBs and kilonovae as electromagnetic counterparts (Li and Paczyński, 1998; Nakar, 2007; Metzger and Berger, 2012; Kasen, Badnell, and Barnes, 2013; Piran, Nakar, and Rosswog, 2013; Tanaka and Hotokezaka, 2013; Tanvir *et al.*, 2013; Grossman *et al.*, 2014; Metzger and Fernández, 2014; Rosswog *et al.*, 2014, 2015, 2017; Fryer *et al.*, 2015; Wanderman and Piran, 2015; Barnes *et al.*, 2016; Fernández and Metzger, 2016; Hotokezaka *et al.*, 2016; Metzger, 2017a; Ascenzi *et al.*, 2019). Although these objects are also of major importance as strong sources for gravitational wave emission (Shibata and Taniguchi, 2011; Baiotti and Rezzolla, 2017), especially after GW170817 (Abbott *et al.*, 2017a), underpinning the importance of multimessenger observations, we focus here on the ejected nucleosynthesis composition. In Secs. VI.B.1–VI.B.3 we concentrate on (i) the dynamic ejecta, (ii) the postmerger neutrino-wind ejecta, and (iii) the late-time viscous or secular outflow from the accretion disk.

1. Dynamic ejecta

The dynamic ejecta consist of two components: a cold component consisting of neutron-rich matter originating from the outer regions of the neutron star that is "thrown out" via tidal interaction in the equatorial plane, and a hotter component originating from the contact interface. The first

component is the only one present in NS-BH mergers, and the second one may constitute most of the unbound material in NS-NS mergers with similar masses. The tidal component was originally found in Newtonian simulations [first investigations by Davies *et al.* (1994) and Rosswog *et al.* (1999) and more detailed discussions by Korobkin *et al.* (2012)], while the contact interface component was found in relativistic simulations, first within the conformal flatness approximation (Oechslin, Janka, and Marek, 2007; Goriely, Bauswein, and Janka, 2011; Bauswein, Goriely, and Janka, 2013) and then in fully relativistic simulations (Hotokezaka, Kiuchi, Kyutoku, Okawa *et al.*, 2013). The latter simulations neglected the impact of weak processes in the ejecta, and hence the ejected material kept the neutron-rich conditions corresponding to β equilibrium in the cold neutron star $Y_e \lesssim 0.01$.

The nucleosynthesis in low Y_e ejecta, as found in BH-NS mergers and the tidal component of NS-NS mergers, has been extensively studied (Freiburghaus, Rosswog, and Thielemann, 1999; Korobkin *et al.*, 2012; Bauswein, Goriely, and Janka, 2013; Rosswog *et al.*, 2014; Eichler *et al.*, 2015; Mendoza-Temis *et al.*, 2015; Martin *et al.*, 2016; Mumpower *et al.*, 2016; Bovard *et al.*, 2017) and found to be independent of the astrophysical conditions (Korobkin *et al.*, 2012) but sensitive to the nuclear physics input (Panov and Thielemann, 2004; Panov, Korneev, and Thielemann, 2008; Bauswein, Goriely, and Janka, 2013; Eichler *et al.*, 2015; Goriely, 2015; Goriely and Martínez-Pinedo, 2015; Mendoza-Temis *et al.*, 2015; Martin *et al.*, 2016; Mumpower *et al.*, 2016; Shibagaki *et al.*, 2016; Thielemann, Eichler, Panov, and Wehmeyer, 2017; Vassh *et al.*, 2019). For extremely neutron-rich ejecta neutron-to-seed ratios can even reach several 1000 and the associated nucleosynthesis becomes insensitive to the initial composition. The temperature evolution is characterized by having a high temperature plateau $T_{\max}$ (see Fig. 14) whose value is determined by a competition between the *r*-process energy generation rate $\dot{Q}$ and the expansion dynamical timescale (Mendoza-Temis *et al.*, 2015)

$$T_{\max} \approx 0.8\ \mathrm{GK}\left[\left(\frac{\rho}{10^5\ \mathrm{g\,cm^{-3}}}\right)\left(\frac{\dot{Q}}{4\ \mathrm{MeV\,s^{-1}}}\right)\left(\frac{\tau_{\mathrm{dyn}}}{10\ \mathrm{ms}}\right)\right]^{1/4}. \tag{13}$$

Independent of the initial conditions, during the phase of neutron captures one can have a hot or cold *r* process; see Sec. III and Fig. 14, where dark gray and brown lines correspond to cold *r*-process conditions and light gray lines to hot *r*-process conditions. Typically the expansion of the material is "slow" enough to allow for all neutrons to be captured. This leads to the occurrence of several fission cycles with large amounts of heavy nuclei prone to fission, mainly around $A \sim 280$, remaining at freeze-out; see Fig. 13. During the final freeze-out phase the fission yields of the heaviest nuclei determine the final abundances of nuclei with $A \lesssim 140$ (Goriely and Martínez-Pinedo, 2015). Fission also produces large amounts of neutrons that tend to be captured on the third *r*-process peak material. Depending on the amount of neutrons produced and the speed at which they are released, the third *r*-process peak can be shifted to higher mass numbers than solar abundances; see Fig. 32, and see Sec. V.D for more details on the effects of fission. This depends on the mass model (see Fig. 23) and β-decay half-lives (Marketin, Huther, and Martínez-Pinedo, 2016; Panov, Lutostansky, and Thielemann, 2016). In particular, shorter β-decay half-lives for heavy nuclei result in smaller abundances in the fissioning region and hence less and faster release of neutrons during freeze-out (Eichler *et al.*, 2015).

Fission rates and yields for neutron-rich heavy and superheavy nuclei are then fundamental for the determination of the *r*-process abundances (Goriely, 2015). This requires not only the determination of the region of the nuclear chart where fission occurs (Thielemann, Metzinger, and Klapdor, 1983; Petermann *et al.*, 2012; Giuliani, Martínez-Pinedo, and Robledo, 2018; Giuliani *et al.*, 2019) but also the modeling of all relevant fission channels, including neutron-induced fission, β-delayed fission, and spontaneous fission (Thielemann, Metzinger, and Klapdor, 1983; Panov and Thielemann, 2004; Panov *et al.*, 2005, 2010; Goriely *et al.*, 2009, 2013; Mumpower *et al.*, 2018; Vassh *et al.*, 2019) and corresponding yields (Kelic, Ricciardi, and Schmidt, 2009; Schmidt *et al.*, 2016; Schmidt and Jurado, 2018; Schmitt, Schmidt, and Jurado, 2018; Vassh *et al.*, 2019). Low Y_e ejecta produce a final abundance distribution that follows the solar *r*-process abundance distribution for $A > 140$ independent of the fission yields used (Goriely and Martínez-Pinedo, 2015). The production of lighter nuclei is rather sensitive to the fission rates and yields used and typically no nuclei below $A \sim 110$ are produced in substantial amounts (Panov, Korneev, and Thielemann, 2008; Goriely *et al.*, 2013; Eichler *et al.*, 2015; Mendoza-Temis *et al.*, 2015; Vassh *et al.*, 2019). Fission is also relevant for the production of actinides with important consequences for late-time kilonova light curves (Barnes *et al.*, 2016; Rosswog *et al.*, 2017; Wanajo, 2018;

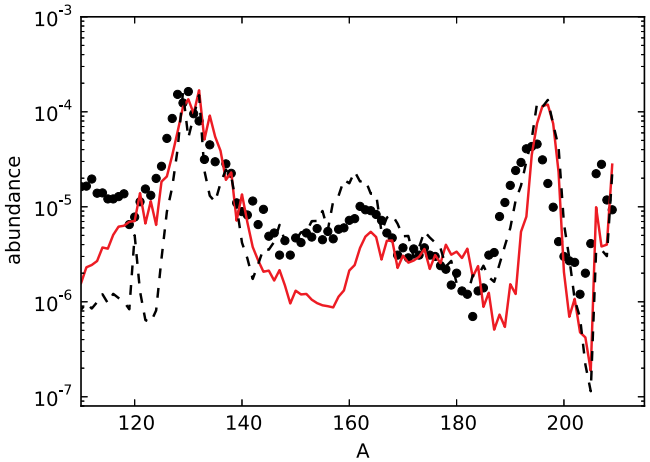

FIG. 32. Resulting *r*-process abundances for dynamic tidal ejecta [compared to solar values (black dots)] from neutron-star merger simulations (Eichler *et al.*, 2015), making use of β-decay half-lives from Möller, Pfeiffer, and Kratz (2003) (red line) and recent β-decay half-life predictions (black line) (Marketin, Huther, and Martínez-Pinedo, 2016) together with the fragment distributions from fissioning nuclei of Kelic, Ricciardi, and Schmidt (2008). From Thielemann, Eichler, Panov, Pignatrari, and Wehmeyer, 2017.

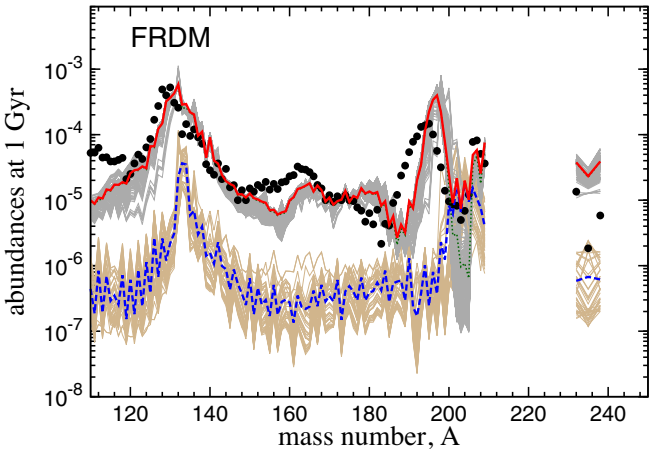

FIG. 33. *r*-process abundances after a decay time of 1 Gyr for all trajectories shown in Fig. 14. The dark gray (light brown) curves correspond to the abundances of the trajectories of the slow (fast) ejecta. The mass-averaged abundances for all trajectories (red solid curves), the slow ejecta (green dotted curves), and the fast ejecta (blue dashed curves) are also shown. The abundances for the slow and fast trajectories and their averages have been scaled by the value of their fractional contribution to the total ejecta. Adapted from Mendoza-Temis *et al.*, 2015.

Zhu *et al.*, 2018; Holmbeck, Sprouse *et al.*, 2019; Wu, Barnes *et al.*, 2019) and U/Th cosmochronometry; see Sec. VIII.D.

Several studies (Goriely *et al.*, 2014; Mendoza-Temis *et al.*, 2015; Metzger *et al.*, 2015; Ishii, Shigeyama, and Tanaka, 2018; Radice, Perego, Hotokezaka, Bernuzzi *et al.*, 2018; Fernández *et al.*, 2019) showed that part of the material, up to 10% in mass, is ejected quickly and reaches such low densities that the timescale for neutron captures becomes much longer than the expansion timescale (see the brown lines in Fig. 14) (Mendoza-Temis *et al.*, 2015). Under such conditions most of the neutrons are not captured, despite having a large neutron-to-seed ratio. The final abundances of this "frustrated" *r* process does not correspond to solar abundances (see Fig. 33), and hence it cannot constitute a major component of the total ejected mass, assuming mergers are a major *r*-process site. However, it can significantly contribute for nuclei around $A \sim 200$ (see the difference between green and red lines in Fig. 33) and can drive an early (timescales of hours) electromagnetic emission that is powered by the radioactive decay of the free neutrons left after completion of the *r* process (Metzger *et al.*, 2015).

Wanajo *et al.* (2014) showed that weak processes operating on the shock-heated ejecta of NS-NS mergers can increase the Y_e. They are particularly efficient in the polar region, where the large neutrino fluxes from the HMNS substantially increase the Y_e of the ejecta, provided that the HMNS does not collapse promptly to a BH. Depending on the neutrino luminosities, Y_e could be increased to values between 0.25 and 0.4. While it is currently accepted that weak processes increase the Y_e of the ejecta, an aspect confirmed by the kilonova observations discussed in Sec. VII, there is still a relatively large spread between the predictions of different groups (Sekiguchi *et al.*, 2015, 2016; Foucart *et al.*, 2016, 2018; Radice *et al.*, 2016; Bovard *et al.*, 2017; Shibata *et al.*, 2017; Radice, Perego, Hotokezaka, Fromm *et al.*, 2018) related to the different approximations in the treatment of neutrino radiation transport and/or to differences in the thermodynamical conditions of matter reached after the merger (Perego, Bernuzzi, and Radice, 2019), as they determine the magnitude of electron and positron capture processes. Dynamic ejecta from NS-NS mergers are expected to contribute to the synthesis of a broad range of *r*-process nuclei, both light and heavy, once weak processes are considered (Wanajo *et al.*, 2014; Goriely *et al.*, 2015; Martin *et al.*, 2018). However, we must keep in mind that the predicted amount of high Y_e matter is typically much smaller than that found in accretion disk outflows.

2. Neutrino winds and the effect of neutrinos

In addition to the dynamic ejecta, related directly to the merging or collision, postmerger ejecta will emerge as well. One component is a "neutrino wind" as found in core-collapse supernovae. For a typical merging system, the hot central NS remnant, supported by high temperatures and differential rotation, will not collapse to a black hole immediately (provided that the combined total mass of the system M_t is smaller than M_c; see the introductory part of Sec. VI.B) and will be surrounded by a hot and dense torus. Hence, the structure of the wind is quite different from the isolated NSs usually found in core-collapse supernovae. The wind outflow occurs mainly in the polar direction (Metzger and Fernández, 2014; Perego *et al.*, 2014; Rosswog *et al.*, 2014; Martin *et al.*, 2015). Matter is exposed to neutrinos long enough for the material to reach an equilibrium between electron neutrino and antineutrino absorption, changing Y_e [see Eq. (10)] from the initial neutron-rich conditions toward higher values that can even be above $Y_e = 0.5$. Because of the much larger $\bar{\nu}_e$ luminosities and energy differences between $\bar{\nu}_e$ and ν_e, found during the postmerger evolution when compared to

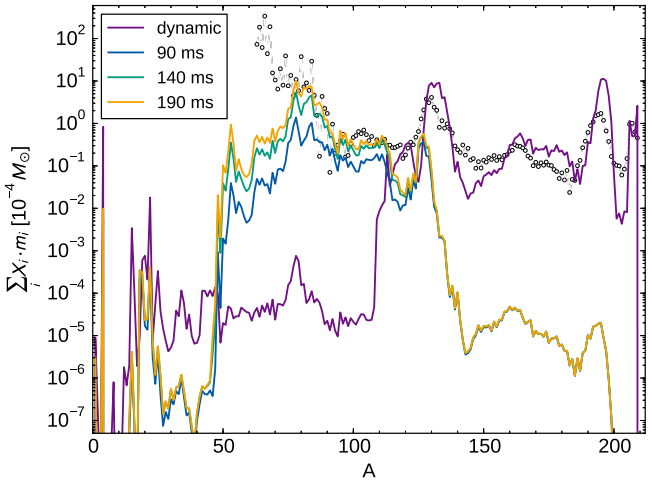

FIG. 34. Neutrino-wind contribution to neutron-star merger ejecta, dependent on the delay time between the merger and BH formation. For comparison the dynamic, tidal ejecta given by Korobkin *et al.* (2012) are also shown. The neutrino wind, ejected dominantly in polar regions, contributes nuclei with $A < 130$ due to the effect of the neutrinos on Y_e. From Martin *et al.*, 2015.

core-collapse supernova (see Fig. 25), the peak of the Y_e distribution is expected to be neutron rich with $Y_e \gtrsim 0.25$ (Martin *et al.*, 2015; Fujibayashi *et al.*, 2017, 2018; Lippuner *et al.*, 2017). This leads to a weak *r* process and produces mainly matter below the second *r*-process peak, i.e., no lanthanides are produced. Figure 34 displays the results of Martin *et al.* (2015) for the neutrino-wind component as a function of the delay time until black hole formation. It can be seen that predominantly nuclei below $A = 130$ are produced, complementing well the abundance features originating from dynamic low Y_e ejecta, which are also displayed and result here from Newtonian simulations (Korobkin *et al.*, 2012).

Similar to the situation in core-collapse supernovae, the properties of neutrino-wind ejecta and particularly Y_e are expected to be sensitive to the spectral differences between ν_e and $\bar{\nu}_e$. This requires an accurate prediction of neutrino luminosities and spectra. Supernova neutrino-wind transport simulations are currently based on accurate numerical solutions of the Boltzmann transport equation (Fischer *et al.*, 2010; Hüdepohl *et al.*, 2010; Roberts, 2012) exploiting the spherically symmetric nature of the problem. In the case of mergers, which require multidimensional treatments, simulations thus far have been based on neutrino leakage schemes (Metzger and Fernández, 2014; Perego *et al.*, 2014; Radice *et al.*, 2016; Ardevol-Pulpillo *et al.*, 2019) and $M1$ schemes (Foucart *et al.*, 2015; Just *et al.*, 2015; Just, Obergaulinger, and Janka, 2015; Fujibayashi *et al.*, 2017, 2018). There are indications that they may not properly capture the energy densities and fluxes of neutrinos in the polar regions (Just *et al.*, 2015), hence affecting the Y_e estimates in the polar region (Foucart *et al.*, 2016, 2018). Additional opacity reactions, like neutrino-pair annihilation, have not yet been considered, but may also play an important role in determining the properties of the ejecta (Just *et al.*, 2016; Fujibayashi *et al.*, 2017, 2018; Perego, Yasin, and Arcones, 2017; Foucart *et al.*, 2018).

Y_e can also be affected by modifications of neutrino and antineutrino spectra due to neutrino flavor conversion. There have been a number of tests to verify such neutrino conversions via matter-neutrino resonances (Malkus *et al.*, 2012; Foucart *et al.*, 2015; Malkus, McLaughlin, and Surman, 2016; Zhu, Perego, and McLaughlin, 2016; Frensel *et al.*, 2017) and fast pairwise flavor conversions (Wu and Tamborra, 2017; Wu, Tamborra *et al.*, 2017). Because of the more complicated geometry of a disk environment in comparison to core-collapse supernovae, most of the calculations are based on single-angle approximations. Spherically symmetric test calculations show that the matter-neutrino resonance still occurs in multiangle models (Vlasenko and McLaughlin, 2018), but with reduced efficiency. Nevertheless, the existing investigations point to a potential effect on Y_e, and thus the resulting nucleosynthesis can be affected.

A further wind component, not addressed here, relates to magnetically driven winds from the central remnant (Kiuchi, Kyutoku, and Shibata, 2012; Siegel, Ciolfi, and Rezzolla, 2014; Ciolfi *et al.*, 2017; Metzger, Thompson, and Quataert, 2018). However, their nucleosynthesis yields and interaction with neutrino-driven winds have not yet been explored.

3. Accretion disk outflows

The long-term evolution $t \sim 1$–10 s of the accretion disk produces outflows of material powered by viscous heating and nuclear recombination (Lee and Ramirez-Ruiz, 2007; Beloborodov, 2008; Metzger, Piro, and Quataert, 2009; Fernández and Metzger, 2013). Those outflows can contain up to 40% of the disk mass. The amount of ejected mass increases with the lifetime of the MNS formed in the merger, but most importantly for nucleosynthesis the Y_e distribution is dramatically affected by the lifetime of the MNS (Metzger and Fernández, 2014). For a long-lived MNS ($t \gtrsim 1$ s), neutrino-irradiation from the MNS results in ejecta with $Y_e > 0.3$ (Metzger and Fernández, 2014; Lippuner *et al.*, 2017; Fujibayashi *et al.*, 2018). The nucleosynthesis in these ejecta is similar to the neutrino-wind ejecta discussed in Sec. VI.B.2.

For a short-lived MNS ($t \lesssim 1$ s), the impact of neutrino irradiation is small and, from the point of view of nucleosynthesis, outflows from accretion disks formed in NS-NS and BH-NS mergers give similar results. Early nucleosynthesis studies were primarily parametric and mainly considered the "neutrino-driven" wind outflow from the surface of the disk (Fujimoto *et al.*, 2003, 2004; Pruet, Woosley, and Hoffman, 2003; Pruet, Thompson, and Hoffman, 2004; McLaughlin and Surman, 2005; Surman, McLaughlin, and Hix, 2006; Metzger, Thompson, and Quataert, 2008; Surman *et al.*, 2008; Dessart *et al.*, 2009; Kizivat *et al.*, 2010; Wanajo and Janka, 2012; Surman *et al.*, 2014). Detailed simulations, based initially on α-viscosity prescriptions and more recently on three-dimensional general-relativistic magnetohydrodynamics (for references see the introductory part of Sec. VI.B), show that neutrino winds from the accretion disk eject little mass and that most of the material is ejected by viscous heating (Just *et al.*, 2015). The results for disk outflows by Wu *et al.* (2016) are displayed in Fig. 35, which shows the integrated abundance pattern of all tracer particles. This underlines that, in

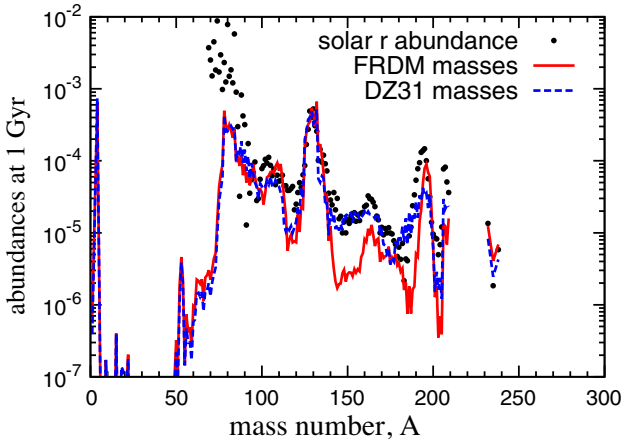

FIG. 35. Resulting *r*-process abundances [compared to solar values (black dots)] from black hole accretion disk simulations, making use of a black hole mass of 3 $M_\odot$, a disk mass of 0.03 $M_\odot$, an initial Y_e of 0.1, entropy per baryon of $8k_b$, an alpha parameter of the viscous disk of 0.03, and a vanishing black hole spin. The impact of two different mass models (FRDM and DZ31) in the final abundances is illustrated. From Wu *et al.*, 2016.

principle, disk outflows alone can produce the entire range of *r*-process nuclei, with a significant production of $A \lesssim 130$ nuclei, also reaching the third peak at $A = 195$ in most of the simulations. The detailed results depend on the disk viscosity, the initial mass or entropy of the torus, the black hole spin, and the nuclear physics input. The latter is illustrated in Fig. 35, which compares the nucleosynthesis results for two different mass models FRDM (Möller *et al.*, 1995) and Duflo-Zuker (Duflo and Zuker, 1995). The production of heavy ($A \gtrsim 195$) nuclei is also affected by the previously discussed uncertainties of the disk properties (Just *et al.*, 2015; Wu *et al.*, 2016; Christie *et al.*, 2019; Fernández *et al.*, 2019; Fujibayashi *et al.*, 2020). Recent α-viscous simulations (Fujibayashi *et al.*, 2020) using torus masses compatible with GW170817 ($M \sim 0.1$–0.2 $M_\odot$) predict relatively large Y_e ejecta mainly due to the disk reaching dynamical beta equilibrium (Arcones *et al.*, 2010) between electron and positron captures. The associated nucleosynthesis is strongly suppressed in $A > 130$ nuclei when compared with solar. However, such a possible deficit can be counterbalanced by the dynamic ejecta, as the total nucleosynthesis of the merger includes the components of the dynamic ejecta, the neutrino wind, and the accretion disk.

Nucleosynthesis studies in mergers are commonly based on simulation data that follow the evolution of the ejecta for timescales shorter (approximately milliseconds) than the *r*-process nucleosynthesis timescale (approximately seconds). This makes it necessary to extrapolate the time evolution of thermodynamic properties like temperature and density to follow the nucleosynthesis to completion. It is commonly assumed that the expansion is homologous ($\rho \sim t^{-3}$), with the temperature evolution determined by the nuclear energy production of the *r* process. It originates mainly from β decays and is in the range $\dot{Q} \approx 1$–4 MeV s^{-1} per nucleon; see the lower panel of Fig. 14. Rosswog *et al.* (2014) performed long-term simulations and found that the *r*-process energy release does not qualitatively alter the properties of dynamic ejecta. Wu *et al.* (2016) found that *r*-process heating can increase the amount of ejecta up to a factor of 2 in viscous outflows from accretion disks and remove an anomalously high abundance of $A = 132$ nuclei; see Fig. 35, as well as Lippuner *et al.* (2017) and Siegel and Metzger (2018). *r*-process heating can critically shape the dynamics of marginally bound ejecta responsible for fallback accretion on timescales of seconds to minutes (Metzger, Arcones *et al.*, 2010; Desai, Metzger, and Foucart, 2019). Late-time fallback accretion has been suggested as a possible mechanism for explaining the extended x-ray emission observed in some short GRBs (Rosswog, 2007). *r*-process heating on timescales of days to weeks after the merger has been found responsible for powering the "kilonova" electromagnetic emission (Li and Paczyński, 1998; Metzger, Martínez-Pinedo *et al.*, 2010), as discussed in Sec. VII.

VII. ELECTROMAGNETIC SIGNATURES OF *r*-PROCESS NUCLEOSYNTHESIS

While we have evidence for the existence of some of the events listed in Sec. VI, i.e., among the sites of Sec. VI.A possibly for electron-capture supernovae (Wanajo *et al.*, 2009; Moriya *et al.*, 2014), for supernovae resulting in magnetars (Vink, 2008; Greiner *et al.*, 2015; Beniamini *et al.*, 2019; Zhou *et al.*, 2019), and for hypernovae and lGRBs (Nomoto *et al.*, 2010), no observational evidence yet exists for their production of heavy *r*-process elements. This is different for compact binary mergers (Sec. VI.B) since GW170817, a neutron-star merger with the combined mass M_t of about 2.74 $M_\odot$ (Abbott *et al.*, 2017b, 2017d, 2019). The observation of an electromagnetic counterpart delivered indications for the existence of heavy *r*-process elements in the ejecta (Metzger, 2017b; Tanaka *et al.*, 2017; Villar *et al.*, 2017), and even identified one element Sr (Watson *et al.*, 2019). This is discussed in detail later. Additional gravitational wave observations now point to further neutron-star mergers (e.g., GW190425 with $M_t \sim 3.4$ $M_\odot$) (B. P. Abbott *et al.*, 2020), or even neutron-star–black hole merger candidates (e.g., GW190426 with M_t in excess of 7 $M_\odot$) (Lattimer, 2019; R. Abbott, 2020b). However, the last two events had no observed accompanying electromagnetic counterpart (Hosseinzadeh *et al.*, 2019; Ackley *et al.*, 2020; Foley *et al.*, 2020), due either to nonexistence or to nondetection, related to a larger distance and/or missing precise directions. This will hopefully change with future gravitational wave events.

The *r* process produces neutron-rich unstable nuclei on timescales of a few seconds that decay to stability by a combination of β, α, and fission decays. These decays produce large amounts of energy and can lead to an observable electromagnetic emission. The first suggestion of such an electromagnetic emission was proposed by Burbidge *et al.* (1956), who attributed type Ia supernova light curves to the decay of ^{254}Cf produced by the *r* process. Today we know that both type Ia and type II supernova light curves are due mainly to the decay of ^{56}Ni. The study of light curves and spectra not only constrains the nucleosynthesis yields (Diehl and Timmes, 1998; Seitenzahl, Timmes, and Magkotsios, 2014) but also provides information about the physical parameters of the progenitor system and the explosion itself (Bersten and Mazzali, 2017; Zampieri, 2017). This illustrates the physics potential of an electromagnetic transient observation associated with *r*-process ejecta. It can identify a site where the *r* process occurs (Metzger, Martínez-Pinedo *et al.*, 2010) and serve as electromagnetic counterpart to the gravitational wave detection following a neutron-star merger (Metzger and Berger, 2012) and the nature of the merging system, NS-NS versus NS-BH, and the remnant (Barbieri *et al.*, 2019; Margalit and Metzger, 2019; Kawaguchi, Shibata, and Tanaka, 2020; Zhu *et al.*, 2020). All these aspects were confirmed by the electromagnetic transient AT 2017gfo following the gravitational wave event GW170817 (Abbott *et al.*, 2017a).

Li and Paczyński (1998) were the first to propose that radioactive ejecta from a NS-NS merger could power a supernovalike transient. However, they did not possess a physical model to describe the origin of the radioactive heating $\dot{Q}$ and considered two possible limiting cases: an exponential-law decay and a power-law $\dot{Q} \sim t^{-1}$. In both cases the normalization was left as a free parameter. Hence, even if the model predicted the right timescale for the peak luminosity, it could not determine the absolute luminosity, spectral peak frequency, or time evolution of the luminosity. Indeed,

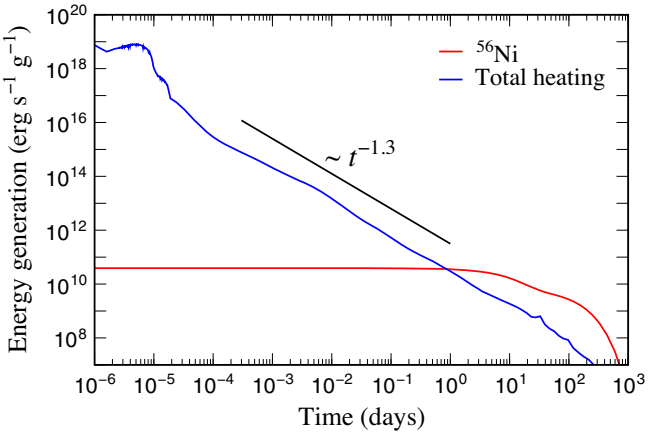

FIG. 36. Specific energy generation rate $\dot{Q}$ in *r*-process ejecta (black line). For comparison the energy production from the decay chain $^{56}\mathrm{Ni} \rightarrow {}^{56}\mathrm{Co} \rightarrow {}^{56}\mathrm{Fe}$ (red line) and the analytical estimate $\dot{Q} \sim t^{-1.3}$ are also shown. Adapted from Metzger, Martínez-Pinedo *et al.*, 2010.

their fiducial model reached extremely high values of the luminosity $\sim 10^{44}$ erg s^{-1} with a spectral peak in the ultraviolet. Kulkarni (2005) considered two possible origins of the heating: neutron and ^{56}Ni decay, and they named such events "macronova." Metzger, Martínez-Pinedo *et al.* (2010) were the first to relate the late-time radioactive heating to the decay of freshly produced *r*-process nuclei. Based on heating rates derived self-consistently from a nuclear reaction network, they showed that the heating rate follows a power law at timescales of a day with a steeper dependence ($\dot{Q} \sim t^{-1.3}$) than the one assumed by Li and Paczyński (1998). As shown in Fig. 36, the heating evolves differently for *r*-process material than for supernovalike ejecta dominated by ^{56}Ni. A power-law dependence is expected whenever the heating is dominated by a broad distribution of nuclei, with all of them decaying exponentially. This can be understood from basic physics of β decay and the properties of neutron-rich nuclei (Metzger, Martínez-Pinedo *et al.*, 2010; Hotokezaka, Sari, and Piran, 2017). A similar dependence is found for the decay rate of terrestrial radioactive waste (Way and Wigner, 1948).

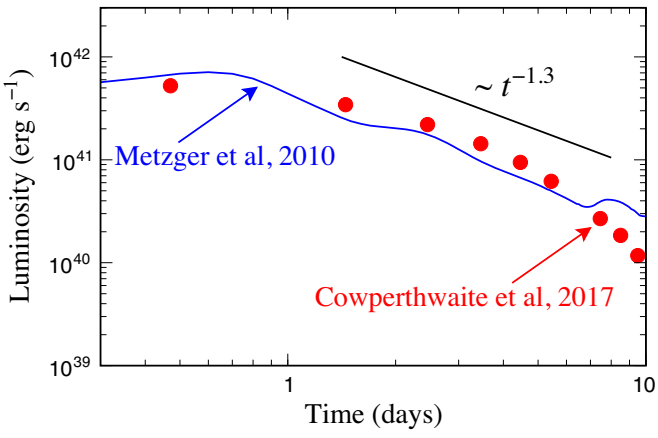

FIG. 37. Bolometric light curve of the optical-infrared counterpart AT 2017gfo of GW170817 (red circles) from multiband photometry (Cowperthwaite *et al.*, 2017) compared to the fiducial model of Metzger, Martínez-Pinedo *et al.* (2010). A line with the approximate power-law decay $\dot{Q} \sim t^{-1.3}$ for *r*-process heating is given for comparison; see Fig. 36.

Metzger, Martínez-Pinedo *et al.* (2010) predicted peak luminosities $\sim 3 \times 10^{41}$ erg s^{-1} for 0.01 $M_\odot$ of ejecta, expanding at $v \sim 0.1c$, and a spectral peak at visual magnitude. As such a value corresponds to 1000 times the luminosity of classical novae they named these events kilonova. Figure 37 compares their prediction with the observation of AT 2017gfo (Cowperthwaite *et al.*, 2017). Similar results were also found by Roberts *et al.* (2011) and Goriely, Bauswein, and Janka (2011).

The physical processes determining the kilonova light curve are as follows [see Fernández and Metzger (2016), Tanaka (2016), and Metzger (2017a) for reviews]:

(a) Radioactive heating. The radioactive heating of *r*-process products is expected to follow a power law whenever a large statistical ensemble of nuclei is produced. This is the case for ejecta with $Y_e \lesssim 0.2$. For higher Y_e ejecta, the heating rate has "bumps" as a function of time caused by being dominated by a few nuclei (Grossman *et al.*, 2014; Lippuner and Roberts, 2015; Martin *et al.*, 2015; Rosswog *et al.*, 2018; Wanajo, 2018). However, when averaged over Y_e distributions, as predicted by simulations, the heating rate at timescales of days to a week (of greatest relevance to determine the peak luminosity) varies only slightly within a factor of a few for $Y_e \lesssim 0.4$ (Lippuner and Roberts, 2015; Wu, Barnes *et al.*, 2019). *r*-process nuclei decay in a variety of channels including β decay, α decay, and fission. The energy production in each channel is important, as the absorption of the energy depends on whether the decay products are electrons, photons, alpha particles, or fission products. For high Y_e ejecta, heating is dominated by β decay and only electrons and photons are relevant, with neutrinos just an energy loss. For low Y_e ejecta, actinides are produced and alpha decay and fission can be substantial for the energy production and sensitive to the underlying mass model (Barnes *et al.*, 2016; Rosswog *et al.*, 2017; Wu, Barnes *et al.*, 2019). The exact form of the heating also depends on the time after the freeze-out of the neutron captures. At early times of a few hours the heating may be dominated by neutron decay, assuming a substantial amount of free neutrons in the outermost layers of the ejecta, producing an ultraviolet or blue precursor to the kilonova emission (Metzger *et al.*, 2015; Metzger, 2017a). Early blue emission can also originate from the hot cocoon that surrounds the GRB jet as it crosses the ejecta (Gottlieb, Nakar, and Piran, 2018). At intermediate times of up to ~10 d, β decays dominate the energy production (Barnes *et al.*, 2016). The heating rate follows a power law ($\dot{Q} \sim t^{-1.3}$), provided that it is determined by the decay of a statistical ensemble of nuclei. As the material expands and the thermalization of the electrons becomes inefficient, the effective heating rate, including thermalization effects (discussed later), follows a power law $\sim t^{-n}$ with a power n that depends on the time evolution of the thermalization efficiency and the confinement of electrons in the plasma due to magnetic fields (Kasen and Barnes, 2019; Waxman, Ofek, and Kushnir, 2019; Hotokezaka and Nakar, 2020). At late times of up to 100 d, the heating is dominated by a few decays [for a complete listing see Wu, Barnes *et al.*

(2019)] due to the scarcity of nuclei with the appropriate half-life, and hence the heating can substantially differ from a power-law dependence.

(b) Thermalization efficiency. At early times the ejected material is extremely dense and the energy produced by radioactive decay, except for neutrinos, is completely reabsorbed. However, with decreasing density an increasing fraction of the energy is lost, and it is incorporated normally via a time-dependent thermalization efficiency of the energy produced by radioactive processes (Barnes *et al.*, 2016). This efficiency depends on bulk properties of the ejecta such as mass and velocity, as they determine the evolution of the density. It also depends on the presence of magnetic fields and their geometry. Furthermore, it varies with the decay product and time evolution of the heating for each decay channel (Kasen and Barnes, 2019), i.e., whether we have a statistical distribution of decaying nuclei or a heating dominated by a few isotopes, which is probably more appropriate for late times. Earlier works considered the thermalization of γ rays (Hotokezaka *et al.*, 2016) and were later extended to consider charged particles (Barnes *et al.*, 2016). This has been recently extended to the case of a few decays dominating the heating (Kasen and Barnes, 2019; Wu, Barnes *et al.*, 2019). Qualitatively one finds that the thermalization efficiency for γ rays decreases rapidly and becomes negligible on timescales of a few tens of days. The thermalization efficiency for charged particles, and particularly alpha particles and fission products, remains substantial at late times. This makes kilonova light curves sensitive to the heating contribution of alpha decays and fission (Barnes *et al.*, 2016; Rosswog *et al.*, 2017; Zhu *et al.*, 2018; Vassh *et al.*, 2019; Wu, Barnes *et al.*, 2019; Giuliani *et al.*, 2020).

(c) Atomic opacities. A significant electromagnetic luminosity is possible only once the density decreases sufficiently such that photons can escape the ejecta on the expansion timescale (Arnett, 1980, 1982). Assuming a homogeneous spherical distribution of ejecta with mass M, expanding homologously with velocity v and radius $R = vt$, the diffusion timescale of the ejecta can be given as $t_{\rm diff} \approx \rho\kappa R^2/(3c)$, with $\rho = 3M/(4\pi R^3)$ the density and κ the opacity of the ejecta. Once the ejecta expand enough to become transparent, they release line radiation. This occurs when the diffusion timescale $t_{\rm diff}$ becomes comparable to the dynamical timescale $t = R/v$ and defines the time at which the maximum of the luminosity is reached (Metzger, Martínez-Pinedo *et al.*, 2010; Fernández and Metzger, 2016)

$$t_{\rm peak} \approx \left(\frac{\kappa M}{4\pi c v}\right)^{1/2} \approx 1.5\ {\rm d}\left(\frac{M}{0.01\ {\rm M}_\odot}\right)^{1/2}\left(\frac{v}{0.1c}\right)^{-1/2}\left(\frac{\kappa}{{\rm cm^2\ g^{-1}}}\right)^{1/2} \quad (14)$$

At timescales beyond the peak time the luminosity can be approximated using Arnett's law (Arnett, 1980, 1982) $L(t) = M\dot{Q}_{\rm dep}(t)$. $\dot{Q}_{\rm dep}$ is the energy deposition rate, corrected by the thermalization efficiency, and can be given as $\dot{Q}_{\rm dep} \approx \varepsilon \times 10^{10}(t/{\rm d})^{-\alpha}\ {\rm erg\ s^{-1}\ g^{-1}}$, with $\varepsilon < 1$ the thermalization efficiency. At peak time the kilonova luminosity is given by

$$L_{\rm peak} \approx 1.1\varepsilon \times 10^{41}\ {\rm erg\ s^{-1}} \times \left(\frac{M}{0.01\ {\rm M}_\odot}\right)^{1-\alpha/2}\left(\frac{v}{0.1c}\right)^{\alpha/2}\left(\frac{\kappa}{{\rm cm^2\ g^{-1}}}\right)^{-\alpha/2}. \quad (15)$$

The effective emission temperature can be obtained from the luminosity using the Stefan-Boltzmann law that, together with the Wien displacement law, gives the characteristic wavelength of the emission

$$\lambda_{\rm peak} \approx 514\ {\rm nm} \times \left(\frac{M}{0.01\ {\rm M}_\odot}\right)^{\alpha/8}\left(\frac{v}{0.1c}\right)^{(2-\alpha)/8}\left(\frac{\kappa}{{\rm cm^2\ g^{-1}}}\right)^{(2+\alpha)/8}. \quad (16)$$

Equations (15) and (16) illustrate several characteristic features of kilonova light curves. Even if the emission mechanism is similar to supernovae the typical ejecta mass is much smaller and the velocity larger. The equations illustrate the important role played by the opacity that is dominated by Doppler-broadened atomic line bound-bound transitions (Kasen, Badnell, and Barnes, 2013; Fontes *et al.*, 2015; Tanaka *et al.*, 2018). Ejecta containing light r-process elements ($A \lesssim 140$) with d-shell valence electrons possess an opacity $\kappa \lesssim 1\ {\rm cm^2\ g^{-1}}$. In this case the emission peaks in the blue after about a day. This was, indeed, the case for AT 2017gfo (Nicholl *et al.*, 2017). If the ejecta contain lanthanide or actinide nuclei ($A \gtrsim 140$), then the optical opacity is high ($\kappa \gtrsim 10 - 100\ {\rm cm^2\ g^{-1}}$) due to the complex structure of f-shell valence electrons for these elements, resulting in a dense forest of lines, and the emission shifts to the red or infrared (Barnes and Kasen, 2013; Kasen, Badnell, and Barnes, 2013; Tanaka and Hotokezaka, 2013; Fontes *et al.*, 2017, 2020). Having a kilonova observation, as in the case of AT 2017gfo, it is possible to adjust the multiwavelength evolution of the light curve using a variation of the previously described model and to determine the amount of ejecta, velocity, and opacity that is a proxy for the composition. As discussed in Sec. II.E, to reproduce the AT 2017gfo observations requires at least two different ejecta components, with three-component models slightly favored (Villar *et al.*, 2017). This result is consistent with the existence of several ejecta components in mergers giving rise to different nucleosynthesis products; see Sec. VI.B. The analysis of sGRB observations (Wu and MacFadyen, 2018) and the kilonova transient (Perego, Radice, and Bernuzzi, 2017) favors an off-axis viewing angle of ~30°. Hence, the early blue phase of the kilonova light curve has been suggested to originate from lanthanide-poor polar ejecta (Kasen *et al.*, 2017); see, however, Kawaguchi, Shibata, and Tanaka (2018) for an alternative explanation. This result is consistent with simulations that predict that weak processes, including electron (anti)neutrino absorption, drive the composition to $Y_e \gtrsim 0.25$. It provides observational evidence of the important role of neutrinos in determining the composition of the ejecta. However, there is a tension between the velocity of the ejecta $v \approx 0.27c$, which is consistent with simulations of dynamical ejecta, and the large ejecta mass $M_{\rm ej} \approx 0.020\ {\rm M}_\odot$, which is not. Additional lanthanide-poor material is expected to originate from the postmerger neutrino-wind ejecta. However, its

velocity is expected to be smaller unless the wind is magnetically accelerated by the strongly magnetized HMNS remnant (Metzger, Thompson, and Quataert, 2018). The amount of material and velocity of material involved in the purple and red components suggest that they originate from postmerger outflows from the accretion disk (Kasen *et al.*, 2017). Simulations predict that the ejecta contain a broad distribution of Y_e and are able to produce both light and heavy *r*-process material including the lanthanides and actinides necessary to account for the high opacity (Just *et al.*, 2015; Wu *et al.*, 2016).

It is, indeed, the observation of the lanthanide-rich red emission that provided the first observational evidence that neutron-star mergers produce *r*-process nuclei. The only element identified in the spectra is Sr (Watson *et al.*, 2019), providing further evidence that weak processes (enhancing Y_e) operate in the ejecta and demonstrating that also first *r*-process-peak elements are produced in mergers. This is consistent with the inferred lanthanide mass fraction $X_{\rm lan} \sim 10^{-3}$–10^{-2} (Kasen *et al.*, 2017; Tanaka *et al.*, 2017; Waxman *et al.*, 2018), which along with the assumption that the GW170817 yield follows solar proportions requires the production of all *r*-process nuclei with additional contributions of trans-iron nuclei (Wu, Barnes *et al.*, 2019). However, if GW170817 represents a typical *r*-process yield from NS mergers, this suggests that an alternative *r*-process site may be responsible for the *r*-process abundances observed in *r*-enhanced metal-poor stars (Ji, Drout, and Hansen, 2019); see also Sec. VIII.A.

No direct spectroscopic evidence has been obtained pointing to the production of heavy *r*-process elements. The high density of lines for lanthanides and actinides together with the large velocities of the ejecta produces line blending and smoothens the spectra (Chornock *et al.*, 2017). This aspect has been used to determine the velocity of the ejecta from spectroscopic information (Chornock *et al.*, 2017). Nevertheless, the spectra present peaks that may probe the abundance of further individual elements beyond Sr; see Fig. 4 given by Kasen *et al.* (2017). However, uncertainties in current atomic data hinder a detailed spectral analysis. The lanthanide and actinide opacities are uncertain because the atomic states and line strengths of these elements are not measured experimentally. Theoretically, such high-Z atoms represent a challenging problem in many-body quantum mechanics, and hence are based on statistical models that must be calibrated to experimental data (Kasen, Badnell, and Barnes, 2013; Fontes *et al.*, 2015; Tanaka *et al.*, 2018, 2020; Radžiūtė *et al.*, 2020). Beyond identifying the line transitions themselves, there is considerable uncertainty in how to translate these data into an effective opacity. The commonly employed "line expansion opacity" formalism (Pinto and Eastman, 2000a, 2000b; Li, 2019), based on the Sobolev approximation and applied to kilonovae by Barnes and Kasen (2013) and Tanaka and Hotokezaka (2013), may break down if the line density is sufficiently high that the wavelength spacing of strong lines becomes comparable to the intrinsic thermal width of the lines (Kasen, Badnell, and Barnes, 2013; Fontes *et al.*, 2015, 2017, 2020).

Lacking a direct spectroscopic identification of the abundance of individual elements, recent work has focused in identifying fingerprints of heavy elements in kilonova light curves. Particularly promising are late-time observations, as the decay heating can be dominated by a few nuclei (Wu, Barnes *et al.*, 2019). Kasliwal *et al.* (2019) suggested heavy isotopes (e.g., ^{140}Ba, ^{143}Pr, ^{147}Nd, ^{156}Eu, ^{191}Os, ^{223}Ra, ^{225}Ra, ^{233}Pa, and ^{234}Th) with β-decay half-lives of around 14 d. Wu, Barnes *et al.* (2019) showed that at time periods consisting of weeks to months, the decay energy input may be dominated by a discrete number of α decays, ^{223}Ra (half-life $t_{1/2} = 11.43$ d), ^{225}Ac ($t_{1/2} = 10.0$ d), following the β decay of ^{225}Ra with $t_{1/2} = 14.9$ d, and the fissioning isotope ^{254}Cf ($t_{1/2} = 60.5$ d) (Zhu *et al.*, 2018), which liberate more energy per decay and thermalize with greater efficiency than β-decay products. Late-time nebular observations of kilonovae, which constrain the radioactive power, provide the potential to identify signatures of these individual isotopes, thus confirming the production of heavy nuclei. To constrain the bolometric light to the required accuracy, multiepoch and wideband observations are required with sensitive instruments like the James Webb Space Telescope.

An alternative mechanism to probe the *in situ* production of *r*-process nuclei is the identification of x-ray or γ-ray lines from their decay similar to the observations of ^{44}Ti γ rays in Cas A (Vink *et al.*, 2001; Renaud *et al.*, 2006) and SN 1987A remnants (Grebenev *et al.*, 2012). Qian, Vogel, and Wasserburg (1998 1999), Wu, Banerjee *et al.* (2019), and Korobkin *et al.* (2020a) provided estimates of γ-ray fluxes for several *r*-process nuclei, and Ripley *et al.* (2014) extended those estimates to x-ray lines. The predicted fluxes are too low to be detected by current missions; however, improvements in detection techniques may allow for the first detection of a merger remnant in our Galaxy; see Wu, Banerjee *et al.* (2019) for a search strategy.

VIII. ABUNDANCE EVOLUTION IN THE GALAXY AND ORIGIN OF THE *r* PROCESS

In Sec. VI we presented possible astrophysical sites and the related abundance predictions. This section addresses some of the additional features like their occurrence frequency and its time evolution throughout galactic history, with the aim of providing an understanding of the impact of these individual sites on the evolution of the Galaxy.

A. Supernova versus *r*-process imprints in early galactic evolution

Based on the nucleosynthesis predictions for regular core collapse and for type Ia supernovae, plus their occurrence rates, one finds that the early phase of the evolution of galaxies is dominated by the ejecta of fast evolving massive stars, i.e., those leading to core-collapse supernovae. While variations for the ejecta composition of different progenitor masses exist, average abundance ratios in the interstellar gas will be found after some time delay when many such explosions and the mixing of their ejecta with the interstellar medium have taken place. These averaged abundance ratios reflect ejecta yields

integrated over the distribution of initial stellar masses [initial mass function (IMF)]. Type Ia supernovae originate from exploding white dwarfs in binary systems, i.e., (a) from slowly evolving stars with initially less than 8 $M_\odot$ in order to become a white dwarf and (b) requiring time delaying mass transfer in a binary system before the type Ia supernova explosion (unless they are produced by rare collisions of white dwarfs). Thus, such events are delayed in comparison to the explosion of massive single stars. Type Ia supernovae, which are only important at later phases in galactic evolution, dominate the overall production of Fe and Ni [typically $0.5-0.6\ M_\odot$ per event] but are only minor contributors to intermediate-mass elements $Z = 8$–22. As core-collapse supernovae produce larger amounts of O, Ne, Mg, Si, S, Ar, Ca, and Ti (so-called α elements) than Fe-group nuclei like Fe and Ni (only of the order 0.1 $M_\odot$), the average ratio of α elements over Fe (α/Fe) is larger than the corresponding solar ratio.

For most stars, with the exception of evolved stars that blew off part of their envelope by stellar winds or stars in binary systems with mass exchange, their surface abundances represent the composition of the interstellar gas out of which they formed. Thus, we can look back into the early history of the Galaxy via the surface abundances of unevolved low-mass stars, witnessing the composition of the interstellar medium at the time of their birth. In Fig. 7 of Sec. II.A some of these aspects were displayed, with [Mg/Fe] plotted as a function of metallicity [Fe/H] for stars in our Galaxy. For Mg (a typical α element) one sees (with a relatively small scatter) a flat value of [Mg/Fe] between 0.3 and 0.5 up to $[\mathrm{Fe/H}] \leq -1$, which decreases down to solar values at $[\mathrm{Fe/H}] = 0$. This can be explained by the early appearance of core-collapse supernovae from fast evolving massive, single stars, producing on average $[\mathrm{Mg/Fe}] = 0.4$ (Woosley, Heger, and Weaver, 2002; Woosley and Heger, 2007; Limongi and Chieffi, 2018) before type Ia supernovae set in. The properties of the latter were reviewed by Hillebrandt *et al.* (2013), Maoz, Mannucci, and Nelemans (2014), Goldstein and Kasen (2018), and Livio and Mazzali (2018) as well as their nucleosynthesis properties (Nomoto and Leung, 2017b; Seitenzahl and Townsley, 2017; Seitenzahl *et al.*, 2019). These basic features of galactic evolution have been understood reasonably well for the majority of elements (Matteucci and Greggio, 1986; Timmes, Woosley, and Weaver, 1995; Nomoto, Kobayashi, and Tominaga, 2013), while open questions remain in stellar evolution and supernova explosion mechanisms. This includes the question of the role of more massive stars, probably ending as black holes (Heger *et al.*, 2003; Ertl *et al.*, 2016, 2020; Sukhbold *et al.*, 2016; Thielemann *et al.*, 2018; Ebinger *et al.*, 2019, 2020), and for sufficiently high angular momentum related to so-called hypernovae–long-duration gamma-ray bursts (see Sec. VI.A) or even more massive pair instability supernovae.

The solar abundance of Eu is more than 90% dominated by those isotopes that are produced in the *r* process (Bisterzo *et al.*, 2015, 2017). Therefore, it is considered a major *r*-process indicator. The ratio Eu/Fe in the Galaxy, already displayed in Fig. 7 of Sec. II.A and as its recent update in Fig. 38, shows a large scatter by more than 2 orders of magnitude at low metallicities, corresponding to early galactic

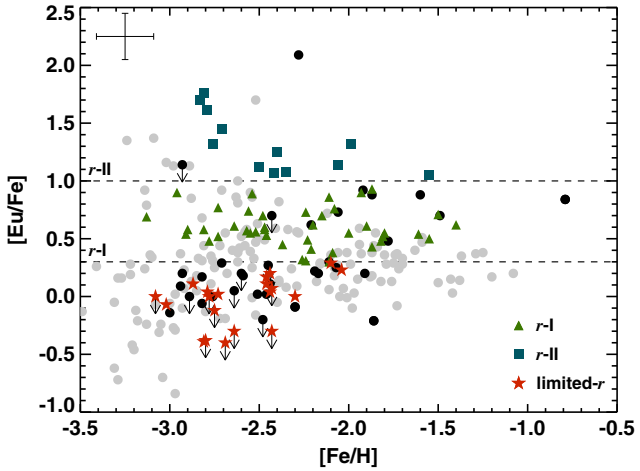

FIG. 38. Derived [Eu/Fe] abundances as a function of metallicity: *r*-I stars (green triangles), *r*-II stars (blue squares), limited-*r* observations (red stars), and non-*r*-process-enhanced stars (black dots); see classifications defined in Sec. II. Upper limits are indicated by black arrows. Gray light dots refer to an earlier overview (Roederer, Preston *et al.*, 2014). From Hansen *et al.*, 2018.

evolution. While the evolution of the average ratio resembles that of the alpha elements (see Fig. 7), being of core-collapse supernova origin and having also experienced a decline to solar ratios for $[\mathrm{Fe/H}] \geq -1$ [for similar trends in Mo and Ru see recent observations by Mishenina, Pignatari, Gorbaneva, Travaglio *et al.* (2019)], it is far more complex to understand Eu and other *r*-process-dominated elements than α elements like Mg. This is also true for elements whose solar abundances are not dominated by the *r* process, but which show a large scatter at low metallicities as well, probably also related to *r*-process contributions [for Sr and Ba, see Hill *et al.* (2019), Mishenina, Pignatari, Gorbaneva, Bisterzo *et al.* (2019), and references therein]. Here we discuss the suggested origins for the *r* process and the possibility of their discrimination. A large scatter seems to indicate a not yet well mixed or averaged interstellar medium, permitting us to see the abundance patterns of individual events. The approach to an average [Eu/Fe] value with a small scatter is observed only in the interval $-2 \leq [\mathrm{Fe/H}] \leq -1$. For [Mg/Fe](but also other alpha elements and Zn and Ge), produced by supernovae, the approach to average values already occurs at about $[\mathrm{Fe/H}] = -3$; see Figs. 7 and 38. A conclusion to take from this would be that *r*-process events occur at a much lower rate than supernovae ones. To be consistent with total solar abundances this would need to be compensated for by larger amounts of their ejecta; see Fig. 39. If the observed abundance ratio of an *r*-process element over Fe ([r/Fe]), for example, [Eu/Fe], scatters at low metallicities due to individual events, this could have one or two origins: (a) the pollution varies dependent on the birth location of the observed star with respect to the *r*-process event and/or (b) the strength of individual *r*-process events varies. The option also exists that a high-frequency weak *r*-process site, related to supernovae, is responsible for the "limited-*r*" sample of Fig. 38, which shows a small scatter only at low metallicities.

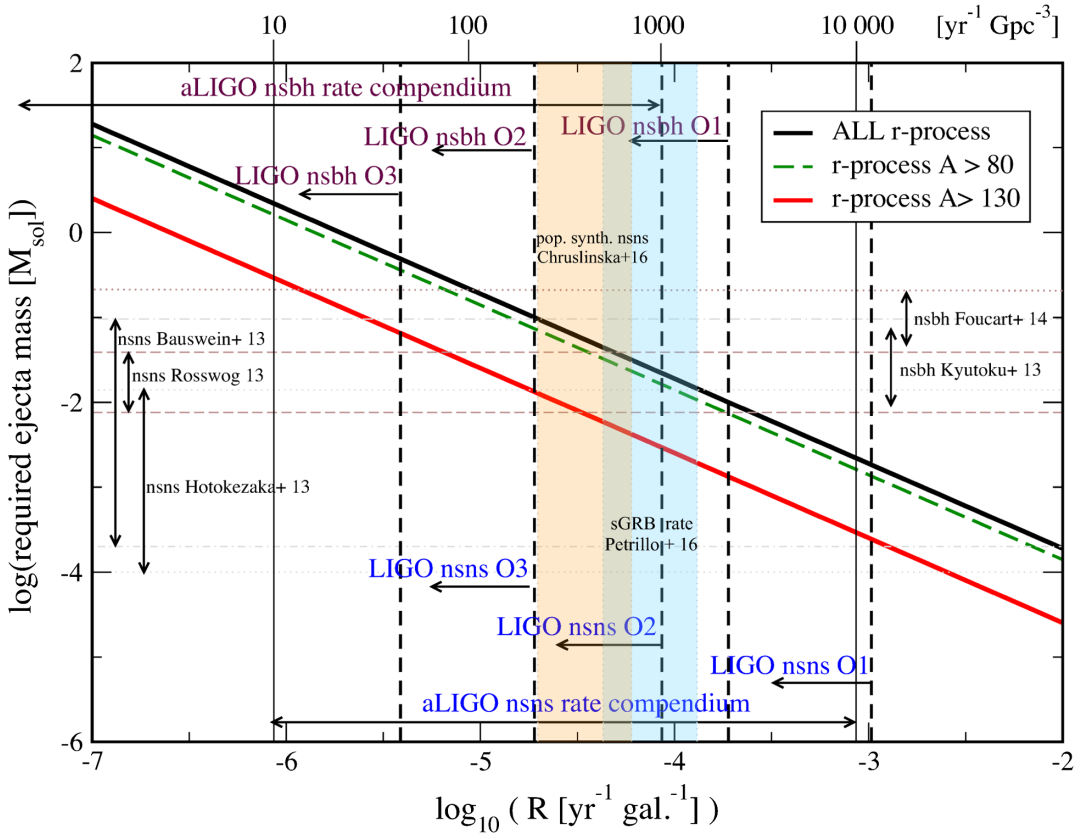

FIG. 39. Required *r*-process ejecta masses as a function of the occurrence frequency of the production site. As shown, on a typical SN frequency of 10^{-2} yr^{-1} about 10^{-4} to 10^{-5} $M_\odot$ of *r*-process matter would need to be produced, for binary merger ejecta with about 10^{-2} $M_\odot$ the frequency must be rarer by a factor of 100 to 1000, and if 1 $M_\odot$ of *r*-process matter is ejected in specific events, the frequency must again be lower by another factor of 100. From Rosswog *et al.*, 2017.

A further interesting aspect of this analysis is related to the question of whether *r*-process elements are correlated or not correlated with other nucleosynthesis products, as well as whether they were coproduced in the same nucleosynthesis site or require a different origin. Cowan *et al.* (2005) compared the abundances of Fe, Ge, Zr, and *r*-process Eu in low-metallicity stars. They found a strong correlation of Ge with Fe, indicating the same nucleosynthesis origin (core-collapse supernovae), a weak correlation of Zr with Fe, indicating that sites other than core-collapse supernovae without or with low Fe ejection contribute as well, and that there is no correlation between Eu and Fe, pointing essentially to a pure *r*-process origin with negligible Fe ejection. More recent data from the SAGA and JINA databases (Suda *et al.*, 2008; Abohalima and Frebel, 2018) permit a weak correlation for [Eu/Fe] < 0.3, i.e., for stars with lower than average *r*-process enrichment. Interpreted in a straightforward way this would point to a negligible Fe/Eu ratio relative to solar ratios in the major *r*-process sources, while a noticeable coproduction of Fe with Eu is possible in weaker *r*-process sources, e.g., possibly with a weak *r* process. Such cases could again be identified with the stars labeled "limited-*r*" in Fig. 38. Not focusing on Eu as a single *r*-process indicator, Ji, Drout, and Hansen (2019) looked for low-metallicity stars ([Fe/H] < -2.5, with compositions indicating an *r*-process origin [Eu/Ba] > 0.4), at the typical lanthanide plus actinide fraction $X_{\rm La}$ among the global *r*-process element distribution. They found for the bulk of low-metallicity stars $\log X_{\rm La} \approx -1.8$, and for the most *r*-process enriched stars $\log X_{\rm La} > -1.5$. This might hint at different sources.

Without pursuing this aspect further, we list here preliminary conclusions for the sites discussed in Sec. VI (see references therein).

(a) Electron-capture supernovae can possibly produce a weak *r* process, not a strong one. If their existence is not ruled out by recent investigations (see Sec. II) and they take place for stars in the interval of 8 to 10 $M_\odot$ of the initial mass function, they are probably not rare. This contradicts a large scatter in [Eu/Fe], but they could be candidates for "limited-*r*" observations.

(b) The neutrino-induced processes in He shells of low-metallicity massive stars would be frequent events at low metallicities, and thus could not lead to a large scatter of [Eu/Fe]. In addition, the related abundance peaks would not be consistent with a strong *r* process.

(c) The regular neutrino-driven core-collapse SNe produce Fe, but at most a weak *r* process (for an extended set of references see Sec. VI.A.1). They are excluded as the site of a strong *r* process because they do not produce the correct abundance pattern and would also be too frequent, not permitting a large scatter in

[Eu/Fe]at low metallicities. However, they could be candidates for limited-*r* observations.

(d) It is not known if quark deconfinement supernovae exist. While present model predictions do not yield a full strong *r* process, the production of elements up to the actinides is possible, however, with the heaviest elements strongly reduced.

(e) Magnetorotational supernovae, starting from a variety of initial magnetic fields, possibly enhanced via magnetorotational (MRI) instabilities, can produce magnetars. While more than 10% of neutron stars seem to be born as magnetars (Beniamini *et al.*, 2019), only progenitors with precollapse magnetic fields of the order of 10^{12}–10^{13} G, and fast rotation can lead to fast jet ejection with a strong *r*-process composition. Smaller fields result in a weak or no *r* process, i.e., following a transition to regular CCSNe. To be consistent with solar *r*-process abundances a core-collapse supernova with these extreme initial conditions should represent 1/100 to 1/1000 of regular core-collapse supernovae (see Fig. 39) and produce also a large [Eu/Fe] scatter. Such events still require observational confirmation.

(f) Collapsars (i.e., high mass stars leading to central black holes, long-duration gamma-ray bursts, hypernovae, and accretion disk outflows) could also be consistent with the overall *r*-process production in the Galaxy, if they would occur more rarely than core-collapse supernovae by more than a factor of 1000 (Siegel, 2019). In such a scenario they would coproduce Fe ($\sim 0.5\ M_\odot$) and *r*-process matter ($> 0.1\ M_\odot$), but with negligible ratios relative to solar (i.e., a ratio of < 5 in mass and about less than 2 in abundances versus about 1000 in a solar composition), and thus not lead to a visible correlation, which is consistent with results given by Cowan *et al.* (2005).

(g) Compact binary mergers lead to *r*-process ejecta masses of the order of $10^{-2}\ M_\odot$ and small occurrence frequencies (less than 1 in 100 CCSNe), which are similar to the ones required for case (e). Their existence and their contribution to heavy elements is observationally proven via gravitational wave and (short) GRB, as well as macronova or kilonova observations. Whether the ejected composition is on average consistent with overall solar *r* abundances will have to be seen in the future.

Summarizing the properties of these events, the following sites remain strong *r*-process candidates: (e) magnetorotational jet supernovae, (f) collapsars, and (g) compact binary mergers. Of these (e) and (f) belong to massive stars, i.e., those occurring during the earliest instances of galactic evolution. Case (g) is related to the coalescence of compact objects resulting from the prior collapse of massive stars and would therefore experience a delay in their appearance.

Macias and Ramirez-Ruiz (2019) suggested a further test to be fulfilled by the site: the maximum pollution a star of the next generation would experience if it is born from a remnant of such an *r*-process event. A Sedov-Taylor blast wave of an explosion with 10^{51} erg results in mixing with about $5 \times 10^4\ M_\odot$ of interstellar medium and about $5 \times 10^5\ M_\odot$ for the more energetic explosions of collapsars. Montes *et al.* (2016) arrived at a similar conclusion for compact binary mergers as for supernovae. Applying this to cases (e), (f), and (g), one would find maximum values of [Eu/Fe] > 3 for collapsars and MHD-jet supernovae, and [Eu/Fe] ∼ 2.3 for compact binary mergers, appearing at [Fe/H] ≈ −3.4, −3.9, and −2.6, if the explosions occurred in a pristine, previously unpolluted interstellar medium (ISM), except for the Fe from two prior CCSNe in the case of compact binary mergers. A comparison of this to Fig. 38 might argue against the first two sites. The question is, however, whether Fe production by earlier CCSNe could have reduced [Eu/Fe]. In a similar way uncertainties in the Fe contribution of the CCSN progenitors of case (g) or further mixing processes could reduce [Fe/H].

In Sec. VIII.B we address the question of how rare and frequent events can be modeled consistently in galactic chemical evolution. Another aspect is how early galactic evolution took place. Indications exist that ultrafaint dwarf galaxies were the earliest building blocks of galactic evolution and that their merger finally led to the evolution of the early Galaxy as a whole. Because of different gas densities they might experience different star formation efficiencies, and due to a low gravitational pull they might lose explosive ejecta more easily. This can have an effect on the point in time and metallicity when the first imprints of explosive ejecta can be observed. These features are addressed as well.

B. Galactic Chemical Evolution Modeling

1. Homogeneous evolution models

In chemical evolution models of galaxies it is still common to use the instantaneous mixing approximation (IMA), i.e., assuming that ejecta compositions were instantaneously and completely mixed throughout the Galaxy. Neglecting this complete mixing can explain radial gradients but would still assume mixing within large and extended volumes (e.g., radial shells). Further developments included infall of primordial matter into and outflow of enriched material out of the Galaxy; for a review of early investigations see Audouze and Tinsley (1976) and Tinsley (1980). When taking into account that explosive stellar ejecta enter the ISM delayed with respect to the birth of a star by the duration of its stellar evolution, detailed predictions for the time evolution of element abundances can be made. Based on nucleosynthesis predictions for stellar deaths, a number of detailed analyses have been performed, from light elements up to the Fe group (Matteucci and Greggio, 1986; Wheeler, Sneden, and Truran, 1989; Timmes, Woosley, and Weaver, 1995; Matteucci and Chiappini, 2001; Kobayashi *et al.*, 2006; Pagel, 2009; Matteucci, 2012; Nomoto, Kobayashi, and Tominaga, 2013). Such approaches have also been applied to understanding the enrichment of heavy elements in the Galaxy (including *r*-process contributions) as a function of time or metallicity [Fe/H] (Ishimaru and Wanajo, 1999; Travaglio *et al.*, 1999; De Donder and Vanbeveren, 2004; Wanajo and Ishimaru, 2006; Matteucci *et al.*, 2014; Ishimaru, Wanajo, and Prantzos, 2015; Vangioni *et al.*, 2016; Côté *et al.*,

2017, 2018, 2019; Hotokezaka, Beniamini, and Piran, 2018; Schönrich and Weinberg, 2019; Siegel, 2019; Grisoni *et al.*, 2020).

The IMA simplifies a chemical evolution model in terms of mass movement. In detail, all event outputs are expected to cool down and mix with the surrounding ISM instantaneously. Thus, a problem of this simplification is this: All stars born at a given time inherit the same averaged abundance patterns of elements and therefore it is impossible to reproduce a scatter in the galactic abundances, which is a crucial aspect, especially at low metallicities. As a consequence a unique relation between galactic evolution time and metallicity [Fe/H] emerges, and for each [Fe/H]only a mean value of $[X/\mathrm{Fe}]$ (X is the element of interest to follow in chemical evolution) is obtained. The IMA approach can be used to get a quick overview of the trends in chemical evolution with a considerably lower computational effort for such a model, and it is probably approximately valid, including in the case of rare r-process events, for $[\mathrm{Fe/H}] > -2$. However, for a detailed study of especially early chemical evolution, including the reproduction of spreads in abundance ratios due to local inhomogeneities, this approach is not sufficient.

2. Inhomogeneous galactic chemical evolution

Local inhomogeneities can be produced if only limited amounts of ISM are polluted by and mixed with the ejecta of an event. The latter effect is of essential importance, especially at low metallicities, where portions of the ISM are already polluted by stellar winds and supernovae, and others are not. Inhomogeneous mixing could produce large element ratios in strongly polluted areas by only one or a few events. This means that the scatter in $[X/\mathrm{Fe}]$ at low metallicities can be a helpful asset in hinting at the origin of element X. Inhomogeneous mixing can experience similar [Fe/H] values in different locations of the Galaxy at different times or different [Fe/H] values at the same time. In addition, different portions of the ISM are polluted by different types of events, leading to a scatter at the same metallicity, which can in fact be utilized as a constraint for these different stellar ejecta. This is especially the case in the early galactic evolution ($[\mathrm{Fe/H}] \leq -2.5$), when locally (out of an entire IMF) only a few stars with varying masses might have exploded and imprinted their stellar neighborhood with their ejecta. Thus, rare events, which produce large amounts of element X, would cause a large scatter, which is helpful for identifying the production site. Therefore, more advanced chemical evolution studies revoked the IMA (Chiappini, Matteucci, and Romano, 2001; Recchi, Matteucci, and D'Ercole, 2001; Argast *et al.*, 2004; Recchi, Calura, and Kroupa, 2009; Spitoni *et al.*, 2009; Cescutti *et al.*, 2015; Hirai *et al.*, 2015, 2017; Shen *et al.*, 2015; Wehmeyer, Pignatari, and Thielemann, 2015; van de Voort *et al.*, 2015, 2020; Haynes and Kobayashi, 2019; Wehmeyer *et al.*, 2019). For the previously summarized reasons, especially for the abundance evolution of r-process elements like Eu, such inhomogeneous chemical evolution models are well suited.

While some of the models mentioned here are of a more stochastic nature, Minchev, Chiappini, and Martig (2014) started with truly chemo "dynamical" galactic evolution models. These models, as well as those given by Hirai *et al.* (2015, 2017), Shen *et al.* (2015), van de Voort *et al.* (2015), Kobayashi (2016), and Haynes and Kobayashi (2019), are based on smoothed-particle hydrodynamics (SPH) simulations. They can model in a self-consistent way massive mergers of galactic subsystems (treated as infall in simpler models), energy feedback from stellar explosions causing outflows (and introduced as such in simpler models), radial migrations in disk galaxies, mixing and diffusion of matter in the ISM, and the initiation of a star formation dependence with progenitor mass. Thus, these global SPH approaches are, on the one hand, most suited to model such environments. However, the mass and smoothing length utilized for the SPH particles will also determine the resolution, as all matter within one particle is treated in a homogeneous fashion. This acts like an artificial mixing on such scales, which are not necessarily related to the real mixing mechanisms. All events within the total mass of one SPH particle are treated within a homogeneous reservoir in this approach. Such effects go into the direction of an IMA on related scales if they are larger than a Sedov blast wave, which mixes only with a limited amount of ISM; see Sec. VIII.A. The chemodynamic code AREPO is probably the most advanced one with the highest resolution, also including MHD and large-scale mixing effects self-consistently (van de Voort *et al.*, 2020), still not resolving Sedov-Taylor blast wave scales, however. This is done in simpler stochastic approaches (Wehmeyer, Pignatari, and Thielemann, 2015; Wehmeyer *et al.*, 2019), which, however, lack most of the advances included in chemodynamic codes.

Within all these approaches a challenge remains: how to model substructures of only about 10^4 $M_\odot$, observed as UFD galaxies, possibly being building blocks of the early Galaxy. In a superposition of IMA treatments Ojima *et al.* (2018), utilizing a variation of sizes of such galactic substructures, made use of related different star formation rates and different outflows according to their gravity and added stochastically neutron-star mergers in these substructures within the range of possible coalescence delay times. The merging of these substructures is expected to eventually represent the early Galaxy as a whole. Tsujimoto and Shigeyama (2014) discussed how Eu of neutron-star merger ejecta is dispersed in UFDs, where, due to ejection velocities of $(0.1 - 0.2)c$, such heavy elements can experience cosmic-ray-type propagation rather than following a hydrodynamical treatment and mix throughout the entire UFD. Komiya and Shigeyama (2016) applied this effect within a chemodynamical model of hierarchical galaxy formation and evolution.

The treatment of compact binary mergers needs to connect the early supernova events that produce the neutron stars and Fe ejecta with the delayed merger event that produces the r-process ejecta. Special binary evolution aspects might apply for such close binary systems and the resulting supernovae (Müller *et al.*, 2018, 2019), not necessarily accompanied by the same amount of Fe/Ni ejecta as for regular CCSNe. Since explosive events give rise to nucleosynthesis inside a supernova remnant bubble (given by a Sedov-Taylor blast wave), the abundances of metals are higher than they are outside such a remnant. A star that is born later inside such a remnant will inherit more metals than a star born outside it. Thus, where a star is born during galactic evolution is of high importance, especially in the early phases. If the later merger, producing

large amounts of *r*-process matter, is occurring within the supernova remnant bubble, the [Fe/H] ratio has already been set by the earlier supernova explosions, and the related [Eu/Fe] ratios will appear at the appropriate [Fe/H] ratio. The main challenge is to have a large [Eu/Fe] ratio at the lowest metallicities, which could be achieved in the following ways: (a) neutron-star kicks during the supernova explosions act in such a way that the actual neutron-star merger takes place outside the initial Fe pollution by the preceding supernovae, (b) neutron-star–black hole mergers would have experienced the Fe ejecta of only one supernova, and (c) large-scale turbulent mixing could lead to the dilution of Fe on timescales shorter than the coalescence delay time of the mergers. Such effects are not yet necessarily treated correctly by present models.

C. Connecting observational constraints on *r*-process abundances with different astrophysical sites

In Sec. VIII.A, we listed possible production sites for a strong *r* process. They need to fulfill the following observational constraints: (i) to lead to a large scatter of $[r/\mathrm{Fe}]$ at low metallicities, these events must be rare relative to regular core-collapse supernovae (this does not preclude the latter from being the site of a weak *r* process), and (ii) if they should be the dominant site responsible for the solar *r* abundances, the combination of their ejecta mass and occurrence frequency must be able to match this requirement. Three of the following listed possible sites may fulfill both criteria: (e) magnetorotational jet supernovae, (f) collapsars, and (g) compact binary mergers. Site (g) is a rare but observed event with ejecta amounts consistent with solar abundances. Sites (e) and (f) are potential *r*-process scenarios that are still lacking observational confirmation. If the required high rotation rates and extreme magnetic fields for magnetorotational jet supernovae can exist, they would eject similar amounts of *r*-process matter as binary mergers. These requirements would also make them rare events. Collapsars [case (f)], also known as hypernovae or observed as lGRBs, have been related to high ^{56}Ni ejecta but recently also postulated to eject more than 0.1 $M_\odot$ of *r*-process matter (Siegel and Metzger, 2017; Janiuk, 2019a; Siegel, Barnes, and Metzger, 2019). In such a case, these events should be rare, even a factor of 10 or more rarer than compact binary mergers.

A further requirement, in addition to the two already discussed (rarity and reproducing the total amount of solar *r* abundances), is that galactic evolution modeling should reproduce the observed metallicity or time evolution. As discussed, homogeneous approaches with IMA are justified if applied for metallicities $[\mathrm{Fe/H}] > -2$. This has especially been utilized for testing the distribution of delay times for neutron-star mergers after the formation of a binary neutron-star system. Early investigations utilized coalescence delay times with a narrow spread. Population synthesis studies, in accordance with the occurrence of sGRBs (related to compact binary mergers), indicate that the possible delay times follow a distribution with a large spread, ranging over orders of magnitude with a t^{-1} behavior. Based on such behavior, studies with the IMA modeling of chemical evolution (Côté *et al.*, 2017, 2018, 2019; Hotokezaka, Beniamini, and Piran, 2018; Siegel, 2019) came to the conclusion that mergers would not be able to reproduce the galactic evolution for metallicities $[\mathrm{Fe/H}] > -2$, including the decline of [Eu/Fe] at $[\mathrm{Fe/H}] = -1$. This would require either a different delay-time distribution (Vigna-Gómez *et al.*, 2018; Beniamini and Piran, 2019; Simonetti *et al.*, 2019) or an additional source for the main, strong *r* process. Schönrich and Weinberg (2019) suggested another solution: star formation takes place only in cooled regions of the ISM; i.e., not all recently ejected matter can already be incorporated and stars contain lower metallicities [Fe/H] than the overall ISM at the time of their birth. This shifts [Eu/Fe] ratios to lower [Fe/H] and has a similar effect as a steeper delay-time distribution.

To address the challenges of explaining the $[r/\mathrm{Fe}]$ scatter at metallicities $[\mathrm{Fe/H}] < -2$, inhomogeneous chemical evolution studies are needed and have been implemented (Argast *et al.*, 2004; Hirai *et al.*, 2015, 2017; Shen *et al.*, 2015; Wehmeyer, Pignatari, and Thielemann, 2015; van de Voort *et al.*, 2015, 2020; Komiya and Shigeyama, 2016; Mennekens and Vanbeveren, 2016; Haynes and Kobayashi, 2019; Wehmeyer *et al.*, 2019). At these low metallicities, there is an important difference among scenarios (e), (f), and (g): MHD supernova and collapsars result from the final phases of a single massive star, while in the merger scenario two supernova explosions are required before the merger happens after a delay. Scenarios (e) and (f) can act at earliest times in galactic evolution, while we have to examine which effect the delay time in scenario (g) plays.

Therefore, the question arises as to whether, in addition to the scatter of *r*-process elements like Eu compared to Fe, [Eu/Fe], covering more than 2 orders of magnitude (see Figs. 7 and 38), especially the early appearance of high [Eu/Fe] values, can be consistent with a "delayed" process like compact binary mergers. Ramirez-Ruiz *et al.* (2015) suggested much shorter delays, because collisions of neutron stars that were dynamically assembled in the first nuclear star clusters could take place shortly after the supernovae occurrences that produced them, in opposition to mergers resulting from binary evolution. However, the "early" appearance at low [Fe/H] values is not related only to "timing." In such a case mergers take place only after the progenitor supernovae have already produced Fe. This is similar to compact binary mergers with a longer delay, as in that case the supernovae responsible for producing at least one neutron-star produced Fe, which shifts the appearance of a typical *r*-process element like Eu to higher metallicities [Fe/H]. This effect has been discussed in inhomogeneous galactic evolution models utilizing neutron-star mergers, i.e., events with two prior supernovae and their Fe ejecta (Argast *et al.*, 2004; Cescutti *et al.*, 2015; Wehmeyer, Pignatari, and Thielemann, 2015; Haynes and Kobayashi, 2019; van de Voort *et al.*, 2020). These researchers came to the conclusion that neutron-star mergers have problems to explain [Eu/Fe] at lowest metallicities, while earlier inhomogenous models came to the conclusion that they can do so (Hirai *et al.*, 2015, 2017; Shen *et al.*, 2015; van de Voort *et al.*, 2015; Komiya and Shigeyama, 2016). The difference is related to resolution and mixing issues discussed in Sec. VIII.B, but it should be noted that the high-resolution run given by van de Voort *et al.* (2015) as well as recent further investigations (see Fig. 40) (van de Voort *et al.*, 2020) indicate

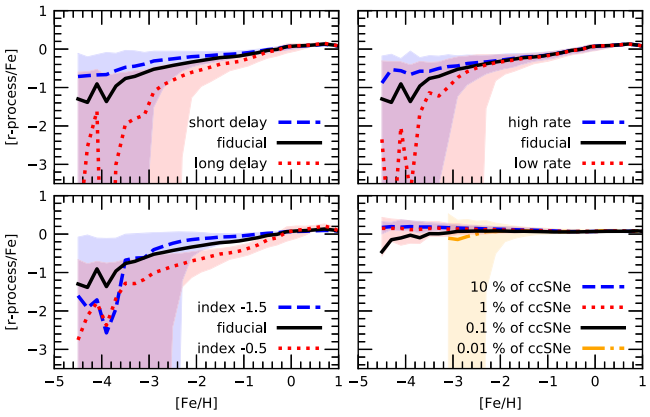

FIG. 40. Results from chemodynamical inhomogeneous evolution models predicting median values (lines) and distributions of $[r/\mathrm{Fe}]$ ratios in newly born stars of the Milky Way for three different neutron-star merger rates, different indices of the coalescence delay-time distributions t^{index}, and an additional admixture of *r*-process events occurring with rates proportional to CCSNe. The combination of additional *r*-process events proportional to the CCSN rate, which were of great importance at low metallicities early in the evolution of the Galaxy, and neutron-star mergers permits an $[r/\mathrm{Fe}]$ dependence on [Fe/H] that does not decline toward low metallicities. From van de Voort *et al.*, 2020.

the rise of [Eu/Fe] to occur at too high of a metallicity. Whether and how much the use of NS-BH mergers, which explode in an environment polluted only with Fe by one prior supernova, improve this situation remains to be seen (Wehmeyer *et al.* (2019); see Fig. 41.

Thus, it would remain to explain the strong *r* process by NS mergers alone. But the path to a binary merger is a complex

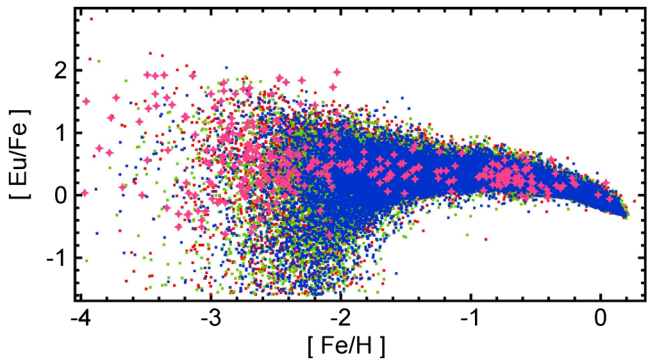

FIG. 41. Evolution of [Eu/Fe] in a stochastic inhomogeneous galactic chemical evolution model, including both neutron-star and neutron-star–black hole mergers as *r*-process sites, under the assumption that all NS-BH mergers eject *r*-process matter. Magenta crosses represent observations, whereas different choices for black hole formation are utilized at low metallicities. Red (green, blue) squares represent models where all stars ≥ 20 $M_\odot$ (≥ 25 $M_\odot$, ≥ 30 $M_\odot$) at metallicites $Z \leq 10^{-2} Z_\odot$ lead to failed SNe and black holes at the end of their life. The combination of these two *r*-process sources also permits a good fit with observations at low metallicities. From Wehmeyer *et al.*, 2019.

one. The mass, ejecta, and explosion energy of the second supernova in a binary system have to be addressed for a full understanding (Müller *et al.*, 2018, 2019). This includes the fact that neutron-star kicks from supernova explosions could move the neutron-star binary far out of reach of the initial supernova remnant that polluted the local ISM with Ni and Fe (Fryer and Kalogera, 1997; Kalogera and Fryer, 1999; Abbott *et al.*, 2017c; Safarzadeh *et al.*, 2019). If in such a way the merger event can be displaced from the original supernovae, Wehmeyer *et al.* (2018) found that mergers could barely be made consistent with the [Eu/Fe] observations if such a displacement were taken into account and short coalescence timescales of 10^6 yr were used. In addition, triple and multiple stellar systems can cause different delay-time distributions for neutron-star mergers (Bonetti *et al.*, 2018; Hamers and Thompson, 2019). And, as mentioned, compact binary mergers also include neutron-star–black hole mergers, which experience the pollution from only one prior supernova (Wehmeyer *et al.*, 2019).

A different issue is the formation of the Galaxy from small substructures like UFDs, which, due to different gas densities, experience different star formation efficiencies and, due to small gravity, the loss of metals from explosive events (Simon, 2019), both shifting the occurrence of abundance features to lower metallicities. The baryonic mass of these UFDs, as small as 10^4 $M_\odot$, is too small to be followed by the previously discussed global simulations, while local simulations have been performed (Corlies, Johnston, and Wise, 2018; Emerick *et al.*, 2018; Tarumi, Yoshida, and Inoue, 2020). The IMA, combined with outflow, can probably be utilized as a first order approximation locally in UFDs. Observations indicate that star formation continues for only about a few 10^8 yr, permitting one to still observe features from type Ia supernovae contributions, leading to the $[\alpha/\mathrm{Fe}]$ downturn at $[\mathrm{Fe/H}] < -2$ (Pakhomov *et al.*, 2019), which takes place in the Milky Way only at -1. As strong *r*-process sites are rare events (by a factor of 100 to 1000 less frequent than both types of supernovae) only a few UFDs show noticeable *r*-process contributions, as observed in Reticulum II and Tucana III (Beniamini, Hotokezaka, and Piran, 2016; Ji *et al.*, 2016; Ji and Frebel, 2018; Marshall *et al.*, 2019), while displaying underabundances in most cases (Ji *et al.*, 2019; Simon, 2019). Only about 10% of UFDs experience a strong early *r*-process contribution (Brauer *et al.*, 2019). An early simpler IMA approach followed by Ishimaru, Wanajo, and Prantzos (2015), recently extended by a stochastic inclusion of neutron-star mergers, which are permitted to vary statistically with respect to coalescence timescales (Ojima *et al.*, 2018), indicates a possible solution to the question of whether neutron-star mergers alone could be responsible for the appearance of *r*-process products at the lowest metallicities. This relates to the question of whether the apparently uniform *r*-process abundances observed in stars of UFDs can be consistent with NS merger scenarios (Tsujimoto and Shigeyama, 2014; Komiya and Shigeyama, 2016; Bonetti *et al.*, 2019; Tarumi, Yoshida, and Inoue, 2020).

The discussion here, focusing on the question of whether galactic chemical evolution studies can determine which of the three sites [(e) magnetorotational jet supernovae, (f) collapsars

and hypernovae, or (g) compact binary mergers] are consistent with or required from observations, came to a still somewhat open result as to whether neutron-star mergers alone can provide the explanation for a strong *r* process throughout and also in the early Galaxy. Ongoing and future observations utilizing dynamical tagging of groups in space with orbital energy as well as angular momentum, combined with their abundance patterns (Gudin *et al.*, 2020; Yuan *et al.*, 2020), might provide further clues. The behavior of [Eu/Fe] around [Fe/H] $= -1$ puts challenges on their delay-time distribution, and the early rise of [Eu/Fe] at lowest metallicities can hardly be achieved within global galactic evolution studies, not resolving scales of ultrafaint dwarf galaxies. These studies argue for a contribution of (e) and/or (f) at early times in galactic evolution. If UFDs are considered, there seems to be a possible way out of this conclusion. However, there are independent observational indications, combining results from the Milky Way and its dwarf galaxy satellites Sagittarius, Fornax, and Sculptor, that there are two distinct *r*-process contributions from an early quick source and a delayed source (Skúladóttir *et al.*, 2019; Skúladóttir and Salvadori, 2020). Thus, the answer is still somewhat in question, also depending on whether on average mergers alone can reproduce the lanthanide fraction X_{La} observed in low-metallicity stars (Ji *et al.*, 2019). It also has to be shown whether the turbulent diffusion coefficients, deduced by Beniamini and Hotokezaka (2020) from occurrence frequencies and production yields of different *r*-process sites to reproduce the abundance scatter at low metallicities, agree with those from self-consistent simulations (van de Voort *et al.*, 2020).

D. Long-lived radioactivities: *r*-process cosmochronometers and actinide-boost stars

A complete list of isotopes with half-lives in the range 10^7–10^{11} yr is given in Table II. They cover a time span from a lower limit in excess of the evolution time of massive stars up to and beyond the age of the Universe. Such nuclei can be utilized as "chronometers" for nucleosynthesis processes in galactic evolution and also serve as a measure for the age of the Galaxy (and thus as a lower limit for the age of the Universe; see the earlier discussion in Sec. II.D). The list is not long. Two of the nuclei require predictions for the production of the ground and isomeric states (^{92}Nb, ^{176}Lu). With the exception of ^{40}K, all of the remaining nuclei are heavier than the "Fe group" and can be made only via neutron capture.

TABLE II. Isotopes with half-lives in the range 10^7–10^{11} yr.

Isotope	Half-life (yr)	Isotope	Half-life (yr)
^{40}K	1.3×10^9	^{205}Pb	1.5×10^7
^{87}Rb	4.8×10^{10}	^{232}Th	1.4×10^{10}
^{92}Nb	3.5×10^7	^{235}U	7.0×10^8
^{129}I	1.6×10^7	^{236}U	2.3×10^7
^{147}Sm	1.1×10^{11}	^{238}U	4.5×10^9
^{176}Lu	3.7×10^{10}	^{244}Pu	8.0×10^7
^{187}Re	4.4×10^{10}	^{247}Cm	1.6×10^7

^{232}Th and ^{238}U have half-lives comparable to the age of the Galaxy and Universe. They, as well as all other actinide isotopes, are products of a single nucleosynthesis process, the *r* process. The possible astrophysical settings were discussed previously. The question is how to predict reliable production ratios for these long-lived isotopes if (a) not even the site is completely clear, and (b) even for a given site nuclear uncertainties enter.

Nevertheless, for many years such chronometers have been utilized to attempt predictions for the age of the Galaxy (Fowler and Hoyle, 1960; Schramm and Wasserburg, 1970; Cowan, Thielemann, and Truran, 1991; Panov *et al.*, 2017). This was performed initially with simplified chemical evolution models (i) via the prediction of ^{232}Th/^{238}U and ^{235}U/^{238}U ratios in *r*-process calculations, (ii) by applying them in galactic evolution models, which include assumptions about the histories of star formation rates and *r*-process production, and finally (iii) by comparing these ratios with meteoritic data, which provide the ^{232}Th/^{238}U and ^{235}U/^{238}U ratios at the formation of the Solar System. An advantage (somewhat decreasing the nuclear uncertainties involved) is that ^{232}Th and ^{235,238}U are populated by α-decay chains, summing up the contributions of a number of nuclei, and therefore uncertainties in the predictions of the individual isotopes involved average out to some extent (Thielemann, Metzinger, and Klapdor, 1983; Cowan, Thielemann, and Truran, 1991; Goriely and Clerbaux, 1999).

Observations of elemental Th and U with respect to the *r*-process reference element Eu in individual old stars can also be used to estimate the age. However, in general this requires a chemical evolution model, except in the case of low-metallicity stars. The metallicities of the halo stars for which neutron-capture element data have become available are in the range $-3 \lesssim$ [Fe/H] $\lesssim -2$. Typical, still simple, galactic chemical evolution calculations suggest approximately the metallicity-age relation [Fe/H] $= -1$ at 10^9 yr, [Fe/H] $= -2$ at 10^8 yr, and [Fe/H] $= -3$ at 10^7 yr [if the IMA could be applied at such low metallicities; see Tsujimoto *et al.* (1997) and Chiappini, Matteucci, and Padoan 2000)]. Even if these estimates are uncertain by a factor of 2 to 3, low-metallicity stars were certainly born when the Galaxy was only 10^7–10^8 yr old, a small fraction of its present age. Thus, the neutron-capture elements observed in low-metallicity stars were generated in only one or at most a few prior nucleosynthesis episodes; see also Beniamini and Hotokezaka (2020). If several events contributed, the time interval between these events had to be short relative to Th decay ages. Thus, it is justified to treat the sum as a single *r*-process abundance distribution which undergoes decay from the time of its incorporation into a low-metallicity star until its detection in present observations.

Such considerations can also be employed for the ratio of Th and U to stable Pb, which has in addition to the *s*-process contribution (i) a direct *r*-process contribution to the $^{206-208}$Pb isotopes, (ii) a contribution due to fast α- and β-decay chains from unstable nuclei produced in the *r* process beyond Pb (decaying within less than 10^6 yr), and finally (iii) a contribution from the long-lived decay chains originating at ^{232}Th and ^{235,238}U (Frebel and Kratz, 2009; Roederer *et al.*, 2009).

The prediction of required isotopic elemental production ratios, lacking until recently site-specific detailed information, has been based on parametrized so-called site-independent fits, utilizing a superposition of neutron densities that reproduce all solar *r*-process abundances from $A = 130$ through the actinides (Cowan *et al.*, 1999; Freiburghaus *et al.*, 1999; Goriely and Arnould, 2001; Schatz *et al.*, 2002; Kratz *et al.*, 2004; Roederer *et al.*, 2009). Alternatively neutrino-wind models were employed with a superposition of contributing entropy components (Freiburghaus *et al.*, 1999; Farouqi *et al.*, 2010; Kratz, Farouqi, and Möller, 2014; Hill *et al.*, 2017). Goriely and Janka (2016) used steady-state neutrino-driven wind models with adiabatic expansion and the superposition of many contributing components.

Making use of such so-called site-independent predictions for standard *r*-process production ratios, combined with observed abundance ratios found in low-metallicity stars, gives an indication of the decay time of radioactive isotopes since the star was born, polluted by an original *r*-process pattern. Typical results for ages of most low-metallicity *r*-process-enhanced stars are in the range of 12–14 Gyr (Cowan *et al.*, 1999; Schatz *et al.*, 2002; Kratz *et al.*, 2004; Roederer *et al.*, 2009; Hill *et al.*, 2017). This approach assumes that the production ratios of the site(s) responsible for these observations are consistent with those reproducing a solar *r* process. We should keep in mind that, independent of the previously discussed uncertainties in abundance predictions, such age determinations are also affected by observational uncertainties. Ludwig *et al.* (2010) provided a detailed analysis of the effects to be expected, which also apply to the forthcoming discussion.

Among the stars with observed Th and U, there are a number of so-called actinide-boost stars with an enhanced ratio of Th/Eu and U/Eu relative to all other *r*-process-enhanced stars (Roederer *et al.*, 2009; Holmbeck *et al.*, 2018), observed especially at low metallicities around $[\mathrm{Fe/H}] \approx -3$. When utilizing as initial abundance patterns the previously discussed parametrized fits (reproducing solar *r* abundances), the age estimates for those stars are unrealistically low or even negative; see the right scale of Fig. 9 in Sec. II. Although it appears that most of the elemental abundances in actinide-boost stars, up to the third *r*-process peak, are close to a solar *r*-process pattern, one should investigate further possible correlations between the actinide boost and other abundance features. The question is whether these features point either to a different site than the dominant one responsible for the solar *r*-process abundances or to variations of conditions in the same type of events, depending on still unknown aspects (Holmbeck, Frebel *et al.*, 2019; Holmbeck, Sprouse *et al.*, 2019).

The actinide-to-Eu ratio is related to the path of the *r* process and the timing (a) when the actinides are reached via the *r*-process flow, and (b) when fission plays a role during the further flow onto heavier nuclei. For this reason, the *r*-process results are dependent on the proton-to-nucleon ratio Y_e in the expanding matter, determining the neutron-to-seed ratio. Intuitively one could expect that the lowest (most neutron-rich) Y_e's would lead to the highest actinide production. Holmbeck, Sprouse *et al.* (2019) showed, with their nuclear physics input, that the ratio is highest for a Y_e in the range

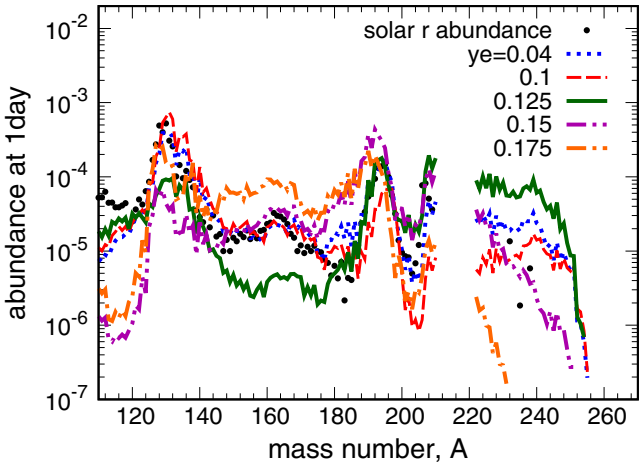

FIG. 42. Utilizing the Duflo-Zuker mass model (Duflo and Zuker, 1995) and trajectories from Barnes *et al.* (2016) permits large variations in actinide production, even at low Y_e. The highest actinide production is found at $Y_e = 0.125$. From M.-R. Wu *et al.* (2017).

0.1–0.15 (see their Figs. 16 and 17), with the highest values found at around $Y_e = 0.125$. Higher Y_e values (i.e., less neutron-rich conditions) lead to a smaller actinide production because of a weaker *r* process. Lower Y_e values (i.e., more or extremely neutron-rich conditions) also lead to smaller ratios. This is due to the fact that an initially higher actinide production is reduced later by fission cycling, which can be effective in destroying the actinides. The details depend on mass models and related fission barriers.

M.-R. Wu *et al.* (2017) presented a similar behavior, as indicated in Fig. 42, using trajectories adapted from Barnes *et al.* (2016), also finding an actinide boost for Y_e conditions close to 0.125. Eichler *et al.* (2019) did an independent study, testing in detail the influence of nuclear physics uncertainties. They found slightly higher Y_e values of 0.15 for the maximum actinide production, but similar conclusions, while also examining the actinide decline for lower Y_e's as a function of the number of resulting fission cycles. In all these cases the Th/U ratio, involving two actinide nuclei close in mass numbers, is not strongly affected by a variation in Y_e.

Holmbeck, Frebel *et al.* (2019) argued that a variety of neutron-star merger characteristics (possible due to different binary masses and/or mass ratios, affecting the total amount of dynamic ejecta, including tidal tails, neutrino wind, and black hole accretion disk outflows) can be responsible for varying outcomes, ranging from solar-type *r*-process patterns to actinide boosts. Wu, Barnes *et al.* (2019) discussed how variations in the produced abundance patterns can affect kilonova light curves and spectra, with the aim of identifying the exact pattern for individual observed events. Ji, Drout, and Hansen (2019) hinted that the observed merger GW170817 is not as lanthanide and actinide rich as required for the dominant solar *r*-process site.

Thus, the question remains, based on low-metallicity observations, as to why most events lead apparently to a solar *r*-process pattern and some others cause an actinide boost (keep in mind also the previous discussion of

observational uncertainties) (Ludwig *et al.*, 2010). And it remains to be seen whether different sites are the reason for these two features or whether one site, i.e., neutron-star mergers, can lead to this variety. Which Y_e interval is resulting from specific events, stopping above 0.125, including 0.125, or also continuing to values below 0.125? What are the dominant conditions in MHD-jet supernovae, what are the properties of accretion disk outflows in collapsars, what is the role of the individual components in compact binary mergers [dynamic ejecta (including prompt ejecta and tidal tails), neutrino winds, and accretion disk outflows], and do all of these subcomponents exist if one of the compact objects is a black hole or the combined mass is sufficiently high, preventing the intermediate existence of a hypermassive neutron star?

Conclusions are still speculative, but variations among the different sites should be investigated further (Nishimura *et al.*, 2017; Eichler *et al.*, 2019; Holmbeck, Frebel *et al.*, 2019; Siegel, 2019; Siegel, Barnes, and Metzger, 2019; Wu, Barnes *et al.*, 2019). Improved predictions for the most probable main *r*-process sites, discussed in Secs. VI and VIII.C, plus possibly exotic scenarios [see Fuller, Kusenko, and Takhistov (2017), but also Camelio, Dietrich, and Rosswog (2018)] can perhaps lead to a one-to-one connection between responsible production sites and observations (although predictions depend on uncertainties with respect to conditions in the astrophysical sites as well as uncertainties in nuclear physics properties).

Independent of these considerations, concerning actinide boosts, it should be kept in mind that chemical evolution findings (Cescutti *et al.*, 2015; Wehmeyer, Pignatari, and Thielemann, 2015; Côté *et al.*, 2017, 2018, 2019; Hotokezaka, Beniamini, and Piran, 2018; Haynes and Kobayashi, 2019; van de Voort *et al.*, 2020) and observations (Skúladóttir *et al.*, 2019; Skúladóttir and Salvadori, 2020) seem to indicate that there are two distinct *r*-process contributions from an early quick source and a delayed source.

In addition to the identification and possible explanation of the abundance pattern in actinide-boost stars related to long-lived unstable Th and U isotopes, shorter-lived radioactive isotopes were addressed by Lugaro, Ott, and Kereszturi (2018), Vescovi *et al.* (2018), and Côté, Yagüe *et al.* (2019). Nuclei with half-lives of a few 10^6 to 10^7 yr permit observers to probe recent nucleosynthesis events in the vicinity of the presolar nebula. In the present context only nuclei of an *r*-process origin are of interest here. Of these Côté, Yagüe *et al.* (2019) pointed out ^{129}I and ^{247}Cm with identical half-lives, and Côté *et al.* (2020) utilized them to measure the strength of the last *r*-process event affecting the presolar nebula, as indicated by meteoritic data. In this respect what composition even later occurring events contribute is also of interest, affecting only the delivery of ^{244}Pu onto Earth and the deposition in deep-sea sediment over the past few hundred million years; see Sec. II.D. Recent investigations by Wallner *et al.* (2019), possibly indicating that ^{60}Fe from the last CCSNe might have been accompanied by a minor ^{244}Pu contribution, would possibly permit a frequent weak *r* process, producing extremely small, but not negligible, amounts of actinides.

IX. FINAL REMARKS AND CONCLUSIONS

In this review we have reported on recent developments and new data from nuclear and atomic physics experiments and constraints from astronomical observations. We have also discussed their impact, combined with advances in astrophysical modeling, on our understanding of the astrophysical *r* process. This includes the operation of the *r* process, its potential astrophysical sites, and its contribution to the chemical evolution of our Galaxy. Despite the tremendous progress achieved since the *r* process was proposed by Burbidge *et al.* (1957) and Cameron (1957), several open questions still remain. In these final remarks we specify these challenges, and also future opportunities for how to overcome them.

With respect to nuclear physics, which enters decisively into producing the abundance pattern of the *r* process, major achievements have been accomplished. This is related to experimental progress in accessing unstable nuclei far from stability, combined with a growing theoretical understanding of their properties.

(1) Novel detection technologies, employed at operational RIB facilities, have allowed us to determine *nuclear masses* for nuclei far from stability with improved precision. This in turn served as stringent constraints to improve empirical and microscopic global mass models that in *r*-process simulations determine the location of the *r*-process path in the nuclear chart. Further improvements are required to remove uncertainties, which have decisive consequences for the *r*-process mass flow across neutron-shell closures shaping the final *r*-process abundance distribution.

(2) The measurement of *β-decay half-lives* for medium-mass neutron-rich nuclei at or near the *r*-process path at RIKEN has been a major recent achievement. The data are of crucial importance for the speed with which the *r* process moves matter to heavier nuclei and (in combination with the location of the *r*-process path) for the height of peaks and the overall final abundance distribution. Progress has also been reached to measure β-delayed neutron emissions (important in the late phases during decay back to stability), particularly for nuclei close to the $N = 126$ shell closure. However, no β-decay data yet exist for $N = 126$ (or heavier) nuclei on the *r*-process path. Such measurements, which can be expected from the next-generation RIB facilities, will be of crucial relevance in determining the amount of matter that is transported beyond the third *r*-process peak into the fission region.

(3) *Fission* plays a crucial role in current *r*-process models, particularly related to high neutron density environments, as in neutron-star mergers. Here fission terminates the flow to heavier nuclei beyond the actinides, causing fission cycling. This returns matter to lighter nuclei and is also a source of neutrons that can shape the final abundance pattern. In these models fission yields contribute strongly to the second *r*-process peak, which needs to be confirmed in future work. Fission also affects the heaviest long-lived nuclei that are produced by the *r* process. Heavy

neutron-rich nuclei, in particular, those at the $N = 184$ shell closure, are still experimentally out of reach. But experimental programs are envisioned to push the measurement of fission rates and yields to more neutron-rich nuclei than are currently accessible. Such improvements are also required to address the question whether superheavy elements can be produced by the *r* process.

(4) Simulations identify *α decays*, especially the decay chains originating from actinide nuclei, as important contributors to the kilonova light curve and to determine the *r*-process Pb abundance. Many of these decays are experimentally studied. It is an open question as to whether α decays can compete with fission for heavy neutron-rich nuclei.

(5) *Neutron captures* (and their inverse photodisintegration) affect the final abundance distribution during the *r*-process freeze-out period. (For a large variety of conditions during the *r*-process buildup a chemical equilibrium between these two reactions can be maintained, and the *r*-process path is determined solely by nuclear masses.) The nuclei involved can have low neutron-separation energies (with a low density of states) so that direct neutron captures might be favored over compound nucleus reactions. Direct measurements of neutron-capture rates for *r*-process nuclei are currently experimentally out of reach. Advances have been made to develop surrogate techniques to constrain the rates indirectly or to reduce nuclear uncertainties entering statistical model capture rate evaluations. If the direct capture is dominated by individual resonances, the rate can be constrained by indirect determination of the resonance parameters.

In the investigation of all these aspects much progress has occurred, but major uncertainties are remaining, as experiments have touched nuclei in the *r*-process path only at a limited number of locations in the nuclear chart. Besides these nuclear aspects, there exist also other challenges in modeling astrophysical sites of the *r* process:

(1) Most environments expected to be sites of a strong *r* process involve objects at high densities and temperatures, making it necessary to determine the *nuclear equation of state* in these extreme conditions. Constraints for the EOS have been obtained in relativistic heavy-ion collisions and by astronomical observations. Decisive progress is expected from upcoming nuclear experiments at heavy-ion facilities and by dedicated experiments probing the nuclear symmetry energy as well as from astronomical observations exploiting upgraded and novel detectors. Improved knowledge of the nuclear EOS is also important to answer the question of whether in compact binary mergers a hypermassive neutron star exists temporarily or even remains as a final outcome.

(2) The modeling of *r*-process sites requires multiscale general-relativistic, multidimensional radiation magnetohydrodynamics simulations. Such calculations are computationally demanding and involve approximations and numerical methods whose reliability needs to be critically assessed.

(3) Many of the discussed effects involve the modeling of *magnetic fields*, possibly as a major ingredient to predict jet ejection. A decisive aspect is whether and how magnetic fields can be enhanced during these events, where the magnetorotational instability MRI plays a major role. High-resolution magnetohydrodynamics modeling is a field only at the brink of getting reliable results for the modeling of complete astrophysical sites.

(4) As reactions mediated by the weak interaction are not in equilibrium, processes like electron and positron captures and *neutrino interactions with matter* have to be explicitly modeled. Neutrino flavor transformations, especially via matter-neutrino resonances and fast pairwise flavor conversion, have been identified as playing an essential role in compact binary mergers. Weak-interaction reactions are also crucial to determine the proton-to-nucleon ratio Y_e, which is a key ingredient for *r*-process nucleosynthesis. The adequate treatment of the neutrino processes requires multidimensional transport simulations. Owing to the complicated geometries involved, studies of neutrino flavor transformations are in their infancy.

(5) In addition to neutrino transport, general *radiation transport via photons* is important for predicting the electromagnetic aftermath of explosions in order to make a connection to observational features like light curves and spectra. Fundamental ingredients for these predictions are the total energy released by radioactive matter, its thermalization, and the still unknown atomic opacities of especially multiply ionized heavy elements. Progress in this field will permit us to test whether the lanthanide fraction X_{La} in observed events is consistent with solar *r*-process abundances.

Based on the presently available input for nuclear properties and the present status with respect to modeling possible *r*-process sites, three major options for sites of a strong *r* process have emerged. For one of these sites (NS mergers) observational evidence exists, while for the other two observational proofs of *r*-process ejecta are still missing.

(1) Models of *compact binary mergers* indicate that they are prolific sites of *r*-process nucleosynthesis, with up to 10^{-2} $M_\odot$ of *r*-process matter in the dynamic ejecta and a few times 10^{-2} $M_\odot$ from accretion disk outflows. When including all components (dynamic ejecta, neutrino winds, and viscous or secular accretion disk outflows) they produce not only the heaviest *r*-process nuclei but also significant amounts of the standard solar *r*-process abundances for mass numbers with $A < 130$. The first observation of a neutron-star merger (GW170817), accompanied by the AT 2017gfo macronova or kilonova thermal afterglow, makes this the first proven and confirmed production site of heavy *r*-process elements; variations, depending on the mass of the merged object, as well as neutron-star—black hole mergers require further observational confirmation and theoretical modeling.

(2) There are observational indications of neutron stars with surface magnetic fields exceeding 10^{15} G (magnetars)

that could be produced by a rare class of *magneto-rotational core-collapse supernovae*. Depending on high initial magnetic field strengths and rotation rates before collapse, they might eject *r*-process matter in polar jets. However, better predictions of these initial parameters from stellar evolution are needed to understand whether fast ejection via jets takes place or whether a MRI will only eventually cause an explosion, ejecting less neutronized matter. Investigating the role of the MRI during the collapse-explosion phase is impossible without high-resolution simulations.

(3) A recent multidimensional MHD simulation for *accretion disk outflows from collapsars*, i.e., objects that result from the final collapse of massive stars and end in the formation of a black hole, suggests that large amounts of *r*-process material ($> 0.1\ M_\odot$) can be ejected. Further simulations are needed, in particular, to understand the relation of collapsars to hypernovae and long-duration GRBs and their potential for the galactic inventory of *r*-process material.

While the three previously mentioned sites are candidates for a strong *r* process, producing heavy elements up to the actinides, there are further options to produce a so-called weak or limited-*r* process, probably also synthesizing elements up to Eu (and possibly beyond), but with a steeper decline as a function of nuclear-mass number than found in the Solar System *r*-abundance pattern; possible such sites include electron-capture supernovae, regular core-collapse supernovae, and also quark deconfinement supernovae.

All of these models have to be confronted and scrutinized by astronomical observations. An interesting aspect is that one of the listed and confirmed sites is related to binary systems, while the others are resulting from the evolution of massive single stars. Observations supporting and constraining *r*-process sites exist in a number of ways:

(1) The requirement to reproduce the total amount of *r*-process matter in the Galaxy puts stringent constraints on the occurrence and frequency of *r*-process events. For compact binary mergers as well as magnetorotational jet supernovae this frequency should be 1 event per 100–1000 regular supernovae. For mergers this would be consistent with population synthesis studies, while collapsars should be less frequent by a factor of about 10.

(2) The *radioactive r-process tracer* ^{244}Pu is found in *deep-sea sediments*; however, the observed amount rules out a quasicontinuous production of *r*-process elements as expected for sites with occurrence frequencies like supernovae and points to much rarer events. There are indications from deep-sea sediment that point to events where ^{60}Fe and ^{244}Pu are coproduced, however, with relative amounts of ^{244}Pu strongly reduced relative to the solar value. Such events could be related to a weak *r* process (discussed earlier).

(3) Observations indicate the presence of *r*-process elements in halo stars at lowest metallicities, showing either a complete or only a partial (or incomplete) *r*-process abundance pattern, in the latter case possibly pointing to a weak *r*-process origin. These abundance detections act as proof for nucleosynthesis early in the history of the Galaxy and provide important clues about the nature of the earliest stars and their *r*-process sites.

(4) Observations of lowest metallicity stars in our Galaxy and ultrafaint dwarf galaxies show substantial variations in *r*-process abundances, indicating a production site with a low event rate and consistently high amounts of *r*-process ejecta in order to explain solar abundances; this is also underlined by the *large scatter of* Eu/Fe (with Eu being an *r*-process element and Fe stemming from core-collapse supernovae at these low metallicities) seen in the earliest stars of the Galaxy; this is explained by a not yet well mixed interstellar medium with respect to contributions of products from regular core-collapse supernovae and the rare *r*-process events.

(5) Because of the availability of experimental atomic data and high-resolution, precise observations, *r*-process abundance determinations have improved significantly over time; this permitted also to detect the presence of long-lived radioactive nuclei like Th and U in the same star, making even a "dating" of old stars possible. Observed variations in the actinide to intermediate-mass *r*-process elements like Eu, leading to so-called actinide-boost stars, would even give clues about different *r*-process sites.

These observations indicate rare events for the strong *r* process, a requirement matched by all three candidate sites. Moreover, the observations related to the overall evolution of heavy *r*-process elements relative to Fe, and especially its large scatter at low metallicities, require inhomogeneous galactic evolution simulations, which can reproduce this behavior and might actually point to favored sites:

(1) A major open question is: Can products of the neutron-star merger *r* process alone explain the observations of a large scatter of Eu/Fe and other *r*-process elements seen already at metallicities of $[\mathrm{Fe/H}] \leq -3$? As the supernovae that produce the neutron stars of a merger already lead to a substantial floor of Fe, they enhance [Fe/H]. Thus, the high [Eu/Fe] due to the new ejecta would then be seen first at the metallicity [Fe/H] inherited from the prior supernovae if the merger ejecta are mixed with the same interstellar medium as the prior supernova ejecta. For a typical explosion energy of 10^{51} erg and typical densities of the interstellar medium, this mixing would occur via a Sedov-Taylor blast wave of about $5 \times 10^4\ M_\odot$. As matter is ejected with similar kinetic energies in neutron-star mergers and supernovae, recent investigations indicate that it would mix with a similar amount of interstellar medium. Stochastic inhomogeneous chemical evolution calculations, utilizing this effect alone, show the appearance of Eu only in the metallicity range $-3 < [\mathrm{Fe/H}] < -2$ for neutron-star mergers. First investigations have been performed on how this would be affected in the case of neutron-star–black hole

mergers, as they would lead to Fe ejecta by only one prior supernova.

(2) Like other hydrodynamic calculations, *large-scale SPH simulations* can suffer from resolution problems, which overestimate the material mixing. This mixes Fe with larger amounts of interstellar medium and thus causes a decrease in the metallicity at which *r*-process nucleosynthesis sets in. Global simulations can handle turbulent mixing of interstellar medium matter in the early Galaxy; however, it is questionable whether they can resolve the relevant length scales. Some of these simulations seem to be able to reproduce the *r*-process behavior of low-metallicity observations with compact binary mergers, but the most recent ones also favor an additional site or source at lowest metallicities.

(3) *Neutron-star kicks*, resulting from a supernova explosion, could have the binary neutron-star system move out of its supernova remnants (polluted with Fe and Ni), and the merger event could take place in galactic regions unpolluted by Fe from earlier supernovae. This could permit the ejection of *r*-process matter in environments with a lower [Fe/H] also in the case of neutron-star mergers. Preliminary simulations with stochastic inhomogeneous models are able to reproduce observations if coalescence delay times are as short as 1 Myr.

(4) Another option is that early on, in galactic substructures of the size of dwarf galaxies, different star formation rates can exist, combined with a loss of nucleosynthesis ejecta out of these galaxies due to less gravity. This can shift the behavior of the [Eu/Fe] ratio as a function of metallicity [Fe/H] to lower metallicities. When also considering a statistical distribution of (down to small) coalescence timescales in the individual substructures, the low-metallicity observations could possibly be matched, while the merging of these substructures within the early Galaxy at later times can be made consistent with the [Eu/Fe] decline (similar to alpha elements) at $[\mathrm{Fe/H}] = -1$. However, we note that in dwarf galaxies indications of two different sources, an early quick and a delayed *r*-process contribution, exist.

(5) In somewhat simpler galactic evolution models, employing the IMA and coalescence delay-time distributions following a t^{-1} power law, as expected from population synthesis studies and statistics of short-duration gamma-ray bursts, apparently no model can reproduce the metallicity dependence of the *r*-process/Fe abundance ratios with neutron-star mergers alone. But further constraints on the delay-time distribution, and consideration of hot and cold phases of the interstellar medium, might help.

This discussion underlines that it is still inconclusive whether binary compact mergers alone can explain low-metallicity observations. Although mergers could be responsible for the dominant amount of *r*-process products in the Solar System and the Galaxy, an additional component that acts at lowest metallicities may still be required. The detection of actinide-boost stars, found, in particular, at metallicities as low as $[\mathrm{Fe/H}] \approx -3$, could be a further argument for such an additional component.

This review of all aspects of the astrophysical *r* process, from nuclear physics via stellar (explosive) modeling, astronomical observations, and galactic evolution, has shown that substantial progress has been made since the *r* process was postulated in the 1950s by Burbidge *et al.* (1957) and Cameron (1957). But it also shows that, despite the first observation of an *r*-process production site (GW170817) in 2017, confirming neutron-star mergers as probably the most important site, many open questions remain and further progress on all fronts is required in an interdisciplinary effort to answer them.

Existing and upcoming nuclear facilities worldwide (FAIR, FRIB, HIAF, RAON, RIKEN, SPIRAL) will allow us to produce neutron-rich nuclei along the *r*-process path and to determine their properties, including, for the first time, nuclei of the third *r*-process peak. Relativistic heavy-ion collision experiments envisioned for FAIR, NICA, and RHIC will generate and investigate nuclear matter at the temperatures and densities as they exist in neutron-star mergers (and core-collapse supernovae). These exciting experimental prospectives will constrain and guide advances in global nuclear models, and together they will decisively reduce the nuclear uncertainties currently hampering *r*-process studies.

Observational programs targeting abundances in low-metallicity stars, like RAVE, Gaia, and APOGEE, will be incorporated in future surveys such as SDSS V, 4MOST, and WEAVE. This will provide the highest quality information about the chemical structure of the galactic disk, the halo, and the bulge. Multimessenger astronomy with present and future gravitational wave detectors like LIGO, VIRGO, KAGRA, and IndIGO is expected to detect up to ten compact binary mergers per year, which can be followed up with observations of related gamma-ray bursts and the electromagnetic afterglow. This permits us to analyze the outcome of many sources with different viewing angles and will help our further understanding of this site and possible variations, producing the heaviest elements in the Universe.

The upcoming experimental facilities and observational tools have to be supplemented by theory advances to lead us to a deeper and more detailed understanding of the origin of the heavy elements spanning from Fe to U produced by the *r* process. These theoretical efforts have to include improved models for the nuclear equation of state and for neutron-rich nuclei far from stability, but also for stellar atmospheres, stellar evolution and explosions, and finally for the chemodynamical history of the Galaxy.

In summary, we are living in interesting times for unraveling the mysteries of *r*-process nucleosynthesis and this research field is evolving at a fast pace (the literature review for this work ended in April 2020).

ACKNOWLEDGMENTS

We thank a large number of colleagues and friends for helpful collaborations and discussions, but Al Cameron and Willy Fowler should especially be mentioned here, as they motivated many of us to explore the topic of this review. We also thank M. Eichler, T. Fischer, S. A. Giuliani, A. Manukyan, A. Perego, B. Wehmeyer, and M.-R. Wu for providing unpublished data and figures, or redrawing figures.

This research was supported in part by NASA Grant No. HST-GO-14232 (J. J. C.), NSF Grant No. AST-1616040 (C. S.), NASA Grant No. NNX16AE96G and NSF Grant No, AST-1516182 (J. E. L.), NSF Grant No. Phys-0758100 and the Joint Institute for Nuclear Astrophysics through NSF Grant No. Phys-0822648 (A. A. and M. W.), NSF Grant No. PHY-1430152 (JINA Center for the Evolution of the Elements) (A. A, J. J. C., and M. W.), NSF Grant No. PHY-1927130 [AccelNet-WOU: International Research Network for Nuclear Astrophysics (IReNA)] (A. A., J. J. C., K. L., G. M.-P., F.-K. T., and M. W.), the Extreme Matter Institute (EMMI) (K. L. and G. M.-P.), the Deutsche Forschungsgemeinschaft (DFG, German Research Foundation) through Project ID No. 279384907–SFB 1245 (G. M.-P.), the Swiss SNF through Grant No. 200020-132816/1, ERC Advanced Grant FISH No. 321263 (F.-K. T.), ERC Advanced Grant KILONOVA No. 885281 (G. M.-P.), and COST Actions NewCompstar No. MP1304 (F.-K. T.) and ChETEC No. CA16117 (F.-K. T. and G. M.-P.).

REFERENCES

Abbott, B. P., *et al.*, 2017a, "Multi-messenger observations of a binary neutron star merger," Astrophys. J. Lett., **848**, L12.

Abbott, B. P., *et al.* (LIGO Scientific and Virgo Collaborations), 2017b, "GW170817: Observation of Gravitational Waves from a Binary Neutron Star Inspiral," Phys. Rev. Lett. **119**, 161101.

Abbott, B. P., *et al.* (LIGO Scientific and Virgo Collaborations), 2017c, "On the progenitor of binary neutron star merger GW170817," Astrophys. J. Lett., **850**, L40.

Abbott, B. P., *et al.* (LIGO Scientific Collaboration and Virgo Collaborations), 2017d, "Estimating the Contribution of Dynamical Ejecta in the Kilonova Associated with GW170817," Astrophys. J. Lett., **850**, L39.

Abbott, B. P., *et al.* (LIGO Scientific, Virgo, Fermi Gamma-ray Burst Monitor, and INTEGRAL Collaborations), 2017e, "Gravitational waves and gamma-rays from a binary neutron star merger: GW170817 and GRB 170817A," Astrophys. J. Lett. **848**, L13.

Abbott, B. P., *et al.* (LIGO Scientific and Virgo Collaborations), 2018, "GW170817: Measurements of Neutron Star Radii and Equation of State," Phys. Rev. Lett. **121**, 161101.

Abbott, B. P., *et al.* (LIGO Scientific and Virgo Collaborations), 2019, "Properties of the Binary Neutron Star Merger GW170817," Phys. Rev. X **9**, 011001.

Abbott, B. P., *et al.*, 2020, "GW190425: Observation of a compact binary coalescence with total mass $\sim 3.4 M_{\odot}$," Astrophys. J. Lett., **892**, L3.

Abbott, R., *et al.*, 2020a, "GW190814: Gravitational waves from the coalescence of a 23 solar mass black hole with a 2.6 solar mass compact object," Astrophys. J. Lett., **896**, L44.

Abbott, R., *et al.*, 2020b, "GWTC-2: Compact binary coalescences observed by LIGO and Virgo during the first half of the third observing run," arXiv:2010.14527.

Abohalima, Abdu, and Anna Frebel, 2018, "JINAbase—A database for chemical abundances of metal-poor stars," Astrophys. J. Suppl. Ser., **238**, 36.

Aboussir, Y., J. M. Pearson, A. K. Dutta, and F. Tondeur, 1995, "Nuclear mass formula via an approximation to the Hartree-Fock method," At. Data Nucl. Data Tables **61**, 127–176.

Ackley, K., *et al.*, 2020, "Observational constraints on the optical and near-infrared emission from the neutron star-black hole binary merger S190814bv," arXiv:2002.01950.

Adrich, P., *et al.* (LAND-FRS Collaboration), 2005, "Evidence for Pygmy and Giant Dipole Resonances in ^{130}Sn and ^{132}Sn," Phys. Rev. Lett. **95**, 132501.

Agramunt, J., *et al.*, 2016, "Characterization of a neutron-beta counting system with beta-delayed neutron emitters," Nucl. Instrum. Methods Phys. Res., Sect. A **807**, 69–78.

Akram, Waheed, Khalil Farouqi, Oliver Hallmann, and Karl-Ludwig Kratz, 2020, "Nucleosynthesis of light trans-Fe isotopes in ccSNe: Implications from presolar SiC-X grains," EPJ Web Conf., **227**, 01009.

Alhassid, Y., G. F. Bertsch, S. Liu, and H. Nakada, 2000, "Parity Dependence of Nuclear Level Densities," Phys. Rev. Lett. **84**, 4313.

Alhassid, Y., S. Liu, and H. Nakada, 1999, "Particle-Number Reprojection in the Shell Model Monte Carlo Method: Application to Nuclear Level Densities," Phys. Rev. Lett. **83**, 4265–4268.

Alhassid, Y., S. Liu, and H. Nakada, 2007, "Spin Projection in the Shell Model Monte Carlo Method and the Spin Distribution of Nuclear Level Densities," Phys. Rev. Lett. **99**, 162504.

Anderson, Matthew, Eric W. Hirschmann, Luis Lehner, Steven L. Liebling, Patrick M. Motl, David Neilsen, Carlos Palenzuela, and Joel E. Tohline, 2008, "Magnetized Neutron-Star Mergers and Gravitational-Wave Signals," Phys. Rev. Lett. **100**, 191101.

Annala, Eemeli, Tyler Gorda, Aleksi Kurkela, and Aleksi Vuorinen, 2018, "Gravitational-Wave Constraints on the Neutron-Star-Matter Equation of State," Phys. Rev. Lett. **120**, 172703.

Antoniadis, John, *et al.*, 2013, "A massive pulsar in a compact relativistic binary," Science **340**, 1233232.

Aoki, M., Y. Ishimaru, W. Aoki, and S. Wanajo, 2017, "Diversity of abundance patterns of light neutron-capture elements in very-metal-poor stars," Astrophys. J. **837**, 8.

Aoki, W., *et al.*, 2013, "High-resolution spectroscopy of extremely metal-poor stars from SDSS/SEGUE. I. Atmospheric parameters and chemical compositions," Astron. J. **145**, 13.

Arcavi, I., *et al.*, 2017, "Optical emission from a kilonova following a gravitational-wave-detected neutron-star merger," Nature (London) **551**, 64–66.

Arcones, A., and H.-T. Janka, 2011, "Nucleosynthesis-relevant conditions in neutrino-driven supernova outflows. II. The reverse shock in two-dimensional simulations," Astron. Astrophys. **526**, A160.

Arcones, A., H.-T. Janka, and L. Scheck, 2007, "Nucleosynthesis-relevant conditions in neutrino-driven supernova outflows. I. Spherically symmetric hydrodynamic simulations," Astron. Astrophys. **467**, 1227–1248.

Arcones, A., and G. Martínez-Pinedo, 2011, "Dynamical *r*-process studies within the neutrino-driven wind scenario and its sensitivity to the nuclear physics input," Phys. Rev. C **83**, 045809.

Arcones, A., G. Martínez-Pinedo, L. F. Roberts, and S. E. Woosley, 2010, "Electron fraction constraints based on nuclear statistical equilibrium with beta equilibrium," Astron. Astrophys. **522**, A25.

Arcones, A., and F. Montes, 2011, "Production of light-element primary process nuclei in neutrino-driven winds," Astrophys. J. **731**, 5.

Arcones, A., and F.-K. Thielemann, 2013, "Neutrino-driven wind simulations and nucleosynthesis of heavy elements," J. Phys. G **40**, 013201.

Ardevol-Pulpillo, Ricard, H. Thomas Janka, Oliver Just, and Andreas Bauswein, 2019, "Improved leakage-equilibration-absorption scheme (ILEAS) for neutrino physics in compact object mergers," Mon. Not. R. Astron. Soc. **485**, 4754–4789.

Argast, D., M. Samland, F.-K. Thielemann, and Y.-Z. Qian, 2004, "Neutron star mergers versus core-collapse supernovae as dominant *r*-process sites in the early Galaxy," Astron. Astrophys. **416**, 997–1011.

Arlandini, C., F. Käppeler, K. Wisshak, R. Gallino, M. Lugaro, M. Busso, and O. Straniero, 1999, "Neutron capture in low-mass asymptotic giant branch stars: Cross sections and abundance signatures," Astrophys. J. **525**, 886–900.

Armbruster, P., *et al.*, 1976, "The recoil separator Lohengrin: Performance and special features for experiments," Nucl. Instrum. Methods **139**, 213–222.

Arnett, W. D., 1980, "Analytic solutions for light curves of supernovae of type II," Astrophys. J. **237**, 541–549.

Arnett, W. D., 1982, "Type I supernovae. I—Analytic solutions for the early part of the light curve," Astrophys. J. **253**, 785–797.

Arnould, M., and S. Goriely, 2003, "The *p*-process of stellar nucleosynthesis: Astrophysics and nuclear physics status," Phys. Rep. **384**, 1–84.

Arnould, M., S. Goriely, and K. Takahashi, 2007, "The *r*-process of stellar nucleosynthesis: Astrophysics and nuclear physics achievements and mysteries," Phys. Rep. **450**, 97–213.

Arzhanov, A., 2017, "Microscopic nuclear mass model for *r*-process nucleosynthesis," Ph.D. thesis (Technische Universität Darmstadt).

Ascenzi, Stefano, *et al.*, 2019, "A luminosity distribution for kilonovae based on short gamma-ray burst afterglows, Mon. Not. R. Astron. Soc. **486**, 672–690.

Asplund, M., N. Grevesse, A. J. Sauval, and P. Scott, 2009, "The chemical composition of the Sun," Annu. Rev. Astron. Astrophys. **47**, 481–522.

Atanasov, D., *et al.*, 2015, "Precision Mass Measurements of $^{129-131}$Cd and Their Impact on Stellar Nucleosynthesis via the Rapid Neutron Capture Process," Phys. Rev. Lett. **115**, 232501.

Audi, G., F. G. Kondev, M. Wang, B. Pfeiffer, X. Sun, J. Blachot, and M. MacCormick, 2012, "The Nubase2012 evaluation of nuclear properties," Chin. Phys. C **36**, 1157.

Audi, G., A. H. Wapstra, and C. Thibault, 2003, "The Ame2003 atomic mass evaluation: II. Tables, graphs and references," Nucl. Phys. **A729**, 337–676.

Audouze, J., and B. M. Tinsley, 1976, "Chemical evolution of galaxies," Annu. Rev. Astron. Astrophys. **14**, 43–79.

Avrigeanu, M., and V. Avrigeanu, 2016, "On deuteron interactions within surrogate reactions and nuclear level density studies," J. Phys. Conf. Ser., **724**, 012003.

Avrigeanu, V., and M. Avrigeanu, 2015, "Consistent optical potential for incident and emitted low-energy α particles," Phys. Rev. C **91**, 064611.

Avrigeanu, V., M. Avrigeanu, and C. Mănăilescu, 2014, "Further explorations of the α-particle optical model potential at low energies for the mass range $A \approx 45$–209," Phys. Rev. C **90**, 044612.

Baade, W., and F. Zwicky, 1934, "Remarks on super-novae and cosmic rays," Phys. Rev. **46**, 76–77.

Baiotti, Luca, and Luciano Rezzolla, 2017, "Binary neutron star mergers: A review of Einstein's richest laboratory," Rep. Prog. Phys. **80**, 096901.

Baldo, M., and G. F. Burgio, 2016, "The nuclear symmetry energy," Prog. Part. Nucl. Phys. **91**, 203–258.

Banerjee, P., W. C. Haxton, and Y.-Z. Qian, 2011, "Long, Cold, Early *r* Process? Neutrino-Induced Nucleosynthesis in He Shells Revisited," Phys. Rev. Lett. **106**, 201104.

Banerjee, P., Y.-Z. Qian, A. Heger, and W. Haxton, 2016, "Neutrino-induced nucleosynthesis in helium shells of early core-collapse supernovae," EPJ Web Conf., **109**, 06001.

Barbieri, C., O. S. Salafia, M. Colpi, G. Ghirlanda, and A. Perego, 2020, "Distinguishing the nature of 'ambiguous' merging systems hosting a neutron star: GW190425 in low-latency," arXiv:2002.09395.

Barbieri, C., O. S. Salafia, M. Colpi, G. Ghirlanda, A. Perego, and A. Colombo, 2019, "Filling the mass gap: How kilonova observations can unveil the nature of the compact object merging with the neutron star," Astrophys. J. Lett., **887**, L35.

Barklem, P. S., N. Christlieb, T. C. Beers, V. Hill, M. S. Bessell, J. Holmberg, B. Marsteller, S. Rossi, F.-J. Zickgraf, and D. Reimers, 2005, "The Hamburg/ESO *R*-process enhanced star survey (HERES). II. Spectroscopic analysis of the survey sample," Astron. Astrophys. **439**, 129–151.

Barnes, J., D. Kasen, M.-R. Wu, and G. Martínez-Pinedo, 2016, "Radioactivity and thermalization in the ejecta of compact object mergers and their impact on kilonova light curves," Astrophys. J. **829**, 110.

Barnes, Jennifer, and Daniel Kasen, 2013, "Effect of a high opacity on the light curves of radioactively powered transients from compact object mergers," Astrophys. J. **775**, 18.

Bartos, I., P. Brady, and S. Márka, 2013, "How gravitational-wave observations can shape the gamma-ray burst paradigm," Classical Quantum Gravity **30**, 123001.

Battistini, C., and T. Bensby, 2016, "The origin and evolution of *r*- and *s*-process elements in the Milky Way stellar disk," Astron. Astrophys. **586**, A49.

Bauge, E., J. P. Delaroche, and M. Girod, 2001, "Lane-consistent, semimicroscopic nucleon-nucleus optical model," Phys. Rev. C **63**, 024607.

Baumgarte, T. W., S. L. Shapiro, and M. Shibata, 2000, "On the maximum mass of differentially rotating neutron stars," Astrophys. J. Lett., **528**, L29–L32.

Bauswein, A., T. W. Baumgarte, and H.-T. Janka, 2013, "Prompt Merger Collapse and the Maximum Mass of Neutron Stars," Phys. Rev. Lett. **111**, 131101.

Bauswein, A., S. Goriely, and H.-T. Janka, 2013, "Systematics of dynamical mass ejection, nucleosynthesis, and radioactively powered electromagnetic signals from neutron-star mergers," Astrophys. J. **773**, 78.

Bauswein, A., and H.-T. Janka, 2012, "Measuring Neutron-Star Properties via Gravitational Waves from Neutron-Star Mergers," Phys. Rev. Lett. **108**, 011101.

Bauswein, A., and N. Stergioulas, 2017, "Semi-analytic derivation of the threshold mass for prompt collapse in binary neutron-star mergers," Mon. Not. R. Astron. Soc. **471**, 4956–4965.

Bauswein, A., and N. Stergioulas, 2019, "Spectral classification of gravitational-wave emission and equation of state constraints in binary neutron star mergers," J. Phys. G **46**, 113002.

Bauswein, A., N. Stergioulas, and H.-T. Janka, 2016, "Exploring properties of high-density matter through remnants of neutron-star mergers," Eur. Phys. J. A **52**, 56.

Bauswein, Andreas, Oliver Just, Hans-Thomas Janka, and Nikolaos Stergioulas, 2017, "Neutron-star radius constraints from GW170817 and future detections," Astrophys. J. Lett., **850**, L34.

Beard, M., E. Uberseder, R. Crowter, and M. Wiescher, 2014, "Comparison of statistical model calculations for stable isotope neutron capture," Phys. Rev. C **90**, 034619.

Beers, T. C., and N. Christlieb, 2005, "The discovery and analysis of very metal-poor stars in the Galaxy," Annu. Rev. Astron. Astrophys. **43**, 531–580.

Belczynski, K., M. Dominik, T. Bulik, R. O'Shaughnessy, C. Fryer, and D. E. Holz, 2010, "The effect of metallicity on the detection prospects for gravitational waves," Astrophys. J. Lett., **715**, L138–L141.

Beloborodov, A. M., 2003, "Nuclear composition of gamma-ray burst fireballs," Astrophys. J. **588**, 931–944.

Beloborodov, A. M., 2008, "Hyper-accreting black holes," AIP Conf. Proc., **1054** 51–70.

Bengtsson, R., and W. M. Howard, 1975, "Mass asymmetric fission and the termination of the astrophysical *r*-process," Phys. Lett. **55B**, 281–285.

Beniamini, Paz, and Kenta Hotokezaka, 2020, "Turbulent mixing of *r*-process elements in the Milky Way," Mon. Not. R. Astron. Soc. **496**, 1891–1901.

Beniamini, Paz, Kenta Hotokezaka, Alexander van der Horst, and Chryssa Kouveliotou, 2019, "Formation rates and evolution histories of magnetars," Mon. Not. R. Astron. Soc. **487**, 1426–1438.

Beniamini, Paz, Kenta Hotokezaka, and Tsvi Piran, 2016, "*r*-process production sites as inferred from Eu abundances in dwarf galaxies," Astrophys. J. **832**, 149.

Beniamini, Paz, and Tsvi Piran, 2019, "The gravitational waves merger time distribution of binary neutron star systems," Mon. Not. R. Astron. Soc. **487**, 4847–4854.

Bensby, T., S. Feltzing, and M. S. Oey, 2014, "Exploring the Milky Way stellar disk. A detailed elemental abundance study of 714 F and G dwarf stars in the solar neighbourhood," Astron. Astrophys. **562**, A71.

Bersten, M. C., and P. A. Mazzali, 2017, "Light curves of type I supernovae," in *Handbook of Supernovae*, edited by A. W. Alsabti, and P. Murdin (Springer International Publishing, Cham, Switzerland).

Bethe, H. A., 1990, "Supernova mechanisms," Rev. Mod. Phys. **62**, 801–866.

Bisterzo, S., R. Gallino, F. Käppeler, M. Wiescher, G. Imbriani, O. Straniero, S. Cristallo, J. Görres, and R. J. deBoer, 2015, "The branchings of the main *s*-process: their sensitivity to α-induced reactions on ^{13}C and ^{22}Ne and to the uncertainties of the nuclear network," Mon. Not. R. Astron. Soc. **449**, 506–527.

Bisterzo, S., C. Travaglio, M. Wiescher, F. Käppeler, and R. Gallino, 2017, "Galactic chemical evolution: The impact of the ^{13}C-pocket structure on the *s*-process distribution," Astrophys. J. **835**, 97.

Blake, J. B., and D. N. Schramm, 1976, "A possible alternative to the *r*-process," Astrophys. J. **209**, 846–849.

Blaum, K., J. Dilling, and W. Nörtershäuser, 2013, "Precision atomic physics techniques for nuclear physics with radioactive beams," Phys. Scr. **T152**, 014017.

Blaum, Klaus, 2006, "High-accuracy mass spectrometry with stored ions," Phys. Rep. **425**, 1–78.

Bohle, D., A. Richter, W. Steffen, A. E. L. Dieperink, N. Lo Iudice, F. Palumbo, and O. Scholten, 1984, "New magnetic dipole excitation mode studied in the heavy deformed nucleus ^{156}Gd by inelastic electron scattering," Phys. Lett. B **137**, 27–31.

Bollig, R., H.-T. Janka, A. Lohs, G. Martínez-Pinedo, C. J. Horowitz, and T. Melson, 2017, "Muon Creation in Supernova Matter Facilitates Neutrino-Driven Explosions," Phys. Rev. Lett. **119**, 242702.

Bonetti, M., A. Perego, P. R. Capelo, M. Dotti, and M. C. Miller, 2018, "*r*-process nucleosynthesis in the early Universe through fast mergers of compact binaries in triple systems," Publ. Astron. Soc. Aust. **35**, e017.

Bonetti, Matteo, Albino Perego, Massimo Dotti, and Gabriele Cescutti, 2019, "Neutron star binary orbits in their host potential: Effect on early *r*-process enrichment," Mon. Not. R. Astron. Soc. **490**, 296–311.

Borzov, I., and S. Goriely, 2000, "Weak interaction rates of neutron-rich nuclei and the *r*-process nucleosynthesis," Phys. Rev. C **62**, 035501.

Borzov, I. N., 2003, "Gamow-Teller and first-forbidden decays near the *r*-process paths at $N = 50$, 82, and 126," Phys. Rev. C **67**, 025802.

Borzov, I. N., J. J. Cuenca-García, K. Langanke, G. Martínez-Pinedo, and F. Montes, 2008, "Beta-decay of $Z < 50$ nuclei near the $N = 82$ closed neutron shell," Nucl. Phys. **A814**, 159–173.

Bovard, Luke, Dirk Martin, Federico Guercilena, Almudena Arcones, Luciano Rezzolla, and Oleg Korobkin, 2017, "*r*-process nucleosynthesis from matter ejected in binary neutron star mergers," Phys. Rev. D **96**, 124005.

Boyd, R. N., M. A. Famiano, B. S. Meyer, Y. Motizuki, T. Kajino, and I. U. Roederer, 2012, "The *r*-process in metal-poor stars and black hole formation," Astrophys. J. **744**, L14.

Brauer, Kaley, Alexander P. Ji, Anna Frebel, Gregory A. Dooley, Facundo A. Gómez, and Brian W. O'Shea, 2019, "The origin of *r*-process enhanced metal-poor halo stars in now-destroyed ultra-faint dwarf galaxies," Astrophys. J. **871**, 247.

Brault, J. W., 1976, "Rapid-scan high-resolution Fourier spectrometer for the visible," J. Opt. Soc. Am. **66**, 1081, https://ui.adsabs.harvard.edu/#abs/1976JOSA...66.1081B/abstract.

Bravo, E., and D. García-Senz, 1999, "Coulomb corrections to the equation of state of nuclear statistical equilibrium matter: Implications for SNIa nucleosynthesis and the accretion-induced collapse of white dwarfs," Mon. Not. R. Astron. Soc. **307**, 984–992.

Brege, Wyatt, Matthew D. Duez, Francois Foucart, M. Brett Deaton, Jesus Caro, Daniel A. Hemberger, Lawrence E. Kidder, Evan O'Connor, Harald P. Pfeiffer, and Mark A. Scheel, 2018, "Black hole-neutron star mergers using a survey of finite-temperature equations of state," Phys. Rev. D **98**, 063009.

Brink, D. M., 1955, Ph.D. thesis, "Some aspects of the interaction of light with matter" (Oxford University), https://ora.ox.ac.uk/objects/uuid:334ec4a3-8a89-42aa-93f4-2e54d070ee09.

Brink, D. M., 1957, "Individual particle and collective aspects of the nuclear photoeffect," Nucl. Phys. **A4**, 215–220.

Brown, B. A., and A. C. Larsen, 2014, "Large Low-Energy $M1$ Strength for ^{56,57}Fe within the Nuclear Shell Model," Phys. Rev. Lett. **113**, 252502.

Bruske, C., K. H. Burkard, W. Hüller, R. Kirchner, O. Klepper, and E. Roeckl, 1981, "Status report on the GSI on-line mass separator facility," Nucl. Instrum. Methods Phys. Res. **186**, 61–69.

Bugli, M., J. Guilet, M. Obergaulinger, P. Cerdá-Durán, and M. A. Aloy, 2020, "The impact of non-dipolar magnetic fields in core-collapse supernovae, Mon. Not. R. Astron. Soc. **492**, 58–71.

Burbidge, E. M., G. R. Burbidge, W. A. Fowler, and F. Hoyle, 1957, "Synthesis of the elements in stars," Rev. Mod. Phys. **29**, 547–650.

Burbidge, G. R., F. Hoyle, E. M. Burbidge, R. F. Christy, and W. A. Fowler, 1956, "Californium-254 and supernovae," Phys. Rev. **103**, 1145–1149.

Burris, D. L., C. A. Pilachowski, T. E. Armandroff, C. Sneden, J. J. Cowan, and H. Roe, 2000, "Neutron-capture elements in the early Galaxy: Insights from a large sample of metal-poor giants," Astrophys. J. **544**, 302–319.

Burrows, A., D. Vartanyan, J. C. Dolence, M. A. Skinner, and D. Radice, 2018, "Crucial physical dependencies of the core-collapse supernova mechanism," Space Sci. Rev. **214**, 33.

Burrows, Adam, 2013, "Colloquium: Perspectives on core-collapse supernova theory," Rev. Mod. Phys. **85**, 245–261.

Burrows, Adam, David Radice, David Vartanyan, Hiroki Nagakura, M. Aaron Skinner, and Joshua C. Dolence, 2020, "The overarching framework of core-collapse supernova explosions as revealed by 3D FORNAX simulations," Mon. Not. R. Astron. Soc. **491**, 2715–2735.

Busso, M., R. Gallino, and G. J. Wasserburg, 1999, "Nucleosynthesis in asymptotic giant branch stars: Relevance for galactic enrichment and Solar System formation," Annu. Rev. Astron. Astrophys. **37**, 239–309.

Caballero, O. L., A. Arcones, I. N. Borzov, K. Langanke, and G. Martinez-Pinedo, 2014, "Local and global effects of beta decays on *r*-process," arXiv:1405.0210.

Caballero-Folch, R., *et al.*, 2016, "First Measurement of Several β-Delayed Neutron Emitting Isotopes beyond $N = 126$," Phys. Rev. Lett. **117**, 012501.

Cabezón, Rubén M., Kuo-Chuan Pan, Matthias Liebendörfer, Takami Kuroda, Kevin Ebinger, Oliver Heinimann, Albino Perego, and Friedrich-Karl Thielemann, 2018, "Core-collapse supernovae in the hall of mirrors. A three-dimensional code-comparison project," Astron. Astrophys. **619**, A118.

Calviño, F., *et al.*, 2014, TDR BEta deLayEd Neutron detector Technical Report No. 1865760 (FAIR), https://edms.cern.ch/document/1865760.

Camelio, Giovanni, Tim Dietrich, and Stephan Rosswog, 2018, "Disc formation in the collapse of supramassive neutron stars," Mon. Not. R. Astron. Soc. **480**, 5272–5285.

Cameron, A. G. W., 1957, "Stellar evolution, nuclear astrophysics, and nucleogenesis," Report No. CRL-41 (Chalk River); reprinted in Kahl, D. M., 2013, Ed., *Stellar Evolution, Nuclear Astrophysics, and Nucleogenesis* (Dover, New York).

Cameron, A. G. W., 1959, "A revised table of abundances of the elements," Astrophys. J. **129**, 676.

Cameron, A. G. W., 2003, "Some nucleosynthesis effects associated with *r*-process jets," Astrophys. J. **587**, 327–340.

Cameron, A. G. W., J. J. Cowan, and J. W. Truran, 1983, "The waiting point approximation in *r*-process calculations," Astrophys. Space Sci. **91**, 235–243.

Capano, Collin D., Ingo Tews, Stephanie M. Brown, Ben Margalit, Soumi De, Sumit Kumar, Duncan A. Brown, Badri Krishnan, and Sanjay Reddy, 2020, "Stringent constraints on neutron-star radii from multimessenger observations and nuclear theory," Nat. Astron. **4**, 625–632.

Caurier, E., K. Langanke, G. Martínez-Pinedo, and F. Nowacki, 1999, "Shell model calculations of stellar weak interaction rates: I. Gamow-Teller distributions and spectra of nuclei in the mass range $A = 45$–65," Nucl. Phys. **A653**, 439–452.

Caurier, E., G. Martínez-Pinedo, Fréderic Nowacki, A. Poves, and A. P. Zuker, 2005, "The shell model as unified view of nuclear structure," Rev. Mod. Phys. **77**, 427–488.

Cayrel, R., *et al.*, 2001, "Measurement of stellar age from uranium decay," Nature (London) **409**, 691–692.

Cayrel, R., *et al.*, 2004, "First stars V—Abundance patterns from C to Zn and supernova yields in the early Galaxy," Astron. Astrophys. **416**, 1117–1138.

Cescutti, G., D. Romano, F. Matteucci, C. Chiappini, and R. Hirschi, 2015, "The role of neutron star mergers in the chemical evolution of the galactic halo," Astron. Astrophys. **577**, A139.

Chawla, Sarvnipun, Matthew Anderson, Michael Besselman, Luis Lehner, Steven L. Liebling, Patrick M. Motl, and David Neilsen, 2010, "Mergers of Magnetized Neutron Stars with Spinning Black Holes: Disruption, Accretion, and Fallback," Phys. Rev. Lett. **105**, 111101.

Chen, B., J. Dobaczewski, K.-L. Kratz, K. Langanke, B. Pfeiffer, F.-K. Thielemann, and P. Vogel, 1995, "Influence of shell-quenching far from stability on the astrophysical *r*-process," Phys. Lett. B **355**, 37–44.

Chiappini, C., F. Matteucci, and P. Padoan, 2000, "The chemical evolution of the Galaxy with variable initial mass functions," Astrophys. J. **528**, 711–722.

Chiappini, C., F. Matteucci, and D. Romano, 2001, "Abundance gradients and the formation of the Milky Way," Astrophys. J. **554**, 1044–1058.

Chornock, R., *et al.*, 2017, "The electromagnetic counterpart of the binary neutron star merger LIGO/Virgo GW170817. IV. Detection of near-infrared signatures of *r*-process nucleosynthesis with Gemini-South," Astrophys. J. Lett., **848**, L19.

Christie, I. M., A. Lalakos, A. Tchekhovskoy, R. Fernández, F. Foucart, E. Quataert, and D. Kasen, 2019, "The role of magnetic field geometry in the evolution of neutron star merger accretion discs," Mon. Not. R. Astron. Soc. **490**, 4811–4825.

Ciolfi, Riccardo, Wolfgang Kastaun, Bruno Giacomazzo, Andrea Endrizzi, Daniel M. Siegel, and Rosalba Perna, 2017, "General relativistic magnetohydrodynamic simulations of binary neutron star mergers forming a long-lived neutron star," Phys. Rev. D **95**, 063016.

Cizewski, J. A., A. Ratkiewicz, J. E. Escher, A. Lepailleur, S. D. Pain, and G. Potel, 2017, "Informing neutron capture nucleosynthesis on short-lived nuclei with (d, p) reactions," in EPJ Web Conf. **165**, 01013.

Clayton, D. D., 1968, *Principles of Stellar Evolution and Nucleosynthesis* (McGraw-Hill, New York).

Cohen, J. G., N. Christlieb, A. McWilliam, S. Shectman, I. Thompson, G. J. Wasserburg, I. Ivans, M. Dehn, T. Karlsson, and J. Melendez, 2004, "Abundances in very metal-poor dwarf stars," Astrophys. J. **612**, 1107–1135.

Cole, A. L., T. S. Anderson, R. G. T. Zegers, Sam M. Austin, B. A. Brown, L. Valdez, S. Gupta, G. W. Hitt, and O. Fawwaz, 2012, "Gamow-Teller strengths and electron-capture rates for pf-shell nuclei of relevance for late stellar evolution," Phys. Rev. C **86**, 015809.

Corlies, Lauren, Kathryn V. Johnston, and John H. Wise, 2018, "Exploring simulated early star formation in the context of the ultrafaint dwarf galaxies," Mon. Not. R. Astron. Soc. **475**, 4868–4880.

Côté, B., *et al.*, 2020, "Constraining the rapid neutron-capture process with meteoritic I-129 and Cm-247," arXiv:2006.04833.

Côté, B., K. Belczynski, C. L. Fryer, C. Ritter, A. Paul, B. Wehmeyer, and B. W. O'Shea, 2017, "Advanced LIGO constraints on neutron star mergers and *r*-process sites," Astrophys. J. **836**, 230.

Côté, B., *et al.*, 2018, "The origin of *r*-process elements in the Milky Way," Astrophys. J. **855**, 99.

Côté, Benoit, Andrés Yagüe, Blanka Világos, and Maria Lugaro, 2019, "Stochastic chemical evolution of radioactive isotopes with a Monte Carlo approach," Astrophys. J. **887**, 213.

Côté, Benoit, *et al.*, 2019, "Neutron star mergers might not be the only source of *r*-process elements in the Milky Way," Astrophys. J. **875**, 106.

Coughlin, Michael W., Tim Dietrich, Ben Margalit, and Brian D. Metzger, 2019, "Multimessenger Bayesian parameter inference of a binary neutron star merger," Mon. Not. R. Astron. Soc. **489**, L91–L96.

Coulter, D. A., *et al.*, 2017, "Swope Supernova Survey 2017a (SSS17a), the optical counterpart to a gravitational wave source," Science **358**, 1556–1558.

Cowan, J. J., A. G. W. Cameron, and J. W. Truran, 1980, "Seed abundances for *r*-processing in the helium shells of supernovae," Astrophys. J. **241**, 1090–1093.

Cowan, J. J., A. G. W. Cameron, and J. W. Truran, 1983, "Explosive helium burning in supernovae—A source of *r*-process elements," Astrophys. J. **265**, 429–442.

Cowan, J. J., A. G. W. Cameron, and J. W. Truran, 1985, "*r*-process nucleosynthesis in dynamic helium-burning environments," Astrophys. J. **294**, 656–662.

Cowan, J. J., B. Pfeiffer, K.-L. Kratz, F.-K. Thielemann, C. Sneden, S. Burles, D. Tytler, and T. C. Beers, 1999, "*r*-process abundances and chronometers in metal-poor stars," Astrophys. J. **521**, 194–205.

Cowan, J. J., and W. K. Rose, 1977, "Production of ^{14}C and neutrons in red giants," Astrophys. J. **212**, 149–158.

Cowan, J. J., C. Sneden, T. C. Beers, J. E. Lawler, J. Simmerer, J. W. Truran, F. Primas, J. Collier, and S. Burles, 2005, "Hubble Space Telescope observations of heavy elements in metal-poor galactic halo stars," Astrophys. J. **627**, 238–250.

Cowan, J. J., F.-K. Thielemann, and J. W. Truran, 1991, "The *r*-process and nucleochronology," Phys. Rep. **208**, 267–394.

Cowan, J. J., *et al.*, 2002, "The chemical composition and age of the metal-poor halo star BD + 17°3248," Astrophys. J. **572**, 861–879.

Cowperthwaite, P. S., *et al.*, 2017, "The electromagnetic counterpart of the binary neutron star merger LIGO/Virgo GW170817. II. UV, optical, and near-infrared light curves and comparison to kilonova models," Astrophys. J. Lett., **848**, L17.

Crease, R. P., and R. W. Seidel, 2000, "Making physics: A biography of Brookhaven National Laboratory, 1946–1972," Phys. Today **53**, No. 1, 55.

Curtis, Sanjana, Kevin Ebinger, Carla Fröhlich, Matthias Hempel, Albino Perego, Matthias Liebendörfer, and Friedrich-Karl Thielemann, 2019, "PUSHing core-collapse supernovae to explosions in spherical symmetry. III. Nucleosynthesis yields," Astrophys. J. **870**, 2.

Cyburt, R. H., B. D. Fields, K. A. Olive, and T.-H. Yeh, 2016, "Big bang nucleosynthesis: Present status," Rev. Mod. Phys. **88**, 015004.

Davies, M. B., W. Benz, T. Piran, and F. K. Thielemann, 1994, "Merging neutron stars. I. Initial results for coalescence of noncorotating systems," Astrophys. J. **431**, 742–753.

Davis, A. M., and K. D. McKeegan, 2014, "Short-lived radionuclides and early Solar System chronology," in *Meteorites and Cosmochemical Processes*, edited by A. M. Davis (Elsevier, Amsterdam), pp. 361–395.

De, Soumi, Daniel Finstad, James M. Lattimer, Duncan A. Brown, Edo Berger, and Christopher M. Biwer, 2018, "Tidal Deformabilities and Radii of Neutron Stars from the Observation of GW170817," Phys. Rev. Lett. **121**, 091102.

De Donder, E., and D. Vanbeveren, 2004, "The influence of neutron star mergers on the galactic chemical enrichment of *r*-process elements," New Astron. **9**, 1–16.

Demetriou, P., C. Grama, and S. Goriely, 2002, "Improved global α-optical model potentials at low energies," Nucl. Phys. **A707**, 253–276.

Demetriou, P., C. Grama, and S. Goriely, 2003, "Improved global α-optical model potential at low energies," Nucl. Phys. **A718**, 510–512.

Demorest, P. B., T. Pennucci, S M. Ransom, M. S. E. Roberts, and J. W. T. Hessels, 2010, "A two-solar-mass neutron star measured using Shapiro delay," Nature (London) **467**, 1081–1083.

Den Hartog, E. A., M. E. Wickliffe, and J. E. Lawler, 2002, "Radiative lifetimes of Eu I, II, and III and transition probabilities of Eu I," Astrophys. J. Suppl. Ser., **141**, 255–265.

Denissenkov, P. A., F. Herwig, U. Battino, C. Ritter, M. Pignatari, S. Jones, and B. Paxton, 2017, "*i*-process nucleosynthesis and mass retention efficiency in He-shell flash evolution of rapidly accreting white dwarfs," Astrophys. J. **834**, L10.

Desai, D., B. D. Metzger, and F. Foucart, 2019, "Imprints of *r*-process heating on fall-back accretion: Distinguishing black hole–neutron star from double neutron star mergers," Mon. Not. R. Astron. Soc. **485**, 4404–4412.

Dessart, L., C. D. Ott, A. Burrows, S. Rosswog, and E. Livne, 2009, "Neutrino signatures and the neutrino-driven wind in binary neutron star mergers," Astrophys. J. **690**, 1681–1705.

Diehl, R., and F. X. Timmes, 1998, "Gamma-ray line emission from radioactive isotopes in stars and galaxies," Publ. Astron. Soc. Pac. **110**, 637–659.

Dillmann, I., *et al.*, 2003, "$N = 82$ Shell Quenching of the Classical *r*-Process 'Waiting-Point' Nucleus ^{130}Cd," Phys. Rev. Lett. **91**, 162503.

Drout, M. R., *et al.*, 2017, "Light curves of the neutron star merger GW170817/SSS17a: Implications for *r*-process nucleosynthesis," Science **358**, 1570–1574.

Duflo, J., and A. P. Zuker, 1995, "Microscopic mass formulas," Phys. Rev. C **52**, R23–R27.

Duncan, R. C., S. L. Shapiro, and I. Wasserman, 1986, "Neutrino-driven winds from young, hot neutron stars," Astrophys. J. **309**, 141–160.

Duncan, R. C., and C. Thompson, 1992, "Formation of very strongly magnetized neutron stars—Implications for gamma-ray bursts," Astrophys. J. Lett., **392**, L9–L13.

Dunlop, R., *et al.*, 2019, "β decay and β-delayed neutron decay of the $N = 82$ nucleus $^{131}_{49}\mathrm{In}_{82}$," Phys. Rev. C **99**, 045805.

Duquette, D. W., S. Salih, and J. E. Lawler, 1981, "Radiative lifetimes in MoI using a novel atomic beam source," Phys. Lett. **83A**, 214–216.

Ebinger, Kevin, Sanjana Curtis, Carla Fröhlich, Matthias Hempel, Albino Perego, Matthias Liebendörfer, and Friedrich-Karl Thielemann, 2019, "PUSHing core-collapse supernovae to explosions in spherical symmetry. II. Explodability and remnant properties," Astrophys. J. **870**, 1.

Ebinger, Kevin, Sanjana Curtis, Somdutta Ghosh, Carla Fröhlich, Matthias Hempel, Albino Perego, Matthias Liebendörfer, and Friedrich-Karl Thielemann, 2020, "PUSHing core-collapse supernovae to explosions in spherical symmetry. IV. Explodability, remnant properties, and nucleosynthesis yields of low-metallicity stars," Astrophys. J. **888**, 91.

Eichler, D., M. Livio, T. Piran, and D. N. Schramm, 1989, "Nucleosynthesis, neutrino bursts and gamma-rays from coalescing neutron stars," Nature (London) **340**, 126–128.

Eichler, M., K. Nakamura, T. Takiwaki, T. Kuroda, K. Kotake, M. Hempel, R. Cabezón, M. Liebendörfer, and F.-K. Thielemann, 2018, "Nucleosynthesis in 2D core-collapse supernovae of 11.2 and 17.0$M_\odot$ progenitors: Implications for Mo and Ru production," J. Phys. G **45**, 014001.

Eichler, M., W. Sayar, A. Arcones, and T. Rauscher, 2019, "Probing the production of actinides under different *r*-process conditions," Astrophys. J. **879**, 47.

Eichler, M., *et al.*, 2015, "The role of fission in neutron star mergers and its impact on the *r*-process peaks," Astrophys. J. **808**, 30.

Ejnisman, R., I. D. Goldman, K. S. Krane, P. Mohr, Y. Nakazawa, E. B. Norman, T. Rauscher, and J. Reel, 1998, "Neutron capture cross section of ^{44}Ti," Phys. Rev. C **58**, 2531–2537.

Eliseev, S., K. Blaum, M. Block, C. Droese, M. Goncharov, E. Minaya Ramirez, D. A. Nesterenko, Y. N. Novikov, and L. Schweikhard, 2013, "Phase-Imaging Ion-Cyclotron-Resonance Measurements for Short-Lived Nuclides," Phys. Rev. Lett. **110**, 082501.

Emerick, Andrew, Greg L. Bryan, Mordecai-Mark Mac Low, Benoit Côté, Kathryn V. Johnston, and Brian W. O'Shea, 2018, "Metal mixing and ejection in dwarf galaxies are dependent on nucleosynthetic source," Astrophys. J. **869**, 94.

Engel, J., M. Bender, J. Dobaczewski, W. Nazarewicz, and R. Surman, 1999, "Beta decay of *r*-process waiting-point nuclei in a self-consistent approach," Phys. Rev. C **60**, 014302.

Epstein, Richard I., Stirling A. Colgate, and Wick C. Haxton, 1988, "Neutrino-Induced *r*-Process Nucleosynthesis," Phys. Rev. Lett. **61**, 2038–2041.

Erler, J., K. Langanke, H. Loens, Gabriel Martínez-Pinedo, and P.-G. Reinhard, 2012, "Fission properties for *r*-process nuclei," Phys. Rev. C **85**, 025802.

Ertl, T., H.-T. Janka, S. E. Woosley, T. Sukhbold, and M. Ugliano, 2016, "A two-parameter criterion for classifying the explodability of massive stars by the neutrino-driven mechanism," Astrophys. J. **818**, 124.

Ertl, T., S. E. Woosley, Tuguldur Sukhbold, and H. T. Janka, 2020, "The explosion of helium stars evolved with mass loss," Astrophys. J. **890**, 51.

Escher, J. E., J. T. Burke, F. S. Dietrich, N. D. Scielzo, I. J. Thompson, and W. Younes, 2012, "Compound-nuclear reaction cross sections from surrogate measurements," Rev. Mod. Phys. **84**, 353–397.

Escher, J. E., and F. S. Dietrich, 2006, "Determining (n, f) cross sections for actinide nuclei indirectly: Examination of the surrogate ratio method," Phys. Rev. C **74**, 054601.

Evans, P. A., *et al.*, 2017, "Swift and NuSTAR observations of GW170817: Detection of a blue kilonova," Science **358**, 1565–1570.

Ezzeddine, Rana, *et al.*, 2020, "The *r*-process alliance: First Magellan/MIKE release from the southern search for *r*-process-enhanced stars," Astrophys. J. **898**, 150.

Faber, Joshua A., Thomas W. Baumgarte, Stuart L. Shapiro, Keisuke Taniguchi, and Frederic A. Rasio, 2006, "Black hole-neutron star binary merger calculations: GRB progenitors and the stability of mass transfer," AIP Conf. Proc. **861** 622–629.

Farouqi, K., K.-L. Kratz, B. Pfeiffer, T. Rauscher, F.-K. Thielemann, and J. W. Truran, 2010, "Charged-particle and neutron-capture processes in the high-entropy wind of core-collapse supernovae," Astrophys. J. **712**, 1359–1377.

Fattoyev, F. J., J. Piekarewicz, and C. J. Horowitz, 2018, "Neutron Skins and Neutron Stars in the Multimessenger Era," Phys. Rev. Lett. **120**, 172702.

Fernández, R., and Brian D. Metzger, 2013, "Delayed outflows from black hole accretion tori following neutron star binary coalescence," Mon. Not. R. Astron. Soc. **435**, 502–517.

Fernández, R., D. Kasen, B. D. Metzger, and E. Quataert, 2015, "Outflows from accretion discs formed in neutron star mergers: Effect of black hole spin," Mon. Not. R. Astron. Soc. **446**, 750–758.

Fernández, R., and B. D. Metzger, 2016, "Electromagnetic signatures of neutron star mergers in the Advanced LIGO era," Annu. Rev. Nucl. Part. Sci. **66**, 23–45.

Fernández, Rodrigo, Alexander Tchekhovskoy, Eliot Quataert, Francois Foucart, and Daniel Kasen, 2019, "Long-term GRMHD simulations of neutron star merger accretion discs: Implications for electromagnetic counterparts, Mon. Not. R. Astron. Soc. **482**, 3373–3393.

Fields, Brian, *et al.*, 2019, "Near-Earth supernova explosions: Evidence, implications, and opportunities," Bull. Am. Astron. Soc. **51**, 410 [arXiv:1903.04589].

Fischer, T., I. Sagert, G. Pagliara, M. Hempel, J. Schaffner-Bielich, T. Rauscher, F.-K. Thielemann, R. Käppeli, G. Martínez-Pinedo, and M. Liebendörfer, 2011, "Core-collapse supernova explosions triggered by a quark-hadron phase transition during the early post-bounce phase," Astrophys. J. Suppl. Ser., **194**, 39.

Fischer, T., S. C. Whitehouse, A. Mezzacappa, F.-K. Thielemann, and M. Liebendörfer, 2010, "Protoneutron star evolution and the neutrino-driven wind in general relativistic neutrino radiation hydrodynamics simulations," Astron. Astrophys. **517**, A80.

Fischer, Tobias, Niels-Uwe F. Bastian, Meng-Ru Wu, Petr Baklanov, Elena Sorokina, Sergei Blinnikov, Stefan Typel, Thomas Klähn, and David B. Blaschke, 2018, "Quark deconfinement as a supernova explosion engine for massive blue supergiant stars," Nat. Astron. **2**, 980–986.

Fischer, Tobias, Gang Guo, Alan A. Dzhioev, Gabriel Martínez-Pinedo, Meng-Ru Wu, Andreas Lohs, and Yong-Zhong Qian, 2020, "Neutrino signal from proto-neutron star evolution: Effects of opacities from charged-current-neutrino interactions and inverse neutron decay," Phys. Rev. C **101**, 025804.

Fischer, Tobias, Meng-Ru Wu, Benjamin Wehmeyer, Niels-Uwe F. Bastian, Gabriel Martínez-Pinedo, and Friedrich-Karl Thielemann, 2020, "Core-collapse supernova explosions driven by the hadron-quark phase transition as rare *r* process site," Astrophys. J. **894**, 9.

Fogelberg, B., *et al.*, 2004, "Decays of ^{131}In, ^{131}Sn, and the position of the $h_{11/2}$ neutron hole state," Phys. Rev. C **70**, 034312.

Foglizzo, T., *et al.*, 2015, "The explosion mechanism of core-collapse supernovae: Progress in supernova theory and experiments," Publ. Astron. Soc. Aust. **32**, e009.

Foley, Ryan J., David A. Coulter, Charles D. Kilpatrick, Anthony L. Piro, Enrico Ramirez-Ruiz, and Josiah Schwab, 2020, "Updated parameter estimates for GW190425 using astrophysical arguments and implications for the electromagnetic counterpart," Mon. Not. R. Astron. Soc. **494**, 190–198.

Fontes, C. J., C. L. Fryer, A. L. Hungerford, P. Hakel, J. Colgan, D. P. Kilcrease, and M. E. Sherrill, 2015, "Relativistic opacities for astrophysical applications," High Energy Density Phys. **16**, 53–59.

Fontes, C. J., C. L. Fryer, A. L. Hungerford, R. T. Wollaeger, and O. Korobkin, 2020, "A line-binned treatment of opacities for the spectra and light curves from neutron star mergers," Mon. Not. R. Astron. Soc. **493**, 4143–4171.

Fontes, Christopher J., Chris L. Fryer, Aimee L. Hungerford, Ryan T. Wollaeger, Stephan Rosswog, and Edo Berger, 2017, "A line-smeared treatment of opacities for the spectra and light curves from macronovae," arXiv:1702.02990.

Forssén, C., F. S. Dietrich, J. Escher, R. D. Hoffman, and K. Kelley, 2007, "Determining neutron capture cross sections via the surrogate reaction technique," Phys. Rev. C **75**, 055807.

Foucart, F., M. B. Deaton, M. D. Duez, L. E. Kidder, I. MacDonald, C. D. Ott, H. P. Pfeiffer, M. A. Scheel, B. Szilagyi, and S. A. Teukolsky, 2013, "Black-hole-neutron-star mergers at realistic mass ratios: Equation of state and spin orientation effects," Phys. Rev. D **87**, 084006.

Foucart, F., M. B. Deaton, M. D. Duez, E. O'Connor, C. D. Ott, R. Haas, L. E. Kidder, H. P. Pfeiffer, M. A. Scheel, and B. Szilagyi, 2014, "Neutron star-black hole mergers with a nuclear equation of state and neutrino cooling: Dependence in the binary parameters," Phys. Rev. D **90**, 024026.

Foucart, F., M. D. Duez, L. E. Kidder, R. Nguyen, H. P. Pfeiffer, and M. A. Scheel, 2018, "Evaluating radiation transport errors in merger simulations using a Monte Carlo algorithm," Phys. Rev. D **98**, 063007.

Foucart, F., E. O'Connor, L. Roberts, M. D. Duez, R. Haas, L. E. Kidder, C. D. Ott, H. P. Pfeiffer, M. A. Scheel, and B. Szilagyi, 2015, "Post-merger evolution of a neutron star-black hole binary with neutrino transport," Phys. Rev. D **91**, 124021.

Foucart, Francois, 2012, "Black-hole-neutron-star mergers: Disk mass predictions," Phys. Rev. D **86**, 124007.

Foucart, Francois, Evan O'Connor, Luke Roberts, Lawrence E. Kidder, Harald P. Pfeiffer, and Mark A. Scheel, 2016, "Impact of an improved neutrino energy estimate on outflows in neutron star merger simulations," Phys. Rev. D **94**, 123016.

Fowler, W. A., and F. Hoyle, 1960, "Nuclear cosmochronology," Ann. Phys. (N.Y.) **10**, 280–302.

François, P., *et al.*, 2007, "First stars. VIII. Enrichment of the neutron-capture elements in the early Galaxy," Astron. Astrophys. **476**, 935–950.

Frebel, A., N. Christlieb, J. E. Norris, C. Thom, T. C. Beers, and J. Rhee, 2007, "Discovery of HE 1523-0901, a strongly *r*-process-enhanced metal-poor star with detected uranium," Astrophys. J. Lett. **660**, L117–L120.

Frebel, A., and K.-L. Kratz, 2009, "Stellar age dating with thorium, uranium and lead," Proc. Int. Astron. Union, **258** 449–456.

Frebel, A., and J. E. Norris, 2015, "Near-field cosmology with extremely metal-poor stars," Annu. Rev. Astron. Astrophys. **53**, 631–688.

Freiburghaus, C., J.-F. Rembges, T. Rauscher, E. Kolbe, F.-K. Thielemann, K.-L. Kratz, B. Pfeiffer, and J. J. Cowan, 1999, "The astrophysical *r*-process: A comparison of calculations following adiabatic expansion with classical calculations based on neutron densities and temperatures," Astrophys. J. **516**, 381–398.

Freiburghaus, C., S. Rosswog, and F.-K. Thielemann, 1999, "*r*-process in neutron star mergers," Astrophys. J. **525**, L121–L124.

Frensel, M., M.-R. Wu, C. Volpe, and A. Perego, 2017, "Neutrino flavor evolution in binary neutron star merger remnants," Phys. Rev. D **95**, 023011.

Frischknecht, U., R. Hirschi, M. Pignatari, A. Maeder, G. Meynet, C. Chiappini, F.-K. Thielemann, T. Rauscher, C. Georgy, and S. Ekström, 2016, "*s*-process production in rotating massive stars at solar and low metallicities," Mon. Not. R. Astron. Soc. **456**, 1803–1825.

Fröhlich, C., G. Martínez-Pinedo, M. Liebendörfer, F.-K. Thielemann, E. Bravo, W. R. Hix, K. Langanke, and N. T. Zinner, 2006, "Neutrino-Induced Nucleosynthesis of $A > 64$ Nuclei: The νp Process," Phys. Rev. Lett. **96**, 142502.

Fröhlich, C., *et al.*, 2006, "Composition of the innermost supernova ejecta," Astrophys. J. **637**, 415–426.

Fryer, C., and V. Kalogera, 1997, "Double neutron star systems and natal neutron star kicks," Astrophys. J. **489**, 244–253.

Fryer, C. L., K. Belczynski, E. Ramirez-Ruiz, S. Rosswog, G. Shen, and A. W. Steiner, 2015, "The fate of the compact remnant in neutron star mergers," Astrophys. J. **812**, 24.

Fujibayashi, S., K. Kiuchi, N. Nishimura, Y. Sekiguchi, and M. Shibata, 2018, "Mass ejection from the remnant of a binary neutron star merger: Viscous-radiation hydrodynamics study," Astrophys. J. **860**, 64.

Fujibayashi, S., Y. Sekiguchi, K. Kiuchi, and M. Shibata, 2017, "Properties of neutrino-driven ejecta from the remnant of a binary neutron star merger: Pure radiation hydrodynamics case," Astrophys. J. **846**, 114.

Fujibayashi, Sho, Masaru Shibata, Shinya Wanajo, Kenta Kiuchi, Koutarou Kyutoku, and Yuichiro Sekiguchi, 2020, "Mass ejection from disks surrounding a low-mass black hole: Viscous neutrino-radiation hydrodynamics simulation in full general relativity," Phys. Rev. D **101**, 083029.

Fujimoto, S.-i., M.-a. Hashimoto, K. Arai, and R. Matsuba, 2004, "Nucleosynthesis inside an accretion disk and disk winds related to gamma-ray bursts," Astrophys. J. **614**, 847–857.

Fujimoto, S.-i., M.-a. Hashimoto, O. Koike, K. Arai, and R. Matsuba, 2003, "*p*-process nucleosynthesis inside supernova-driven supercritical accretion disks," Astrophys. J. **585**, 418–428.

Fujimoto, S.-i., M.-a. Hashimoto, K. Kotake, and S. Yamada, 2007, "Heavy-element nucleosynthesis in a collapsar," Astrophys. J. **656**, 382–392.

Fujimoto, S.-i., K. Kotake, S. Yamada, M.-a. Hashimoto, and K. Sato, 2006, "Magnetohydrodynamic simulations of a rotating massive star collapsing to a black hole," Astrophys. J. **644**, 1040–1055.

Fujimoto, S.-i., N. Nishimura, and M.-a. Hashimoto, 2008, "Nucleosynthesis in magnetically driven jets from collapsars," Astrophys. J. **680**, 1350–1358.

Fulbright, J. P., 2000, "Abundances and kinematics of field halo and disk stars. I. Observational data and abundance analysis," Astron. J. **120**, 1841–1852.

Fuller, G. M., W. A. Fowler, and M. J. Newman, 1980, "Stellar weak-interaction rates for *sd*-shell nuclei. I—Nuclear matrix element systematics with application to Al-26 and selected nuclei of importance to the supernova problem," Astrophys. J. Suppl. Ser. **42**, 447–473.

Fuller, George M., Alexander Kusenko, and Volodymyr Takhistov, 2017, "Primordial Black Holes and *r*-Process Nucleosynthesis," Phys. Rev. Lett. **119**, 061101.

Galama, T. J., *et al.*, 1998, "An unusual supernova in the error box of the γ-ray burst of 25 April 1998," Nature (London) **395**, 670–672.

Geissel, H., *et al.*, 1992, "The GSI projectile fragment separator (FRS): A versatile magnetic system for relativistic heavy ions," Nucl. Instrum. Methods Phys. Res., Sect. B **70**, 286–297.

Giacomazzo, B., L. Rezzolla, and L. Baiotti, 2009, "Can magnetic fields be detected during the inspiral of binary neutron stars?," Mon. Not. R. Astron. Soc. **399**, L164–L168.

Giacomazzo, B., J. Zrake, P. C. Duffell, A. I. MacFadyen, and R. Perna, 2015, "Producing magnetar magnetic fields in the merger of binary neutron stars," Astrophys. J. **809**, 39.

Gilroy, K. K., C. Sneden, C. A. Pilachowski, and J. J. Cowan, 1988, "Abundances of neutron capture elements in population II stars," Astrophys. J. **327**, 298–320.

Giuliani, S. A., Z. Matheson, W. Nazarewicz, E. Olsen, P.-G. Reinhard, J. Sadhukhan, B. Schuetrumpf, N. Schunck, and P. Schwerdtfeger, 2019, "Colloquium: Superheavy elements: Oganesson and beyond," Rev. Mod. Phys. **91**, 011001.

Giuliani, Samuel A, Luis M. Robledo, and R. Rodríguez-Guzmán, 2014, "Dynamic versus static fission paths with realistic interactions," Phys. Rev. C **90**, 054311.

Giuliani, Samuel A., Gabriel Martínez-Pinedo, and Luis M. Robledo, 2018, "Fission properties of superheavy nuclei for *r*-process calculations," Phys. Rev. C **97**, 034323.

Giuliani, Samuel A., Gabriel Martínez-Pinedo, Meng-Ru Wu, and Luis M. Robledo, 2020, "Fission and the *r*-process nucleosynthesis of translead nuclei," Phys. Rev. C **102**, 045804.

Giunti, C., M. Laveder, Y. F. Li, Q. Y. Liu, and H. W. Long, 2012, "Update of short-baseline electron neutrino and antineutrino disappearance," Phys. Rev. D **86**, 113014.

Godzieba, Daniel A, David Radice, and Sebastiano Bernuzzi, 2020, "On the maximum mass of neutron stars and GW190814," arXiv:2007.10999.

Goldstein, D. A., and D. Kasen, 2018, "Evidence for sub-Chandrasekhar mass type Ia supernovae from an extensive survey of radiative transfer models," Astrophys. J. **852**, L33.

Gómez-Hornillos, M. B., *et al.*, 2011, "First measurements with the BEta deLayEd Neutron Detector (BELEN-20) at JYFLTRAP," J. Phys. Conf. Ser. **312**, 052008.

Gompertz, B. P., *et al.*, 2018, "The diversity of kilonova emission in short gamma-ray bursts," Astrophys. J. **860**, 62.

Goriely, S., 1997, "Direct neutron captures and the *r*-process nucleosynthesis," Astron. Astrophys. **325**, 414–424, https://ui.adsabs.harvard.edu/#abs/1997A&A...325..414G/abstract.

Goriely, S., 1998, "Radiative neutron captures by neutron-rich nuclei and the *r*-process nucleosynthesis," Phys. Lett. B **436**, 10–18.

Goriely, S., 1999, "Uncertainties in the Solar System *r*-abundance distribution," Astron. Astrophys. **342**, 881–891, https://ui.adsabs.harvard.edu/#abs/1999A&A...342..881G/abstract.

Goriely, S., 2015, "The fundamental role of fission during *r*-process nucleosynthesis in neutron star mergers," Eur. Phys. J. A **51**, 22.

Goriely, S., and M. Arnould, 2001, "Actinides: How well do we know their stellar production?," Astron. Astrophys. **379**, 1113–1122.

Goriely, S., A. Bauswein, H. T. Janka, J. L. Sida, J. F. Lemaître, S. Panebianco, N. Dubray, and S. Hilaire, 2014, "The *r*-process nucleosynthesis during the decompression of neutron star crust material," AIP Conf. Proc. **1594** 357–364.

Goriely, S., A. Bauswein, and H.-T. Janka, 2011, "*r*-process nucleosynthesis in dynamically ejected matter of neutron star mergers," Astrophys. J. **738**, L32.

Goriely, S., A. Bauswein, O. Just, E. Pllumbi, and H.-T. Janka, 2015, "Impact of weak interactions of free nucleons on the *r*-process in dynamical ejecta from neutron star mergers," Mon. Not. R. Astron. Soc. **452**, 3894–3904.

Goriely, S., N. Chamel, and J. M. Pearson, 2010, "Further explorations of Skyrme-Hartree-Fock-Bogoliubov mass formulas. XII. Stiffness and stability of neutron-star matter," Phys. Rev. C **82**, 035804.

Goriely, S., N. Chamel, and J. M. Pearson, 2016, "Further explorations of Skyrme-Hartree-Fock-Bogoliubov mass formulas. XVI. Inclusion of self-energy effects in pairing," Phys. Rev. C **93**, 034337.

Goriely, S., and B. Clerbaux, 1999, "Uncertainties in the Th cosmochronometry," Astron. Astrophys. **346**, 798–804, https://ui.adsabs.harvard.edu/abs/1999A%26A...346..798G/abstract.

Goriely, S., and J.-P. Delaroche, 2007, "The isovector imaginary neutron potential: A key ingredient for the *r*-process nucleosynthesis," Phys. Lett. B **653**, 178–183.

Goriely, S., S. Hilaire, and M. Girod, 2012, "Latest development of the combinatorial model of nuclear level densities," J. Phys. Conf. Ser. **337**, 012027.

Goriely, S., S. Hilaire, and A. J. Koning, 2008, "Improved microscopic nuclear level densities within the Hartree-Fock-Bogoliubov plus combinatorial method," Phys. Rev. C **78**, 064307.

Goriely, S., S. Hilaire, A. J. Koning, M. Sin, and R. Capote, 2009, "Towards a prediction of fission cross sections on the basis of microscopic nuclear inputs," Phys. Rev. C **79**, 024612.

Goriely, S., S. Hilaire, S. Péru, and K. Sieja, 2018, "Gogny-HFB +QRPA dipole strength function and its application to radiative nucleon capture cross section," Phys. Rev. C **98**, 014327.

Goriely, S., and H.-T. Janka, 2016, "Solar *r*-process-constrained actinide production in neutrino-driven winds of supernovae," Mon. Not. R. Astron. Soc. **459**, 4174–4182.

Goriely, S., and E. Khan, 2002, "Large-scale QRPA calculation of E1-strength and its impact on the neutron capture cross section," Nucl. Phys. **A706**, 217–232.

Goriely, S., E. Khan, and M. Samyn, 2004, "Microscopic HFB + QRPA QRPA predictions of dipole strength for astrophysics applications," Nucl. Phys. **A739**, 331–352.

Goriely, S., and G. Martínez-Pinedo, 2015, "The production of transuranium elements by the *r*-process nucleosynthesis," Nucl. Phys. **A944**, 158–176.

Goriely, S., J.-L. Sida, J.-F. Lemaître, S. Panebianco, N. Dubray, S. Hilaire, A. Bauswein, and H.-T. Janka, 2013, "New Fission Fragment Distributions and *r*-Process Origin of the Rare-Earth Elements," Phys. Rev. Lett. **111**, 242502.

Görres, J., M. Wiescher, and F.-K. Thielemann, 1995, "Bridging the waiting points: The role of two-proton capture reactions in the *rp* process," Phys. Rev. C **51**, 392–400.

Gottlieb, Ore, Ehud Nakar, and Tsvi Piran, 2018, "The cocoon emission—An electromagnetic counterpart to gravitational waves from neutron star mergers," Mon. Not. R. Astron. Soc. **473**, 576–584.

Grawe, H., K. Langanke, and G. Martínez-Pinedo, 2007, "Nuclear structure and astrophysics," Rep. Prog. Phys. **70**, 1525–1582.

Grebenev, S. A., A. A. Lutovinov, S. S. Tsygankov, and C. Winkler, 2012, "Hard-x-ray emission lines from the decay of ^{44}Ti in the remnant of supernova 1987A," Nature (London) **490**, 373–375.

Greiner, J., *et al.*, 2015, "A very luminous magnetar-powered supernova associated with an ultra-long γ-ray burst," Nature (London) **523**, 189–192.

Grichener, Aldana, and Noam Soker, 2019, "The common envelope jet supernova (CEJSN) *r*-process scenario," Astrophys. J. **878**, 24.

Griffin, R., B. Gustafsson, T. Vieira, and R. Griffin, 1982, "HD 115444—A barium star of extreme population II, Mon. Not. R. Astron. Soc. **198**, 637–658.

Grisoni, V., G. Cescutti, F. Matteucci, R. Forsberg, H. Jönsson, and N. Ryde, 2020, "Modelling the chemical evolution of Zr, La, Ce, and Eu in the galactic discs and bulge," Mon. Not. R. Astron. Soc. **492**, 2828–2834.

Grossjean, M. K., and H. Feldmeier, 1985, "Level density of a Fermi gas with pairing interactions," Nucl. Phys. **A444**, 113–132.

Grossman, D., O. Korobkin, S. Rosswog, and T. Piran, 2014, "The long-term evolution of neutron star merger remnants—II. Radioactively powered transients," Mon. Not. R. Astron. Soc. **439**, 757–770.

Gudin, D., *et al.*, "The *R*-Process Alliance: Chemo-dynamically tagged groups of halo *r*-process-enhanced stars reveal a shared chemical-evolution history," arXiv:2012.13808.

Guerrero, C., C. Domingo-Pardo, F. Käppeler, J. Lerendegui-Marco, F. R. Palomo, J. M. Quesada, and R. Reifarth, 2017, "Prospects for direct neutron capture measurements on *s*-process branching point isotopes," Eur. Phys. J. A **53**, 87.

Guilet, J., A. Bauswein, O. Just, and H.-T. Janka, 2017, "Magneto-rotational instability in neutron star mergers: Impact of neutrinos," Mon. Not. R. Astron. Soc. **471**, 1879–1887.

Guttormsen, M., T. Ramsøy, and J. Rekstad, 1987, "The first generation of γ-rays from hot nuclei," Nucl. Instrum. Methods Phys. Res., Sect. A **255**, 518–523.

Guttormsen, M., *et al.*, 2005, "Radiative strength functions in $^{93-98}$Mo," Phys. Rev. C **71**, 044307.

Haensel, P., A. Y. Potekhin, and D. G. Yakovlev, 2007, *Neutron Stars 1: Equation of State and Structure*, Astrophysics and Space Science Library Vol. 326 (Springer, New York).

Halevi, G., and P. Mösta, 2018, "*r*-process nucleosynthesis from three-dimensional jet-driven core-collapse supernovae with magnetic misalignments," Mon. Not. R. Astron. Soc. **477**, 2366–2375.

Hamers, Adrian S., and Todd A. Thompson, 2019, "Double neutron star mergers from hierarchical triple-star systems," Astrophys. J. **883**, 23.

Hannaford, P., and R. M. Lowe, 1981, "Determination of atomic lifetimes using pulsed laser excitation of sputtered metal vapours," J. Phys. B **14**, L5–L9.

Hansen, C. J., and F. Primas, 2011, "The origin of palladium and silver," Astron. Astrophys. **525**, L5.

Hansen, C. J., F. Primas, H. Hartman, K. L. Kratz, S. Wanajo, B. Leibundgut, K. Farouqi, O. Hallmann, N. Christlieb, and H. Nilsson, 2012, "Silver and palladium help unveil the nature of a second *r*-process," Astron. Astrophys. **545**, A31.

Hansen, T. T., *et al.* (DES Collaboration), 2017, "An *r*-process enhanced star in the dwarf galaxy Tucana III," Astrophys. J. **838**, 44.

Hansen, Terese T., Erika M. Holmbeck, Timothy C. Beers, Vinicius M. Placco, Ian U. Roederer, Anna Frebel, Charli M. Sakari, Joshua D. Simon, and Ian B. Thompson, 2018, "The *r*-process alliance: First release from the southern search for *r*-process-enhanced stars in the galactic halo," Astrophys. J. **858**, 92.

Harikae, Seiji, Tomoya Takiwaki, and Kei Kotake, 2009, "Long-term evolution of slowly rotating collapsar in special relativistic magnetohydrodynamics," Astrophys. J. **704**, 354–371.

Hartmann, D., S. E. Woosley, and M. F. El Eid, 1985, "Nucleosynthesis in neutron-rich supernova ejecta," Astrophys. J. **297**, 837–845.

Hatarik, R., *et al.*, 2010, "Benchmarking a surrogate reaction for neutron capture," Phys. Rev. C **81**, 011602.

Hausmann, M., *et al.*, 2000, "First isochronous mass spectrometry at the experimental storage ring ESR," Nucl. Instrum. Methods Phys. Res., Sect. A **446**, 569–580.

Hausmann, M., *et al.*, 2001, "Isochronous mass measurements of hot exotic nuclei," Hyperfine Interact. **132**, 289–295.

Haxton, W. C., K. Langanke, Y.-Z. Qian, and P. Vogel, 1997, "Neutrino-Induced Nucleosynthesis and the Site of the *r* Process," Phys. Rev. Lett. **78**, 2694–2697.

Hayek, W., *et al.*, 2009, "The Hamburg/ESO *r*-process enhanced star survey (HERES). IV. Detailed abundance analysis and age dating of the strongly *r*-process enhanced stars CS 29491-069 and HE 1219-0312," Astron. Astrophys. **504**, 511–524.

Haynes, Christopher J., and Chiaki Kobayashi, 2019, "Galactic simulations of *r*-process elemental abundances," Mon. Not. R. Astron. Soc. **483**, 5123–5134.

Hebeler, K., J. D. Holt, J. Menéndez, and A. Schwenk, 2015, "Nuclear forces and their impact on neutron-rich nuclei and neutron-rich matter," Annu. Rev. Nucl. Part. Sci. **65**, 457–484.

Hebeler, K., J. M. Lattimer, C. J. Pethick, and A. Schwenk, 2013, "Equation of state and neutron star properties constrained by nuclear physics and observation," Astrophys. J. **773**, 11.

Heger, A., C. L. Fryer, S. E. Woosley, N. Langer, and D. H. Hartmann, 2003, "How massive single stars end their life," Astrophys. J. **591**, 288–300.

Heger, A., E. Kolbe, W. C. Haxton, K. Langanke, G. Martínez-Pinedo, and S. E. Woosley, 2005, "Neutrino nucleosynthesis," Phys. Lett. B **606**, 258–264.

Hewish, A., and S. E. Okoye, 1965, "Evidence for an unusual source of high radio brightness temperature in the Crab Nebula," Nature (London) **207**, 59–60.

Hilaire, S., S. Goriely, M. Girod, A. J. Koning, R. Capote, and M. Sin, 2010, "Combinatorial level densities for practical applications," EPJ Web Conf. **2**, 04005.

Hill, V., N. Christlieb, T. C. Beers, P. S. Barklem, K. L. Kratz, B. Nordström, B. Pfeiffer, and K. Farouqi, 2017, "The Hamburg/ESO *r*-process enhanced star survey (HERES). XI. The highly *r*-process-enhanced star CS 29497-004," Astron. Astrophys. **607**, A91.

Hill, V., *et al.*, 2002, "First stars. I. The extreme *r*-element rich, iron-poor halo giant CS 31082-001. Implications for the *r*-process site(s) and radioactive cosmochronology," Astron. Astrophys. **387**, 560–579.

Hill, V., *et al.*, 2019, "VLT/FLAMES high-resolution chemical abundances in Sculptor: A textbook dwarf spheroidal galaxy," Astron. Astrophys. **626**, A15.

Hillebrandt, W., 1978, "The rapid neutron-capture process and the synthesis of heavy and neutron-rich elements," Space Sci. Rev. **21**, 639–702.

Hillebrandt, W., K. Takahashi, and T. Kodama, 1976, "*r*-process nucleosynthesis: A dynamical model," Astron. Astrophys. **52**, 63–68, https://ui.adsabs.harvard.edu/#abs/1976A&A....52...63H/abstract.

Hillebrandt, W., M. Kromer, F. K. Röpke, and A. J. Ruiter, 2013, "Towards an understanding of type Ia supernovae from a synthesis of theory and observations," Front. Phys. **8**, 116–143.

Hillebrandt, W., F. K. Thielemann, H. V. Klapdor, and T. Oda, 1981, "The *r*-process during explosive helium burning in supernovae," Astron. Astrophys. **99**, 195–198, https://ui.adsabs.harvard.edu/#abs/1981A&A....99..195H/abstract.

Hirai, Y., Y. Ishimaru, T. R. Saitoh, M. S. Fujii, J. Hidaka, and T. Kajino, 2015, "Enrichment of *r*-process elements in dwarf spheroidal galaxies in chemo-dynamical evolution model," Astrophys. J. **814**, 41.

Hirai, Y., Y. Ishimaru, T. R. Saitoh, M. S. Fujii, J. Hidaka, and T. Kajino, 2017, "Early chemo-dynamical evolution of dwarf galaxies deduced from enrichment of *r*-process elements," Mon. Not. R. Astron. Soc. **466**, 2474–2487.

Hix, W. R., E. J. Lentz, S. W. Bruenn, A. Mezzacappa, O. E. B. Messer, E. Endeve, J. M. Blondin, J. A. Harris, P. Marronetti, and K. N. Yakunin, 2016, "The multi-dimensional character of core-collapse supernovae," Acta Phys. Pol. B **47**, 645.

Hix, W. R., and B. S. Meyer, 2006, "Thermonuclear kinetics in astrophysics," Nucl. Phys. **A777**, 188–207.

Hix, W. R., and F.-K. Thielemann, 1999, "Silicon burning. II. Quasi-equilibrium and explosive burning," Astrophys. J. **511**, 862–875.

Hix, W. Raphael, Suzanne T. Parete-Koon, Christian Freiburghaus, and Friedrich-Karl Thielemann, 2007, "The QSE-reduced nuclear reaction network for silicon burning," Astrophys. J. **667**, 476–488.

Hix, W. Raphael, and Friedrich-Karl Thielemann, 1999, "Computational methods for nucleosynthesis and nuclear energy generation," J. Comput. Appl. Math. **109**, 321–351.

Hoffman, R. D., S. E. Woosley, and Y.-Z. Qian, 1997, "Nucleosynthesis in neutrino-driven winds. II. Implications for heavy element synthesis," Astrophys. J. **482**, 951–962.

Holmbeck, E. M., *et al.*, 2018, "The *r*-process alliance: 2MASS J09544277+5246414, the most actinide-enhanced R-II star known," Astrophys. J. **859**, L24.

Holmbeck, Erika M., Anna Frebel, G. C. McLaughlin, Matthew R. Mumpower, Trevor M. Sprouse, and Rebecca Surman, 2019, "Actinide-rich and actinide-poor *r*-process-enhanced metal-poor stars do not require separate *r*-process progenitors," Astrophys. J. **881**, 5.

Holmbeck, Erika M., Trevor M. Sprouse, Matthew R. Mumpower, Nicole Vassh, Rebecca Surman, Timothy C. Beers, and Toshihiko Kawano, 2019, "Actinide production in the neutron-rich ejecta of a neutron star merger," Astrophys. J. **870**, 23.

Honda, S., W. Aoki, Y. Ishimaru, and S. Wanajo, 2007, "Neutron-capture elements in the very metal-poor star HD 88609: Another star with excesses of light neutron-capture elements," Astrophys. J. **666**, 1189–1197.

Honda, S., W. Aoki, Y. Ishimaru, S. Wanajo, and S. G. Ryan, 2006, "Neutron-capture elements in the very metal poor star HD 122563," Astrophys. J. **643**, 1180–1189.

Honda, S., W. Aoki, T. Kajino, H. Ando, T. C. Beers, H. Izumiura, K. Sadakane, and M. Takada-Hidai, 2004, "Spectroscopic studies of extremely metal-poor stars with the Subaru high dispersion spectrograph. II. The *r*-process elements, including thorium," Astrophys. J. **607**, 474–498.

Horowitz, C. J., 2002, "Weak magnetism for antineutrinos in supernovae," Phys. Rev. D **65**, 043001.

Horowitz, C. J., G. Shen, Evan O'Connor, and Christian D. Ott, 2012, "Charged-current neutrino interactions in core-collapse supernovae in a virial expansion," Phys. Rev. C **86**, 065806.

Horowitz, C. J., *et al.*, 2019, "*r*-process nucleosynthesis: Connecting rare-isotope beam facilities with the cosmos," J. Phys. G **46**, 083001.

Hosmer, P., *et al.*, 2010, "Half-lives and branchings for β-delayed neutron emission for neutron-rich Co-Cu isotopes in the *r*-process," Phys. Rev. C **82**, 025806.

Hosmer, P. T., *et al.*, 2005, "Half-Life of the Doubly Magic *r*-Process Nucleus ^{78}Ni," Phys. Rev. Lett. **94**, 112501.

Hosseinzadeh, G., *et al.*, 2019, "Follow-up of the neutron star bearing gravitational-wave candidate events S190425z and S190426c with MMT and SOAR," Astrophys. J. Lett., **880**, L4.

Hotokezaka, K., P. Beniamini, and T. Piran, 2018, "Neutron star mergers as sites of *r*-process nucleosynthesis and short gamma-ray bursts," Int. J. Mod. Phys. D **27**, 1842005.

Hotokezaka, K., K. Kyutoku, and M. Shibata, 2013, "Exploring tidal effects of coalescing binary neutron stars in numerical relativity," Phys. Rev. D **87**, 044001.

Hotokezaka, K., T. Piran, and M. Paul, 2015, "Short-lived ^{244}Pu points to compact binary mergers as sites for heavy *r*-process nucleosynthesis," Nat. Phys. **11**, 1042.

Hotokezaka, K., S. Wanajo, M. Tanaka, A. Bamba, Y. Terada, and T. Piran, 2016, "Radioactive decay products in neutron star merger ejecta: Heating efficiency and γ-ray emission," Mon. Not. R. Astron. Soc. **459**, 35–43.

Hotokezaka, Kenta, Kenta Kiuchi, Koutarou Kyutoku, Takayuki Muranushi, Yu-ichiro Sekiguchi, Masaru Shibata, and Keisuke Taniguchi, 2013, "Remnant massive neutron stars of binary neutron star mergers: Evolution process and gravitational waveform," Phys. Rev. D **88**, 044026.

Hotokezaka, Kenta, Kenta Kiuchi, Koutarou Kyutoku, Hirotada Okawa, Yu-ichiro Sekiguchi, Masaru Shibata, and Keisuke Taniguchi, 2013, "Mass ejection from the merger of binary neutron stars," Phys. Rev. D **87**, 024001.

Hotokezaka, Kenta, Koutarou Kyutoku, Hirotada Okawa, Masaru Shibata, and Kenta Kiuchi, 2011, "Binary neutron star mergers: Dependence on the nuclear equation of state," Phys. Rev. D **83**, 124008.

Hotokezaka, Kenta, and Ehud Nakar, 2020, "Radioactive heating rate of *r*-process elements and macronova light curve," Astrophys. J. **891**, 152.

Hotokezaka, Kenta, Re'em Sari, and Tsvi Piran, 2017, "Analytic heating rate of neutron star merger ejecta derived from Fermi's theory of beta decay," Mon. Not. R. Astron. Soc. **468**, 91–96.

Howard, W. M., W. D. Arnett, D. D. Clayton, and S. E. Woosley, 1972, "Nucleosynthesis of rare nuclei from seed nuclei in explosive carbon burning," Astrophys. J. **175**, 201.

Howard, W. M., and P. Möller, 1980, "Calculated fission barriers, ground-state masses, and particle separation energies for nuclei with $76 \leq Z \leq 100$ and $140 \leq N \leq 184$," At. Data Nucl. Data Tables **25**, 219.

Hüdepohl, L., B. Müller, H.-T. Janka, A. Marek, and G. G. Raffelt, 2010, "Neutrino Signal of Electron-Capture Supernovae from Core Collapse to Cooling," Phys. Rev. Lett. **104**, 251101.

Hulse, R. A., and J. H. Taylor, 1975, "Discovery of a pulsar in a binary system," Astrophys. J. **195**, L51–L53.

Iliadis, C., 2007, *Nuclear Physics of Stars* (Wiley-VCH Verlag, Wenheim, Germany).

Ishii, Ayako, Toshikazu Shigeyama, and Masaomi Tanaka, 2018, "Free neutron ejection from shock breakout in binary neutron star mergers," Astrophys. J. **861**, 25.

Ishimaru, Y., and S. Wanajo, 1999, "Enrichment of the *r*-process element europium in the galactic halo," Astrophys. J. **511**, L33–L36.

Ishimaru, Y., S. Wanajo, and N. Prantzos, 2015, "Neutron star mergers as the origin of *r*-process elements in the galactic halo based on the sub-halo clustering scenario," Astrophys. J. **804**, L35.

Ivans, I. I., J. Simmerer, C. Sneden, J. E. Lawler, J. J. Cowan, R. Gallino, and S. Bisterzo, 2006, "Near-ultraviolet observations of HD 221170: New insights into the nature of *r*-process-rich stars," Astrophys. J. **645**, 613–633.

Iwamoto, K., *et al.*, 1998, "A hypernova model for the supernova associated with the γ-ray burst of 25 April 1998," Nature (London) **395**, 672–674.

Janiuk, A., 2014, "Nucleosynthesis of elements in gamma-ray burst engines," Astron. Astrophys. **568**, A105.

Janiuk, Agnieszka, 2017, "Microphysics in the gamma-ray burst central engine," Astrophys. J. **837**, 39.

Janiuk, Agnieszka, 2019a, "Nucleosynthesis from dynamical outflows of long gamma-ray burst accretion disks" (private communication).

Janiuk, Agnieszka, 2019b, "The *r*-process nucleosynthesis in the outflows from short GRB accretion disks," Astrophys. J. **882**, 163.

Janiuk, Agnieszka, and Kostas Sapountzis, 2018, "Gamma ray bursts. Progenitors, accretion in the central engine, jet acceleration mechanisms," arXiv:1803.07873.

Janiuk, Agnieszka, Petra Sukova, and Ishika Palit, 2018, "Accretion in a dynamical spacetime and the spinning up of the black hole in the gamma-ray burst central engine," Astrophys. J. **868**, 68.

Janka, H.-T., 2017a, "Neutrino-driven explosions," in *Handbook of Supernovae*, edited by A. W. Alsabti, and P. Murdin (Springer International Publishing, Cham, Switzerland).

Janka, H.-T., 2017b, "Neutrino emission from supernovae," in *Handbook of Supernovae*, edited by A. W. Alsabti, and P. Murdin (Springer International Publishing, Cham, Switzerland).

Janka, H.-T., B. Müller, F. S. Kitaura, and R. Buras, 2008, "Dynamics of shock propagation and nucleosynthesis conditions in O-Ne-Mg core supernovae," Astron. Astrophys. **485**, 199–208.

Janka, Hans-Thomas, Tobias Melson, and Alexander Summa, 2016, "Physics of core-collapse supernovae in three dimensions: A sneak preview," Annu. Rev. Nucl. Part. Sci. **66**, 341–375.

Jeukenne, J.-P., A. Lejeune, and C. Mahaux, 1977, "Optical-model potential in finite nuclei from Reid's hard core interaction," Phys. Rev. C **16**, 80–96.

Ji, A. P., A. Frebel, J. D. Simon, and A. Chiti, 2016, "Complete element abundances of nine stars in the *r*-process galaxy Reticulum II," Astrophys. J. **830**, 93.

Ji, Alexander P., Maria R. Drout, and Terese T. Hansen, 2019, "The lanthanide fraction distribution in metal-poor stars: A test of neutron star mergers as the dominant *r*-process site," Astrophys. J. **882**, 40.

Ji, Alexander P., and Anna Frebel, 2018, "From actinides to zinc: Using the full abundance pattern of the brightest star in Reticulum II to distinguish between different *r*-process sites," Astrophys. J. **856**, 138.

Ji, Alexander P., Joshua D. Simon, Anna Frebel, Kim A. Venn, and Terese T. Hansen, 2019, "Chemical abundances in the ultra-faint dwarf galaxies Grus I and Triangulum II: Neutron-capture elements as a defining feature of the faintest dwarfs," Astrophys. J. **870**, 83.

Jin, Zhi-Ping, Stefano Covino, Neng-Hui Liao, Xiang Li, Paolo D'Avanzo, Yi-Zhong Fan, and Da-Ming Wei, 2020, "A kilonova associated with GRB 070809," Nat. Astron. **4**, 77–82.

Jin, Zhi-Ping, Kenta Hotokezaka, Xiang Li, Masaomi Tanaka, Paolo D'Avanzo, Yi-Zhong Fan, Stefano Covino, Da-Ming Wei, and Tsvi Piran, 2016, "The macronova in GRB 050709 and the GRB-macronova connection," Nat. Commun. **7**, 12898.

Jin, Zhi-Ping, Xiang Li, Zach Cano, Stefano Covino, Yi-Zhong Fan, and Da-Ming Wei, 2015, "The light curve of the macronova associated with the long-short burst GRB 060614," Astrophys. J. Lett. **811**, L22.

Johnson, C. W., S. E. Koonin, G. H. Lang, and W. E. Ormand, 1992, "Monte Carlo Methods for the Nuclear Shell Model," Phys. Rev. Lett. **69**, 3157–3160.

Jones, K. L., *et al.*, 2010, "The magic nature of ^{132}Sn explored through the single-particle states of ^{133}Sn," Nature (London) **465**, 454–457.

Jones, S., R. Hirschi, and K. Nomoto, 2014, "The final fate of stars that ignite neon and oxygen off-center: Electron capture or iron core-collapse supernova?," Astrophys. J. **797**, 83.

Jones, S., C. Ritter, F. Herwig, C. Fryer, M. Pignatari, M. G. Bertolli, and B. Paxton, 2016, "H ingestion into He-burning convection

zones in super-AGB stellar models as a potential site for intermediate neutron-density nucleosynthesis," Mon. Not. R. Astron. Soc. **455**, 3848–3863.

Jones, S., F. K. Röpke, R. Pakmor, I. R. Seitenzahl, S. T. Ohlmann, and P. V. F. Edelmann, 2016, "Do electron-capture supernovae make neutron stars? First multidimensional hydrodynamic simulations of the oxygen deflagration," Astron. Astrophys. **593**, A72.

Junghans, A. R., M. de Jong, H.-G. Clerc, A. V. Ignatyuk, G. A. Kudyaev, and K.-H. Schmidt, 1998, "Projectile-fragment yields as a probe for the collective enhancement in the nuclear level density," Nucl. Phys. **A629**, 635–655.

Juodagalvis, A., Karlheinz Langanke, W. R. Hix, Gabriel Martínez-Pinedo, and J. M. Sampaio, 2010, "Improved estimate of electron capture rates on nuclei during stellar core collapse," Nucl. Phys. **A848**, 454–478.

Just, O., A. Bauswein, R. A. Pulpillo, S. Goriely, and H.-T. Janka, 2015, "Comprehensive nucleosynthesis analysis for ejecta of compact binary mergers," Mon. Not. R. Astron. Soc. **448**, 541–567.

Just, O., M. Obergaulinger, and H. T. Janka, 2015, "A new multidimensional, energy-dependent two-moment transport code for neutrino-hydrodynamics," Mon. Not. R. Astron. Soc. **453**, 3386.

Just, O., M. Obergaulinger, H.-T. Janka, A. Bauswein, and N. Schwarz, 2016, "Neutron-star merger ejecta as obstacles to neutrino-powered jets of gamma-ray bursts," Astrophys. J. **816**, L30.

Kajino, T., W. Aoki, A. B. Balantekin, R. Diehl, M. A. Famiano, and G. J. Mathews, 2019, "Current status of *r*-process nucleosynthesis," Prog. Part. Nucl. Phys. **107**, 109–166.

Kajino, T., and G. J. Mathews, 2017, "Impact of new data for neutron-rich heavy nuclei on theoretical models for *r*-process nucleosynthesis," Rep. Prog. Phys. **80**, 084901.

Kalogera, V., and C. L. Fryer, 1999, "Formation of the observed double neutron star systems," Astron. Astrophys. Trans. **18**, 515–520.

Kaplan, J. D., C. D. Ott, E. P. O'Connor, K. Kiuchi, L. Roberts, and M. Duez, 2014, "The influence of thermal pressure on equilibrium models of hypermassive neutron star merger remnants," Astrophys. J. **790**, 19.

Käppeler, F., 1999, "The origin of the heavy elements: The *s* process," Prog. Part. Nucl. Phys. **43**, 419–483.

Käppeler, F., R. Gallino, S. Bisterzo, and W. Aoki, 2011, "The *s* process: Nuclear physics, stellar models, and observations," Rev. Mod. Phys. **83**, 157–194.

Karakas, A. I., and J. C. Lattanzio, 2014, "The Dawes Review 2: Nucleosynthesis and stellar yields of low- and intermediate-mass single stars," Publ. Astron. Soc. Aust. **31**, e030.

Kasen, D., N. R. Badnell, and J. Barnes, 2013, "Opacities and spectra of the *r*-process ejecta from neutron star mergers," Astrophys. J. **774**, 25.

Kasen, D., and L. Bildsten, 2010, "Supernova light curves powered by young magnetars," Astrophys. J. **717**, 245–249.

Kasen, Daniel, and Jennifer Barnes, 2019, "Radioactive heating and late time kilonova light curves," Astrophys. J. **876**, 128.

Kasen, Daniel, Brian Metzger, Jennifer Barnes, Eliot Quataert, and Enrico Ramirez-Ruiz, 2017, "Origin of the heavy elements in binary neutron-star mergers from a gravitational-wave event," Nature (London) **551**, 80–84.

Kasliwal, M. M., *et al.*, 2017, "Illuminating gravitational waves: A concordant picture of photons from a neutron star merger," Science **358**, 1559–1565.

Kasliwal, Mansi M., *et al.*, 2019, "Spitzer mid-infrared detections of neutron star merger GW170817 suggests synthesis of the heaviest elements," Mon. Not. R. Astron. Soc. Lett. (to be published).

Kaspi, V. M., and A. M. Beloborodov, 2017, "Magnetars," Annu. Rev. Astron. Astrophys. **55**, 261–301.

Kastaun, W., R. Ciolfi, and B. Giacomazzo, 2016, "Structure of stable binary neutron star merger remnants: A case study," Phys. Rev. D **94**, 044060.

Kawaguchi, Kyohei, Koutarou Kyutoku, Masaru Shibata, and Masaomi Tanaka, 2016, "Models of kilonova/macronova emission from black hole–neutron star mergers," Astrophys. J. **825**, 52.

Kawaguchi, Kyohei, Masaru Shibata, and Masaomi Tanaka, 2018, "Radiative transfer simulation for the optical and near-infrared electromagnetic counterparts to GW170817," Astrophys. J. **865**, L21.

Kawaguchi, Kyohei, Masaru Shibata, and Masaomi Tanaka, 2020, "Diversity of kilonova light curves," Astrophys. J. **889**, 171.

Kelic, A., M. V. Ricciardi, and K.-H. Schmidt, 2008, "New insight into the fission process from experiments with relativistic heavy-ion beams," in *Dynamical Aspects of Nuclear Fission*, edited by J. Kliman, M. G. Itkis, and Š. Gmuca (World Scientific, Singapore), pp. 203–215.

Kelic, Aleksandra, M. Valentina Ricciardi, and Karl-Heinz Schmidt, 2009, "ABLA07—Towards a complete description of the decay channels of a nuclear system from spontaneous fission to multi-fragmentation," arXiv:0906.4193.

Kirby, E. N., J. G. Cohen, P. Guhathakurta, L. Cheng, J. S. Bullock, and A. Gallazzi, 2013, "The universal stellar mass-stellar metallicity relation for dwarf galaxies," Astrophys. J. **779**, 102.

Kirsebom, O. S., *et al.*, 2019a, "Discovery of an Exceptionally Strong β -Decay Transition of ^{20}F and Implications for the Fate of Intermediate-Mass Stars," Phys. Rev. Lett. **123**, 262701.

Kirsebom, O. S., *et al.*, 2019b, "Measurement of the $2^+ \rightarrow 0^+$ ground-state transition in the β decay of ^{20}F," Phys. Rev. C **100**, 065805.

Kirson, M. W., 2008, "Mutual influence of terms in a semi-empirical mass formula," Nucl. Phys. **A798**, 29–60.

Kiss, G. G., *et al.*, 2009, "High precision ^{89}Y$(\alpha,\alpha)^{89}$Y scattering at low energies," Phys. Rev. C **80**, 045807.

Kitaura, F. S., H.-T. Janka, and W. Hillebrandt, 2006, "Explosions of O-Ne-Mg cores, the Crab supernova, and subluminous type II-P supernovae," Astron. Astrophys. **450**, 345–350.

Kiuchi, K., P. Cerdá-Durán, K. Kyutoku, Y. Sekiguchi, and M. Shibata, 2015, "Efficient magnetic-field amplification due to the Kelvin-Helmholtz instability in binary neutron star mergers," Phys. Rev. D **92**, 124034.

Kiuchi, Kenta, Koutarou Kyutoku, and Masaru Shibata, 2012, "Three-dimensional evolution of differentially rotating magnetized neutron stars," Phys. Rev. D **86**, 064008.

Kiuchi, Kenta, Yuichiro Sekiguchi, Masaru Shibata, and Keisuke Taniguchi, 2009, "Long-term general relativistic simulation of binary neutron stars collapsing to a black hole," Phys. Rev. D **80**, 064037.

Kizivat, L.-T., G. Martínez-Pinedo, K. Langanke, R. Surman, and G. C. McLaughlin, 2010, "γ-ray bursts black hole accretion disks as a site for the νp process," Phys. Rev. C **81**, 025802.

Klapdor, H. V., T. Oda, J. Metzinger, W. Hillebrandt, and F. K. Thielemann, 1981, "The beta strength function and the astrophysical site of the *r*-process," Z. Phys. A **299**, 213–229.

Knie, K., G. Korschinek, T. Faestermann, E. A. Dorfi, G. Rugel, and A. Wallner, 2004, "^{60}Fe Anomaly in a Deep-Sea Manganese Crust and Implications for a Nearby Supernova Source," Phys. Rev. Lett. **93**, 171103.

Knöbel, R., *et al.*, 2016, "First direct mass measurements of stored neutron-rich 129,130,131Cd isotopes with FRS-ESR," Phys. Lett. B **754**, 288–293.

Kobayashi, C., 2016, "Inhomogeneous chemical enrichment in the galactic halo," in *The General Assembly of Galaxy Halos: Structure, Origin and Evolution*, IAU Symposium Vol. 317, edited by A. Bragaglia, M. Arnaboldi, M. Rejkuba, and D. Romano (Cambridge University Press, Cambridge, England), pp. 57–63.

Kobayashi, C., H. Umeda, K. Nomoto, N. Tominaga, and T. Ohkubo, 2006, "Galactic chemical evolution: Carbon through zinc," Astrophys. J. **653**, 1145–1171.

Kodama, Takeshi, and Kohji Takahashi, 1975, "*r*-process nucleosynthesis and nuclei far from the region of beta-stability," Nucl. Phys. **A239**, 489–510.

Kolbe, E., K. Langanke, G. Martínez-Pinedo, and P. Vogel, 2003, "Neutrino nucleus reactions and nuclear structure," J. Phys. G **29**, 2569–2596.

Komiya, Yutaka, and Toshikazu Shigeyama, 2016, "Contribution of neutron star mergers to the *r*-process chemical evolution in the hierarchical galaxy formation," Astrophys. J. **830**, 76.

Koning, A. J., and J. P. Delaroche, 2003, "Local and global nucleon optical models from 1 keV to 200 MeV," Nucl. Phys. **A713**, 231–310.

Koning, A. J., S. Hilaire, and S. Goriely, 2008, "Global and local level density models," Nucl. Phys. **A810**, 13–76.

Koonin, S. E., D. J. Dean, and K. Langanke, 1997, "Shell model Monte Carlo methods," Phys. Rep. **278**, 1–77.

Korobkin, O., S. Rosswog, A. Arcones, and C. Winteler, 2012, "On the astrophysical robustness of the neutron star merger *r*-process," Mon. Not. R. Astron. Soc. **426**, 1940–1949.

Korobkin, Oleg, *et al.*, 2020a, "Gamma rays from kilonova: A potential probe of *r*-process nucleosynthesis," Astrophys. J. **889**, 168.

Korobkin, Oleg, *et al.*, 2020b, "Axisymmetric radiative transfer models of kilonovae," arXiv:2004.00102.

Kotake, K., K. Sumiyoshi, S. Yamada, T. Takiwaki, T. Kuroda, Y. Suwa, and H. Nagakura, 2012, "Core-collapse supernovae as supercomputing science: A status report toward six-dimensional simulations with exact Boltzmann neutrino transport in full general relativity," Prog. Theor. Exp. Phys. **2012**, 01A301.

Koura, H., T. Tachibana, M. Uno, and M. Yamada, 2005, "Nuclidic mass formula on a spherical basis with an improved even-odd term," Prog. Theor. Phys. **113**, 305–325.

Kozub, R. L., *et al.*, 2012, "Neutron Single Particle Structure in ^{131}Sn and Direct Neutron Capture Cross Sections," Phys. Rev. Lett. **109**, 172501.

Kramer, M., 2009, "Pulsars & magnetars," in *Cosmic Magnetic Fields: From Planets, to Stars and Galaxies*, IAU Symposium Vol. 259, edited by K. G. Strassmeier, A. G. Kosovichev, and J. E. Beckman (Cambridge University Press, Cambridge, England), pp. 485–492.

Kratz, K.-L., 1984, "β-strength function phenomena of exotic nuclei: A critical examination of the significance of nuclear model predictions," Nucl. Phys. **A417**, 447–476.

Kratz, K.-L., 2001, "Measurements of *r*-process nuclei," Nucl. Phys. **A688**, 308–317.

Kratz, K.-L., J. Bitouzet, F. Thielemann, P. Moeller, and B. Pfeiffer, 1993, "Isotopic *r*-process abundances and nuclear structure far from stability—Implications for the *r*-process mechanism," Astrophys. J. **403**, 216–238.

Kratz, K. L., H. Gabelmann, W. Hillebrandt, B. Pfeiffer, K. Schlösser, and F. K. Thielemann, 1986, "The beta-decay half-life of $^{130}_{48}Cd_{82}$ and its importance for astrophysical *r*-process scenarios," Z. Phys. A **325**, 489–490.

Kratz, K. L., and G. Herrmann, 1973, "Systematics of neutron emission probabilities from delayed neutron precursors," Z. Phys. **263**, 435–442.

Kratz, K.-L., K. Farouqi, and P. Möller, 2014, "A high-entropy-wind *r*-process study based on nuclear-structure quantities from the new finite-range droplet model FRDM(2012)," Astrophys. J. **792**, 6.

Kratz, K.-L., P. Möller, B. Pfeiffer, and W. B. Walters, 2000, "New information on *r*-process nuclei," AIP Conf. Proc. **529**, 295.

Kratz, K.-L., B. Pfeiffer, F.-K. Thielemann, and W. B. Walters, 2000, "Nuclear structure studies at ISOLDE and their impact on the astrophysical *r*-process," Hyperfine Interact. **129**, 185–221.

Kratz, K.-L., B. Pfeiffer, J. J. Cowan, and C. Sneden, 2004, "*r*-process chronometers," New Astron. Rev. **48**, 105–108.

Kratz, K.-L., F.-K. Thielemann, W. Hillebrandt, P. Möller, V. Harms, A. Wohr, and J. W. Truran, 1988, "Constraints on *r*-process conditions from beta-decay properties far off stability and *r*-abundances," J. Phys. G **14**, S331–S342.

Kratz, K.-L., W. Ziegert, W. Hillebrandt, and F.-K. Thielemann, 1983, "Determination of stellar neutron-capture rates for radioactive nuclei with the aid of beta-delayed neutron emission," Astron. Astrophys. **125**, 381–387, https://ui.adsabs.harvard.edu/#abs/1983A&A...125..381K/abstract.

Kratz, K.-L., *et al.*, 1979, "Investigation of beta strength functions by neutron and gamma-ray spectroscopy. I. The decay of ^{87}Br, ^{137}I, ^{85}As and ^{135}Sb," Nucl. Phys. **A317**, 335–362.

Kratz, K.-L., *et al.*, 1982, "Beta-delayed neutron emission from ^{93100}Rb to excited states in the residual Sr isotopes," Z. Phys. A **306**, 239–257.

Kugler, E., D. Fiander, B. Johnson, H. Haas, A. Przewloka, H. L. Ravn, D. J. Simon, K. Zimmer, and Isolde Collaboration, 1992, "The new CERN-ISOLDE on-line mass-separator facility at the PS-booster," Nucl. Instrum. Methods Phys. Res., Sect. B **70**, 41–49.

Kulkarni, S. R., 2005, "Modeling supernova-like explosions associated with gamma-ray bursts with short durations," arXiv:astro-ph/0510256.

Kurcewicz, J., *et al.*, 2012, "Discovery and cross-section measurement of neutron-rich isotopes in the element range from neodymium to platinum with the FRS," Phys. Lett. B **717**, 371–375.

Kuroda, T., K. Kotake, T. Takiwaki, and F.-K. Thielemann, 2018, "A full general relativistic neutrino radiation-hydrodynamics simulation of a collapsing very massive star and the formation of a black hole," Mon. Not. R. Astron. Soc. **477**, L80–L84.

Kyutoku, K., K. Ioka, H. Okawa, M. Shibata, and K. Taniguchi, 2015, "Dynamical mass ejection from black hole-neutron star binaries," Phys. Rev. D **92**, 044028.

Kyutoku, K., K. Ioka, and M. Shibata, 2013, "Anisotropic mass ejection from black hole-neutron star binaries: Diversity of electromagnetic counterparts," Phys. Rev. D **88**, 041503.

Kyutoku, K., K. Kiuchi, Y. Sekiguchi, M. Shibata, and K. Taniguchi, 2018, "Neutrino transport in black hole-neutron star binaries: Neutrino emission and dynamical mass ejection," Phys. Rev. D **97**, 023009.

Kyutoku, Koutarou, Sho Fujibayashi, Kota Hayashi, Kyohei Kawaguchi, Kenta Kiuchi, Masaru Shibata, and Masaomi Tanaka, 2020, "On the possibility of GW190425 being a black hole-neutron star binary merger," Astrophys. J. Lett., **890**, L4.

Landau, L. D., 1932, "On the theory of star," Phys. Z. Sowjetunion **1**, 285–288, https://ui.adsabs.harvard.edu/#abs/1932PhyZS...1..285L/abstract.

Langanke, K., 1998, "Shell model Monte Carlo level densities for nuclei with A~50," Phys. Lett. B **438**, 235–241.

Langanke, K., 2006, "Shell model Monte Carlo studies of pairing correlations and level densities in medium-mass nuclei," Nucl. Phys. **A778**, 233–246.

Langanke, K., and E. Kolbe, 2001, "Neutrino-induced charged-current reaction rates for *r*-process nuclei," At. Data Nucl. Data Tables **79**, 293–315.

Langanke, K., and E. Kolbe, 2002, "Neutrino-induced neutral-current reaction rates for *r*-process nuclei," At. Data Nucl. Data Tables **82**, 191–209.

Langanke, K., and G. Martínez-Pinedo, 2000, "Shell-model calculations of stellar weak interaction rates: II. Weak rates for nuclei in the mass range $A = 45$–65 in supernovae environment," Nucl. Phys. **A673**, 481–508.

Langanke, K., and G. Martínez-Pinedo, 2001, "Rate tables for the weak processes of pf-shell nuclei in stellar environments," At. Data Nucl. Data Tables **79**, 1–46.

Langanke, K., and G. Martínez-Pinedo, 2003, "Nuclear weak-interaction processes in stars," Rev. Mod. Phys. **75**, 819–862.

Larsen, A. C., and S. Goriely, 2010, "Impact of a low-energy enhancement in the γ-ray strength function on the neutron-capture cross section," Phys. Rev. C **82**, 014318.

Larsen, A. C., A. Spyrou, S. N. Liddick, and M. Guttormsen, 2019, "Novel techniques for constraining neutron-capture rates relevant for *r*-process heavy-element nucleosynthesis," Prog. Part. Nucl. Phys. **107**, 69–108.

Larsen, A. C., *et al.*, 2006, "Microcanonical entropies and radiative strength functions of ^{50,51}V," Phys. Rev. C **73**, 064301.

Larsen, A. C., *et al.*, 2007, "Nuclear level densities and γ-ray strength functions in ^{44,45}Sc," Phys. Rev. C **76**, 044303.

Larsen, A. C., *et al.*, 2015, "Upbend and M1 scissors mode in neutron-rich nuclei—Consequences for *r*-process (n,γ) reaction rates," Acta Phys. Pol. B **46**, 509.

Larson, N., *et al.*, 2013, "High efficiency beta-decay spectroscopy using a planar germanium double-sided strip detector," Nucl. Instrum. Methods Phys. Res., Sect. A **727**, 59–64.

Lattimer, J. M., 2012, "The nuclear equation of state and neutron star masses," Annu. Rev. Nucl. Part. Sci. **62**, 485–515.

Lattimer, J. M., and D. N. Schramm, 1974, "Black-hole-neutron-star collisions," Astrophys. J. **192**, L145–L147.

Lattimer, J. M., and D. N. Schramm, 1976, "The tidal disruption of neutron stars by black holes in close binaries," Astrophys. J. **210**, 549–567.

Lattimer, James M., 2019, "The properties of a black hole-neutron star merger candidate," arXiv:1908.03622.

Lawler, J. E., E. A. Den Hartog, C. Sneden, and J. J. Cowan, 2006, "Improved laboratory transition probabilities for Sm II and application to the samarium abundances of the Sun and three *r*-process-rich, metal-poor stars," Astrophys. J. Suppl. Ser., **162**, 227–260.

Lawler, J. E., E. A. Hartog, C. Sneden, and J. J. Cowan, 2008, "Comparison of Sm II transition probabilities," Can. J. Phys. **86**, 1033–1038.

Lawler, J. E., C. Sneden, J. J. Cowan, I. I. Ivans, and E. A. Den Hartog, 2009, "Improved laboratory transition probabilities for Ce II, application to the cerium abundances of the Sun and five *r*-process-rich, metal-poor stars, and rare earth lab data summary," Astrophys. J. Suppl. Ser., **182**, 51–79.

Lee, William H., and Enrico Ramirez-Ruiz, 2007, "The progenitors of short gamma-ray bursts," New J. Phys. **9**, 17–17.

Lehner, L., S. L. Liebling, C. Palenzuela, O. L. Caballero, E. O'Connor, M. Anderson, and D. Neilsen, 2016, "Unequal mass binary neutron star mergers and multimessenger signals," Classical Quantum Gravity **33**, 184002.

Leist, B., W. Ziegert, M. Wiescher, K.-L. Kratz, and F.-K. Thielemann, 1985, "Neutron capture cross sections for neutron-rich isotopes," Z. Phys. A **322**, 531–532.

Lhersonneau, G., H. Gabelmann, B. Pfeiffer, and K.-L. Kratz, 1995, "Structure of the highly deformed nucleus $^{101}Sr_{63}$ and evidence for identical $K = 3/2$ bands," Z. Phys. A **352**, 293–301.

Lhersonneau, G., B. Pfeiffer, M. Huhta, A. Wöhr, I. Klöckl, K. L. Kratz, and J. Äystö, 1995, "First evidence for the 2^+ level in the very neutron-rich nucleus ^{102}Sr," Z. Phys. A **351**, 357–358.

Li, Hai-Ning, Wako Aoki, Satoshi Honda, Gang Zhao, Norbert Christlieb, and Takuma Suda, 2015, "Discovery of a strongly *r*-process enhanced extremely metal-poor star LAMOST J110901.22+075441.8," Res. Astron. Astrophys. **15**, 1264.

Li, L.-X., and B. Paczyński, 1998, "Transient events from neutron star mergers," Astrophys. J. **507**, L59–L62.

Li, Li-Xin, 2019, "Line expansion opacity in relativistically expanding media," Astrophys. J. **887**, 60.

Liddick, S. N., *et al.*, 2016, "Experimental Neutron Capture Rate Constraint Far from Stability," Phys. Rev. Lett. **116**, 242502.

Liebendörfer, M., M. Rampp, H.-T. Janka, and A. Mezzacappa, 2005, "Supernova simulations with Boltzmann neutrino transport: A comparison of methods," Astrophys. J. **620**, 840–860.

Liebendörfer, M., S. C. Whitehouse, and T. Fischer, 2009, "The isotropic diffusion source approximation for supernova neutrino transport," Astrophys. J. **698**, 1174–1190.

Limongi, M., and A. Chieffi, 2018, "Presupernova evolution and explosive nucleosynthesis of rotating massive stars in the metallicity range $-3 \leq [\mathrm{Fe/H}] \leq 0$," Astrophys. J. Suppl. Ser., **237**, 13.

Lippuner, J., R. Fernández, L. F. Roberts, F. Foucart, D. Kasen, B. D. Metzger, and C. D. Ott, 2017, "Signatures of hypermassive neutron star lifetimes on *r*-process nucleosynthesis in the disc ejecta from neutron star mergers," Mon. Not. R. Astron. Soc. **472**, 904–918.

Lippuner, J., and L. F. Roberts, 2017, "SkyNet: A modular nuclear reaction network library," Astrophys. J. Suppl. Ser., **233**, 18.

Lippuner, Jonas, and Luke F. Roberts, 2015, "*r*-process lanthanide production and heating rates in kilonovae," Astrophys. J. **815**, 82.

Litvinov, Y. A., *et al.*, 2004, "Precision experiments with time-resolved Schottky mass spectrometry," Nucl. Phys. **A734**, 473–476.

Litvinova, E., and N. Belov, 2013, "Low-energy limit of the radiative dipole strength in nuclei," Phys. Rev. C **88**, 031302.

Litvinova, E., H. P. Loens, K. Langanke, G. Martínez-Pinedo, T. Rauscher, P. Ring, F.-K. Thielemann, and V. Tselyaev, 2009, "Low-lying dipole response in the relativistic quasiparticle time blocking approximation and its influence on neutron capture cross sections," Nucl. Phys. **A823**, 26–37.

Liu, Min, Ning Wang, Yangge Deng, and Xizhen Wu, 2011, "Further improvements on a global nuclear mass model," Phys. Rev. C **84**, 014333.

Liu, Yuk Tung, Stuart L. Shapiro, Zachariah B. Etienne, and Keisuke Taniguchi, 2008, "General relativistic simulations of magnetized binary neutron star mergers," Phys. Rev. D **78**, 024012.

Livio, M., and P. Mazzali, 2018, "On the progenitors of type Ia supernovae," Phys. Rep. **736**, 1–23.

Lodders, K., H. Palme, and H.-P. Gail, 2009, "Abundances of the elements in the Solar System," in *Astronomy, Astrophysics, and Cosmology*, edited by J. E. Trümper, Landolt-Börnstein, New Series Vol. 4B, Pt. 712 (Springer-Verlag, Berlin), https://doi.org/10.1007/978-3-540-88055-4_34.

Loens, H. P., K. Langanke, G. Martínez-Pinedo, T. Rauscher, and F.-K. Thielemann, 2008, "Complete inclusion of parity-dependent level densities in the statistical description of astrophysical reaction rates," Phys. Lett. B **666**, 395–399.

Loens, H. P., K. Langanke, G. Martínez-Pinedo, and K. Sieja, 2012, "M1 strength functions from large-scale shell-model calculations and their effect on astrophysical neutron capture cross-sections," Eur. Phys. J. A **48**, 34.

Lorusso, G., *et al.*, 2015, "β-Decay Half-Lives of 110 Neutron-Rich Nuclei across the $N = 82$ Shell Gap: Implications for the Mechanism and Universality of the Astrophysical *r* Process," Phys. Rev. Lett. **114**, 192501.

Ludwig, H. G., E. Caffau, M. Steffen, P. Bonifacio, and L. Sbordone, 2010, "Accuracy of spectroscopy-based radioactive dating of stars," Astron. Astrophys. **509**, A84.

Ludwig, P., *et al.*, 2016, "Time-resolved 2-million-year-old supernova activity discovered in Earth's microfossil record," Proc. Natl. Acad. Sci. U.S.A. **113**, 9232–9237.

Lugaro, M., U. Ott, and Á. Kereszturi, 2018, "Radioactive nuclei from cosmochronology to habitability," Prog. Part. Nucl. Phys. **102**, 1–47.

MacFadyen, A. I., and S. E. Woosley, 1999, "Collapsars: Gamma-ray bursts and explosions in 'failed supernovae,' " Astrophys. J. **524**, 262–289.

MacFadyen, A. I., S. E. Woosley, and A. Heger, 2001, "Supernovae, jets, and collapsars," Astrophys. J. **550**, 410–425.

Macias, Phillip, and Enrico Ramirez-Ruiz, 2019, "Constraining collapsar *r*-process models through stellar abundances," Astrophys. J. Lett., **877**, L24.

Malkus, A., J. P. Kneller, G. C. McLaughlin, and R. Surman, 2012, "Neutrino oscillations above black hole accretion disks: Disks with electron-flavor emission," Phys. Rev. D **86**, 085015.

Malkus, A., G. C. McLaughlin, and R. Surman, 2016, "Symmetric and standard matter neutrino resonances above merging compact objects," Phys. Rev. D **93**, 045021.

Mamdouh, A., J. M. Pearson, M. Rayet, and F. Tondeur, 2001, "Fission barriers of neutron-rich and superheavy nuclei calculated with the ETFSI method," Nucl. Phys. **A679**, 337–358.

Manning, B., *et al.*, 2019, "Informing direct neutron capture on tin isotopes near the $N = 82$ shell closure," Phys. Rev. C **99**, 041302.

Maoz, D., F. Mannucci, and G. Nelemans, 2014, "Observational clues to the progenitors of type Ia supernovae," Annu. Rev. Astron. Astrophys. **52**, 107–170.

Marek, A., H. Dimmelmeier, H. Th. Janka, E. Müller, and R. Buras, 2006, "Exploring the relativistic regime with Newtonian hydrodynamics: An improved effective gravitational potential for supernova simulations," Astron. Astrophys. **445**, 273–289.

Margalit, Ben, and Brian Metzger, 2017, "Constraining the maximum mass of neutron stars from multi-messenger observations of GW170817," Astrophys. J. Lett., **850**, L19.

Margalit, Ben, and Brian D. Metzger, 2019, "The multi-messenger matrix: The future of neutron star merger constraints on the nuclear equation of state," Astrophys. J. Lett., **880**, L15.

Marketin, T., L. Huther, and G. Martínez-Pinedo, 2016, "Large-scale evaluation of β -decay rates of *r*-process nuclei with the inclusion of first-forbidden transitions," Phys. Rev. C **93**, 025805.

Marketin, T., L. Huther, J. Petković, N. Paar, and G. Martínez-Pinedo, 2016, "Beta decay rates of neutron-rich nuclei," AIP Conf. Proc. **1743**, 040006.

Marketin, T., D. Vretenar, and P. Ring, 2007, "Calculation of beta-decay rates in a relativistic model with momentum-dependent self-energies," Phys. Rev. C **75**, 024304.

Marshall, J. L., *et al.* (DES Collaboration), 2019, "Chemical abundance analysis of Tucana III, the second *r*-process enhanced ultra-faint dwarf galaxy," Astrophys. J. **882**, 177.

Martin, D., A. Arcones, W. Nazarewicz, and E. Olsen, 2016, "Impact of Nuclear Mass Uncertainties on the *r* Process," Phys. Rev. Lett. **116**, 121101.

Martin, D., A. Perego, A. Arcones, F.-K. Thielemann, O. Korobkin, and S. Rosswog, 2015, "Neutrino-driven winds in the aftermath of a neutron star merger: Nucleosynthesis and electromagnetic transients," Astrophys. J. **813**, 2.

Martin, D., A. Perego, W. Kastaun, and A. Arcones, 2018, "The role of weak interactions in dynamic ejecta from binary neutron star mergers," Classical Quantum Gravity **35**, 034001.

Martin, W. C., R. Zalubas, and L. Hagan, 1978, "Atomic energy levels—The rare-earth elements," NBS, National Standards Reference Data Series—No. **60** (U.S. GPO, Washington, DC).

Martínez-Pinedo, Gabriel, Tobias Fischer, Karlheinz Langanke, Andreas Lohs, Andre Sieverding, and Meng-Ru Wu, 2017, "Neutrinos and their impact on core-collapse supernova nucleosynthesis," in *Handbook of Supernovae*, edited by A. W. Alsabti, and P. Murdin (Springer International Publishing, Cham, Switzerland).

Martínez-Pinedo, G., T. Fischer, and L. Huther, 2014, "Supernova neutrinos and nucleosynthesis," J. Phys. G **41**, 044008.

Martínez-Pinedo, G., T. Fischer, A. Lohs, and L. Huther, 2012, "Charged-Current Weak Interaction Processes in Hot and Dense Matter and Its Impact on the Spectra of Neutrinos Emitted from Protoneutron Star Cooling," Phys. Rev. Lett. **109**, 251104.

Martínez-Pinedo, G., Y. H. Lam, K. Langanke, R. G. T. Zegers, and C. Sullivan, 2014, "Astrophysical weak-interaction rates for selected $A = 20$ and $A = 24$ nuclei," Phys. Rev. C **89**, 045806.

Martínez-Pinedo, G., D. Mocelj, N. T. Zinner, A. Kelić, K. Langankea, I. Panov, B. Pfeiffer, T. Rauscher, K.-H. Schmidt, and F.-K. Thielemann, 2007, "The role of fission in the *r*-process," Prog. Part. Nucl. Phys. **59**, 199–205.

Mashonkina, L., N. Christlieb, and K. Eriksson, 2014, "The Hamburg/ESO *r*-process Enhanced Star survey (HERES). X. HE 2252-4225, one more *r*-process enhanced and actinide-boost halo star," Astron. Astrophys. **569**, A43.

Mathews, G. J., A. Mengoni, F.-K. Thielemann, and W. A. Fowler, 1983, "Neutron capture rates in the *r*-process—The role of direct radiative capture," Astrophys. J. **270**, 740–745.

Matteucci, F., and C. Chiappini, 2001, "The evolution of the oxygen abundance in the Galaxy, New Astron. Rev. **45**, 567–570.

Matteucci, F., and L. Greggio, 1986, "Relative roles of type I and II supernovae in the chemical enrichment of the interstellar gas," Astron. Astrophys. **154**, 279–287, https://ui.adsabs.harvard.edu/#abs/1986A&A...154..279M/abstract.

Matteucci, F., D. Romano, A. Arcones, O. Korobkin, and S. Rosswog, 2014, "Europium production: Neutron star mergers versus core-collapse supernovae," Mon. Not. R. Astron. Soc. **438**, 2177–2185.

Matteucci, Francesca, 2012, *Chemical Evolution of Galaxies*, Astronomy and Astrophysics Library (Springer-Verlag, Berlin).

McConnell, J. R., and W. L. Talbert, 1975, "The Tristan on-line isotope separator facility," Nucl. Instrum. Methods **128**, 227–243.

McFadden, L., and G. R. Satchler, 1966, "Optical-model analysis of the scattering of 24.7 MeV alpha particles," Nucl. Phys. **A84**, 177–200.

McKinney, J. C., A. Tchekhovskoy, and R. D. Blandford, 2013, "Alignment of magnetized accretion disks and relativistic jets with spinning black holes," Science **339**, 49.

McLaughlin, G. C., J. M. Fetter, A. B. Balantekin, and G. M. Fuller, 1999, "Active-sterile neutrino transformation solution for *r*-process nucleosynthesis," Phys. Rev. C **59**, 2873–2887.

McLaughlin, G. C., and R. Surman, 2005, "Prospects for obtaining an *r* process from gamma ray burst disk winds," Nucl. Phys. **A758**, 189–196.

Meisel, Z., and S. George, 2013, "Time-of-flight mass spectrometry of very exotic systems," Int. J. Mass Spectrom. **349–350**, 145–150.

Mendoza-Temis, Joel Jesús, Meng-Ru Wu, Karlheinz Langanke, Gabriel Martínez-Pinedo, Andreas Bauswein, and Hans-Thomas Janka, 2015, "Nuclear robustness of the *r* process in neutron-star mergers," Phys. Rev. C **92**, 055805.

Mendoza-Temis, Joel Jesús, 2014, "Nuclear masses and their impact in *r*-process nucleosynthesis," Ph.D. thesis (Technische Universität Darmstadt).

Mennekens, N., and D. Vanbeveren, 2014, "Massive double compact object mergers: Gravitational wave sources and *r*-process element production sites," Astron. Astrophys. **564**, A134.

Mennekens, N., and D. Vanbeveren, 2016, "The delay time distribution of massive double compact star mergers," Astron. Astrophys. **589**, A64.

Mention, G., M. Fechner, Th. Lasserre, Th. A. Mueller, D. Lhuillier, M. Cribier, and A. Letourneau, 2011, "Reactor antineutrino anomaly," Phys. Rev. D **83**, 073006.

Merrill, P. W., 1952, "Spectroscopic observations of stars of class," Astrophys. J. **116**, 21.

Metzger, B. D., 2017a, "Kilonovae," Living Rev. Relativity **20**, 3.

Metzger, B. D., 2017b, "Welcome to the multi-messenger era! Lessons from a neutron star merger and the landscape ahead," arXiv:1710.05931.

Metzger, B. D., A. Arcones, E. Quataert, and G. Martínez-Pinedo, 2010, "The effects of *r*-process heating on fallback accretion in compact object mergers," Mon. Not. R. Astron. Soc. **402**, 2771–2777.

Metzger, B. D., A. Bauswein, S. Goriely, and D. Kasen, 2015, "Neutron-powered precursors of kilonovae," Mon. Not. R. Astron. Soc. **446**, 1115–1120.

Metzger, B. D., and E. Berger, 2012, "What is the most promising electromagnetic counterpart of a neutron star binary merger?," Astrophys. J. **746**, 48.

Metzger, B. D., and R. Fernández, 2014, "Red or blue? A potential kilonova imprint of the delay until black hole formation following a neutron star merger," Mon. Not. R. Astron. Soc. **441**, 3444–3453.

Metzger, B. D., G. Martínez-Pinedo, S. Darbha, E. Quataert, A. Arcones, D. Kasen, R. Thomas, P. Nugent, I. V. Panov, and N. T. Zinner, 2010, "Electromagnetic counterparts of compact object mergers powered by the radioactive decay of *r*-process nuclei, Mon. Not. R. Astron. Soc. **406**, 2650–2662.

Metzger, B. D., A. L. Piro, and E. Quataert, 2009, "Neutron-rich freeze-out in viscously spreading accretion discs formed from compact object mergers," Mon. Not. R. Astron. Soc. **396**, 304–314.

Metzger, B. D., T. A. Thompson, and E. Quataert, 2008, "On the conditions for neutron-rich gamma-ray burst outflows," Astrophys. J. **676**, 1130–1150.

Metzger, B. D., T. A. Thompson, and E. Quataert, 2018, "A magnetar origin for the kilonova ejecta in GW170817," Astrophys. J. **856**, 101.

Meyer, B. S., 1993, "Entropy and nucleosynthesis," Phys. Rep. **227**, 257–267.

Meyer, B. S., G. J. Mathews, W. M. Howard, S. E. Woosley, and R. D. Hoffman, 1992, "*r*-process nucleosynthesis in the high-entropy supernova bubble," Astrophys. J. **399**, 656–664.

Meyer, B. S., G. C. McLaughlin, and G. M. Fuller, 1998, "Neutrino capture and *r*-process nucleosynthesis," Phys. Rev. C **58**, 3696–3710.

Meyer, B. S., and D. N. Schramm, 1988, "Nucleosynthesis from the decompression of initially cold neutron star matter," in *Origin and Distribution of the Elements*, edited by G. J. Mathews (World Scientific, Singapore), p. 610.

Minchev, I., C. Chiappini, and M. Martig, 2014, "Chemodynamical evolution of the Milky Way disk. II. Variations with galactic radius and height above the disk plane," Astron. Astrophys. **572**, A92.

Mirizzi, A., 2015, "Breaking the symmetries in self-induced flavor conversions of neutrino beams from a ring," Phys. Rev. D **92**, 105020.

Mirizzi, A., G. Mangano, and N. Saviano, 2015, "Self-induced flavor instabilities of a dense neutrino stream in a two-dimensional model," Phys. Rev. D **92**, 021702.

Mirizzi, A., I. Tamborra, H.-T. Janka, N. Saviano, K. Scholberg, R. Bollig, L. Hüdepohl, and S. Chakraborty, 2016, "Supernova neutrinos: Production, oscillations and detection," Riv. Nuovo Cimento Soc. Ital. Fis. **39**, 1–112.

Mishenina, T., M. Pignatari, T. Gorbaneva, S. Bisterzo, C. Travaglio, F. K. Thielemann, and C. Soubiran, 2019, "Enrichment of the galactic disc with neutron capture elements: Sr," Mon. Not. R. Astron. Soc. **484**, 3846–3864.

Mishenina, T., M. Pignatari, T. Gorbaneva, C. Travaglio, B. Côté, F. K. Thielemann, and C. Soubiran, 2019, "Enrichment of the galactic disc with neutron-capture elements: Mo and Ru," Mon. Not. R. Astron. Soc. **489**, 1697–1708.

Mocelj, D., T. Rauscher, G. Martínez-Pinedo, K. Langanke, L. Pacearescu, A. Faessler, F.-K. Thielemann, and Y. Alhassid, 2007, "Large-scale prediction of the parity distribution in the nuclear level density and application to astrophysical reaction rates," Phys. Rev. C **75**, 045805.

Mohr, P., Zs. Fülöp, Gy. Gyürky, G. G. Kiss, and T. Szücs, 2020, "Successful Prediction of Total α-Induced Reaction Cross Sections at Astrophysically Relevant Sub-Coulomb Energies Using a Novel Approach," Phys. Rev. Lett. **124**, 252701.

Mohr, P., G. Gyürky, and Z. Fülöp, 2017, "Statistical model analysis of α -induced reaction cross sections of ^{64}Zn at low energies," Phys. Rev. C **95**, 015807.

Mohr, P., G. G. Kiss, Z. Fülöp, D. Galaviz, G. Gyürky, and E. Somorjai, 2013, "Elastic alpha scattering experiments and the alpha-nucleus optical potential at low energies," At. Data Nucl. Data Tables **99**, 651–679.

Möller, P., W. D. Myers, H. Sagawa, and S. Yoshida, 2012, "New Finite-Range Droplet Mass Model and Equation-of-State Parameters," Phys. Rev. Lett. **108**, 052501.

Möller, P., J. R. Nix, and K.-L. Kratz, 1997, "Nuclear properties for astrophysical and radioactive-ion beam applications," At. Data Nucl. Data Tables **66**, 131–343.

Möller, P., J. R. Nix, W. D. Myers, and W. J. Swiatecki, 1995, "Nuclear ground-state masses and deformations," At. Data Nucl. Data Tables **59**, 185.

Möller, P., B. Pfeiffer, and K.-L. Kratz, 2003, "New calculations of gross beta-decay properties for astrophysical applications: Speeding-up the classical *r* process," Phys. Rev. C **67**, 055802.

Möller, P., A. J. Sierk, R. Bengtsson, H. Sagawa, and T. Ichikawa, 2012, "Nuclear shape isomers," At. Data Nucl. Data Tables **98**, 149–300.

Möller, P., A. J. Sierk, T. Ichikawa, A. Iwamoto, and M. Mumpower, 2015, "Fission barriers at the end of the chart of the nuclides," Phys. Rev. C **91**, 024310.

Möller, P., A. J. Sierk, T. Ichikawa, and H. Sagawa, 2016, "Nuclear ground-state masses and deformations: FRDM(2012)," At. Data Nucl. Data Tables **109-110**, 1–204.

Montes, F., *et al.*, 2006, "β-decay half-lives and β-delayed neutron emission probabilities for neutron rich nuclei close to the $N = 82$ *r*-process path," Phys. Rev. C **73**, 035801.

Montes, G., E. Ramirez-Ruiz, J. Naiman, S. Shen, and W. H. Lee, 2016, "Transport and mixing of *r*-process elements in neutron star binary merger blast waves," Astrophys. J. **830**, 12.

Mooley, K. P., *et al.*, 2018, "A mildly relativistic wide-angle outflow in the neutron-star merger event GW170817," Nature (London) **554**, 207–210.

Moore, C. E., 1971, "Atomic energy levels," NBS, National Standards Reference Data Series—No. 35, Vols. **I–III** (U.S. GPO, Washington, DC), https://nvlpubs.nist.gov/nistpubs/Legacy/NSRDS/nbsnsrds35v1.pdf, https://nvlpubs.nist.gov/nistpubs/Legacy/NSRDS/nbsnsrds35v2.pdf, https://nvlpubs.nist.gov/nistpubs/Legacy/NSRDS/nbsnsrds35v3.pdf.

Moriya, Takashi J., Nozomu Tominaga, Norbert Langer, Ken'ichi Nomoto, Sergei I. Blinnikov, and Elena I. Sorokina, 2014, "Electron-capture supernovae exploding within their progenitor wind," Astron. Astrophys. **569**, A57.

Most, Elias R., Lukas R. Weih, Luciano Rezzolla, and Jürgen Schaffner-Bielich, 2018, "New Constraints on Radii and Tidal Deformabilities of Neutron Stars from GW170817," Phys. Rev. Lett. **120**, 261103.

Mösta, P., C. D. Ott, D. Radice, L. F. Roberts, E. Schnetter, and R. Haas, 2015, "A large-scale dynamo and magnetoturbulence in rapidly rotating core-collapse supernovae," Nature (London) **528**, 376–379.

Mösta, P., S. Richers, C. D. Ott, R. Haas, A. L. Piro, K. Boydstun, E. Abdikamalov, C. Reisswig, and E. Schnetter, 2014, "Magnetorotational core-collapse supernovae in three dimensions," Astrophys. J. **785**, L29.

Mösta, P., L. F. Roberts, G. Halevi, C. D. Ott, J. Lippuner, R. Haas, and E. Schnetter, 2018, "*r*-process nucleosynthesis from three-dimensional magnetorotational core-collapse supernovae," Astrophys. J. **864**, 171.

Mueller, E., 1986, "Nuclear-reaction networks and stellar evolution codes—The coupling of composition changes and energy release in explosive nuclear burning," Astron. Astrophys. **162**, 103–108, https://ui.adsabs.harvard.edu/abs/1986A%26A...162..103M/abstract.

Müller, B., 2016, "The status of multi-dimensional core-collapse supernova models," Publ. Astron. Soc. Aust. **33**, e048.

Müller, B., D. W. Gay, A. Heger, T. M. Tauris, and S. A. Sim, 2018, "Multidimensional simulations of ultrastripped supernovae to shock breakout," Mon. Not. R. Astron. Soc. **479**, 3675–3689.

Müller, Bernhard, Thomas M. Tauris, Alexander Heger, Projjwal Banerjee, Yong-Zhong Qian, Jade Powell, Conrad Chan, Daniel W. Gay, and Norbert Langer, 2019, "Three-dimensional simulations of neutrino-driven core-collapse supernovae from low-mass single and binary star progenitors," Mon. Not. R. Astron. Soc. **484**, 3307–3324.

Mumpower, M. R., P. Jaffke, M. Verriere, and J. Randrup, 2020, "Primary fission fragment mass yields across the chart of nuclides," Phys. Rev. C **101**, 054607.

Mumpower, M. R., T. Kawano, T. M. Sprouse, N. Vassh, E. M. Holmbeck, R. Surman, and P. Möller, 2018, "β-delayed fission in *r*-process nucleosynthesis," Astrophys. J. **869**, 14.

Mumpower, M. R., T. Kawano, J. L. Ullmann, M. Krtička, and T. M. Sprouse, 2017, "Estimation of M1 scissors mode strength for deformed nuclei in the medium- to heavy-mass region by statistical Hauser-Feshbach model calculations," Phys. Rev. C **96**, 024612.

Mumpower, M. R., G. C. McLaughlin, R. Surman, and A. W. Steiner, 2017, "Reverse engineering nuclear properties from rare earth abundances in the *r* process," J. Phys. G **44**, 034003.

Mumpower, M. R., R. Surman, D.-L. Fang, M. Beard, P. Möller, T. Kawano, and A. Aprahamian, 2015, "Impact of individual nuclear masses on *r*-process abundances," Phys. Rev. C **92**, 035807.

Mumpower, M. R., R. Surman, G. C. McLaughlin, and A. Aprahamian, 2016, "The impact of individual nuclear properties on *r*-process nucleosynthesis," Prog. Part. Nucl. Phys. **86**, 86–126.

Munson, J. M., *et al.*, 2018, "Recoil-ion detection efficiency for complex β decays studied using the beta-decay Paul trap," Nucl. Instrum. Methods Phys. Res., Sect. A **898**, 60–66.

Münzel, J., H. Wollnik, B. Pfeiffer, and G. Jung, 1981, "A high-temperature ion source for the on-line separator OSTIS," Nucl. Instrum. Methods Phys. Res. **186**, 343–347.

Mustafa, M. G., M. Blann, A. V. Ignatyuk, and S. M. Grimes, 1992, "Nuclear level densities at high excitations," Phys. Rev. C **45**, 1078–1083.

Mustonen, M. T., and J. Engel, 2016, "Global description of β^- decay in even-even nuclei with the axially-deformed Skyrme finite-amplitude method," Phys. Rev. C **93**, 014304.

Myers, W. D., and W. J. Świątecki, 1999, "Thomas-Fermi fission barriers," Phys. Rev. C **60**, 014606.

Nadyozhin, D. K., and I. V. Panov, 2007, "Weak *r*-process component as a result of the neutrino interaction with the helium shell of a supernova," Astron. Lett. **33**, 385–389.

Nagataki, S., 2011, "GRB-SN connection: Central engine of long GRBs and explosive nucleosynthesis," Int. J. Mod. Phys. D **20**, 1975–1978.

Nagataki, S., R. Takahashi, A. Mizuta, and T. Takiwaki, 2007, "Numerical study of gamma-ray burst jet formation in collapsars," Astrophys. J. **659**, 512–529.

Nakada, H., and Y. Alhassid, 1997, "Total and Parity-Projected Level Densities of Iron-Region Nuclei in the Auxiliary Fields Monte Carlo Shell Model," Phys. Rev. Lett. **79**, 2939–2942.

Nakamura, K., T. Kajino, G. J. Mathews, S. Sato, and S. Harikae, 2015, "*r*-process nucleosynthesis in the MHD+neutrino-heated collapsar jet," Astron. Astrophys. **582**, A34.

Nakamura, T., H. Umeda, K. Iwamoto, K. Nomoto, M.-a. Hashimoto, W. R. Hix, and F.-K. Thielemann, 2001, "Explosive nucleosynthesis in hypernovae," Astrophys. J. **555**, 880–899.

Nakar, Ehud, 2007, "Short-hard gamma-ray bursts," Phys. Rep. **442**, 166–236.

National Research Council, 2003, *Connecting Quarks with the Cosmos: Eleven Science Questions for the New Century* (National Academies Press, Washington, DC).

Neufcourt, Léo, Yuchen Cao, Witold Nazarewicz, and Frederi Viens, 2018, "Bayesian approach to model-based extrapolation of nuclear observables," Phys. Rev. C **98**, 034318.

Ney, E. M., J. Engel, and N. Schunck, 2020, "Global description of beta decay with the axially-deformed skyrme finite amplitude method: Extension to odd-mass and odd-odd nuclei," arXiv:2005.12883.

Nicholl, M., J. Guillochon, and E. Berger, 2017, "The magnetar model for type I superluminous supernovae. I. Bayesian analysis of the full multicolor light-curve sample with MOSFiT," Astrophys. J. **850**, 55.

Nicholl, M., *et al.*, 2017, "The electromagnetic counterpart of the binary neutron star merger LIGO/Virgo GW170817. III. Optical and UV spectra of a blue kilonova from fast polar ejecta," Astrophys. J. Lett., **848**, L18.

Nishimura, N., T. Rauscher, R. Hirschi, A. S. J. Murphy, G. Cescutti, and C. Travaglio, 2018, "Uncertainties in the production of *p* nuclides in thermonuclear supernovae determined by Monte Carlo variations," Mon. Not. R. Astron. Soc. **474**, 3133–3139.

Nishimura, N., H. Sawai, T. Takiwaki, S. Yamada, and F.-K. Thielemann, 2017, "The intermediate *r*-process in core-collapse supernovae driven by the magneto-rotational instability," Astrophys. J. **836**, L21.

Nishimura, N., T. Takiwaki, and F.-K. Thielemann, 2015, "The *r*-process nucleosynthesis in the various jet-like explosions of magnetorotational core-collapse supernovae," Astrophys. J. **810**, 109.

Nishimura, S., K. Kotake, M.-a. Hashimoto, S. Yamada, N. Nishimura, S. Fujimoto, and K. Sato, 2006, "*r*-process nucleosynthesis in magnetohydrodynamic jet explosions of core-collapse supernovae," Astrophys. J. **642**, 410–419.

Nolden, F., *et al.*, 2011, "A fast and sensitive resonant Schottky pick-up for heavy ion storage rings," Nucl. Instrum. Methods Phys. Res., Sect. A **659**, 69–77.

Nomoto, K., 2017, "Nucleosynthesis in hypernovae associated with gamma-ray bursts," in *Handbook of Supernovae*, edited by A. W. Alsabti, and P. Murdin (Springer International Publishing, Cham, Switzerland), p. 1931.

Nomoto, K., C. Kobayashi, and N. Tominaga, 2013, "Nucleosynthesis in stars and the chemical enrichment of galaxies," Annu. Rev. Astron. Astrophys. **51**, 457–509.

Nomoto, K., F.-K. Thielemann, and S. Miyaji, 1985, "The triple alpha reaction at low temperatures in accreting white dwarfs and neutron stars," Astron. Astrophys. **149**, 239–245, https://ui.adsabs.harvard.edu/abs/1985A%26A...149..239N/abstract.

Nomoto, K., N. Tominaga, H. Umeda, C. Kobayashi, and K. Maeda, 2006, "Nucleosynthesis yields of core-collapse supernovae and hypernovae, and galactic chemical evolution," Nucl. Phys. **A777**, 424–458.

Nomoto, Ken'ichi, and Shing-Chi Leung, 2017a, "Electron capture supernovae from super asymptotic giant branch stars," in *Handbook of Supernovae*, edited by A. W. Alsabti, and P. Murdin (Springer International Publishing, Cham, Switzerland), https://doi.org/10.1007/978-3-319-21846-5_118.

Nomoto, Ken'ichi, and Shing-Chi Leung, 2017b, "Thermonuclear explosions of Chandrasekhar mass white dwarfs," in *Handbook of Supernovae*, edited by Athem W. Alsabti and Paul Murdin (Springer International Publishing, Cham, Switzerland), https://doi.org/10.1007/978-3-319-21846-5_62.

Nomoto, Ken'ichi, Masaomi Tanaka, Nozomu Tominaga, and Keiichi Maeda, 2010, "Hypernovae, gamma-ray bursts, and first stars," New Astron. Rev. **54**, 191–200.

Nunokawa, H., J. T. Peltoniemi, A. Rossi, and J. W. F. Valle, 1997, "Supernova bounds on resonant active-sterile neutrino conversions," Phys. Rev. D **56**, 1704–1713.

Obergaulinger, M., M. A. Aloy, and E. Müller, 2010, "Local simulations of the magnetized Kelvin-Helmholtz instability in neutron-star mergers," Astron. Astrophys. **515**, A30.

Obergaulinger, M., and M. Á. Aloy, 2020, "Magnetorotational core collapse of possible GRB progenitors—I. Explosion mechanisms," Mon. Not. R. Astron. Soc. **492**, 4613–4634.

Obergaulinger, M., O. Just, and M. A. Aloy, 2018, "Core collapse with magnetic fields and rotation," J. Phys. G **45**, 084001.

Oechslin, R., H.-T. Janka, and A. Marek, 2007, "Relativistic neutron star merger simulations with non-zero temperature equations of state. I. Variation of binary parameters and equation of state," Astron. Astrophys. **467**, 395–409.

Oechslin, R., S. Rosswog, and F.-K. Thielemann, 2002, "Conformally flat smoothed particle hydrodynamics application to neutron star mergers," Phys. Rev. D **65**, 103005.

Oechslin, R., K. Uryū, G. Poghosyan, and F. K. Thielemann, 2004, "The influence of quark matter at high densities on binary neutron star mergers," Mon. Not. R. Astron. Soc. **349**, 1469–1480.

Oertel, M., M. Hempel, T. Klähn, and S. Typel, 2017, "Equations of state for supernovae and compact stars," Rev. Mod. Phys. **89**, 015007.

Ojima, T., Y. Ishimaru, S. Wanajo, N. Prantzos, and P. François, 2018, "Stochastic chemical evolution of galactic subhalos and the origin of *r*-process elements," Astrophys. J. **865**, 87.

Ono, M., M. Hashimoto, S. Fujimoto, K. Kotake, and S. Yamada, 2012, "Explosive nucleosynthesis in magnetohydrodynamical jets from collapsars. II—Heavy-element nucleosynthesis of *s*, *p*, *r*-processes," Prog. Theor. Phys. **128**, 741–765.

Orford, R., *et al.*, 2018, "Precision Mass Measurements of Neutron-Rich Neodymium and Samarium Isotopes and Their Role in Understanding Rare-Earth Peak Formation," Phys. Rev. Lett. **120**, 262702.

Ormand, W. E., 1997, "Estimating the nuclear level density with the Monte Carlo shell model," Phys. Rev. C **56**, R1678–R1682.

Otsuki, K., A. Burrows, G. Martinez-Pinedo, S. Typel, K. Langanke, and M. Matos, 2010, "*r*-process in type II supernovae and the role of direct capture," AIP Conf. Proc. **1238**, 240–242.

Otsuki, K., H. Tagoshi, T. Kajino, and S. Wanajo, 2000, "General relativistic effects on neutrino-driven winds from young, hot neutron stars and *r*-process nucleosynthesis," Astrophys. J. **533**, 424–439.

Özel, Feryal, and Paulo Freire, 2016, "Masses, radii, and the equation of state of neutron stars," Annu. Rev. Astron. Astrophys. **54**, 401–440.

Özen, C., Y. Alhassid, and H. Nakada, 2015, "Nuclear state densities of odd-mass heavy nuclei in the shell model Monte Carlo approach," Phys. Rev. C **91**, 034329.

Pagel, B. E. J., 2009, *Nucleosynthesis and Chemical Evolution of Galaxies* (Cambridge University Press, Cambridge, England).

Pain, S. D., *et al.*, 2007, "Development of a high solid-angle silicon detector array for measurement of transfer reactions in inverse kinematics," Nucl. Instrum. Methods Phys. Res., Sect. B **261**, 1122–1125.

Pakhomov, Yu. V., L. I. Mashonkina, T. M. Sitnova, and P. Jablonka, 2019, "Contribution of type Ia supernovae to the chemical enrichment of the ultra-faint dwarf galaxy Boötes I," Astron. Lett. **45**, 259–275.

Palenzuela, Carlos, Steven L. Liebling, David Neilsen, Luis Lehner, O. L. Caballero, Evan O'Connor, and Matthew Anderson, 2015, "Effects of the microphysical equation of state in the mergers of magnetized neutron stars with neutrino cooling," Phys. Rev. D **92**, 044045.

Pan, K.-C., M. Liebendörfer, S. M. Couch, and F.-K. Thielemann, 2018, "Equation of state dependent dynamics and multi-messenger signals from stellar-mass black hole formation," Astrophys. J. **857**, 13.

Pan, Kuo-Chuan, Carlos Mattes, Evan P. O'Connor, Sean M. Couch, Albino Perego, and Almudena Arcones, 2019, "The impact of different neutrino transport methods on multidimensional core-collapse supernova simulations," J. Phys. G **46**, 014001.

Panov, I. V., E. Kolbe, B. Pfeiffer, T. Rauscher, K.-L. Kratz, and F.-K. Thielemann, 2005, "Calculations of fission rates for *r*-process nucleosynthesis," Nucl. Phys. **A747**, 633–654.

Panov, I. V., I. Y. Korneev, Y. S. Lutostansky, and F.-K. Thielemann, 2013, "Probabilities of delayed processes for nuclei involved in the *r*-process," Phys. At. Nucl. **76**, 88–101.

Panov, I. V., I. Y. Korneev, T. Rauscher, G. Martínez-Pinedo, A. Kelić-Heil, N. T. Zinner, and F.-K. Thielemann, 2010, "Neutron-induced astrophysical reaction rates for translead nuclei," Astron. Astrophys. **513**, A61.

Panov, I. V., I. Y. Korneev, and F.-K. Thielemann, 2008, "The *r*-process in the region of transuranium elements and the contribution of fission products to the nucleosynthesis of nuclei with $A \leq 130$," Astron. Lett. **34**, 189–197.

Panov, I. V., Y. S. Lutostansky, M. Eichler, and F.-K. Thielemann, 2017, "Determination of the Galaxy age by the method of uranium-thorium-plutonium isotopic ratios," Phys. At. Nucl. **80**, 657–665.

Panov, I. V., Y. S. Lutostansky, and F.-K. Thielemann, 2016, "Beta-decay half-lives for the *r*-process nuclei," Nucl. Phys. **A947**, 1–11.

Panov, I. V., and F.-K. Thielemann, 2004, "Fission and the *r*-process: Competition between neutron-induced and beta-delayed fission," Astron. Lett. **30**, 647–655.

Papenfort, L. Jens, Roman Gold, and Luciano Rezzolla, 2018, "Dynamical ejecta and nucleosynthetic yields from eccentric binary neutron-star mergers," Phys. Rev. D **98**, 104028.

Pardo, Richard C., Guy Savard, and Robert V. F. Janssens, 2016, "ATLAS with CARIBU: A laboratory portrait," Nucl. Phys. News **26**, 5–11.

Patat, F., A. Piemonte, C. Lidman, T. Augusteijn, O. R. Hainaut, H. Boehnhardt, B. Leibundgut, and J. Brewer, 1998, "Supernova 1998bw in ESO 184-G82," IAU Symp. **7017**, 2, https://ui.adsabs.harvard.edu/#abs/1998IAUC.7017....2P/abstract.

Perego, A., D. Radice, and S. Bernuzzi, 2017, "AT 2017gfo: An anisotropic and three-component kilonova counterpart of GW170817," Astrophys. J. **850**, L37.

Perego, A., S. Rosswog, R. M. Cabezón, O. Korobkin, R. Käppeli, A. Arcones, and M. Liebendörfer, 2014, "Neutrino-driven winds from neutron star merger remnants," Mon. Not. R. Astron. Soc. **443**, 3134–3156.

Perego, A., H. Yasin, and A. Arcones, 2017, "Neutrino pair annihilation above merger remnants: Implications of a long-lived massive neutron star," J. Phys. G **44**, 084007.

Perego, Albino, Sebastiano Bernuzzi, and David Radice, 2019, "Thermodynamics conditions of matter in neutron star mergers," Eur. Phys. J. A **55**, 124.

Pereira, J., *et al.*, 2009, "β-decay half-lives and β-delayed neutron emission probabilities of nuclei in the region $A \lesssim 110$, relevant for the *r* process," Phys. Rev. C **79**, 035806.

Pereira, J., *et al.*, 2010, "The neutron long counter NERO for studies of β-delayed neutron emission in the *r*-process," Nucl. Instrum. Methods Phys. Res., Sect. A **618**, 275–283.

Petermann, I., K. Langanke, G. Martínez-Pinedo, I. V. Panov, P.-G. Reinhard, and F.-K. Thielemann, 2012, "Have superheavy elements been produced in nature?," Eur. Phys. J. A **48**, 122.

Pfeiffer, B., K. L. Kratz, and F. K. Thielemann, 1997, "Analysis of the Solar System *r*-process abundance pattern with the new ETFSI-Q mass formula," Z. Phys. A **357**, 235–238.

Pfeiffer, B., K.-L. Kratz, F.-K. Thielemann, and W. B. Walters, 2001, "Nuclear structure studies for the astrophysical *r*-process," Nucl. Phys. **A693**, 282–324.

Pian, E., *et al.*, 2017, "Spectroscopic identification of *r*-process nucleosynthesis in a double neutron-star merger," Nature (London) **551**, 67–70.

Pinto, P. A., and R. G. Eastman, 2000a, "The physics of type IA supernova light curves. I. Analytic results and time dependence," Astrophys. J. **530**, 744–756.

Pinto, P. A., and R. G. Eastman, 2000b, "The physics of type IA supernova light curves. II. Opacity and diffusion," Astrophys. J. **530**, 757–776.

Piran, T., 2005, "The physics of gamma-ray bursts," Rev. Mod. Phys. **76**, 1143–1210.

Piran, T., E. Nakar, and S. Rosswog, 2013, "The electromagnetic signals of compact binary mergers," Mon. Not. R. Astron. Soc. **430**, 2121–2136.

Pitrou, C., A. Coc, J.-P. Uzan, and E. Vangioni, 2018, "Precision big bang nucleosynthesis with improved helium-4 predictions, Phys. Rep. **754**, 1–66.

Placco, V. M., *et al.*, 2017, "RAVE J203843.2-002333: The first highly *r*-process-enhanced star identified in the RAVE survey," Astrophys. J. **844**, 18.

Pllumbi, Else, Irene Tamborra, Shinya Wanajo, Hans-Thomas Janka, and Lorenz Hüdepohl, 2015, "Impact of neutrino flavor oscillations on the neutrino-driven wind nucleosynthesis of an electron-capture supernova," Astrophys. J. **808**, 188.

Potel, G., F. M. Nunes, and I. J. Thompson, 2015, "Establishing a theory for deuteron-induced surrogate reactions," Phys. Rev. C **92**, 034611.

Prantzos, N., 2012, "Production and evolution of Li, Be, and B isotopes in the Galaxy," Astron. Astrophys. **542**, A67.

Price, D. J., and S. Rosswog, 2006, "Producing ultrastrong magnetic fields in neutron star mergers," Science **312**, 719–722.

Pruet, J., R. D. Hoffman, S. E. Woosley, H.-T. Janka, and R. Buras, 2006, "Nucleosynthesis in early supernova winds. II. The role of neutrinos," Astrophys. J. **644**, 1028–1039.

Pruet, J., T. A. Thompson, and R. D. Hoffman, 2004, "Nucleosynthesis in outflows from the inner regions of collapsars," Astrophys. J. **606**, 1006–1018.

Pruet, J., S. E. Woosley, and R. D. Hoffman, 2003, "Nucleosynthesis in gamma-ray burst accretion disks," Astrophys. J. **586**, 1254–1261.

Qian, Y.-Z., W. C. Haxton, K. Langanke, and P. Vogel, 1997, "Neutrino-induced neutron spallation and supernova *r*-process nucleosynthesis," Phys. Rev. C **55**, 1532–1544.

Qian, Y.-Z., P. Vogel, and G. J. Wasserburg, 1998, "Supernovae as the site of the *r*-process: Implications for gamma-ray astronomy," Astrophys. J. **506**, 868–873.

Qian, Y.-Z., P. Vogel, and G. J. Wasserburg, 1999, "Probing *r*-process production of nuclei beyond ^{209}Bi with gamma rays," Astrophys. J. **524**, 213–219.

Qian, Y.-Z., and G. J. Wasserburg, 2007, "Where, oh where has the *r*-process gone?," Phys. Rep. **442**, 237–268.

Qian, Y.-Z., and S. E. Woosley, 1996, "Nucleosynthesis in neutrino-driven winds. I. The physical conditions," Astrophys. J. **471**, 331–351.

Qian, Yong-Zhong, 2014, "Diverse, massive-star-associated sources for elements heavier than Fe and the roles of neutrinos," J. Phys. G **41**, 044002.

Quinn, M., *et al.*, 2012, "β decay of nuclei around ^{90}Se: Search for signatures of a $N = 56$ subshell closure relevant to the *r* process," Phys. Rev. C **85**, 035807.

Radice, D., F. Galeazzi, J. Lippuner, L. F. Roberts, C. D. Ott, and L. Rezzolla, 2016, "Dynamical mass ejection from binary neutron star mergers," Mon. Not. R. Astron. Soc. **460**, 3255–3271.

Radice, D., A. Perego, K. Hotokezaka, S. Bernuzzi, S. A. Fromm, and L. F. Roberts, 2018, "Viscous-dynamical ejecta from binary neutron star mergers," Astrophys. J. Lett., **869**, L35.

Radice, D., A. Perego, K. Hotokezaka, S. A. Fromm, S. Bernuzzi, and L. F. Roberts, 2018, "Binary neutron star mergers: Mass ejection, electromagnetic counterparts, and nucleosynthesis," Astrophys. J. **869**, 130.

Radice, David, Sebastiano Bernuzzi, and Albino Perego, 2020, "The dynamics of binary neutron star mergers and of GW170817," Annu. Rev. Nucl. Part. Sci. **70**, 95–119.

Radon, T., *et al.*, 2000, "Schottky mass measurements of stored and cooled neutron-deficient projectile fragments in the element range of $57 \leq Z \leq 84$," Nucl. Phys. **A677**, 75–99.

Radžiūtė, Laima, Gediminas Gaigalas, Daiji Kato, Pavel Rynkun, and Masaomi Tanaka, 2020, "Extended calculations of energy levels and transition rates for singly ionized lanthanide elements I: Pr—Gd," Astrophys. J. Suppl. Ser., **248**, 17.

Raman, S., B. Fogelberg, J. A. Harvey, R. L. Macklin, P. H. Stelson, A. Schröder, and K.-L. Kratz, 1983, "Overlapping beta decay and

resonance neutron spectroscopy of levels in ^{87}Kr," Phys. Rev. C **28**, 602–622.

Ramirez-Ruiz, E., M. Trenti, M. MacLeod, L. F. Roberts, W. H. Lee, and M. I. Saladino-Rosas, 2015, "Compact stellar binary assembly in the first nuclear star clusters and *r*-process synthesis in the early Universe," Astrophys. J. **802**, L22.

Rauscher, T., 2011, "The path to improved reaction rates for astrophysics," Int. J. Mod. Phys. E **20**, 1071–1169.

Rauscher, T., 2013, "Suppression of excited-state contributions to stellar reaction rates," Phys. Rev. C **88**, 035803.

Rauscher, T., R. Bieber, H. Oberhummer, K. L. Kratz, J. Dobaczewski, P. Möller, and M. M. Sharma, 1998, "Dependence of direct neutron capture on nuclear-structure models," Phys. Rev. C **57**, 2031–2039.

Rauscher, T., N. Dauphas, I. Dillmann, C. Fröhlich, Z. Fülöp, and G. Gyürky, 2013, "Constraining the astrophysical origin of the *p*-nuclei through nuclear physics and meteoritic data," Rep. Prog. Phys. **76**, 066201.

Rauscher, T., and F.-K. Thielemann, 2000, "Astrophysical reaction rates from statistical model calculations," At. Data Nucl. Data Tables **75**, 1–351.

Rauscher, T., and F.-K. Thielemann, 2001, "Tables of nuclear cross sections and reaction rates: An addendum to the paper 'Astrophysical reaction rates from statistical model calculations,' " At. Data Nucl. Data Tables **79**, 47–64.

Rauscher, T., F.-K. Thielemann, and K.-L. Kratz, 1997, "Nuclear level density and the determination of thermonuclear rates for astrophysics," Phys. Rev. C **56**, 1613–1625.

Rauscher, Thomas, 2008, "Astrophysical relevance of γ transition energies," Phys. Rev. C **78**, 032801.

Ravn, H. L., S. Sundell, and L. Westgaard, 1975, "Target techniques for the ISOLDE on-line isotope separator," Nucl. Instrum. Methods **123**, 131–144.

Recchi, S., F. Calura, and P. Kroupa, 2009, "The chemical evolution of galaxies within the IGIMF theory: The [α/Fe] ratios and downsizing," Astron. Astrophys. **499**, 711–722.

Recchi, S., F. Matteucci, and A. D'Ercole, 2001, "Dynamical and chemical evolution of gas-rich dwarf galaxies," Mon. Not. R. Astron. Soc. **322**, 800–820.

Reddy, B. E., D. L. Lambert, and C. Allende Prieto, 2006, "Elemental abundance survey of the galactic thick disc," Mon. Not. R. Astron. Soc. **367**, 1329–1366.

Reddy, B. E., J. Tomkin, D. L. Lambert, and C. Allende Prieto, 2003, "The chemical compositions of galactic disc F and G dwarfs," Mon. Not. R. Astron. Soc. **340**, 304–340.

Rehse, S. J., R. Li, T. J. Scholl, A. Sharikova, R. Chatelain, R. A. Holt, and S. D. Rosner, 2006, "Fast-ion-beam laser-induced-fluorescence measurements of spontaneous-emission branching ratios and oscillator strengths in SmII," Can. J. Phys. **84**, 723–771.

Reichert, M., M. Obergaulinger, and A. Arcones, 2020, "*r*-process in magneto-rotational supernova explosions," arXiv:2010.02227.

Reifarth, R., K. Göbel, T. Heftrich, M. Weigand, B. Jurado, F. Käppeler, and Y. A. Litvinov, 2017, "Spallation-based neutron target for direct studies of neutron-induced reactions in inverse kinematics," Phys. Rev. Accel. Beams **20**, 044701.

Reifarth, R., C. Lederer, and F. Käppeler, 2014, "Neutron reactions in astrophysics," J. Phys. G **41**, 053101.

Reifarth, R., and Y. A. Litvinov, 2014, "Measurements of neutron-induced reactions in inverse kinematics," Phys. Rev. ST Accel. Beams **17**, 014701.

Reiter, M. P., *et al.*, 2020, "Mass measurements of neutron-rich gallium isotopes refine production of nuclei of the first *r*-process abundance peak in neutron-star merger calculations," Phys. Rev. C **101**, 025803.

Rembges, F., C. Freiburghaus, T. Rauscher, F.-K. Thielemann, H. Schatz, and M. Wiescher, 1997, "An approximation for the *rp*-process," Astrophys. J. **484**, 412–423.

Renaud, M., *et al.*, 2006, "The signature of ^{44}Ti in Cassiopeia A revealed by IBIS/ISGRI on *INTEGRAL*," Astrophys. J. Lett., **647**, L41–L44.

Rezzolla, Luciano, Elias R. Most, and Lukas R. Weih, 2018, "Using gravitational-wave observations and quasi-universal relations to constrain the maximum mass of neutron stars," Astrophys. J. **852**, L25.

Richers, S., H. Nagakura, C. D. Ott, J. Dolence, K. Sumiyoshi, and S. Yamada, 2017, "A detailed comparison of multidimensional Boltzmann neutrino transport methods in core-collapse supernovae," Astrophys. J. **847**, 133.

Ripley, J. L., B. D. Metzger, A. Arcones, and G. Martínez-Pinedo, 2014, "X-ray decay lines from heavy nuclei in supernova remnants as a probe of the *r*-process origin and the birth periods of magnetars," Mon. Not. R. Astron. Soc. **438**, 3243–3254.

Roberts, L. F., 2012, "A new code for proto-neutron star evolution," Astrophys. J. **755**, 126.

Roberts, L. F., J. Lippuner, M. D. Duez, J. A. Faber, F. Foucart, J. C. Lombardi, Jr., S. Ning, C. D. Ott, and M. Ponce, 2017, "The influence of neutrinos on *r*-process nucleosynthesis in the ejecta of black hole-neutron star mergers," Mon. Not. R. Astron. Soc. **464**, 3907–3919.

Roberts, L. F., S. Reddy, and G. Shen, 2012, "Medium modification of the charged-current neutrino opacity and its implications," Phys. Rev. C **86**, 065803.

Roberts, L. F., G. Shen, V. Cirigliano, J. A. Pons, S. Reddy, and S. E. Woosley, 2012, "Protoneutron Star Cooling with Convection: The Effect of the Symmetry Energy," Phys. Rev. Lett. **108**, 061103.

Roberts, L. F., S. E. Woosley, and R. D. Hoffman, 2010, "Integrated nucleosynthesis in neutrino-driven winds," Astrophys. J. **722**, 954–967.

Roberts, Luke F., Dan Kasen, William H. Lee, and Enrico Ramirez-Ruiz, 2011, "Electromagnetic transients powered by nuclear decay in the tidal tails of coalescing compact binaries," Astrophys. J. **736**, L21.

Roberts, Luke F., and Sanjay Reddy, 2017, "Charged current neutrino interactions in hot and dense matter," Phys. Rev. C **95**, 045807.

Rodríguez, Tomás R., Alexander Arzhanov, and Gabriel Martínez-Pinedo, 2015, "Toward global beyond-mean-field calculations of nuclear masses and low-energy spectra," Phys. Rev. C **91**, 044315.

Roederer, I. U., 2013, "Are there any stars lacking Neutron-capture elements? Evidence from strontium and barium," Astron. J. **145**, 26.

Roederer, I. U., 2017, "The origin of the heaviest metals in most ultra-faint dwarf galaxies," Astrophys. J. **835**, 23.

Roederer, I. U., J. J. Cowan, A. I. Karakas, K.-L. Kratz, M. Lugaro, J. Simmerer, K. Farouqi, and C. Sneden, 2010, "The ubiquity of the rapid neutron-capture process," Astrophys. J. **724**, 975–993.

Roederer, I. U., A. I. Karakas, M. Pignatari, and F. Herwig, 2016, "The diverse origins of neutron-capture elements in the metal-poor star HD 94028: Possible detection of products of *i*-process nucleosynthesis," Astrophys. J. **821**, 37.

Roederer, I. U., K.-L. Kratz, A. Frebel, N. Christlieb, B. Pfeiffer, J. J. Cowan, and C. Sneden, 2009, "The end of nucleosynthesis: Production of lead and thorium in the early Galaxy," Astrophys. J. **698**, 1963–1980.

Roederer, I. U., and J. E. Lawler, 2012, "Detection of elements at all three *r*-process peaks in the metal-poor star HD 160617," Astrophys. J. **750**, 76.

Roederer, I. U., J. E. Lawler, J. J. Cowan, T. C. Beers, A. Frebel, I. I. Ivans, H. Schatz, J. S. Sobeck, and C. Sneden, 2012, "Detection of the second *r*-process peak element tellurium in metal-poor stars," Astrophys. J. Suppl. Ser., **747**, L8.

Roederer, I. U., H. Schatz, J. E. Lawler, T. C. Beers, J. J. Cowan, A. Frebel, I. I. Ivans, C. Sneden, and J. S. Sobeck, 2014, "New detections of arsenic, selenium, and other heavy elements in two metal-poor stars," Astrophys. J. **791**, 32.

Roederer, I. U., C. Sneden, J. E. Lawler, and J. J. Cowan, 2010, "New abundance determinations of cadmium, lutetium, and osmium in the *r*-process enriched star BD +17 3248," Astrophys. J. **714**, L123–L127.

Roederer, Ian U., Kohei Hattori, and Monica Valluri, 2018, "Kinematics of highly *r*-process-enhanced field stars: Evidence for an accretion origin and detection of several groups from disrupted satellites," Astron. J. **156**, 179.

Roederer, Ian U., George W. Preston, Ian B. Thompson, Stephen A. Shectman, Christopher Sneden, Gregory S. Burley, and Daniel D. Kelson, 2014, "A search for stars of very low metal abundance. VI. Detailed abundances of 313 metal-poor stars," Astron. J. **147**, 136.

Rolfs, C. E., and W. S. Rodney, 1988, *Cauldrons in the Cosmos: Nuclear Astrophysics* (University of Chicago Press, Chicago).

Rosswog, S., 2005, "Mergers of neutron star-black hole binaries with small mass ratios: Nucleosynthesis, gamma-ray bursts, and electromagnetic transients," Astrophys. J. **634**, 1202–1213.

Rosswog, S., 2007, "Fallback accretion in the aftermath of a compact binary merger," Mon. Not. R. Astron. Soc. **376**, L48–L51.

Rosswog, S., M. B. Davies, F.-K. Thielemann, and T. Piran, 2000, "Merging neutron stars: Asymmetric systems," Astron. Astrophys. **360**, 171–184, https://ui.adsabs.harvard.edu/#abs/2000A&A...360..171R/abstract.

Rosswog, S., U. Feindt, O. Korobkin, M.-R. Wu, J. Sollerman, A. Goobar, and G. Martinez-Pinedo, 2017, "Detectability of compact binary merger macronovae," Classical Quantum Gravity **34**, 104001.

Rosswog, S., O. Korobkin, A. Arcones, F.-K. Thielemann, and T. Piran, 2014, "The long-term evolution of neutron star merger remnants—I. The impact of *r*-process nucleosynthesis," Mon. Not. R. Astron. Soc. **439**, 744–756.

Rosswog, S., M. Liebendörfer, F.-K. Thielemann, M. B. Davies, W. Benz, and T. Piran, 1999, "Mass ejection in neutron star mergers," Astron. Astrophys. **341**, 499–526, https://ui.adsabs.harvard.edu/#abs/1999A&A...341..499R/abstract.

Rosswog, S., J. Sollerman, U. Feindt, A. Goobar, O. Korobkin, R. Wollaeger, C. Fremling, and M. M. Kasliwal, 2018, "The first direct double neutron star merger detection: Implications for cosmic nucleosynthesis," Astron. Astrophys. **615**, A132.

Rosswog, Stephan, 2015, "The multi-messenger picture of compact binary mergers," Int. J. Mod. Phys. D **24**, 1530012.

Rrapaj, Ermal, J. W. Holt, Alexander Bartl, Sanjay Reddy, and A. Schwenk, 2015, "Charged-current reactions in the supernova neutrino-sphere," Phys. Rev. C **91**, 035806.

Ruffert, M., and H.-T. Janka, 2001, "Coalescing neutron stars—A step towards physical models. III. Improved numerics and different neutron star masses and spins," Astron. Astrophys. **380**, 544–577.

Ruffert, M., H.-T. Janka, and G. Schaefer, 1996, "Coalescing neutron stars—A step towards physical models. I. Hydrodynamic evolution and gravitational-wave emission.," Astron. Astrophys. **311**, 532–566, https://ui.adsabs.harvard.edu/#abs/1996A&A...311..532R/abstract.

Ruffert, M., H.-T. Janka, K. Takahashi, and G. Schaefer, 1997, "Coalescing neutron stars—A step towards physical models. II. Neutrino emission, neutron tori, and gamma-ray bursts," Astron. Astrophys. **319**, 122–153, https://ui.adsabs.harvard.edu/#abs/1997A&A...319..122R/abstract.

Ruiz, Milton, Stuart L. Shapiro, and Antonios Tsokaros, 2018, "GW170817, general relativistic magnetohydrodynamic simulations, and the neutron star maximum mass," Phys. Rev. D **97**, 021501.

Sadhukhan, J., W. Nazarewicz, and N. Schunck, 2016, "Microscopic modeling of mass and charge distributions in the spontaneous fission of ^{240}Pu," Phys. Rev. C **93**, 011304.

Sadhukhan, Jhilam, Samuel A. Giuliani, Zachary Matheson, and Witold Nazarewicz, 2020, "Efficient method for estimation of fission fragment yields of *r*-process nuclei," Phys. Rev. C **101**, 065803.

Sadhukhan, Jhilam, K. Mazurek, A. Baran, J. Dobaczewski, W. Nazarewicz, and J. A. Sheikh, 2013, "Spontaneous fission lifetimes from the minimization of self-consistent collective action," Phys. Rev. C **88**, 064314.

Safarzadeh, Mohammadtaher, Enrico Ramirez-Ruiz, Jeff. J. Andrews, Phillip Macias, Tassos Fragos, and Evan Scannapieco, 2019, "*r*-process enrichment of the ultra-faint dwarf galaxies by fast-merging double-neutron stars," Astrophys. J. **872**, 105.

Sagert, I., T. Fischer, M. Hempel, G. Pagliara, J. Schaffner-Bielich, A. Mezzacappa, F.-K. Thielemann, and M. Liebendörfer, 2009, "Signals of the QCD Phase Transition in Core-Collapse Supernovae," Phys. Rev. Lett. **102**, 081101.

Sakari, Charli M., *et al.*, 2018, "The *r*-process alliance: First release from the northern search for *r*-process-enhanced metal-poor stars in the galactic halo," Astrophys. J. **868**, 110.

Salih, S., and J. E. Lawler, 1983, "Pulsed ion source for laser spectroscopy: Application to Nb II," Phys. Rev. A **28**, 3653–3655.

Sato, K., 1974, "Formation of elements in neutron rich ejected matter of supernovae. II—Dynamical *r*-process stage," Prog. Theor. Phys. **51**, 726–744.

Schäfer, F. P., W. Schmidt, and J. Volze, 1966, "Organic dye solution laser," Appl. Phys. Lett. **9**, 306–309.

Schatz, H., R. Toenjes, B. Pfeiffer, T. C. Beers, J. J. Cowan, V. Hill, and K.-L. Kratz, 2002, "Thorium and uranium chronometers applied to CS 31082-001," Astrophys. J. **579**, 626–638.

Schiller, A., L. Bergholt, M. Guttormsen, E. Melby, J. Rekstad, and S. Siem, 2000, "Extraction of level density and γ strength function from primary γ spectra," Nucl. Instrum. Methods Phys. Res., Sect. A **447**, 498–511.

Schmidt, K.-H., B. Jurado, C. Amouroux, and C. Schmitt, 2016, "General description of fission observables: GEF model code," Nucl. Data Sheets **131**, 107–221.

Schmidt, Karl-Heinz, and Beatriz Jurado, 2018, "Review on the progress in nuclear fission—Experimental methods and theoretical descriptions," Rep. Prog. Phys. **81**, 106301.

Schmitt, C., K.-H. Schmidt, and B. Jurado, 2018, "Benchmark of the GEF code for fission-fragment yields over an enlarged range in fissioning nucleus mass, excitation energy, and angular momentum," Phys. Rev. C **98**, 044605.

Schönrich, Ralph A., and David H. Weinberg, 2019, "The chemical evolution of *r*-process elements from neutron star mergers: The role of a 2-phase interstellar medium, Mon. Not. R. Astron. Soc. **487**, 580–594.

Schramm, D. N., 1973, "Explosive *r*-process nucleosynthesis," Astrophys. J. **185**, 293–302.

Schramm, D. N., and G. J. Wasserburg, 1970, "Nucleochronologies and the mean age of the elements," Astrophys. J. **162**, 57.

Schwengner, R., S. Frauendorf, and B. A. Brown, 2017, "Low-Energy Magnetic Dipole Radiation in Open-Shell Nuclei," Phys. Rev. Lett. **118**, 092502.

Schwengner, R., S. Frauendorf, and A. C. Larsen, 2013, "Low-Energy Enhancement of Magnetic Dipole Radiation," Phys. Rev. Lett. **111**, 232504.

Seeger, P. A., W. A. Fowler, and D. D. Clayton, 1965, "Nucleosynthesis of heavy elements by neutron capture," Astrophys. J. Suppl. Ser., **11**, 121–166.

Seitenzahl, I. R., P. Ghavamian, J. M. Laming, and F. P. A. Vogt, 2019, "Optical Tomography of Chemical Elements Synthesized in Type Ia Supernovae," Phys. Rev. Lett. **123**, 041101.

Seitenzahl, I. R., F. X. Timmes, and G. Magkotsios, 2014, "The light curve of SN 1987A revisited: Constraining production masses of radioactive nuclides," Astrophys. J. **792**, 10.

Seitenzahl, I. R., and D. M. Townsley, 2017, "Nucleosynthesis in thermonuclear supernovae," in *Handbook of Supernovae*, edited by A. W. Alsabti, and P. Murdin (Springer International Publishing, Cham, Switzerland).

Sekiguchi, Y., K. Kiuchi, K. Kyutoku, and M. Shibata, 2015, "Dynamical mass ejection from binary neutron star mergers: Radiation-hydrodynamics study in general relativity," Phys. Rev. D **91**, 064059.

Sekiguchi, Y., K. Kiuchi, K. Kyutoku, M. Shibata, and K. Taniguchi, 2016, "Dynamical mass ejection from the merger of asymmetric binary neutron stars: Radiation-hydrodynamics study in general relativity," Phys. Rev. D **93**, 124046.

Sekiguchi, Y., and M. Shibata, 2011, "Formation of black hole and accretion disk in a massive high-entropy stellar core collapse," Astrophys. J. **737**, 6.

Sekiguchi, Yuichiro, Kenta Kiuchi, Koutarou Kyutoku, and Masaru Shibata, 2011, "Gravitational Waves and Neutrino Emission from the Merger of Binary Neutron Stars," Phys. Rev. Lett. **107**, 051102.

Shafer, T., J. Engel, C. Fröhlich, G. C. McLaughlin, M. Mumpower, and R. Surman, 2016, "β decay of deformed r-process nuclei near $a = 80$ and $a = 160$, including odd-a and odd-odd nuclei, with the Skyrme finite-amplitude method," Phys. Rev. C **94**, 055802.

Shen, S., R. J. Cooke, E. Ramirez-Ruiz, P. Madau, L. Mayer, and J. Guedes, 2015, "The history of r-process enrichment in the Milky Way," Astrophys. J. **807**, 115.

Shetrone, M., K. A. Venn, E. Tolstoy, F. Primas, V. Hill, and A. Kaufer, 2003, "VLT/UVES abundances in four nearby dwarf spheroidal galaxies. I. Nucleosynthesis and abundance ratios," Astron. J. **125**, 684–706.

Shetrone, M. D., M. Bolte, and P. B. Stetson, 1998, "Keck HIRES abundances in the dwarf spheroidal galaxy Draco," Astron. J. **115**, 1888–1893.

Shibagaki, S., T. Kajino, G. J. Mathews, S. Chiba, S. Nishimura, and G. Lorusso, 2016, "Relative contributions of the weak, main, and fission-recycling r-process," Astrophys. J. **816**, 79.

Shibata, M., and K. Taniguchi, 2011, "Coalescence of black hole-neutron star binaries," Living Rev. Relativity **14**, 6.

Shibata, Masaru, 2018, "Mass ejection from neutron star mergers," lecture presented at the EMMI Rapid Reaction Task Force: The physics of neutron star mergers at GSI/FAIR.

Shibata, Masaru, Sho Fujibayashi, Kenta Hotokezaka, Kenta Kiuchi, Koutarou Kyutoku, Yuichiro Sekiguchi, and Masaomi Tanaka, 2017, "Modeling GW170817 based on numerical relativity and its implications," Phys. Rev. D **96**, 123012.

Shibata, Masaru, and Kenta Hotokezaka, 2019, "Merger and mass ejection of neutron star binaries," Annu. Rev. Nucl. Part. Sci. **69**, 41–64.

Shibata, Masaru, and Keisuke Taniguchi, 2006, "Merger of binary neutron stars to a black hole: Disk mass, short gamma-ray bursts, and quasinormal mode ringing," Phys. Rev. D **73**, 064027.

Shibata, Masaru, Keisuke Taniguchi, and Kōji Uryū, 2005, "Merger of binary neutron stars with realistic equations of state in full general relativity," Phys. Rev. D **71**, 084021.

Shibata, Masaru, and Kōji Uryū, 2000, "Simulation of merging binary neutron stars in full general relativity: $\Gamma = 2$ case," Phys. Rev. D **61**, 064001.

Shibata, Masaru, and Kōji Uryū, 2006, "Merger of black hole-neutron star binaries: Nonspinning black hole case," Phys. Rev. D **74**, 121503.

Siegel, D. M., and B. D. Metzger, 2018, "Three-dimensional GRMHD simulations of neutrino-cooled accretion disks from neutron star mergers," Astrophys. J. **858**, 52.

Siegel, Daniel M., 2019, "GW170817—The first observed neutron star merger and its kilonova: Implications for the astrophysical site of the r-process," Eur. Phys. J. A **55**, 203.

Siegel, Daniel M., Jennifer Barnes, and Brian D. Metzger, 2019, "Collapsars as a major source of r-process elements," Nature (London) **569**, 241–244.

Siegel, Daniel M., Riccardo Ciolfi, and Luciano Rezzolla, 2014, "Magnetically driven winds from differentially rotating neutron stars and x-ray afterglows of short gamma-ray bursts," Astrophys. J. Lett., **785**, L6.

Siegel, Daniel M., and Brian D. Metzger, 2017, "Three-Dimensional General-Relativistic Magnetohydrodynamic Simulations of Remnant Accretion Disks from Neutron Star Mergers: Outflows and r-Process Nucleosynthesis," Phys. Rev. Lett. **119**, 231102.

Siegl, K., *et al.*, 2018, "Recoil ions from the β decay of ^{134}Sb confined in a Paul trap," Phys. Rev. C **97**, 035504.

Sieja, K., 2017, "Electric and Magnetic Dipole Strength at Low Energy," Phys. Rev. Lett. **119**, 052502.

Sieja, K., 2018, "Shell-model study of the $M1$ dipole strength at low energy in the $A > 100$ nuclei," Phys. Rev. C **98**, 064312.

Sieverding, A., K. Langanke, G. Martínez-Pinedo, R. Bollig, H. T. Janka, and A. Heger, 2019, "The ν-process with fully time-dependent supernova neutrino emission spectra," Astrophys. J. **876**, 151.

Simmerer, J., C. Sneden, J. J. Cowan, J. Collier, V. M. Woolf, and J. E. Lawler, 2004, "The rise of the s-process in the Galaxy," Astrophys. J. **617**, 1091–1114.

Simon, Joshua D., 2019, "The faintest dwarf galaxies," Annu. Rev. Astron. Astrophys. **57**, 375–415.

Simonetti, Paolo, Francesca Matteucci, Laura Greggio, and Gabriele Cescutti, 2019, "A new delay time distribution for merging neutron stars tested against galactic and cosmic data," Mon. Not. R. Astron. Soc. **486**, 2896–2909.

Siqueira, Mello, *et al.*, 2013, "First stars. XVI. HST/STIS abundances of heavy elements in the uranium-rich metal-poor star CS 31082-001," Astron. Astrophys. **550**, A122.

Skúladóttir, Á., C. J. Hansen, S. Salvadori, and A. Choplin, 2019, "Neutron-capture elements in dwarf galaxies. I. Chemical clocks and the short timescale of the r-process," Astron. Astrophys. **631**, A171.

Skúladóttir, Á., and S. Salvadori, 2020, "Evidence for $\gtrsim$4 Gyr timescales of neutron star mergers from galactic archaeology," Astron. Astrophys. **634**, L2.

Smartt, S. J., *et al.*, 2017, "A kilonova as the electromagnetic counterpart to a gravitational-wave source," Nature (London) **551**, 75–79.

Sneden, C., J. J. Cowan, and R. Gallino, 2008, "Neutron-capture elements in the early Galaxy," Annu. Rev. Astron. Astrophys. **46**, 241–288.

Sneden, C., J. E. Lawler, J. J. Cowan, I. I. Ivans, and E. A. Den Hartog, 2009, "New rare earth element abundance distributions for the Sun and five r-process-rich very metal-poor stars," Astrophys. J. Suppl. Ser., **182**, 80–96.

Sneden, C., A. McWilliam, G. W. Preston, J. J. Cowan, D. L. Burris, and B. J. Armosky, 1996, "The ultra-metal-poor, neutron-capture-rich giant star CS 22892-052," Astrophys. J. **467**, 819.

Sneden, C., and M. Parthasarathy, 1983, "The *r*- and *s*-process nuclei in the early history of the galaxy—HD 122563," Astrophys. J. **267**, 757–778.

Sneden, C., G. W. Preston, A. McWilliam, and L. Searle, 1994, "Ultrametal-poor halo stars: The remarkable spectrum of CS 22892-052," Astrophys. J. Lett. **431**, L27–L30.

Sneden, C., *et al.*, 2003, "The extremely metal-poor, neutron capture-rich star CS 22892-052: A comprehensive abundance analysis," Astrophys. J. **591**, 936–953.

Sneden, Christopher, and John J. Cowan, 2003, "Genesis of the heaviest elements in the Milky Way Galaxy," Science **299**, 70–75.

Soares-Santos, M., *et al.*, 2017, "The electromagnetic counterpart of the binary neutron star merger LIGO/Virgo GW170817. I. Discovery of the optical counterpart using the dark energy camera," Astrophys. J. Lett., **848**, L16.

Söderström, P.-A., *et al.*, 2013, "Installation and commissioning of EURICA—Euroball-RIKEN cluster array," Nucl. Instrum. Methods Phys. Res., Sect. B **317**, 649–652.

Sørensen, M., H. Svensmark, and U. Gråe Jørgensen, 2017, "Near-Earth supernova activity during the past 35 Myr," arXiv:1708.08248.

Sorokin, P. P., and J. R. Lankard, 1966, "Stimulated emission observed from an organic dye chloro-aluminum phthalocynine," IBM J. Res. Dev. **10**, 162.

Spitoni, E., F. Matteucci, S. Recchi, G. Cescutti, and A. Pipino, 2009, "Effects of galactic fountains and delayed mixing in the chemical evolution of the Milky Way," Astron. Astrophys. **504**, 87–96.

Spyrou, A., *et al.*, 2014, "Novel Technique for Constraining *r*-Process (n,γ) Reaction Rates," Phys. Rev. Lett. **113**, 232502.

Spyrou, A., *et al.*, 2017, "Neutron-capture rates for explosive nucleosynthesis: The case of $^{68}\mathrm{Ni}(n,\gamma)^{69}\mathrm{Ni}$," J. Phys. G **44**, 044002.

Steinberg, E. P., and B. D. Wilkins, 1978, "Implications of fission mass distributions for the astrophysical *r*-process," Astrophys. J. **223**, 1000–1014.

Suda, Takuma, Yutaka Katsuta, Shimako Yamada, Tamon Suwa, Chikako Ishizuka, Yutaka Komiya, Kazuo Sorai, Masayuki Aikawa, and Masayuki Y. Fujimoto, 2008, "Stellar Abundances for the Galactic Archeology (SAGA) database—Compilation of the characteristics of known extremely metal-poor stars," Publ. Astron. Soc. Jpn. **60**, 1159.

Sukhbold, T., T. Ertl, S. E. Woosley, J. M. Brown, and H.-T. Janka, 2016, "Core-collapse supernovae from 9 to 120 solar masses based on neutrino-powered explosions," Astrophys. J. **821**, 38.

Sumiyoshi, K., M. Terasawa, G. J. Mathews, T. Kajino, S. Yamada, and H. Suzuki, 2001, "*r*-process in prompt supernova explosions revisited," Astrophys. J. **562**, 880–886.

Sun, B., *et al.*, 2008, "Nuclear structure studies of short-lived neutron-rich nuclei with the novel large-scale isochronous mass spectrometry at the FRS-ESR facility," Nucl. Phys. **A812**, 1–12.

Sun, B.-H., and J. Meng, 2008, "Challenge on the astrophysical *r*-process calculation with nuclear mass models," Chin. Phys. Lett. **25**, 2429–2431.

Surman, R., O. L. Caballero, G. C. McLaughlin, O. Just, and H.-T. Janka, 2014, "Production of ^{56}Ni in black hole-neutron star merger accretion disc outflows," J. Phys. G **41**, 044006.

Surman, R., J. Engel, J. R. Bennett, and B. S. Meyer, 1997, "Source of the Rare-Earth Element Peak in *r*-Process Nucleosynthesis," Phys. Rev. Lett. **79**, 1809–1812.

Surman, R., G. C. McLaughlin, and W. R. Hix, 2006, "Nucleosynthesis in the outflow from gamma-ray burst accretion disks," Astrophys. J. **643**, 1057–1064.

Surman, R., G. C. McLaughlin, M. Ruffert, H.-T. Janka, and W. R. Hix, 2008, "*r*-process nucleosynthesis in hot accretion disk flows from black hole-neutron star mergers," Astrophys. J. **679**, L117.

Suzuki, T., and T. Kajino, 2013, "Element synthesis in the supernova environment and neutrino oscillations," J. Phys. G **40**, 083101.

Suzuki, Toshio, Takashi Yoshida, Toshitaka Kajino, and Takaharu Otsuka, 2012, "β decays of isotones with neutron magic number of $N = 126$ and *r*-process nucleosynthesis," Phys. Rev. C **85**, 015802.

Svanberg, S., J. Larsson, A. Persson, and C.-G. Wahlström, 1994, "Lund high-power laser facility—Systems and first results," Phys. Scr. **49**, 187–197.

Symbalisty, E., and D. N. Schramm, 1982, "Neutron star collisions and the *r*-process," Astrophys. Lett. **22**, 143–145, https://ui.adsabs.harvard.edu/#abs/1982ApL....22..143S/abstract.

Symbalisty, E. M. D., D. N. Schramm, and J. R. Wilson, 1985, "An expanding vortex site for the *r*-process in rotating stellar collapse," Astrophys. J. **291**, L11–L14.

Szücs, T., P. Mohr, Gy. Gyürky, Z. Halász, R Huszánk, G. G. Kiss, T. N. Szegedi, Zs. Török, and Zs. Fülöp, 2020, "Activation measurement of α-induced cross sections for ^{197}Au: Analysis in the statistical model and beyond," J. Phys. Conf. Ser. **1668**, 012042.

Tachibana, T., M. Yamada, and Y. Yoshida, 1990, "Improvement of the gross theory of β-decay. II: One-particle strength function," Prog. Theor. Phys. **84**, 641–657.

Takahashi, K., J. Witti, and H.-Th. Janka, 1994, "Nucleosynthesis in neutrino-driven winds from protoneutron stars. II. The *r*-process," Astron. Astrophys. **286**, 857–869, https://ui.adsabs.harvard.edu/#abs/1994A&A...286..857T/abstract.

Takiwaki, T., and K. Kotake, 2011, "Gravitational wave signatures of magnetohydrodynamically driven core-collapse supernova explosions," Astrophys. J. **743**, 30.

Takiwaki, T., K. Kotake, and K. Sato, 2009, "Special relativistic simulations of magnetically dominated jets in collapsing massive stars," Astrophys. J. **691**, 1360–1379.

Talbert, W. L., F. K. Wohn, J. C. Hill, A. R. Landin, M. A. Cullison, and R. L. Gill, 1979, "Tristan II: Extension of the Tristan facility to the study of non-gaseous activities," Nucl. Instrum. Methods **161**, 431–437.

Tamborra, Irene, Bernhard Müller, Lorenz Hüdepohl, Hans-Thomas Janka, and Georg Raffelt, 2012, "High-resolution supernova neutrino spectra represented by a simple fit," Phys. Rev. D **86**, 125031.

Tanaka, M., 2016, "Kilonova/macronova emission from compact binary mergers," Adv. Astron. **2016**, 634197.

Tanaka, M., *et al.*, 2017, "Kilonova from post-merger ejecta as an optical and near-infrared counterpart of GW170817," Publ. Astron. Soc. Jpn. **69**, 102.

Tanaka, M., *et al.*, 2018, "Properties of kilonovae from dynamical and post-merger ejecta of neutron star mergers," Astrophys. J. **852**, 109.

Tanaka, Masaomi, and Kenta Hotokezaka, 2013, "Radiative transfer simulations of neutron star merger ejecta," Astrophys. J. **775**, 113.

Tanaka, Masaomi, Daiji Kato, Gediminas Gaigalas, and Kyohei Kawaguchi, 2020, "Systematic opacity calculations for kilonovae," Mon. Not. R. Astron. Soc. **496**, 1369–1392.

Tang, T. L., *et al.*, 2020, "First Exploration of Neutron Shell Structure below Lead and beyond $N = 126$," Phys. Rev. Lett. **124**, 062502.

Tanvir, N. R., A. J. Levan, A. S. Fruchter, J. Hjorth, R. A. Hounsell, K. Wiersema, and R. L. Tunnicliffe, 2013, "A 'kilonova' associated with the short-duration γ-ray burst GRB 130603B," Nature (London) **500**, 547–549.

Tanvir, N. R., *et al.*, 2017, "The emergence of a lanthanide-rich kilonova following the merger of two neutron stars," Astrophys. J. Lett., **848**, L27.

Tarumi, Yuta, Naoki Yoshida, and Shigeki Inoue, 2020, "*r*-process enrichment in ultrafaint dwarf galaxies," Mon. Not. R. Astron. Soc. **494**, 120–128.

Terasawa, M., K. Langanke, T. Kajino, G. J. Mathews, and E. Kolbe, 2004, "Neutrino effects before, during, and after the freezeout of the *r*-process," Astrophys. J. **608**, 470–479.

Terasawa, M., K. Sumiyoshi, T. Kajino, G. J. Mathews, and I. Tanihata, 2001, "New nuclear reaction flow during *r*-process nucleosynthesis in supernovae: Critical role of light, neutron-rich nuclei," Astrophys. J. **562**, 470–479.

Tews, I., J. Margueron, and S. Reddy, 2018, "Critical examination of constraints on the equation of state of dense matter obtained from GW170817," Phys. Rev. C **98**, 045804.

Tews, I., J. Margueron, and S. Reddy, 2019, "Confronting gravitational-wave observations with modern nuclear physics constraints," Eur. Phys. J. A **55**, 97.

Thielemann, F.-K., M. Arnould, and W. Hillebrandt, 1979, "Meteoritic anomalies and explosive neutron processing of helium-burning shells," Astron. Astrophys. **74**, 175–185, https://ui.adsabs.harvard.edu/#abs/1979A&A....74..175T/abstract.

Thielemann, F.-K., A. G. W. Cameron, and J. J. Cowan, 1989, "Fission in the astrophysical *r*-process," in *50 Years with Nuclear Fission*, edited by J. Behrens and A. D. Carlson (American Nuclear Society, La Grange Park, IL), p. 592.

Thielemann, F.-K., R. Diehl, A. Heger, R. Hirschi, and M. Liebendörfer, 2018, "Massive stars and their supernovae," in *Astrophysics with Radioactive Isotopes*, Astrophysics and Space Science Library Vol. 453, edited by R. Diehl, D. H. Hartmann, and N. Prantzos (Springer, Cham, Switzerland), pp. 173–286.

Thielemann, F.-K., M. Eichler, I. V. Panov, M. Pignatari, and B. Wehmeyer, 2017, "Making the heaviest elements in a rare class of supernovae," in *Handbook of Supernovae*, edited by A. W. Alsabti, and P. Murdin (Springer International Publishing, Cham, Switzerland).

Thielemann, F.-K., M. Eichler, I. V. Panov, and B. Wehmeyer, 2017, "Neutron star mergers and nucleosynthesis of heavy elements," Annu. Rev. Nucl. Part. Sci. **67**, 253–274.

Thielemann, F.-K., R. Hirschi, M. Liebendörfer, and R. Diehl, 2011, "Massive stars and their supernovae," in *Astronomy with Radioactivities*, Lecture Notes in Physics Vol. 812, edited by Roland Diehl, Dieter, H. Hartmann, and Nikos Prantzos (Springer, Berlin), pp. 153–231.

Thielemann, F.-K., J. Metzinger, and H. V. Klapdor, 1983, "Beta-delayed fission and neutron emission: Consequences for the astrophysical *r*-process and the age of the Galaxy," Z. Phys. A **309**, 301–317.

Thielemann, F.-K., K. Nomoto, and K. Yokoi, 1986, "Explosive nucleosynthesis in carbon deflagration models of type I supernovae," Astron. Astrophys. **158**, 17–33, https://ui.adsabs.harvard.edu/#abs/1986A&A...158...17T/abstract.

Thielemann, F.-K., *et al.*, 2011, "What are the astrophysical sites for the *r*-process and the production of heavy elements?," Prog. Part. Nucl. Phys. **66**, 346–353.

Thielemann, Friedrich-Karl, Masa-Aki Hashimoto, and Ken'ichi Nomoto, 1990, "Explosive nucleosynthesis in SN 1987A. II. Composition, radioactivities, and the neutron star mass," Astrophys. J. **349**, 222.

Thielemann, Friedrich-Karl, Karl-Ludwig Kratz, Bernd Pfeiffer, Thomas Rauscher, Laura van Wormer, and Michael C. Wiescher, 1994, "Astrophysics and nuclei far from stability," Nucl. Phys. **A570**, 329–343.

Thielemann, Friedrich-Karl, Ken'ichi Nomoto, and Masa-Aki Hashimoto, 1996, "Core-collapse supernovae and their ejecta," Astrophys. J. **460**, 408.

Thielemann, Friedrich-Karl, and James W. Truran, 1986, "General implementation of screening effects in thermonuclear reaction rates," in *Advances in Nuclear Astrophysics*, edited by Elisabeth Vangioni-Flam, Jean Audouze, Michel Casse, Jean-Pierre Chieze, and J. Tran Thanh Van (Editions Frontières, Gif-sur-Yvette, France), pp. 541–551.

Thompson, T. A., A. Burrows, and B. S. Meyer, 2001, "The physics of proto-neutron star winds: Implications for *r*-process nucleosynthesis," Astrophys. J. **562**, 887–908.

Timmes, F. X., 1999, "Integration of nuclear reaction networks for stellar hydrodynamics," Astrophys. J. Suppl. Ser., **124**, 241–263.

Timmes, F. X., S. E. Woosley, and T. A. Weaver, 1995, "Galactic chemical evolution: Hydrogen through zinc," Astrophys. J. Suppl. Ser., **98**, 617.

Tinsley, B. M., 1980, "Evolution of the stars and gas in galaxies," Fundam. Cosmic Phys. **5**, 287–388, https://ui.adsabs.harvard.edu/#abs/1980FCPh....5..287T/abstract.

Tornyi, T. G., *et al.*, 2014, "Level density and γ-ray strength function in the odd-odd ^{238}Np nucleus," Phys. Rev. C **89**, 044323.

Travaglio, C., D. Galli, R. Gallino, M. Busso, F. Ferrini, and O. Straniero, 1999, "Galactic chemical evolution of heavy elements: From barium to europium," Astrophys. J. **521**, 691–702.

Travaglio, C., R. Gallino, E. Arnone, J. Cowan, F. Jordan, and C. Sneden, 2004, "Galactic evolution of Sr, Y, and Zr: A multiplicity of nucleosynthetic processes," Astrophys. J. **601**, 864–884.

Travaglio, C., T. Rauscher, A. Heger, M. Pignatari, and C. West, 2018, "Role of core-collapse supernovae in explaining Solar System abundances of *p* nuclides," Astrophys. J. **854**, 18.

Truran, J. W., J. J. Cowan, and A. G. W. Cameron, 1978, "The helium-driven *r*-process in supernovae," Astrophys. J. **222**, L63–L67.

Tsujimoto, T., and T. Shigeyama, 2014, "Enrichment history of *r*-process elements shaped by a merger of neutron star pairs," Astron. Astrophys. **565**, L5.

Tsujimoto, T., Y. Yoshii, K. Nomoto, F. Matteucci, F.-K. Thielemann, and M. Hashimoto, 1997, "A new approach to determine the initial mass function in the solar neighborhood," Astrophys. J. **483**, 228–234.

Ural, U., G. Cescutti, A. Koch, J. Kleyna, S. Feltzing, and M. I. Wilkinson, 2015, "An inefficient dwarf: Chemical abundances and the evolution of the Ursa Minor dwarf spheroidal galaxy," Mon. Not. R. Astron. Soc. **449**, 761–770.

van de Voort, F., E. Quataert, P. F. Hopkins, D. Kereš, and C.-A. Faucher-Giguère, 2015, "Galactic *r*-process enrichment by neutron star mergers in cosmological simulations of a Milky Way–mass galaxy," Mon. Not. R. Astron. Soc. **447**, 140–148.

van de Voort, Freeke, Rüdiger Pakmor, Robert J. J. Grand, Volker Springel, Facundo A. Gómez, and Federico Marinacci, 2020, "Neutron star mergers and rare core-collapse supernovae as sources of *r*-process enrichment in simulated galaxies," Mon. Not. R. Astron. Soc. **494**, 4867–4883.

Vangioni, E., S. Goriely, F. Daigne, P. François, and K. Belczynski, 2016, "Cosmic neutron-star merger rate and gravitational waves constrained by the *r*-process nucleosynthesis," Mon. Not. R. Astron. Soc. **455**, 17–34.

Vassh, N., *et al.*, 2019, "Using excitation-energy dependent fission yields to identify key fissioning nuclei in *r*-process nucleosynthesis," J. Phys. G **46**, 065202.

Vassh, Nicole, Matthew R. Mumpower, Gail C. McLaughlin, Trevor M. Sprouse, and Rebecca Surman, 2020, "Co-production of light and heavy *r*-process elements via fission deposition," Astrophys. J. **896**, 28.

Venn, K. A., E. Tolstoy, A. Kaufer, E. D. Skillman, S. M. Clarkson, S. J. Smartt, D. J. Lennon, and R. P. Kudritzki, 2003, "The chemical composition of two supergiants in the dwarf irregular galaxy WLM," Astron. J. **126**, 1326–1345.

Vescovi, D., M. Busso, S. Palmerini, O. Trippella, S. Cristallo, L. Piersanti, A. Chieffi, M. Limongi, P. Hoppe, and K.-L. Kratz, 2018, "On the origin of early Solar System radioactivities: Problems with the asymptotic giant branch and massive star scenarios," Astrophys. J. **863**, 115.

Vigna-Gómez, Alejandro, *et al.*, 2018, "On the formation history of galactic double neutron stars," Mon. Not. R. Astron. Soc. **481**, 4009–4029.

Vilen, M., *et al.*, 2018, "Precision Mass Measurements on Neutron-Rich Rare-Earth Isotopes at JYFLTRAP: Reduced Neutron Pairing and Implications for *r*-Process Calculations," Phys. Rev. Lett. **120**, 262701.

Villar, V. A., *et al.*, 2017, "The combined ultraviolet, optical, and near-infrared light curves of the kilonova associated with the binary neutron star merger GW170817: Unified data set, analytic models, and physical implications," Astrophys. J. Lett., **851**, L21.

Villar, V. A., *et al.*, 2018, "Spitzer Space Telescope infrared observations of the binary neutron star merger GW170817," Astrophys. J. Lett., **862**, L11.

Vink, J., J. M. Laming, J. S. Kaastra, J. A. M. Bleeker, H. Bloemen, and U. Oberlack, 2001, "Detection of the 67.9 and 78.4 keV lines associated with the radioactive decay of ^{44}Ti in Cassiopeia A," Astrophys. J. Lett. **560**, L79–L82.

Vink, Jacco, 2008, "Supernova remnants with magnetars: Clues to magnetar formation," Adv. Space Res. **41**, 503–511.

Vlasenko, Alexey, and G. C. McLaughlin, 2018, "Matter-neutrino resonance in a multiangle neutrino bulb model," Phys. Rev. D **97**, 083011.

Wallner, A., *et al.*, 2015, "Abundance of live ^{244}Pu in deep-sea reservoirs on Earth points to rarity of actinide nucleosynthesis," Nat. Commun. **6**, 5956.

Wallner, A., *et al.*, 2016, "Recent near-Earth supernovae probed by global deposition of interstellar radioactive ^{60}Fe," Nature (London) **532**, 69–72.

Wallner, A., *et al.*, 2019 (private communication).

Wanajo, S., 2007, "Cold *r*-process in neutrino-driven winds," Astrophys. J. **666**, L77–L80.

Wanajo, S., and Y. Ishimaru, 2006, "*r*-process calculations and galactic chemical evolution," Nucl. Phys. **A777**, 676–699.

Wanajo, S., and H.-T. Janka, 2012, "The *r*-process in the neutrino-driven wind from a black-hole torus," Astrophys. J. **746**, 180.

Wanajo, S., H.-T. Janka, and B. Müller, 2013, "Electron-capture supernovae as sources of ^{60}Fe," Astrophys. J. **774**, L6.

Wanajo, S., T. Kajino, G. J. Mathews, and K. Otsuki, 2001, "The *r*-process in neutrino-driven winds from nascent, 'compact' neutron stars of core-collapse supernovae," Astrophys. J. **554**, 578–586.

Wanajo, S., B. Müller, H.-T. Janka, and A. Heger, 2018, "Nucleosynthesis in the innermost ejecta of neutrino-driven supernova explosions in two dimensions," Astrophys. J. **852**, 40.

Wanajo, S., K. Nomoto, H.-T. Janka, F. S. Kitaura, and B. Müller, 2009, "Nucleosynthesis in electron capture supernovae of asymptotic giant branch stars," Astrophys. J. **695**, 208–220.

Wanajo, S., Y. Sekiguchi, N. Nishimura, K. Kiuchi, K. Kyutoku, and M. Shibata, 2014, "Production of all the *r*-process nuclides in the dynamical ejecta of neutron star mergers," Astrophys. J. **789**, L39.

Wanajo, Shinya, 2006, "The *rp*-process in neutrino-driven winds," Astrophys. J. **647**, 1323–1340.

Wanajo, Shinya, 2018, "Physical conditions for the *r*-process. I. Radioactive energy sources of kilonovae," Astrophys. J. **868**, 65.

Wanajo, Shinya, Hans-Thomas Janka, and Bernhard Müller, 2011, "Electron-capture supernovae as the origin of elements beyond iron," Astrophys. J. **726**, L15.

Wanderman, D., and T. Piran, 2015, "The rate, luminosity function and time delay of non-collapsar short GRBs," Mon. Not. R. Astron. Soc. **448**, 3026–3037.

Wang, M., G. Audi, A. H. Wapstra, F. G. Kondev, M. MacCormick, X. Xu, and B. Pfeiffer, 2012, "The Ame2012 atomic mass evaluation: II. Tables, graphs and references," Chin. Phys. C **36**, 1603–2014.

Wang, Ning, Min Liu, and Xizhen Wu, 2010, "Modification of nuclear mass formula by considering isospin effects," Phys. Rev. C **81**, 044322.

Watson, Darach, *et al.*, 2019, "Identification of strontium in the merger of two neutron stars," Nature (London) **574**, 497–500.

Waxman, E., E. O. Ofek, D. Kushnir, and A. Gal-Yam, 2018, "Constraints on the ejecta of the GW170817 neutron star merger from its electromagnetic emission," Mon. Not. R. Astron. Soc. **481**, 3423–3441.

Waxman, Eli, Eran O. Ofek, and Doron Kushnir, 2019, "Late-time kilonova light curves and implications to GW170817," Astrophys. J. **878**, 93.

Way, K., and E. P. Wigner, 1948, "The rate of decay of fission products," Phys. Rev. **73**, 1318–1330.

Wehmeyer, B., C. Fröhlich, B. Côté, M. Pignatari, and F. K. Thielemann, 2019, "Using failed supernovae to constrain the galactic *r*-process element production," Mon. Not. R. Astron. Soc. **487**, 1745–1753.

Wehmeyer, B., M. Pignatari, and F.-K. Thielemann, 2015, "Galactic evolution of rapid neutron capture process abundances: The inhomogeneous approach," Mon. Not. R. Astron. Soc. **452**, 1970–1981.

Wehmeyer, B., *et al.*, 2018 (private communication).

Weisberg, J. M., and Y. Huang, 2016, "Relativistic measurements from timing the binary pulsar PSR B1913+16," Astrophys. J. **829**, 55.

Westin, J., C. Sneden, B. Gustafsson, and J. J. Cowan, 2000, "The *r*-process-enriched low-metallicity giant HD 115444," Astrophys. J. **530**, 783–799.

Whaling, W., M. T. Carle, and M. L. Pitt, 1993, "Argon branching ratios for spectrometer response calibration," J. Quant. Spectrosc. Radiat. Transfer **50**, 7–18.

Wheeler, J. C., J. J. Cowan, and W. Hillebrandt, 1998, "The *r*-process in collapsing O/Ne/Mg cores," Astrophys. J. **493**, L101–L104.

Wheeler, J. C., C. Sneden, and J. W. Truran, Jr., 1989, "Abundance ratios as a function of metallicity," Annu. Rev. Astron. Astrophys. **27**, 279–349.

Winteler, C., R. Käppeli, A. Perego, A. Arcones, N. Vasset, N. Nishimura, M. Liebendörfer, and F.-K. Thielemann, 2012, "Magnetorotationally driven supernovae as the origin of early Galaxy *r*-process elements?," Astrophys. J. **750**, L22.

Wisshak, K., F. Voss, C. Arlandini, F. Käppeler, and L. Kazakov, 2000, "Stellar neutron capture cross sections of the Yb isotopes," Phys. Rev. C **61**, 065801.

Witti, J., H.-Th. Janka, and K. Takahashi, 1994, "Nucleosynthesis in neutrino-driven winds from protoneutron stars. I. The α-process," Astron. Astrophys. **286**, 841–856, https://ui.adsabs.harvard.edu/#abs/1994A&A...286..841W/abstract.

Wojczuk, K., and A. Janiuk, 2018, "Nucleosynthesis in black hole accretion flows feeding short GRBs," in *XXXVIII Polish Astronomical Society Meeting*, Vol. 7, edited by A. Różańska (Polish Astronomical Society, Warsaw), pp. 337–340.

Woosley, S. E., 1993, "Gamma-ray bursts from stellar mass accretion disks around black holes," Astrophys. J. **405**, 273.

Woosley, S. E., W. David Arnett, and Donald D. Clayton, 1973, "The explosive burning of oxygen and silicon," Astrophys. J. Suppl. Ser., **26**, 231.

Woosley, S. E., Ronald G. Eastman, and Brian P. Schmidt, 1999, "Gamma-ray bursts and type Ic supernova SN 1998BW," Astrophys. J. **516**, 788–796.

Woosley, S. E., D. H. Hartmann, R. D. Hoffman, and W. C. Haxton, 1990, "The ν-process," Astrophys. J. **356**, 272–301.

Woosley, S. E., and A. Heger, 2007, "Nucleosynthesis and remnants in massive stars of solar metallicity," Phys. Rep. **442**, 269–283.

Woosley, S. E., A. Heger, and T. A. Weaver, 2002, "The evolution and explosion of massive stars," Rev. Mod. Phys. **74**, 1015–1071.

Woosley, S. E., and R. D. Hoffman, 1992, "The α-process and the r-process," Astrophys. J. **395**, 202–239.

Woosley, S. E., J. R. Wilson, G. J. Mathews, R. D. Hoffman, and B. S. Meyer, 1994, "The r-process and neutrino-heated supernova ejecta," Astrophys. J. **433**, 229–246.

Wu, J., *et al.*, 2017, "94 β-Decay Half-Lives of Neutron-Rich $_{55}$Cs to $_{67}$Ho: Experimental Feedback and Evaluation of the r-Process Rare-Earth Peak Formation," Phys. Rev. Lett. **118**, 072701.

Wu, M.-R., R. Fernández, G. Martínez-Pinedo, and B. D. Metzger, 2016, "Production of the entire range of r-process nuclides by black hole accretion disc outflows from neutron star mergers, Mon. Not. R. Astron. Soc. **463**, 2323–2334.

Wu, M.-R., T. Fischer, L. Huther, G. Martínez-Pinedo, and Y.-Z. Qian, 2014, "Impact of active-sterile neutrino mixing on supernova explosion and nucleosynthesis," Phys. Rev. D **89**, 061303(R).

Wu, M.-R., *et al.*, 2017 (private communication).

Wu, Meng-Ru, Projjwal Banerjee, Brian D. Metzger, Gabriel Martínez-Pinedo, Tsuguo Aramaki, Eric Burns, Charles J. Hailey, Jennifer Barnes, and Georgia Karagiorgi, 2019, "Finding the remnants of the Milky Way's last neutron star mergers," Astrophys. J. **880**, 23.

Wu, Meng-Ru, J. Barnes, G. Martínez-Pinedo, and B. D. Metzger, 2019, "Fingerprints of Heavy-Element Nucleosynthesis in the Late-Time Lightcurves of Kilonovae," Phys. Rev. Lett. **122**, 062701.

Wu, Meng-Ru, Yong-Zhong Qian, Gabriel Martínez-Pinedo, Tobias Fischer, and Lutz Huther, 2015, "Effects of neutrino oscillations on nucleosynthesis and neutrino signals for an $18M_{\odot}$ supernova model," Phys. Rev. D **91**, 065016.

Wu, Meng-Ru, and Irene Tamborra, 2017, "Fast neutrino conversions: Ubiquitous in compact binary merger remnants," Phys. Rev. D **95**, 103007.

Wu, Meng-Ru, Irene Tamborra, Oliver Just, and Hans-Thomas Janka, 2017, "Imprints of neutrino-pair flavor conversions on nucleosynthesis in ejecta from neutron-star merger remnants," Phys. Rev. D **96**, 123015.

Wu, Yiyang, and Andrew MacFadyen, 2018, "Constraining the outflow structure of the binary neutron star merger event GW170817/GRB170817A with a Markov chain Monte Carlo analysis," Astrophys. J. **869**, 55.

Wünsch, K.-D., 1978, "An on-line mass-separator for thermically ionisable fission products: OSTIS," Nucl. Instrum. Methods **155**, 347–351.

Xu, Y., and S. Goriely, 2012, "Systematic study of direct neutron capture," Phys. Rev. C **86**, 045801.

Xu, Y., S. Goriely, A. J. Koning, and S. Hilaire, 2014, "Systematic study of neutron capture including the compound, pre-equilibrium, and direct mechanisms," Phys. Rev. C **90**, 024604.

Yakovlev, D. G., L. R. Gasques, A. V. Afanasjev, M. Beard, and M. Wiescher, 2006, "Fusion reactions in multicomponent dense matter," Phys. Rev. C **74**, 035803.

Yan, X. L., K. Blaum, Y. A. Litvinov, X. L. Tu, H. S. Xu, Y. H. Zhang, and X. H. Zhou (ESR and CSRe Collaborations on In-Ring Mass Measurements), 2016, "Recent results on mass measurements of exotic nuclides in storage rings," J. Phys. Conf. Ser. **665**, 012053.

Yang, Bin, Zhi-Ping Jin, Xiang Li, Stefano Covino, Xian-Zhong Zheng, Kenta Hotokezaka, Yi-Zhong Fan, Tsvi Piran, and Da-Ming Wei, 2015, "A possible macronova in the late afterglow of the long-short burst GRB 060614," Nat. Commun. **6**, 7323.

Yee, R. M., *et al.*, 2013, "β-Delayed Neutron Spectroscopy Using Trapped Radioactive Ions," Phys. Rev. Lett. **110**, 092501.

Yeh, T.-R., D. D. Clark, G. Scharff-Goldhaber, R. E. Chrien, L.-J. Yuan, M. Shmid, R. L. Gill, A. E. Evans, H. Dautet, and J. Lee, 1983, "High resolution measurements of delayed neutron emission spectra from fission products," in *Nuclear Data for Science and Technology*, edited by K. H. Böckhoff (Springer Netherlands, Dordrecht), pp. 261–264.

Yong, D., J. E. Norris, G. S. Da Costa, L. M. Stanford, A. I. Karakas, L. J. Shingles, R. Hirschi, and M. Pignatari, 2017, "A chemical signature from fast-rotating low-metallicity massive stars: ROA 276 in ω Centauri," Astrophys. J. **837**, 176.

Yuan, Zhen, *et al.*, 2020, "Dynamical relics of the ancient galactic halo," Astrophys. J. **891**, 39.

Zampieri, L., 2017, "Light curves of type II supernovae," in *Handbook of Supernovae*, edited by A. W. Alsabti, and P. Murdin (Springer International Publishing, Cham, Switzerland).

Zhang, C. L., B. Schuetrumpf, and W. Nazarewicz, 2016, "Nucleon localization and fragment formation in nuclear fission," Phys. Rev. C **94**, 064323.

Zhi, Q., E. Caurier, J. J. Cuenca-García, K. Langanke, G. Martínez-Pinedo, and K. Sieja, 2013, "Shell-model half-lives including first-forbidden contributions for r-process waiting-point nuclei," Phys. Rev. C **87**, 025803.

Zhou, Ping, Jacco Vink, Samar Safi-Harb, and Marco Miceli, 2019, "Spatially resolved x-ray study of supernova remnants that host magnetars: Implication of their fossil field origin," Astron. Astrophys. **629**, A51.

Zhu, Jin-Ping, Yuan-Pei Yang, Liang-Duan Liu, Yan Huang, Bing Zhang, Zhuo Li, Yun-Wei Yu, and He Gao, 2020, "Kilonova emission from black hole-neutron star mergers. I. Viewing-angle-dependent lightcurves," Astrophys. J. **897**, 20.

Zhu, Y., *et al.*, 2018, "Californium-254 and kilonova light curves," Astrophys. J. **863**, L23.

Zhu, Y. L., A. Perego, and G. C. McLaughlin, 2016, "Matter-neutrino resonance transitions above a neutron star merger remnant," Phys. Rev. D **94**, 105006.

Zrake, J., and A. I. MacFadyen, 2013, "Magnetic energy production by turbulence in binary neutron star mergers," Astrophys. J. **769**, L29.